

Development of Carbonaceous Nanomaterial Based Heterogeneous Catalytic Systems for Organic Transformations

Ph.D. Thesis

By
Biju Majumdar



DISCIPLINE OF CHEMISTRY
INDIAN INSTITUTE OF TECHNOLOGY INDORE
OCTOBER 2017

Development of Carbonaceous Nanomaterial Based Heterogeneous Catalytic Systems for Organic Transformations

A THESIS

*Submitted in partial fulfillment of the
requirements for the award of the degree*

of

DOCTOR OF PHILOSOPHY

by

BIJU MAJUMDAR



DISCIPLINE OF CHEMISTRY
INDIAN INSTITUTE OF TECHNOLOGY INDORE
OCTOBER 2017



INDIAN INSTITUTE OF TECHNOLOGY INDORE

CANDIDATE'S DECLARATION

I hereby certify that the work which is being presented in the thesis entitled **Development of Carbonaceous Nanomaterial Based Heterogeneous Catalytic Systems for Organic Transformations** in the partial fulfillment of the requirements for the award of the degree of **DOCTOR OF PHILOSOPHY** and submitted in the **DISCIPLINE OF CHEMISTRY, Indian Institute of Technology Indore**, is an authentic record of my own work carried out during the time period from July, 2012 to September, 2017 under the supervision of Dr. Tridib Kumar Sarma, Assistant professor, Discipline of Chemistry, IIT Indore.

The matter presented in this thesis has not been submitted by me for the award of any other degree of this or any other institute.

**Signature of the student with date
(BIJU MAJUMDAR)**

This is to certify that the above statement made by the candidate is correct to the best of my knowledge.

**Signature of Thesis Supervisor with date
(Dr. TRIDIB KUMAR SARMA)**

BIJU MAJUMDAR has successfully given his Ph.D. Oral Examination held on

Signature of Chairperson (OEB)
Date:

Signature of External Examiner
Date:

Signature of Thesis Supervisor
Date:

Signature of PSPC Member #1
Date:

Signature of PSPC Member #2
Date:

Signature of Convener, DPGC
Date:

Signature of Head of Discipline
Date:

ACKNOWLEDGEMENT

It is my great pleasure to express my deep sense of gratitude to Dr. Tridib Kumar Sarma who has been an excellent supervisor. He created a cool scientific environment in the laboratory and gave me the freedom to explore my own scientific interest. I feel fortunate to work under him. He always motivated me to achieve great things in life. I am greatly indebted to him for his constant guidance, encouragement and belief in my research abilities. Apart from being a good supervisor, he is also a good human being. The knowledge and experience he shared to deal with different aspects of life will have a huge impact in my career.

I am thankful to my PSPC committee members, Dr. Sampak Samanta and Dr. Ram Bilas Pachori for their valuable suggestions and guidance. Further, I am also grateful to Dr. Deepa Dey for her constant support, help and encouragement.

I wish to express my gratitude to Prof. Pradeep Mathur, Director, IIT Indore for his continuous support in every aspect.

I would like to thank IIT Indore and SIC, IIT Indore for providing financial support and instrumentation facility respectively. I would also like to thank Dr. Satya S. Bulusu, Dr. Anjan Chakraborty, Dr. Sanjay Kumar Singh, Dr. Biswarup Pathak, Dr. Tushar Kanti Mukherjee, Dr. Suman Mukhopadhyay, Dr. Apurba Kumar Das, Dr. Shaikh M. Mobin, Dr. Rajneesh Misra, Dr. Chelvam Venkatesh and Dr. Amarendra Kumar Singh for their guidance and help during various activities in the department. Specially, I would like to thank Dr. Chelvam Venkatesh for allowing me to use his lab facilities.

I take this opportunity to extend my heartiest gratitude to my three seniors from our group Dr. Tamalika Bhattacharya, Dr. Bhagwati Sharma and Dr. Sonam Mandani and my groupmates Mr. Anurag Sharma, Mr. Siddarth Jain, Ms. Neha Thakur, Mr. Abhiram Panigrahi and Ms. Daisy Sarma for their selfless cooperation and help in making the PhD journey memorable and successful. I am also grateful to Mr. Manjeet Yadav and Ms. Riniki Ragini Kaushik for their smiley support.

I wish to thank the technical staff from Sophisticated Instrumentation Centre (SIC), IIT Indore, Ms. Sarita Batra, Mr. Kinny Pandey, Dr. Ravinder Kumar, Mr. Ghanshyam Bhavsar, Mr. Manish Kushwaha, Mr. Nitin Upadhyay and Ms. Vinita Kothari for their patience and timely technical support without which it would never have been possible to complete my work. I would also like to thank Ms. Anjali Bandiwadekar, Mr. Rajesh Kumar, Mr. Gati Krushna Nayak and other library staff and Mr. Manoj Pal, Mr. Vinod Pal, Mr. Nitin Bhate and other technical staff for their constant help, whenever required. I am also grateful to the transport and house-keeping department of IIT Indore for making things smoother during the PhD tenure.

I am thankful to University Grants Commission (UGC), New Delhi for fellowship. Further, I would like to acknowledge SAIF, NEHU, Shillong, SAIF, IIT Bombay, Department of Physics, Pune University, UGC-DAE Consortium for Scientific Research, Indore and IISER Bhopal for instrumentation support.

I would also like to thank all my co-researchers at IIT Indore. It has been a wonderful experience to work with many friends during my Ph.D who really helped me in many aspects. I would like to record my thanks to Dr. Bhausahab, Dr. Dnyaneswar, Dr. Rajendar, Dr. Raina, Dr. Anupam, Dr. Indrajit, Dr. Shivendra, Dr. Maruthi, Dr. Debashis, Dr. Thaksen, Dr. Anvita, Dr. Veenu, Dr. Surajit, Dr. Arup, Dr. Rohit, Dr. Deepika, Kavita, Kuber, Roopali, Arpan, Mriganka, Soumen, Anuradha, Soumitra, Soumya, Nishu, Miraj, Bidyut, Sagnik, Ramesh, Premansh, Krishna, Amit, Sagar and many others for their generous help and cooperation. I express my heartiest gratitude to my good friends outside the institute, especially, Dr. Hemanta Deka, Dr. Bidyut Bikash Sarma and Mr. Nipu Kalita who have been with me in every ups and downs of my professional and personal life. I also would like to thank my uncle Mr. Kamala Das for inspiring me to choose Chemistry as my career.

I also take this opportunity to express my love and gratitude to all my teachers from Borigog Hajo Higher Secondary School, Rangia Higher Secondary School, Department of Chemistry, B. Borooah College, Department of Chemistry, Gauhati University for their encouragement, love and guidance. I am grateful to

my beloved teachers Mr. Sunanda Mahanta, Dr. Diganta Choudhary and Dr. Dibakar Chandra Deka for their all time inspiration.

Most importantly, it would have been impossible for me to reach here without the support, care and love of my family. I express my respect, love and gratitude to my beloved parents, my brother and my sister for their unconditional love and support.

There are many more who have directly or indirectly contributed in making this journey successful, I wish I could thank them all, but time and space compel me to stop here.

BIJU MAJUMDAR

Dedicated to My Beloved Family

And

My Motherland

Abstract

Within the broad area of nanoscience, catalysis plays an important role in academic scientific research as well as industrial production. Traditional homogeneous catalytic systems are highly efficient because the catalytic activity can be defined on a molecular level and the catalysts as well as the reactants are in sufficient contact in the reaction medium. However, removing them from the reaction medium without contamination of the target products requires tedious purification procedure. With the ecological and economical demands towards sustainable chemical methods, the recovery and reuse of catalysts is an important factor. With this motivation, various heterogeneous catalytic systems including mesoporous materials, metal-organic frameworks, metal oxides/sulphides, noble-metal nanoparticles etc. have been developed for photochemical and electrochemical catalysis, environmental remediation as well as catalyst for important organic transformations.

As one of the most abundant elements on the earth, carbon is very attractive for catalytic applications. Several polytypes of carbon which include fullerenes, nanotubes, graphene, nanodiamonds and amorphous porous carbon represent a rich class of solid carbonaceous materials with environmental acceptability and reusability. Their excellent thermal and chemical stability and adjustable surface functionality make them suitable for many applications ranging from catalysis, electrochemistry and adsorption to separation. In heterogeneous catalytic processes carbon materials are predominantly being used as support for other active catalysts. However, the recent developments involving various carbonaceous materials as efficient metal-free catalysts for several organic reactions has generated a new area of research broadly known as carbocatalysis. The catalytic activities of carbon materials are proportionately related to their defects, structure and surface chemistry. The unparalleled flexibility in tailoring their physical (surface area and porosity) and chemical (surface functional groups) properties and their role in enhancing catalytic activity have generated a great interest in the scientific community.

In this thesis, we explored the intrinsic catalytic activity of two important carbonaceous nanomaterials namely carbon dots and graphene oxide for various

important organic transformations. Further their composite with noble-metal nanoparticles and iron oxide nanoparticles have been explored for different oxidation reactions. The thesis is divided into the following chapters.

Chapter 1: Introduction

In this chapter, a general discussion and literature survey of homogeneous and heterogeneous catalysis including carbonaceous nanomaterials, their synthesis and application in organic reactions have been inscribed.

Chapter 2: Graphene oxide as metal-free catalyst in oxidative dehydrogenative C–N coupling leading to α -ketoamides and importance of dual catalytic activity

In this chapter, we have shown graphene oxide (GO) as a heterogeneous, inexpensive and environmentally friendly carbocatalyst that enables the formation of α -ketoamides from activated aldehydes and amines through a cross-dehydrogenative coupling pathway.

Several controlled experiments and spectroscopic investigation revealed formation of hemiaminal as the intermediate. The dual catalytic activity of graphene oxide towards the C-N coupling reaction was established where the acidic character catalyzed the initial formation of hemiaminal intermediate and the oxidizing character catalyzed the oxidation of hemiaminal to α -ketoamide. Mechanistic studies by different experimental evidence proved that it was the carboxylic acid group that was only responsible for the observed catalytic activity of graphene oxide.

Chapter 3: Probing carbocatalytic activity of carbon nanodots for the synthesis of biologically active dihydro/spiro/glyco quinazolinones and aza-Michael adducts

In this chapter, we have shown carbon nanodots (CNDs) as an effective and recyclable carbocatalyst for the generation of carbon-hetero atom bond leading to quinazolinone derivatives and aza-Michael adducts under mild reaction conditions. The mild acidity imparted by the surface CO₂H groups of this nanoscale form of carbon could act as an alternative carbocatalyst to several

traditional acid catalysts for important acid catalyzed organic transformations. We choose β -carotene as the carbon source for the synthesis of CNDs. The main motive of using β -carotene as the carbon source was that unlike other carbon sources used to make CNDs, β -carotene does not have any oxygen functionality in it. The catalytic activity is driven only by the surface CO_2H group generated during the carbonization of β -carotene. The catalyst showed excellent activity towards the synthesis of variety of dihydro/spiro/glyco quinazolinones with structurally perplexing substituent. The mild acidic behaviour of CNDs could also be extended towards the synthesis of aza-Michael adducts at room temperature.

Chapter 4: Au nanoparticle-polydopamine-reduced graphene oxide ternary nanocomposite as efficient catalyst for selective oxidation of benzylic $\text{C}(\text{sp}^3)\text{-H}$ bonds under mild conditions

In this chapter, we have shown the excellent catalytic activity of a ternary nanocomposite comprising of Au nanoparticles (NPs), polydopamine and reduced graphene oxide towards oxidation of C-H bond in benzylic hydrocarbons under mild conditions in presence of *N*-hydroxyphthalimide (NHPI). The composite was synthesized by modifying the surface of graphene oxide by polydopamine followed by immobilization of Au nanoparticles. The composite was characterized by several spectroscopic and microscopic techniques.

The nanocomposite could be used towards C-H oxidation in wide range of compounds with high activity and selectivity. All the components in the nanocomposite played important role in the effectiveness of the catalyst. Sufficient electron transfer from polydopamine/reduced graphene oxide to Au NPs made the nanoparticle surface more negatively charged favourable for molecular oxygen activation leading to C-H bond oxidation. The reaction followed a free-radical pathway as evidenced by detailed mechanistic studies. Further, easy separation and excellent reusability without significant loss in activity over several iterations fortify the ternary nanocomposite as excellent heterogeneous catalyst for C-H oxidation reactions.

Chapter 5: One-pot magnetic iron oxide carbon nanodots composite catalyzed cyclooxidative aqueous tandem synthesis of quinazolinones in presence of *tert*-butyl hydroperoxide

In this chapter, we have shown carbon nanodots stabilized iron oxide nanoparticles ($\text{Fe}_3\text{O}_4\text{-CNDs}$) as effective magnetically recoverable heterogeneous catalyst for the one-pot synthesis of quinazolinones using *tert*-butyl hydroperoxide (TBHP) as the principal oxidant in aqueous medium. Controlled experiments showed involvement of benzaldehyde and dihydroquinazolinone as the intermediates. The reaction followed a free radical pathway as evident from the experiment using radical scavenger. The catalyst can be recovered easily from the reaction mixture by using a simple magnet and reused for multiple cycles without significant loss in catalytic activity. The stability of the reactive oxygen species derived from *tert*-butylhydroperoxide bound to iron oxide surface may be the driving force for the exceptional activity of the catalyst.

Chapter 6: Conclusion and Future Outlook

This chapter summarizes the works described in the thesis. Further, the relevance and future prospects of the works have been discussed.

LIST OF PUBLICATIONS

1. **Majumdar B.**, Sarma D., Bhattacharya T., Sarma T. K. (2017), Graphene oxide as metal-free catalyst in oxidative dehydrogenative C-N coupling leading to α -ketoamides: Importance of dual catalytic activity, ACS Sustainable Chem. Eng., 5, 9286-9294 (DOI: 10.1021/acssuschemeng.7b02267)
2. **Majumdar B.**, Mandani S., Bhattacharya T., Sarma D., Sarma T. K. (2017), Probing carbocatalytic activity of carbon nanodots for the synthesis of biologically active dihydro/spiro/glyco quinazolinones and aza-Michael adducts, J. Org. Chem., 82, 2097-2106 (DOI: 10.1021/acs.joc.6b02914)
3. **Majumdar B.**, Bhattacharya T., Sarma T. K. (2016), Gold nanoparticle–polydopamine–reduced graphene oxide ternary nanocomposite as an efficient catalyst for selective oxidation of benzylic C(sp³)-H bonds under mild conditions, ChemCatChem, 8, 1825-1835 (DOI : 10.1002/cctc.201600136)
4. **Majumdar B.**, Sarma D., Jain S., Sarma T. K. One-pot magnetic iron oxide carbon nanodots composite catalyzed cyclooxidative aqueous tandem synthesis of quinazolinones in presence of *tert*-butyl hydroperoxide (Manuscript under preparation)
5. Bhattacharya T., **Majumdar B.**, Dey D., Sarma T. K. (2014), Ultrasound mediated synthesis of α -aminophosphonates and 3,4-dihydropyrimidin-2-ones using graphene oxide as a recyclable catalyst under solvent-free conditions, RSC Adv., 4, 45831–45837 (DOI: 10.1039/c4ra08533g)
6. Bhattacharya T., **Majumdar B.**, Sarma T. K. (2016), Compositional effect in AuPd bimetallic nanoparticles towards product selectivity during aerobic oxidation of α -hydroxy esters and phosphonates, Chemistry Select, 1, 5265-5269 (DOI: 10.1002/slct.201601021)
7. Dey D., Bhattacharya T., **Majumdar B.**, Mandani S., Sharma B., Sarma T. K. (2013), Carbon dot reduced palladium nanoparticles as active catalyst for carbon-carbon bond formation, Dalton Trans., 42, 13821-13825 (DOI: 10.1039/c3dt51234g)

8. Bhattacharya T., **Majumdar B.**, Sarma T. K. Heterogeneous spherical Au-Pd bimetallic nanoparticles for aerobic oxidative cross-dehydrogenative C-N coupling: Synthesis of α -ketoamide (Manuscript communicated)

- Publications 5-8 are not a part of this thesis.

TABLE OF CONTENTS

1. List of Figures	
2. List of Schemes	
3. List of Tables	
4. Acronyms	
5. Nomenclature	
Chapter 1: General Introduction and Background	1-44
1.1 Introduction	3
1.2 Nanocatalysis	4
1.2.1 Role of support	5
1.2.2 Carbocatalysis	7
1.2.3 Graphene Oxide as a carbocatalyst	10
1.2.4 Carbon nanodots	15
1.2.4.1 Synthesis of Carbon nanodots	17
1.2.4.2 Applications of Carbon nanodots	19
1.2.5 Magnetic nanoparticles	19
1.2.5.1 Synthesis of magnetic nanoparticles	20
1.2.5.2 Application of magnetic nanoparticles	21
1.3 Organization of the Thesis	22
1.4 References	24
Chapter 2: Graphene Oxide as Metal-Free Catalyst in Oxidative Dehydrogenative C-N Coupling leading to α-Ketoamides: Importance of Dual Catalytic Activity	45-102
2.1 Introduction	47
2.2 Results and Discussion	49
2.2.1 Synthesis and characterization of graphene oxide	49
2.2.2 Optimization studies and substrate scope	50
2.2.3 Conservation of mass and formation of byproducts	55
2.2.4 Large scale synthesis	56
2.2.5 Recovery and recyclability	56
2.2.6 Synthesis of bioactive compound	57

2.2.7 Mechanistic Investigation	57
2.2.8 Leaching Test	65
2.3 Conclusion	66
2.4 Experimental Section	66
2.4.1 General Information	66
2.4.2 Materials	67
2.4.3 Reaction procedure for the synthesis of α -ketoamide	67
2.4.4 Isolation of hemiaminal intermediate	67
2.4.5 Synthesis of starting materials	68
2.4.6 HPLC analysis	69
2.4.7 Preparation of arylglyoxal	69
2.4.8 Characterisation data	69
2.4.8.1 Characterization data for hemiaminal intermediate	69
2.4.8.2 Characterization data for α -ketoamides	70
2.5 References	76
Appendix-Chapter 2	85
^1H and ^{13}C NMR spectra of Hemiaminal Intermediate and α -Ketoamides	
Chapter 3: Probing Carbocatalytic Activity of Carbon Nanodots for the Synthesis of Biologically Active Dihydro/Spiro/Glyco Quinazolinones and Aza-Michael Adducts	103-176
3.1 Introduction	105
3.2 Results and Discussion	107
3.2.1 Synthesis and characterization of CNDs	107
3.2.2 Catalytic activity of carbon nanodots towards cyclocondensation reaction	109
3.2.2.1 Optimization with respect to catalyst loading, temperature, co-solvents and various acid catalysts	110
3.2.2.2 Substrate scope for the cyclocondensation reaction	112
3.2.3 Activity of CNDs towards Aza-Michael addition reaction	115
3.2.4 Recovery and recyclability	116
3.2.5 Mechanism	117

3.3 Conclusion	118
3.4 Experimental Section	118
3.4.1 General Information	118
3.4.2 Materials and Methods	119
3.4.3 Synthesis of carbon nanodots (CNDs)	119
3.4.4 Quantum yield of CNDs	120
3.4.5 The measurement of quantity of total functional groups (-OH and -CO ₂ H groups)	120
3.4.6 The measurement of quantity of -CO ₂ H functional groups	121
3.4.7 General method of synthesis of 2, 3-dihydroquinazolinones	121
3.4.8 General method of synthesis of aza-Michael adducts	121
3.4.9 Reusability of the catalyst	122
3.4.10 Synthesis of 4-formylphenyl 2,3,4,6-tetra-O-acetyl-β-D-galactopyranoside	122
3.4.11 Characterisation data	122
3.5 References	131
Appendix-Chapter 3	141
¹ H and ¹³ C NMR spectra of Dihydro/Spiro/Glyco Quinazolinones and Aza-Michael Adducts	

Chapter 4: Au Nanoparticle-Polydopamine-Reduced Graphene Oxide Ternary Nanocomposite as Efficient Catalyst for Selective Oxidation of Benzylic C(sp³)-H Bonds Under Mild Conditions **177-230**

4.1 Introduction	179
4.2 Results and Discussion	181
4.2.1 Synthesis and characterization of nanocomposite	181
4.2.2 Catalytic Performance of Au-pDA-rGO composite at variable Au loading	186
4.2.3 Optimization and scope of reaction	189
4.2.4 Conservation of mass and large scale synthesis	194
4.2.5 Initial activity studies	195
4.2.6 Recovery and reusability studies	195

4.2.7 Leaching test	196
4.2.8 Mechanistic Studies	198
4.3 Conclusion	202
4.4 Experimental Section	203
4.4.1 Materials	203
4.4.2 Instrumentation and characterization	203
4.4.3 Synthesis of graphene oxide	204
4.4.4 Synthesis of Au-pDA-rGO nanocomposite	204
4.4.5 Synthesis of Au-rGO composite (Au-rGO ^b)	205
4.4.6 Synthesis of other Au catalysts	205
4.4.6.1 Synthesis of Au-TiO ₂ and Au-CeO ₂	205
4.4.6.2 Synthesis of Au-C	206
4.4.6.3 Synthesis of Au-PVP	206
4.4.7 Aerobic sp ³ C-H bond oxidation	206
4.4.8 Characterization data	207
4.5 References	210
Appendix-Chapter 4	222
¹ H and ¹³ C NMR of Oxidized Products	
Chapter 5: One-Pot Magnetic Iron Oxide Carbon Nanodots	231-268
Composite Catalyzed Cyclooxidative Aqueous Tandem	
Synthesis of Quinazolinones in Presence of Tert-butyl	
hydroperoxide	
5.1 Introduction	233
5.2 Results and Discussion	235
5.2.1 Synthesis of CND and CND stabilized (Fe ₃ O ₄) NPs (Fe ₃ O ₄ -CNDs)	235
5.2.2 Characterization of Fe ₃ O ₄ -CND composite	236
5.2.3 Catalytic activity of Fe ₃ O ₄ -CND composite towards the formation of quinazolinones	240
5.2.4 Investigation of reaction mechanism	243
5.2.5 Recovery and reusability	245
5.3 Conclusion	246

5.4 Experimental section	247
5.4.1 Generation Information	247
5.4.2 Materials and methods	247
5.4.3 Cyclooxidative synthesis of quinazolinones	247
5.4.4 Characterization data of quinazolinones	248
5.5 References	251
Appendix-Chapter 5	260
^1H and ^{13}C NMR spectra of Quinazolinones	
Chapter 6: Conclusion and Future Outlook	269-272
6.1 Conclusion	271
6.2 Future Outlook	271

LIST OF FIGURES

Chapter 1: General Introduction and Background

Figure 1.1	Different forms of carbon nanomaterials	9
Figure 1.2	Possibilities of covalent functionalization of GO	11
Figure 1.3	Schematic diagram of active sites of graphene-based nanomaterials	12
Figure 1.4	Schematic illustration of the two broad categories of C-dots	16
Figure 1.5	Schematic illustration of synthesis of CNDs via top-down and bottom-up approaches and further modification including functionalization, doping and nanohybrid formation	18

Chapter 2: Graphene Oxide as Metal-Free Catalyst in Oxidative Dehydrogenative C-N Coupling leading to α -Ketoamides: Importance of Dual Catalytic Activity

Figure 2.1	a) TEM image; scale bar 500 nm, b) AFM image (inset height profile of GO), c) Powder X-ray diffraction pattern, d) C1s core level XPS spectrum e) UV-visible spectrum and f) FTIR spectrum of GO	50
Figure 2.2	a) Product yield after different cycle of catalytic reactions using recovered GO after subsequent reactions as catalyst and b) XPS O1s core level spectrum of GO and GO recovered after 5 th catalytic cycle for the model coupling reaction	56
Figure 2.3	Time-dependent HPLC-MS analysis of the coupling reaction of phenyl glyoxal monohydrate and pyrrolidine with its corresponding ESI-MS.	58
Figure 2.4	a) Catalytic activity (inset, relative C/O ratio with increasing temperature), GO-5th denotes the catalyst after 5th cycle, b) XPS survey spectra, c) O1s core level	60

XPS spectra d) Raman spectra of GO annealed at different temperature

Figure 2.5 Transmission infrared differential spectra of GO 61 showing relative amounts and distribution of oxygenated functional groups at different annealing temperature regime. It presents the changes in functional groups at various elevated temperature

Figure 2.6 Zeta potential measurement of GO samples annealed at 61 different temperature

Figure 2.7 (a, b, c, d and e) SEM images of GO annealed at 62 different temperature (pristine GO, 200, 400, 600 and 800 °C respectively) showing no apparent changes in surface morphology

Figure 2.8 Transmission infrared absorption spectra for a) GO 63 (black), bGO (blue), baGO (magenta) and b) baGO (purple), R-baGO(magenta) and R-baGO* (navy).

Figure 2.9 Formation of α -ketoamide as a function of time under 65 standard condition (red line) and removal of GO catalyst after 2 hour (blue line).

Chapter 3: Probing Carbocatalytic Activity of Carbon Nanodots for the Synthesis of Biologically Active Dihydro/Spiro/Glyco Quinazolinones and Aza-Michael Adducts

Figure 3.1 a) Digital images of (1) β -carotene dispersed in water, 107 (2) CNDs hydrothermally obtained in daylight and (3) C-dot solution showing blue fluorescence under UV light (λ_{ex} = 365 nm), b) UV-visible spectrum and c) Excitation dependent emission spectrum of CNDs.

Figure 3.2 a) TEM image of CNDs (scale bar 10 nm), particle size 108 distribution histogram (inset a) and b) High resolution transmission electron microscopy image of CNDs.

Figure 3.3 a) AFM image and b) powder X-ray diffraction pattern 109

	of CNDs.	
Figure 3.4	a) C1s XPS and b) FTIR spectrum of CNDs.	109
Figure 3.5	a) Transmission electron microscopy image and b) X-ray photoelectron spectroscopy study of C1s core level of CNDs recovered after 3 rd cycle of reaction, c) Normalized fluorescence spectra and d) Zeta potential values of CNDs before and after reaction.	117
Chapter 4: Au Nanoparticle-Polydopamine-Reduced Graphene Oxide Ternary Nanocomposite as Efficient Catalyst for Selective Oxidation of Benzylic C(sp³)-H Bonds Under Mild Conditions		
Figure 4.1	A pictorial depiction for the formation of Au NPs supported on pDA-rGO nanosheets	182
Figure 4.2	Transmission electron micrograph of a) graphene oxide; scale bar 500 nm, b) Au-pDA-rGO composite; scale bar 100 nm, c) High Resolution (HR-TEM)TEM image of Au-pDA-rGO composite, scale bar 2 nm and d) selected area electron diffraction (SAED) pattern of Au-pDA-rGO composite	183
Figure 4.3	Atomic force microscopy studies of GO and Au-pDA-rGO; a) low resolution image of GO; (b, c) high resolution image and corresponding height profile of GO; d) AFM image of Au-pDA-rGO and e) corresponding height profile.	184
Figure 4.4	a) UV-Visible spectra (inset: enlarged view of Au surface Plasmon resonance band); b) powder X-ray diffraction pattern; c) Raman spectra and d) FTIR spectra of GO (black line) and Au-pDA-rGO (red line).	185
Figure 4.5	a) XPS survey spectra of (i) GO, (ii) pDA-rGO and (iii) Au-pDA-rGO; b) and c) XPS C1s core-level spectrum of GO and pDA-rGO respectively and d) Au4f core-level spectrum	186

Figure 4.6	TEM images and corresponding particle size distribution histogram (below) of Au-pDA-rGO nanocomposite with different Au loading a) 0.5 wt%, b) 2 wt%, c) 4 wt% and d) 6 wt%	188
Figure 4.7	a) TEM image of Polydopamine stabilized Au nanoparticle (Au-pDA), b) TEM micrograph of Au-rGO ^b composite synthesized by simultaneous reduction of Au ³⁺ and GO using NaBH ₄ ; scale bar 20 nm and c) corresponding SAED pattern. The particles showed an average size of 7.6 ± 1.6 nm	190
Figure 4.8	Gram scale oxidation reaction of cyclohexane	194
Figure 4.9	Percentage deactivation showing the initial activity of catalyst upon reuse; Au-pDA-rGO (black line) and Au-pDA (dashed line) over three diphenylmethane oxidation recycle test. Each reaction was performed under the standard conditions of diphenylmethane oxidation; substrate/metal molar ratio 1000; O ₂ pressure 10 bar; stirring rate 1000 rpm; Reaction temperature 60 °C; NHPI 10 mol%; Reaction time 4 h	195
Figure 4.10	Reusability studies of Au-pDA-rGO nanocomposite on the oxidation of diphenylmethane	196
Figure 4.11	TEM image and corresponding particle size distribution of Au-pDA-rGO a) after 3rd cycle (scale bar 50 nm) and b) after 5th cycle (scale bar 50 nm)	197
Figure 4.12	Formation of diphenylketone as a function of time under standard condition (red line) and removal of Au-pDA-rGO catalyst after 4 hour (blue line). Standard reaction conditions of diphenylmethane oxidation (Substrate to metal molar ratio 1000; stirring rate 1000rpm, O ₂ pressure 10 bar; 60 °C, NHPI 10 mol%) were employed in both the cases	197
Figure 4.13	O ₂ activation by pDA-rGO supported Au NPs forming the superoxo species	198

Figure 4.14	Plausible mechanistic cycle for oxidation of benzylic hydrocarbons by the Au-pDA-rGO/NHPI system	199
Figure 4.15	Comparative Au4f core-level XPS study of a) Au-rGO ^b , b) Au-pDA and c) Au-pDA-rGO	200
Figure 4.16	High resolution mass spectra of the Diphenylmethyl-TEMPO adduct	201
Figure 4.17	UV-Visible spectrum of DPPH and DPPH-radical adduct (inset digital images of the two solutions respectively)	201
Figure 4.18	DMPO trapped EPR spectra with or without Au-pDA-rGO. DMPO binds with superoxide radicals ($\bullet\text{O}_2^-$) formed on Au NP surface	202

Chapter 5: One-Pot Magnetic Iron Oxide Carbon Nanodots Composite Catalyzed Cyclooxidative Aqueous Tandem Synthesis of Quinazolinones in Presence of Tert-butyl hydroperoxide

Figure 5.1	a) Powder X-ray diffraction pattern of Fe ₃ O ₄ -CND composite, b) and c) Emission spectra and FTIR spectra for CNDs and Fe ₃ O ₄ -CND respectively	237
Figure 5.2	a) Wide scan XPS spectrum of Fe ₃ O ₄ -CND, b) Fe2p, c) C1s and d) O1s core level XPS spectrum of Fe ₃ O ₄ -CND	238
Figure 5.3	a) TEM image of Fe ₃ O ₄ -CND with scale bar 20 nm (inset a: high resolution TEM image), b) SAED pattern, c) SEM image and d), e), f) elemental mapping of Fe ₃ O ₄ -CND representing Fe, O and C respectively (inset f: EDS spectrum)	239
Figure 5.4	Magnetization curve for CND stabilized iron oxide nanoparticles	239
Figure 5.5	a) Digital image showing dispersion of Fe ₃ O ₄ -CND nanoparticles in presence and absence of external magnet, b) reusability study of Fe ₃ O ₄ -CND for the	246

model reaction and c) TEM image of Fe₃O₄-CND
recovered after 3rd cycles of reaction

LIST OF SCHEMES

Chapter 2: Graphene Oxide as Metal-Free Catalyst in Oxidative Dehydrogenative C-N Coupling leading to α -Ketoamides: Importance of Dual Catalytic Activity

Scheme 2.1	Biologically active α -Ketoamides	47
Scheme 2.2	Synthetic methods for α -ketoamides	48
Scheme 2.3	Gram scale synthesis for the coupling reaction of phenylglyoxal and pyrrolidine	56
Scheme 2.4	Synthesis of orexin receptor antagonist (I)	57
Scheme 2.5	Formation of hemiaminal intermediate followed by α -ketoamide	59
Scheme 2.6	Comparison of benzaldehyde and phenylglyoxal towards α -ketoamide formation	59

Chapter 3: Probing Carbocatalytic Activity of Carbon Nanodots for the Synthesis of Biologically Active Dihydro/Spiro/Glyco Quinazolinones and Aza-Michael Adducts

Scheme 3.1	Model cyclocondensation reaction leading to the formation of 2,3-dihydroquinazolinon-4(1H)-one	110
Scheme 3.2	Synthesis of spirocyclized quinazolinones	114
Scheme 3.3	Synthesis of Glycosidic bond	115
Scheme 3.4	Plausible mechanism for CNDs catalyzed cyclocondensation reaction of carbonyl compound and 2-aminobenzamide	117

Chapter 4: Au Nanoparticle-Polydopamine-Reduced Graphene Oxide Ternary Nanocomposite as Efficient Catalyst for Selective Oxidation of Benzylic C(sp³)-H Bonds Under Mild

Conditions

- Scheme 4.1** Schematic of the ternary nanocomposite consisting of Au nanoparticles supported on polydopamine and reduced graphene oxide as catalysts for benzylic C-H bond oxidation 181

Chapter 5: One-Pot Magnetic Iron Oxide Carbon Nanodots Composite Catalyzed Cyclooxidative Aqueous Tandem Synthesis of Quinazolinones in Presence of Tert-butyl hydroperoxide

- Scheme 5.1** One-pot synthesis of quinazolinones with alcohols and 2-aminobenzamides as the starting materials 234
- Scheme 5.2** C-H amidation leading to dihydroquinazolinone and quinazolinone 240
- Scheme 5.3** Control experiments with benzaldehyde and 2-aminobenzamide as the starting materials 244
- Scheme 5.4** Presence of radical inhibitor indicating free radical process 244
- Scheme 5.5** All the reactions were carried out using 0.5 mmol substrate, 1.0 mmol TBHP, 0.5 mmol BHT, 10 mg catalyst and 2 mL H₂O at 90 °C 245

LIST OF TABLES

Chapter 1: General Introduction and Background

Table 1.1	Few reactions catalyzed by carbon catalysts	8
Table 1.2	Catalytic reactions by GO and chemically converted GO (Adapted from reference 82). Graphene (G), X-doped G (X denotes B, N and Si), (B, N)-doped holy G [(BN)HoIG], carbon-nitride (g-C ₃ N ₄), reduced graphene oxide (rGO), N-doped rGO [(N)rGO], triethylamine modified rGO (rGO-NEt ₃), rGO/GO functionalized with -SO ₃ H (rGO-SO ₃ H/GO-SO ₃ H), poly(amidoamine)-modified rGO (rGO-PAMAM), amino-functionalized GO with 3-[2-(2-amino ethyl amino)ethylamino] propyl-trimethoxy silane (AEPTMS) and aryl -SO ₃ H groups (GO-AEPTMS/SO ₃ H)	13

Chapter 2: Graphene Oxide as Metal-Free Catalyst in Oxidative Dehydrogenative C-N Coupling leading to α -Ketoamides: Importance of Dual Catalytic Activity

Table 2.1	Oxidative coupling of 1a with 2a under various conditions	51
Table 2.2	Optimization studies of coupling reaction of 1a and 2a	52
Table 2.3	GO catalyzed oxidative coupling of variety of α -keto aldehydes and aliphatic secondary/primary amines.	53
Table 2.4	Oxidative coupling of 1a and 4a under various reaction conditions	54
Table 2.5	GO catalyzed oxidative coupling of different α -carbonyl aldehydes with variety of primary amines	55
Table 2.6	Surface area of Graphene Oxide annealed at different temperature	62
Table 2.7	Catalytic activity of modified GO	64

Chapter 3: Probing Carbocatalytic Activity of Carbon Nanodots for the Synthesis of Biologically Active Dihydro/Spiro/Glyco Quinazolinones and Aza-Michael Adducts

Table 3.1	Optimization with respect to catalyst loading and temperature	110
Table 3.2	Optimization with respect to co-solvents	111
Table 3.3	Catalytic activity of different carbon based catalysts and acid catalysts	112
Table 3.4	Substrate scope of the cyclocondensation reaction with various aromatic/heteroaromatic/aliphatic aldehydes	113
Table 3.5	Aza-Michael addition of Amines and α , β -unsaturated compounds using CNDs	115
Table 3.6	Quantum yield of quinine sulphate and CNDs	120

Chapter 4 : Au Nanoparticle-Polydopamine-Reduced Graphene Oxide Ternary Nanocomposite as Efficient Catalyst for Selective Oxidation of Benzylic C(sp³)-H Bonds Under Mild Conditions

Table 4.1	ICP-AES analysis and TON of Au catalysts with varying Au loading	187
Table 4.2	Effect of Au loading on the aerobic oxidation of diphenylmethane	188
Table 4.3	Effect of rGO: Au ratio in the catalytic conversion of diphenylmethane oxidation	189
Table 4.4	Optimization of reaction conditions	191
Table 4.5	Comparison of catalytic activity of different Au catalysts at elevated temperature	192
Table 4.6	The Oxidation of benzylic hydrocarbons catalysed by Au-pDA-rGO nanocomposite	193

Chapter 5 : One-Pot Magnetic Iron Oxide Carbon Nanodots Composite Catalyzed Cyclooxidative

**Aqueous Tandem Synthesis of Quinazolinones in
Presence of Tert-butyl hydroperoxide**

Table 5.1	Oxidative coupling of (1a) and (2a) under various conditions	241
Table 5.2	Synthesis of quinazolinones catalyzed by Fe ₃ O ₄ -CND composite	243

ACRONYMS

CNT	Carbon nanotubes
CDC	Cross-dehydrogenative coupling
CNDs	Carbon nanodots
GQD	Graphene quantum dots
PL	Photoluminescence
UV-Vis	UV-Visible Spectroscopy
XPS	X-ray Photoelectron Spectroscopy
SAED	Selected area electron diffraction
TEM	Transmission electron microscopy
SEM	Scanning electron microscopy
EDS	Energy dispersive spectrum
HRTEM	High-resolution transmission electron microscopy
PXRD	Powder X-ray Diffraction
FTIR	Fourier Transform Infrared
QY	Quantum yield
AFM	Atomic-force Microscopy
FRET	Forster Resonance Energy Transfer
TCSPC	Time-Correlated Single Photon Counting
NP	Nanoparticle
K_{SV}	Stern-Volmer quenching constant
GO	Graphene oxide
AC	Activated carbon
CB	Carbon black
MRI	Magnetic resonance imaging
EPR	Electron paramagnetic resonance
NMR	Nuclear magnetic resonance
HPLC	High performance liquid chromatography
PPM	Parts per million
BE	Binding energy
TLC	Thin layer chromatography
ICP-AES	Inductively coupled plasma atomic emission spectroscopy

TON	Turnover number
RPM	Rotation per minute
TOF	Turnover frequency
PPB	Parts per billion
PEG	Polyethylene glycol

NOMENCLATURE

λ	Wavelength
nm	Nanometer
π	Pi
eV	Electron-volt
\AA	Angstrom
ns	Nanoseconds
M	Molar concentration
μM	Micromolar
mM	Millimolar
mg	Milligram
mV	Millivolt
Hz	Hertz
rpm	Revolutions per minute
a.u.	Arbitrary unit
cps	Counts per second
mL	Milliliter
μL	Microliter
μm	Micrometer
$^{\circ}\text{C}$	Degree Centigrade
α	Alpha
β	Beta
γ	Gamma

Chapter 1

General Introduction and Background

Chapter 1

1.1 Introduction

In recent years, there has been tremendous focus towards developing greener synthetic methods for the industrial production of fine and commodity chemicals. Towards the development of economical and environmentally friendly pathway for the large scale synthesis at the industrial level, the ideal protocols are characterized by four parameters: catalytic activity, selectivity, atom-economy and step-selectivity. Among them, development of catalytic systems with high activity and selectivity plays the most important role. A catalyst provides an alternative pathway with a lower activation energy barrier for the rate-determining step in an organic reaction without being transformed itself.^[1] If there are several products and several reaction barriers, a catalyst can drive the reaction selectivity with a particular product. The efficiency of a catalyst lies on the formation of the desired product with high yield and selectivity at relatively milder reaction conditions. Hence, the search for suitable catalytic systems to achieve green and sustainable production of chemicals is growing continuously, that promotes reduction of toxic and hazardous chemicals, stoichiometric amount of promoter, less consumption of energy, fewer side products and less number of steps involved.

In the past, the main objective of catalysis was to enhance the activity and selectivity of a catalyst, the recovery and reusability of a catalyst was rarely a major concern. Traditional homogeneous organocatalysts, transition metal catalysts as well as bio-catalytic systems are highly efficient because the catalytic activity can be defined on a molecular level. These single site catalysts are highly accessible to reactant molecules, readily soluble in reaction medium and often give rise to high catalytic activity and selectivity even under mild conditions.^[2-3] However, often use of expensive metal salts, expensive ligands, expensive and tedious purification steps as well as recovery of the catalyst is the major issue. A variety of homogeneous and heterogeneous catalysts have been developed, however there is still a vast scope for development of suitable catalysts that not only offers high activity and selectivity, but also greenly acceptable. Fabricating single step synthetic methods using heterogeneous catalysts is a challenging goal as it aims at decreasing the energy and time consumption by operation of multi-

Chapter 1

steps at a time which eliminates the need of separation of products from the reaction mixture again and again.^[4-13]

1.2 Nanocatalysis

In the area of heterogeneous catalysis, the primary focus is towards development of materials with high surface area as the reactions involve surface initiated pathway. As high surface area to volume ratio is achieved as the sizes go down from bulk to nanometer level, hence research activities involving nanoparticles (NPs) as catalysts have grown rapidly in a variety of areas such as pharmaceuticals, fine chemicals, renewable energy and biotransformations. The key objective of nanocatalysis research is to produce catalysts with 100% selectivity with extremely high activity, low energy consumption, and long lifetime. This can be achieved only by precisely controlling the size, shape, spatial distribution, surface composition and electronic structure, and thermal and chemical stability of the individual nanocomponents. In addition, surface atoms which are at the edges or in the corners are more active than those in planes, and their number also increases with decreasing particle size. Thus nanoparticles have shown tremendous applicability at the interface between homogeneous and heterogeneous catalysis.^[14-30] Homogeneous nanocatalysts are used in the same medium as the reactants. The main concern with homogeneous nanocatalysts is their recovery from the solution for repeated cycles as nanoparticles are extremely difficult to be removed from a solution and the extra steps needed to do so could completely negate the process simplification. If the nanoparticles cannot be recovered, they pose an environmental risk, as well as threatening the profitability of the process. For easy recovery and recyclability, the active nanocatalysts are often immobilized on a solid inert matrix, which is in a different phase to the reactants. The solid catalysts can in most cases simply be filtered out and used for the next cycle of reactions, making the process economical and greener. Due to the complex physico-chemical properties at the nanometer level and possibility of multiple surface initiated reactions at the active site, synthesis-structure-catalysis performance relationships are poorly understood in many catalytic systems. A variety of heterogeneous catalytic systems based on metal nanoparticles, semiconductors, oxides/sulphides,

mesoporous materials, metal-organic framework etc. and their combinations have been developed for photochemical and electrochemical catalysis, environmental remediation as well as catalysis for important chemical conversions. Other metal-free nanomaterials such as fullerene, graphite, graphene oxide (GO), carbon nanotube (CNT) and carbon nanodots (CNDs) have also been studied either as effective carbocatalyst or as support for metal/oxide for various catalytic applications.

1.2.1 Role of support

In heterogeneous catalysis, the modus operandi is through surface mediated reactions. Therefore, availability of large surface area is a prerequisite for high catalytic conversions.^[29-47] Although, unsupported nanoparticles with well-defined surface structure and clean exposed facets are predicted to be highly active for catalysis as shown by several theoretical studies, their applicability in real catalysis is a challenge. Due to high surface energy resulting from the large fraction of atoms present on the surface of NPs, they tend to reduce the surface energy and stabilize themselves through agglomeration and coagulation, resulting in decreased active surface area.^[31-36] This leads to an exponential decrease in the surface area for effective catalysis and the prime objective of using nanoparticles for repeated cycles with high activity is practically lost. For example, in case of Au nanoparticles, size plays a critical role during oxidation reactions, as nanoparticles with the diameter 1-5 nm are highly active, whereas larger nanoparticles becomes inactive. The protection of nanoparticle surface from agglomeration can be achieved by using a surface stabilizing agent or immobilizing the NPs into a solid matrix with high surface areas.^[37-47] Soft organic materials such as polymers,^[48-50] surfactants,^[51-53] dendrimers,^[54-60] and ionic liquids have been used as effective capping agents.^[61-62] These systems often show high catalytic performances^[63-64] e.g. reduction of nitrobenzene,^[65] olefin hydrogenation and CO oxidation at low temperatures by Au nanoparticles,^[66] C-C coupling^[67-68] or hydrosilylation reactions of olefins by Pd nanoparticles.^[69] However, these polymeric supports suffer certain disadvantages such as providing low surface area which limits the interface between the catalyst and the reaction substrate. Moreover, soft nature of the materials and low

Chapter 1

mechanical stability often leads to separation of the support from the NPs surface after repeated reaction cycles which eventually results in agglomeration of the particles and decrease in catalytic activity. Alternatively, nanoparticles have been immobilized or grafted onto solid supports to improve their stabilization and recycling ability.^[37-42] “Inert” porous solid materials such as zeolites, charcoals, metal-organic frameworks, layered-double hydroxides etc. have been used for immobilization of active metal catalysts. Being inert and hard, these materials are highly stable even under harsh reaction conditions and can be easily recovered from the reaction mixture for further applications. Porous materials also allow control over the nanoparticle growth in the porous matrix, prevents agglomeration and enhances active site exposure.^[70] The host support materials stabilizes the nanoparticles, however they have no role in manipulating the activity of the nanoparticles for catalysis. In the last few years, there has been tremendous focus on the development of “active” supports, which along with stabilizing the nanoparticles also contribute towards overall catalytic activity in synergy with the nanoparticles.^[71-72] For example, the charge state of the Au nanoparticles is known to influence their reactivity, in the case of the negatively charged Au nanoparticles, an extra electron from the gold readily transfers to the anti-bonding $2\pi^*$ orbital of the adsorbed O_2 , which weakens the O–O bond and activates oxygen molecule for further catalytic reaction. On the other hand, the positive charge accumulated on the gold can promote adsorption of some reactants, such as CO and hydrocarbons. An active support can transfer charges to/from the active catalytic surface, hence influencing the activity of the reaction. For example, Au nanoparticles anchored on rutile $TiO_2(110)$ surface shows high activity for the oxidation of CO to CO_2 . Along with providing significant exposed catalytic active sites for the reaction, TiO_2 also involves in charge transfer process with the Au NPs making the NPs surface highly negative for dioxygen activation leading to oxidation of CO to CO_2 .^[73] Recently, research works involving GO as a support for immobilizing active metal nanoparticles have gained attention. GO, not only provides a large surface area with high exposure of active catalysts, but also can influence the catalytic activity.^[74-75] Possible surface to metal electron transfer from GO to nanoparticles activating dioxygen molecule over NPs surface for several oxidation reactions has been reported.^[75]

Hence, choice of a suitable support for NPs stabilization with possible cooperativity might play an important role in controlling the reaction yield and selectivity of products.

1.2.2 Carbocatalysis

Carbon is one of the most abundant elements on earth and is central to life. Hence, catalytic application of carbon is very attractive and both organic and inorganic carbons play a key role in catalysis. A huge amount of organic compounds act as highly efficient homogeneous catalysts, forming a dedicated branch of chemistry “organocatalysis”. Carbon is often the main constituent of the organic ligands surrounding the metallic center in organometallics. In enzymatic catalysis it constitutes the backbone of the active species. In heterogeneous catalysis, carbon materials act as unique catalyst supports by anchoring different active species through its active site and can also act as catalysts by themselves. The physical and chemical properties of carbon materials, such as their tunable porosity and surface chemistry, make them suitable for application in many catalytic processes.

Among the carbon catalysts developed, activated carbon (AC) and carbon black (CB) are the most commonly used carbon supports. The typically large surface area and high porosity of activated carbon catalysts favor the dispersion of the active phase over the support and increase its resistance to sintering at high metal loadings. The pore size distribution can be tuned to suit the requirements of active supports and substrates. The activated carbon shows several advantages owing to their several outstanding properties, such as low cost, resistance to acids and bases, high stability even at elevated temperature, high surface area ($> 1000 \text{ m}^2/\text{gm}$) and easy removal etc. Moreover, metal salts can be reduced to active metallic forms in these mesoporous materials, making them highly competent as metal supports.

Carbocatalysis is the study of chemical reactions using carbonaceous materials as catalysts. These catalytic materials are prepared and used in powder or monolith form, and the reactions are therefore heterogeneous. Carbocatalysis has been known for decades since the first discovery of catalytic activities of

Chapter 1

carbon materials^[76] when Wright *et al.* (1925) discovered the charcoal catalyzed oxidation of oxalic acid, which was among the first reports of carbocatalysis.^[77] Moreover, 45 years earlier also, carbon materials were found to be able to catalyze the conversion of halogenated hydrocarbon.^[76] Some relevant reactions catalyzed by activated carbon materials are summarized in Table 1.1.^[78]

Table 1.1. Few reactions catalyzed by carbon catalysts

General Classification	Examples
Oxidation–reduction	$\text{SO}_2 + 1/2\text{O}_2 \longrightarrow \text{SO}_3$ $\text{NO} + 1/2\text{O}_2 \longrightarrow \text{NO}_2$
Hydrogenation-dehydrogenation	$\text{RX} + \text{H}_2 \longrightarrow \text{RH} + \text{HX} \text{ (X= Cl, Br)}$ $\text{HCOOH} \longrightarrow \text{CO}_2 + \text{H}_2$
Combination with halogens	$\text{H}_2 + \text{Br}_2 \longrightarrow 2\text{HBr}$ $\text{CO} + \text{Cl}_2 \longrightarrow \text{COCl}_2 \text{ (phosgene)}$
Decomposition	$2\text{H}_2\text{O}_2 \longrightarrow 2\text{H}_2\text{O} + \text{O}_2$ $\text{CH}_4 \longrightarrow \text{C} + 2\text{H}_2$
Dehydration, isomerization and polymerization	$\text{HCOOH} \longrightarrow \text{H}_2\text{O} + \text{CO}$ $3\text{C}_2\text{H}_2 \longrightarrow \text{C}_6\text{H}_6$ $\alpha\text{-olefins} \longrightarrow \text{poly}(\alpha\text{-olefins})$
Emerging applications	Oxygen reduction reactions

With the development of fullerenes, the research activities for the growth of nanocarbon materials have gained momentum. Several polytypes of carbon which include fullerenes, nanotubes, graphene, nanodiamonds and amorphous porous carbon and their derivatives represent a rich class of solid carbonaceous materials with environmental acceptability and reusability and all are found to be catalytically active in certain reactions. However, most of these carbon materials are highly hydrophobic without any functional groups on their surface.

Fullerene black is an efficient catalyst for dehydrogenation, cracking, methylation, and demethylation reactions. C_{60} and C_{70} were found to be suitable catalysts for the reduction of nitrobenzene, using hydrogen gas under UV light.^[79] Further, several organometallic compounds involving fullerene as a ligand

Chapter 1

have been developed that showed efficient catalytic activity for several organic transformations.^[80-82]

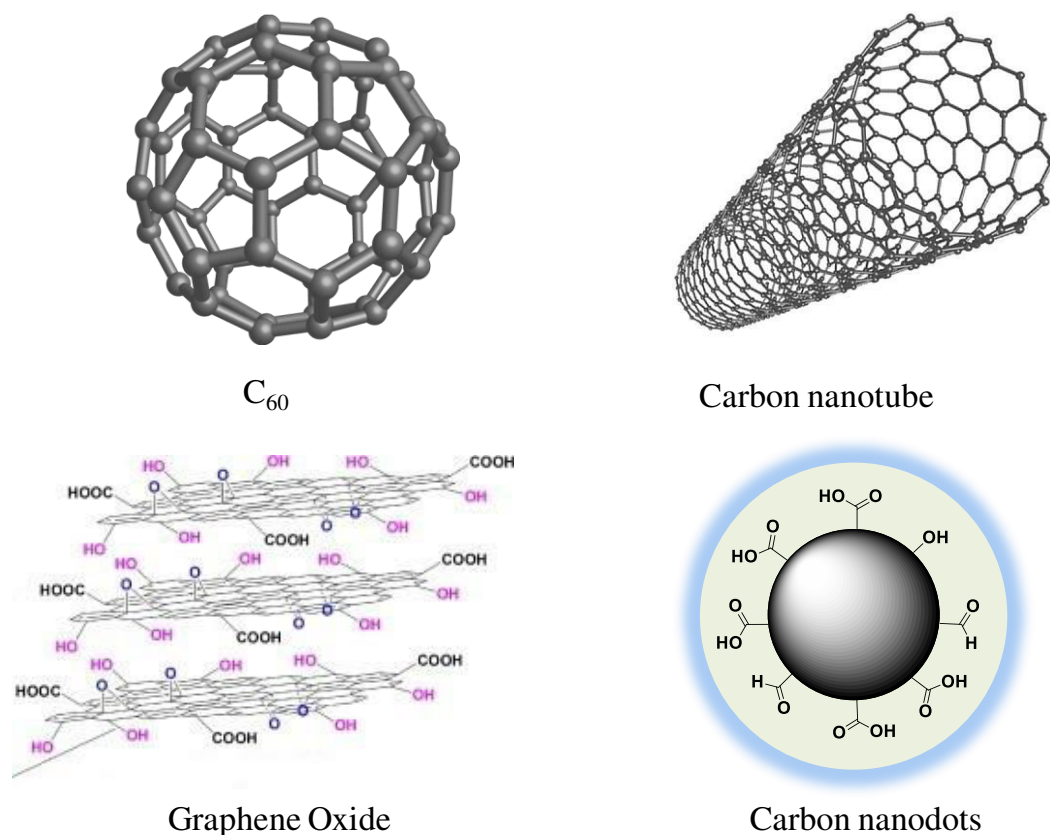


Figure 1.1. Different forms of carbon nanomaterials

The 1D and 2D carbon materials such as carbon nanotubes and graphene offered high surface area and continuous efforts are focused on surface functionalization of these materials, both through covalent and non-covalent approach. Oxidation in presence of strong acids and oxidants could introduce oxyfunctionalized groups on the surfaces of these carbon materials, making them hydrophilic and suitable for anchoring several active catalytic groups on their surfaces. The work on the oxidative dehydrogenation reaction by Schlögl^[83] and Su^[84] *et al.* opened a new window in carbocatalysis. Carbon nanotubes, in its oxygenated forms, showed efficient catalysis for oxidative dehydrogenations e.g. conversion of n-butane to 1-butene.^[84] In the catalytic hydrogenation of ethylbenzene to styrene, a process of high industrial relevance, CNTs performed better than activated carbon and graphite as catalysts. It was reasoned that the reactant molecules were first adsorbed on the CNT surface via π -interactions next

Chapter 1

to basic oxygen moieties, which facilitated dehydrogenation with concomitant formation of surface hydroxy groups.^[83] Taking advantage of surface modification techniques, various nanoparticle as well as molecular catalysts could be anchored on carbon nanotubes.^[85-87]

1.2.3 Graphene Oxide as a carbocatalyst

Graphene and other two-dimensional sp^2 -hybridized carbon scaffolds are expected to have large impacts in the area of catalysis, mainly because of their unique electronic properties and high surface area in comparison to other carbon materials.^[88] Although graphene was known to exist within graphite materials, it was assumed to be thermodynamically unstable in distinct 2D structures at finite temperatures.^[89] Geim *et al.* (2004) mechanically exfoliated single sheets from the π -stack layers in graphite for the first time.^[90] The unique electron transfer properties of graphene, such as a half-integer quantum Hall effect, the massless Dirac fermion behavior of its charge carriers, and quantum capacitance, have been extensively studied making them one of the most important materials in opto-electronics utility.^[91] The use of graphene-based nanomaterials as catalyst support was hampered by the high price associated with the laborious synthesis and processing (e.g., sublimation of silicon from silicon carbide wafers,^[92] chemical vapor deposition,^[93] oxidation/reduction protocols^[94] etc. However, the process for liquid phase exfoliation through oxidation of graphite in presence of strong oxidizing agents generating the graphene analogue with oxygenated functionalities on their surface (popularly known as Hummer's method) has brought tremendous excitement in the nanocatalyst research community. These materials termed as "graphene oxide" can be obtained in sufficient quantities from commercially available graphite through reliable, now well-established preparation procedures. Further potential chemical modifications of the graphene surface introduces different newer catalytically active site important for specific catalytic reactions (Fig. 1.2).^[95]

Chapter 1

reactions.^[99] Further, reduction of graphene oxides can be performed using common reducing agents such as hydrogen, metal ion borohydride and hydrazine. Moreover, the graphene oxide surfaces can be reduced by heating at elevated temperature. Various heteroatoms such as N, B, P, Se, S, F, and Cl^[100-101] can be incorporated into the lattice of graphene sheets. Functional groups such as $-\text{SO}_3\text{H}$ groups can also be grafted onto graphene sheets by organic reactions.^[102] Based on the various functionalities of catalytic importance, a pictorial representation of graphitic surface is represented in Fig. 1.3.

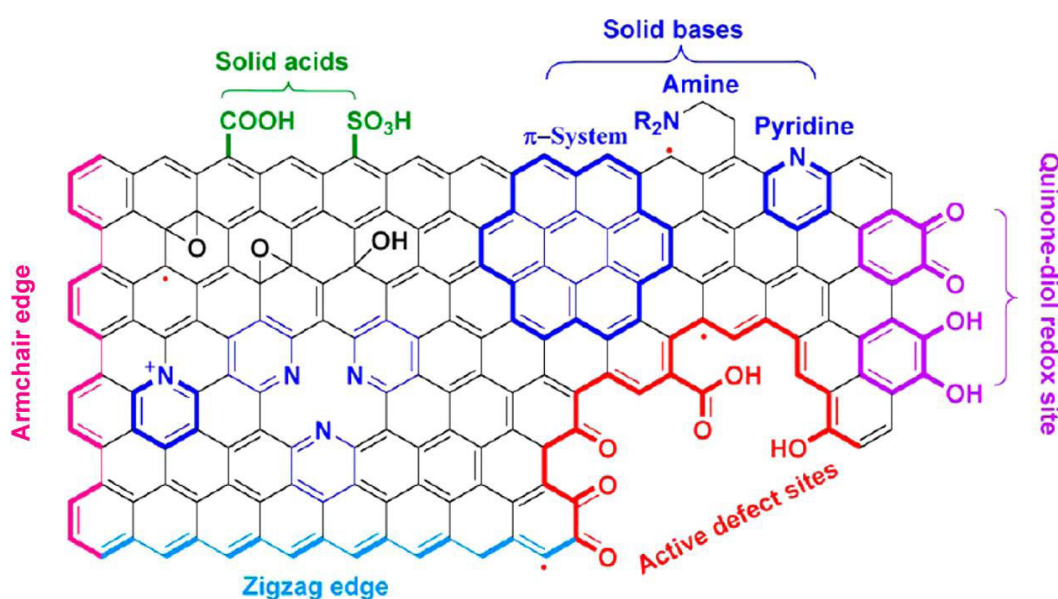


Figure 1.3. Schematic diagram of active sites of graphene-based nanomaterials (Adapted from reference 103)

GO and their chemically converted forms have shown broad spectrum of catalytic activity ranging from oxidation reactions and thermal decomposition reactions. Bielawski *et al.*, first demonstrated catalytic activity of graphene oxide for liquid phase organic transformations.^[98] Since then, a variety of organic transformations have been explored taking advantage of the functional groups present on the graphitic surface. Table 1.2 summarizes a variety of reported reactions catalyzed by GO and chemically converted GO.^[82]

Chapter 1

Table 1.2. Catalytic reactions by GO and chemically converted GO (Adapted from reference 82). Graphene (G), X-doped G (X denotes B, N and Si), (B, N)-doped holy G [(BN)HolG], carbon-nitride (g-C₃N₄), reduced graphene oxide (rGO), N-doped rGO [(N)rGO], triethylamine modified rGO (rGO-NEt₃), rGO/GO functionalized with -SO₃H (rGO-SO₃H/GO-SO₃H), poly(amidoamine)-modified rGO (rGO-PAMAM), amino-functionalized GO with 3-[2-(2-aminoethylamino)ethylamino] propyl-trimethoxysilane(AEPTMS) and aryl -SO₃H groups (GO-AEPTMS/SO₃H)

catalyst	reactions	active sites
	Oxidation reactions (promoted by molecular O₂)	
(N)rGO	Aerobic oxidation of benzylic alcohols	Doped N atoms are active sites
(B,N)G	Aerobic oxidation of benzylic hydrocarbons	Synergism of doped B and N atoms
G/g-C ₃ N ₄	Hydrocarbon oxidation	Synergism between G and C ₃ N ₄
(BN)HolG	Aerobic oxidation of amines	Doped N and B are active sites
GO	Aerobic oxidation of benzylic alcohols	Oxygen functional groups
GO	Dehydrogenation of propane to propene	Epoxy and hydroxyl functional groups
	Oxidation reactions (promoted by other oxidants)	
HG	Fenton-like reactions (H ₂ O ₂)	Reduction site on HG surface
(N)G	Oxidation of benzylic positions (TBHP)	Doped N atoms are active sites
rGO	Oxidation of pollutants (H ₂ O ₂)	Electron rich oxygen groups
GO/rGO	Polymerization of 3-aminophenylboronic acid ((NH ₄) ₂ S ₂ O ₈)	Electronic interaction between rGO and 3-aminophenylboronic acid favors the catalytic activity
	Reduction reactions	
B, N or O doped G ribbon edges	H ₂ dissociative adsorption chemisorption on G ribbon edge	Beneficial B doping
(Si)G	NO _x reduction	Enhanced adsorption /reduction
rGO or (N)rGO	4-nitrophenol reduction (NaBH ₄)	
	Acid reactions	

Chapter 1

rGO	Synthesis of dipyrromethane /calix[4]pyrrole/1-H tetrazoles	Acidic sites are active sites
rGO-SO ₃ H	Dehydration of xylose to furfural	-SO ₃ H are active sites
GO	Hydration of alkynes	
GO	Ring opening of epoxides	-SO ₃ H functional groups
GO	Michael/aza-Michael addition	Oxygen functional groups
GO-SO ₃ H	Glucose/fructose to levulinic acid	
	Base reactions	
rGO-NEt ₃	Hydrolysis of ethyl acetate	Amino groups are active sites
rGO-PAMAM	Knoevenagel condensation	Basic sites of the catalyst
GO-AEPTMS/SO ₃ H	Deacetalization-nitroaldol reaction	Acid/basic groups
	Thermal decomposition reaction	
rGO	Thermal dehydrogenation and rehydrogenation of LiBH ₄	
GO-AB	Dehydrogenation of ammonia borane	

Further, the two-dimensional surface of graphene based materials can be used to anchor other active catalysts as well as biocatalysts. For example, the catalytic activity of several enzymes including cytochromes, peroxidases, myoglobins, and hemoglobins supported on graphene surface enhances several folds compared to the unsupported enzymes towards the oxidation reaction of pyrogallol.^[104] The importance of oxygen functional groups on GO surface has been exploited towards C-H activation reaction in biaryl construction as well as friedel-crafts alkylation reactions.^[105-106] On the other hand graphene surface can also be used as support for immobilization of several metal/metal oxide nanoparticles and used for several electrocatalysis, photocatalysis and organic transformations.^[107-113] For example, Pd nanoparticle immobilized on graphene oxide gave remarkable turnover frequencies (TOF > 39 000h⁻¹) in Suzuki–Miyaura cross-coupling reactions.^[114] Microwave assisted reduction of well-

dispersed GO and palladium salt to form Pd/rGO^[115] demonstrated outstanding catalytic activity for the Suzuki–Miyaura coupling reaction (TOF up to 108 000 h⁻¹) under ligand-free conditions, which was attributed to the high concentration of well dispersed Pd-NPs.

1.2.4 Carbon nanodots

Carbon nanodots (CNDs), a recently discovered fluorescent form of carbon nanomaterials with dimension less than 10 nm have attracted tremendous research activities in recent years. “CNDs” is a comprehensive term for various nanosized fluorescent carbogenic materials with an outer shell composed of oxygen or other heteroatom rich functional groups and an inner core rich in sp² hybridized carbon atoms.^[116] In general, CNDs have a high content of sp² hybridized carbon atoms along with some sp³ carbon atoms and are rich in oxygen (up to 40%) due to presence of carbonyl, carboxyl and epoxy groups at the surface.^[117] Further, the surface functionality of CNDs can be modified, simply by varying precursor molecules for carbonization. For example, carbon dots can be doped with N, S, B, P etc. by varying precursors and controlling the carbonization temperature.^[118-119] The opto-electronic properties of the CNDs largely depend on the surface functionality.

Depending on the method of synthesis, fluorescent carbon nanodots are subdivided into graphene quantum dots (GQDs) and carbon nanodots (CNDs). GQDs are obtained by top-down approach through acid hydrolysis of graphene. They retain the crystallinity of graphene, consist of one or a few layers of graphene and their lateral dimensions are substantially larger than their height. CNDs are quasi-spherical in shape with typical size under 10 nm and are obtained through a bottom up approach through carbonization of carbon-rich small molecules. Depending on the synthetic techniques CNDs can be obtained both in amorphous or crystalline form.^[116]

Carbon materials such as fullerene, carbon black or graphene are water insoluble and exhibit weak fluorescence properties.^[120] On the other hand, due to surface functionality, CNDs are highly water-soluble and show tunable photoluminescence (PL) properties due to which they are often referred to as

Chapter 1

carbon nanolights.^[121] The origin of excitation dependent emission properties of CNDs are mechanistically not clear and both the carbon core and the surface functionality are assumed to contribute towards emissive behavior of these tiny dots. However, their ease of synthesis from inexpensive carbon precursors, easy

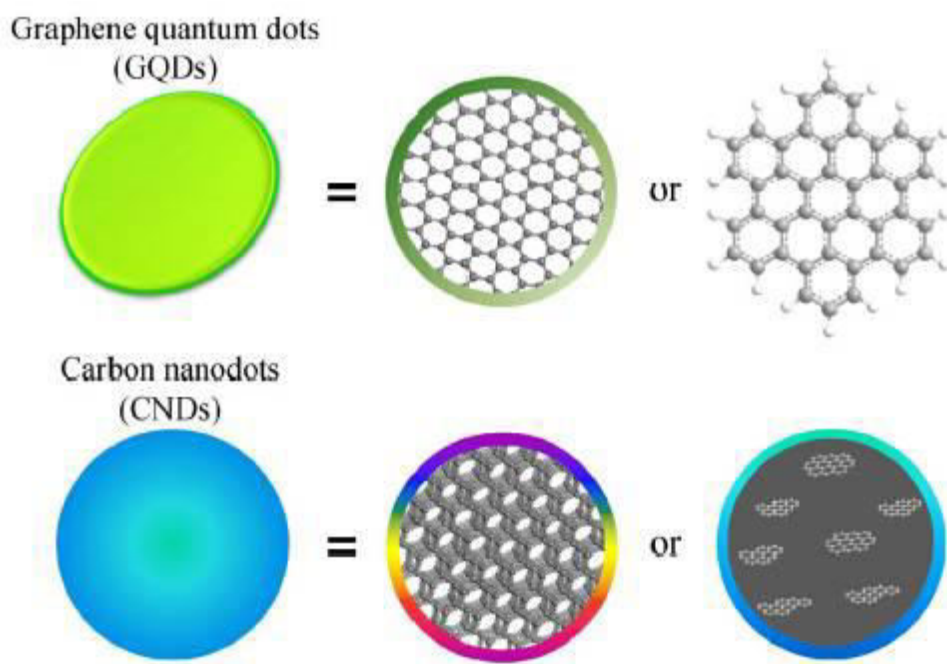


Figure 1.4. Schematic illustration of the two broad categories of C-dots (Adapted from reference 116)

functionalization, resistance to photo bleaching, biocompatibility and lower toxicity have made CNDs an attractive nanomaterial with application potential in diverse areas.^[122] Significant progress in the field of CNDs synthesis, properties and application has been achieved in the past few years.^[120, 122] Many synthetic methods that involve tuning of the optical properties of CNDs by controlling their core size, crystallinity and surface chemistry have been developed.^[123-124] The inherent fluorescence property of CNDs has found wide applications in energy and catalysis.^[125-126] High biocompatibility as well as low toxicity of CNDs compared to other traditional semiconductor quantum dots has generated potential in biosensing and biomedical applications.^[127] The photoluminescence

of CNDs is affected upon interaction with electron donor or acceptor molecules which has formed the basis of development of a huge number of optical sensors for metal ions, biomolecules, drugs, pollutants, etc.^[128] Furthermore, CNDs demonstrate enzyme-mimetic activity, that can be used for several biological applications.

1.2.4.1 Synthesis of Carbon nanodots

The synthetic pathway and precursors of CNDs determine their physicochemical properties such as the size, crystallinity, oxygen/nitrogen content, emission characteristics including quantum yield (QY), colloidal stability and compatibility with a particular solvent.^[129]

Synthesis of CNDs includes “top-down” or bottom-up approaches. A top-down approach is essentially the breaking of larger carbon materials such as graphite, coal, CNTs, etc. to smaller nanoparticles through techniques such as laser ablation, oxidative cutting, plasma treatment, etc.^[130-132] On the other hand, bottom-up method relies on the use of molecular precursors which upon carbonization lead to formation of CNDs.^[133-134] Bottom-up approaches include solvothermal treatment, alkali/acid-assisted ultrasonic treatment, pyrolytic thermal oxidation and nitric acid reflux oxidation.^[135] The resulting CNDs are purified by centrifugation, dialysis, electrophoresis or other separation techniques. These approaches typically yield CNDs with abundant doping states and surface functional groups, and utilize molecular carbon precursors such as glucose, citric acid, and amino acids. Xu et al. (2004) first discovered CNDs during the purification of single-wall carbon nanotubes by gel electrophoresis.^[136]

Top-down approach involves the fragmentation of carbon sources such as graphite, carbon fibres, CNTs or even candle soot. The frequently used method to synthesis luminescent CNDs are oxidizing agents like HNO_3 and H_2SO_4 .^[137] Hens et al. demonstrated that the time of oxidation of various graphite structures in the mixture of H_2SO_4 and HNO_3 (3:1) determines the emission maxima of resultant CNDs.^[138] Wei et al. showed that even the same-size CNDs with different surface charge can exhibit PL from blue to orange.^[139] CNDs have also been obtained by laser irradiation of carbon powders dispersed in various

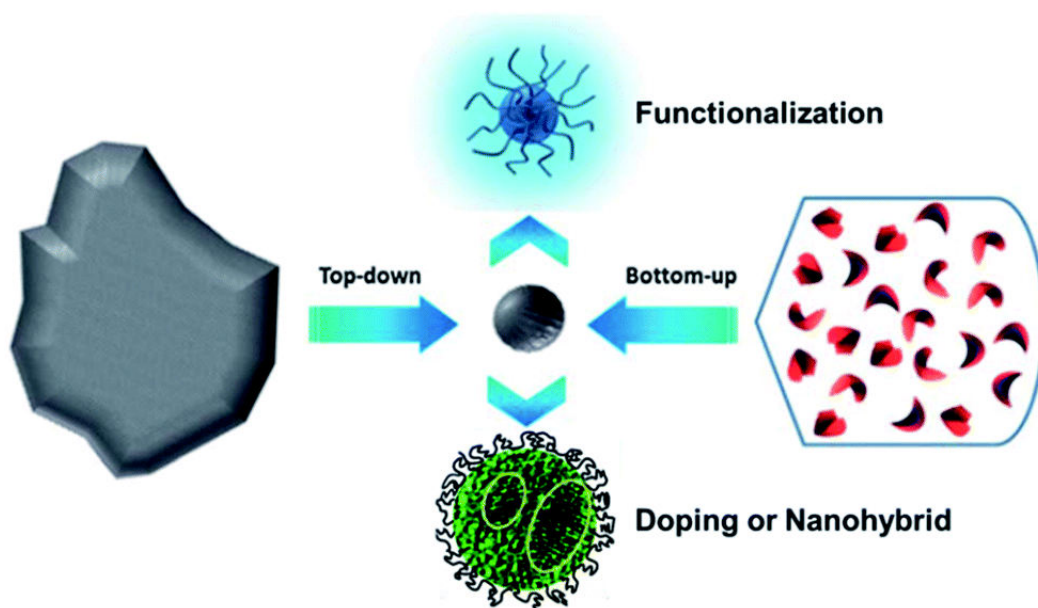


Figure 1.5. Schematic illustration of synthesis of CNDs via top-down and bottom-up approaches and further modification including functionalization, doping and nanohybrid formation (Adapted from reference 120)

solvents which were further oxidized and surface passivated to increase the quantum yield.^[140]

In bottom-up approach, carbonization of organic biomolecules/polymers results in formation of CNDs. High temperature treatment of organic precursors may give rise to CNDs which has been widely reported.^[141-142] CNDs have been found to be present in food caramels and instant coffee where the preparation involves heating of carbohydrates and other carbon rich biomolecules.^[143-144] CNDs are also found to be present in materials available in nature, such as honey and humic acid. Thermal oxidation is the most convenient synthetic route for CNDs which involve oxidation of organic precursors such as amino acids, polyethylene glycol, sugars, citric acid, ethylene diamine, etc.^[145-146] Thermal oxidation can be carried out in presence of air, inert atmosphere, by heating in microwave or autoclaving solutions of the organic precursors. Controlling the carbonization conditions through selection of precursors, properties of resulting CNDs can also be tuned. For example, Wei et al. reported that CNDs resulted from microwave treatment of a solution of glucose and amino acids show varying physicochemical properties with varying side-chain of amino acid.^[147]

1.2.4.2 Applications of Carbon nanodots

CNDs have attracted enormous attention in bio imaging,^[148] drug delivery,^[149] and sensors^[150] due to their unique properties such as intense photoluminescence (PL), excellent photo stability, and high biocompatibility. Increasingly, CNDs are finding application in photo catalytic solar-to-energy conversion due to their ease of synthesis, low cost, excellent performance, and non-toxicity.^[151] The presence of -COOH functionality on the CND surface can also be exploited for the acid catalyzed organic transformations to achieve an efficient and sustainable synthesis of organic feedstock following green protocols.^[152] The photo catalytic activity of CNDs has been explored for H₂ production, environmental remediation, anticancer drug delivery, CO₂ reduction and organic synthesis.^[143, 153-156] CNDs have also been investigated as surface stabilizing agents for nanoparticles for effective catalytic activities.^[157-158]

1.2.5 Magnetic nanoparticles

Homogeneous catalysts are quite efficient in catalyzing organic reactions. However, their recyclability remains an important issue in the sustainable and large-scale production of fine chemicals. The catalyst can be recycled under liquid–liquid interface of two immiscible solvents in a process called phase separation. However, the process is limited to solubility of the reactants in catalyst medium (usually water) and mass transfer through the interface.^[159] Solid–liquid techniques are based on the immobilization of catalytically active metal particles or compounds on solid supports. In the case of solid particles suspended in a liquid, the rate of transfer of reactants within the liquid to the catalyst is inversely proportional to the particle diameter. Thus, the activity (and the selectivity) of the suspended catalyst will benefit from decreasing the particle size.^[160] It is worth mentioning that due to large particle size the dispersion of most conventional heterogeneous catalysts in liquid media is poor and in most cases distinct solid–liquid separation occurs, even after vigorous stirring. One way to overcome this drawback is to keep the size of the particles as small as possible.^[37-42] Nanoparticles have recently emerged as efficient alternatives for the immobilization of homogeneous catalysts and as catalysts themselves.^[10, 36] Unlike conventional micrometer-sized particles, nanoparticles can be easily

Chapter 1

dispersed in a liquid medium to form stable suspensions. However, particles with diameters of less than 100 nm are difficult to separate by filtration techniques. In such cases, expensive ultracentrifugation is often the only way to separate the product and catalyst. This drawback can be overcome by using magnetic nanoparticles (MNPs), which can be easily removed from the reaction mixture by magnetic separation.

Most of the magnetic nanoparticles include colloidal metals (Fe, Co and Ni), alloys (FePt and FePt₃), metal oxides (FeO, Fe₂O₃ and Fe₃O₄) or ferrites (CoFe₂O₄ and MnFe₂O₄). Iron chloride, acetate, sulphate, acetylacetonate and carbonyls are commonly used precursors for the synthesis of iron oxide nanoparticles.^[161] Iron pentacarbonyl ([Fe(CO)₅]) is a widely used precursor for the synthesis of Fe nanoparticles.^[162] The synthesis of pure metal nanoparticles is considered to be a difficult task, since metals such as iron are readily oxidized under ambient conditions. This means that at least the surface of such particles is covered by various native oxides. Among the iron oxides, δ -Fe₂O₃ (maghemite) and Fe₃O₄ (magnetite) have received more attention than FeO since smaller FeO nanoparticles are again quite sensitive towards oxygen.^[163] In maghemite, the iron ions are distributed in the octahedral (Oh) and tetrahedral (Td) sites of the spinel structure, with cationic vacancies within the octahedral sites.^[164]

1.2.5.1 Synthesis of magnetic nanoparticles

Although the synthesis of magnetic nanoparticles include a wide variety of methods such as co-precipitation, thermal decomposition, synthesis in microemulsions or under hydrothermal conditions, and laser pyrolysis techniques,^[43-45] co-precipitation and hydrothermal synthesis are considered to be the most facile way to synthesis iron oxides in water. Co-precipitation synthesis is typically carried out with an aqueous solution containing Fe²⁺/Fe³⁺ salts and added base under inert conditions at ambient temperatures. However, the nanoparticles tend to aggregate when treated without any protection agents, thus nullifying their unique properties derived from their small size.^[165] Organic coatings such as long-chain fatty acids, diols, or alkyl amines are commonly used to prevent aggregation of the particles. The surfactants used as stabilizing agents play a vital role in determining the nucleation, growth, size, shape, magnetic and

other chemical properties of the developing nanoparticles in the solution. Although most studies have focused on the development of polymer or silica protective coatings, carbon-based materials protected magnetic nanoparticles are receiving huge attention, due to much higher chemical and thermal stability as well as biocompatibility of carbon materials over silica or other polymers.^[43]

1.2.5.2 Application of magnetic nanoparticles

A stabilizing agent not only serves to protect the magnetic nanoparticles against degradation, but can also be used for further functionalization with specific components, such as catalytically active species, various drugs, specific binding sites, or other functional groups. Magnetic iron oxide nanoparticles have widely been used in variety of biomedical applications such as early detection of inflammatory cancer and diabetes, magnetic resonance imaging (MRI), hyperthermia, gene therapy etc.^[43, 166] Moreover, the easy separation and controlled placement of these functionalized magnetic nanoparticles by means of an external magnetic field enables their application as catalyst and catalyst supports in several organic reactions such as C-C bond formation,^[167-168] hydrogenation,^[169] hydroformylation,^[170] oxidation and epoxidation,^[171-172] organocatalysis,^[173-174] enantioselective catalysis^[175-176] and acid-base reactions.^[177-178]

1.3 Organization of the Thesis

In this thesis, we explored the intrinsic catalytic activity of two important carbonaceous nanomaterials namely carbon dots and graphene oxide for various important organic transformations. Further their composite with noble-metal nanoparticles and iron oxide nanoparticles have been explored for different oxidation reactions.

Chapter 2 describes carbocatalytic activity of metal-free, inexpensive, heterogeneous graphene oxide towards cross-dehydrogenative C-N coupling of activated aldehydes and amines leading to the formation of α -ketoamides. The oxygenated functionalities on the surface of graphene oxide impart acidic as well as oxidizing properties to the material. Both these properties of graphene oxide were instrumental in the formation of α -ketoamides. Carboxylic acid groups and π - π basal plane were found to be responsible for the catalytic activity evident from different control experiments.

Chapter 3 describes inherent catalytic property of carbon nanodots in organic synthesis. The surface carboxylic group on carbon nanodots surface acted as active catalytic site towards acid catalyzed formation of dihydroquinazolinones and aza-Michael adducts. The mild surface acidity of carbon nanodots was the driving force to synthesize diverse range of quinazolinones/spiroquinazolinone and glycoquinazolinone with structurally perplexing substrates.

Chapter 4 describes the catalytic activity of polydopamine-reduced graphene oxide stabilized Au nanoparticle, a ternary nanocomposite toward selective C-H oxidation in benzylic hydrocarbons in presence of *N*-hydroxyphthalimide and oxygen. Electron transfer from support to nanoparticle surface followed by dioxygen activation was the preliminary steps of the oxidation reaction. A radical mechanism was found to be involved as evidenced by several mechanistic studies.

Chapter 5 describes synthesis of inexpensive, magnetically recoverable carbon dots stabilized iron oxide nanoparticles and its catalytic activity towards oxidative synthesis of quinazolinones from benzyl alcohols and 2-aminobenzamides in presence of *tert*-butylhydroperoxide under aqueous medium.

Chapter 1

Control experiments showed involvement of radical process and formation of bezaldehyde and 2, 3-dihydroquinazolinones as the reaction intermediates.

Chapter 6 discusses the relevance of the works done by us as well as their future scope for future application.

1.4 References

1. Chorkendorff I., Niemantsverdriet J. W., (2007) Concepts of modern catalysis and kinetics, second ed. Wiley-VCH Verlag GmbH & Co. KGaA, Weinheim.
2. Gladysz J. A. (2002), Introduction: Recoverable catalysts and reagents-perspective and prospective, *Chem. Rev.*, 102, 3215-3216 (DOI: 10.1021/cr020068s)
3. Gladysz J. A. (2001), Recoverable catalysts. Ultimate goals, criteria of evaluation, and the green chemistry interface, *Pure Appl. Chem.*, 73, 1319-1324 (DOI: 10.1351/pac200173081319)
4. Grunes J., Zhu J., Somorjai G. A. (2003), Catalysis and nanoscience, *Chem. Commun.*, 2257-2260 (DOI: 10.1039/B305719B)
5. Bell A. T. (2003), The impact of nanoscience on heterogeneous catalysis, *Science*, 299, 1688-1691 (DOI: 10.1126/science.1083671)
6. Schlögl R., Abd Hamid S. B. (2004), Nanocatalysis: Mature science revisited or something really new?, *Angew. Chem. Int. Ed.*, 43, 1628-1637 (DOI: 10.1002/anie.200301684)
7. Jana R., Pathak T. P., Sigman M. S. (2011), Advances in transition metal (Pd, Ni, Fe)-catalyzed cross-coupling reactions using alkyl-organometallics as reaction partners, *Chem. Rev.*, 111, 1417-1492 (DOI: 10.1021/cr100327p)
8. Sherry B. D., Fürstner A. (2008), The promise and challenge of iron-catalyzed cross coupling, *Acc. Chem. Res.*, 2008, 41, 1500-1511 (DOI: 10.1021/ar800039x)
9. Punniyamurthy T., Velusamy S., Iqbal J. (2005), Recent advances in transition metal catalyzed oxidation of organic substrates with molecular oxygen, *Chem. Rev.*, 105, 2329-2364 (DOI: 10.1021/cr050523v)
10. Cole-Hamilton D. J. (2003), Homogeneous catalysis-new approaches to catalyst separation, recovery, and recycling, *Science*, 299, 1702-1706 (DOI: 10.1126/science.1081881)
11. Sheldon R. A., Van Bekkum H., (2001) Fine chemicals through heterogeneous catalysis, Wiley-VCH, Weinheim.

Chapter 1

12. Sheldon R. A. (2008), E factors, green chemistry and catalysis: An odyssey, *Chem. Commun.*, 3352-3365 (DOI: 10.1039/b803584a)
13. Sheldon R. A. (2008), Why green chemistry and sustainability of resources are essential to our future, *J. Environ. Monit.*, 10, 406-407 (DOI: 10.1039/b801651h)
14. Ahmadi T. S., Wang Z. L., Green T. C., Henglein A., El-Sayed M. A. (1996), Shape-controlled synthesis of colloidal platinum nanoparticles, *Science*, 272, 1924-1925 (DOI: 10.1126/science.272.5270.1924)
15. Narayanan R., El-Sayed M. A. (2004), Shape-dependent catalytic activity of platinum nanoparticles in colloidal solution, *Nano Lett.*, 4, 1343-1348 (DOI: 10.1021/nl0495256)
16. Narayanan R., El-Sayed M. A. (2005), Effect of colloidal nanocatalysis on the metallic nanoparticle shape: The Suzuki reaction, *Langmuir*, 21, 2027-2033 (DOI: 10.1021/la047600m)
17. Teranishi T., Miyake M. (1998), Size control of palladium nanoparticles and their crystal structures, *Chem. Mater.*, 10, 594-600 (DOI: 10.1021/cm9705808)
18. Li Y., El-Sayed M. A. (2001), The effect of stabilizers on the catalytic activity and stability of Pd colloidal nanoparticles in the Suzuki reactions in aqueous solution, *J. Phys. Chem. B*, 105, 8938-8943 (DOI: 10.1021/jp010904m)
19. Narayanan R., El-Sayed M. A. (2004), Effect of colloidal catalysis on the nanoparticle size distribution: Dendrimer-Pd vs PVP-Pd nanoparticles catalyzing the Suzuki coupling reaction, *J. Phys. Chem. B*, 108, 8572-8580 (DOI: 10.1021/jp037169u)
20. Sau T. K., Pal A., Pal T. (2001), Size regime dependent catalysis by gold nanoparticles for the reduction of eosin, *J. Phys. Chem. B*, 105, 9266-9272 (DOI: 10.1021/jp011420t)
21. Astruc D., (2008) *Nanoparticles and Catalysis*, Wiley-VCH, Weinheim.
22. Narayanan R., El-Sayed M. A. (2005), Catalysis with transition metal nanoparticles in colloidal solution: Nanoparticle shape dependence and stability, *J. Phys. Chem. B*, 109, 12663-12676 (DOI: 10.1021/jp051066p)

Chapter 1

23. Kim S.-W., Son S. U., Lee S. S., Hyeon T., Chung Y. K. (2001), Colloidal cobalt nanoparticles: a highly active and reusable Pauson–Khand catalyst, *Chem. Commun.*, 2212-2213 (DOI: 10.1039/b107577m)
24. Son S. U., Lee S. I., Chung Y. K., Kim S.-W., Hyeon T. (2002), The first intramolecular Pauson–Khand reaction in water using aqueous colloidal cobalt nanoparticles as catalysts, *Org. Lett.*, 4, 277-279 (DOI: 10.1021/ol017043k)
25. Schmid G. (1992), Large clusters and colloids. Metals in the embryonic state, *Chem. Rev.*, 92, 1709-1727 (DOI: 10.1021/cr00016a002)
26. Lewis L. N. (1993), Chemical catalysis by colloids and clusters, *Chem. Rev.*, 93, 2693-2730 (DOI: 10.1021/cr00024a006)
27. Daniel M. C., Astruc D. (2004), Gold nanoparticles: Assembly, supramolecular chemistry, quantum-size-related properties, and applications toward biology, catalysis, and nanotechnology, *Chem. Rev.*, 104, 293-346 (DOI: 10.1021/cr030698)
28. Astruc D., Lu F., Aranzas J. R. (2005), Nanoparticles as recyclable catalysts: the frontier between homogeneous and heterogeneous catalysis, *Angew. Chem. Int. Ed.*, 44, 7852-7872 (DOI: 10.1002/anie.200500766)
29. Dahl J. A., Maddux B. L. S., Hutchinson J. E. (2007), Toward greener nanosynthesis, *Chem. Rev.*, 107, 2228-2269 (DOI: 10.1021/cr050943k)
30. Roucoux A., Schulz J., Patin H. (2002), Reduced transition metal colloids: A novel family of reusable catalysts?, *Chem. Rev.*, 102, 3757-3778 (DOI: 10.1021/cr010350j)
31. Rao C. N. R., Muller A., Cheetham A. K., (2004) *The chemistry of nanomaterials: Synthesis and applications*, Vol. 1, Wiley-VCH, Weinheim.
32. Anastas P. T., Kirchhoff M. M., (2002) Origins, current status, and future challenges of green chemistry, *Acc. Chem. Res.*, 35, 686-694 (DOI: 10.1021/ar010065m)
33. Schmid G., Maihack V., Lantermann F., Peschel S. (1996), Ligand-stabilized metal clusters and colloids: Properties and applications, *J. Chem. Soc. Dalton Trans.*, 589 – 595 (DOI: 10.1039/dt9960000589)

Chapter 1

34. Yan W., Mahurin S. M., Overbury S. H., Dai S. (2006), Nanoengineering catalyst supports via layer-by-layer surface functionalization, *Top. Catal.*, 39, 199-212 (DOI: 10.1007/s11244-006-0058-x)
35. Rioux R. M., Song H., Hoefelmeyer J. D., Yang P., Somorjai G. A. (2005), High-surface-area catalyst design: Synthesis, characterization, and reaction studies of platinum nanoparticles in mesoporous SBA-15 silica, *J. Phys. Chem. B*, 109, 2192-2202 (DOI: 10.1021/jp048867x)
36. Budroni G., Corma A. (2006), Gold–organic–inorganic high-surface area materials as precursors of highly active catalysts, *Angew. Chem. Int. Ed.*, 45, 3328-3331 (DOI: 10.1002/anie.200600552)
37. Campelo J. M., Luna D., Luque R., Marinas J. M., Romero A. A. (2009), Sustainable preparation of supported metal nanoparticles and their applications in catalysis, *ChemSusChem*, 2, 18 – 45 (DOI: 10.1002/cssc.200800227)
38. Glaspell G., Hassan H. M. A., Elzatahry A., Abdalsayed V., El-Shall M. S. (2008), Nanocatalysis on supported oxides for CO oxidation, *Top. Catal.*, 47, 22-31 (DOI: 10.1007/s11244-007-9036-1)
39. Claus P., Brückner A., Mohr C., Hofmeister H. (2000), Supported gold nanoparticles from quantum dot to mesoscopic size scale: Effect of electronic and structural properties on catalytic hydrogenation of conjugated functional groups, *J. Am. Chem. Soc.*, 122, 11430-11439 (DOI: 10.1021/ja0012974)
40. Martino A., Yamanaka S. A., Kawola J. S., Loy D. A. (1997), Encapsulation of gold nanoclusters in silica materials via an inverse micelle/sol–gel synthesis, *Chem. Mater.*, 9, 423-429 (DOI: 10.1021/cm9604625)
41. Mu X. -D., Evans D. G., Kou Y. (2004), A general method for preparation of PVP-stabilized noble metal nanoparticles in room temperature ionic liquids, *Catal. Lett.*, 97, 151-154 (DOI: 10.1023/B:CATL.0000038577.18441.bf)
42. Hwang C. -B., Fu Y. -S., Lu Y. -L., Jang S. -W., Chou P. -T., Wang C. -R., Yu S. -J. (2000), Synthesis, characterization and highly efficient catalytic

Chapter 1

- reactivity of suspended palladium nanoparticles, *J. Catal.*, 195, 336-341 (DOI: 10.1006/jcat.2000.2992).
43. Lu A. -H., Salabas E. L., Schüth F. (2007), Magnetic nanoparticles: Synthesis, protection, functionalization, and application, *Angew. Chem. Int. Ed.*, 46, 1222-1244 (DOI: 10.1002/anie.200602866)
44. Jeong U., Teng X., Wang Y., Yang H., Xia Y. (2007), Superparamagnetic colloids: Controlled synthesis and niche applications, *Adv. Mater.*, 19, 33-60 (DOI: 10.1002/adma.200600674)
45. Jun Y. -W., Seo J. -W., Cheon J. (2008), Nanoscaling laws of magnetic nanoparticles and their applicabilities in biomedical sciences, *Acc. Chem. Res.*, 41, 179-189 (DOI: 10.1021/ar700121f)
46. Borodko Y., Habas S. E., Koebel M., Yang P., Frei H., Somorjai G. A. (2006), Probing the interaction of poly(vinylpyrrolidone) with platinum nanocrystals by UV-Raman and FTIR, *J. Phys. Chem. B*, 110, 23052-23059 (DOI: 10.1021/jp063338)
47. Washio I., Xiong Y., Yin Y., Xia Y. (2006), Reduction by the end groups of poly(vinyl pyrrolidone): A new and versatile route to the kinetically controlled synthesis of Ag triangular nanoplates, *Adv. Mater.*, 18, 1745-1749 (DOI: 10.1002/adma.200600675)
48. Narayanan R., El-Sayed M. A. (2003), Effect of catalysis on the stability of metallic nanoparticles: Suzuki reaction catalyzed by PVP-palladium nanoparticles, *J. Am. Chem. Soc.*, 125, 8340-8347 (DOI: 10.1021/ja035044x)
49. Chauhan B. P. S., Rathore J. S., Bando T. (2004), Polysiloxane-Pd⁰ nanocomposites as recyclable chemoselective hydrogenation catalysts, *J. Am. Chem. Soc.*, 126, 8493-8500 (DOI: 10.1021/ja049604j)
50. Gröschel L., Haidar R., Beyer A., Reichert K.-H., Schomäcker R. (2004), Characterization of palladium nanoparticles adsorpt on polyacrylic acid particles as hydrogenation catalyst, *Catal. Lett.*, 95, 67-75 (DOI: 10.1023/B:CATL.0000023724.17132.16)
51. Schulz J., Roucoux A., Patin H. (2000), Stabilized rhodium(0) nanoparticles: A reusable hydrogenation catalyst for arene derivatives in a biphasic water-liquid system, *Chem. Eur. J.*, 6, 618-624 (DOI:

Chapter 1

- 10.1002/(SICI)1521-3765(20000218)6:4<618::AID-CHEM618>3.0.CO;2-A)
52. Mévellec V., Roucoux A., Ramirez E., Philippot K., Chaudret B. (2004) Surfactant-stabilized aqueous iridium(0) colloidal suspension: An efficient reusable catalyst for hydrogenation of arenes in biphasic media, *Adv. Synth. Catal.*, 346, 72-76 (DOI: 10.1002/adsc.200303157)
53. Yang C. -C., Wan C. -C., Wang Y. -Y. (2004), Synthesis of Ag/Pd nanoparticles via reactive micelles as templates and its application to electroless copper deposition, *J. Colloid Interface Sci.*, 279, 433-439 (DOI: 10.1016/j.jcis.2004.06.098)
54. Zhao M., Sun L., Crooks R. M. (1998), Preparation of Cu nanoclusters within dendrimer templates, *J. Am. Chem. Soc.*, 120, 4877-4878 (DOI: 10.1021/ja980438n)
55. Crooks R. M., Zhao M., Sun L., Chechik V., Yeung L. K. (2001), Dendrimer-encapsulated metal nanoparticles: Synthesis, characterization, and applications to catalysis, *Acc. Chem. Res.*, 34, 181-190 (DOI: 10.1021/ar000110a)
56. Zhao M., Crooks R. M. (1999), Homogeneous hydrogenation catalysis with monodisperse, dendrimer-encapsulated Pd and Pt nanoparticles, *Angew. Chem. Int. Ed.*, 38, 364-366 (DOI: 10.1002/(SICI)1521-3773(19990201)38:3<364::AID-ANIE364>3.0.CO;2-L)
57. Balogh L., Tomalia D. A. (1998), Poly(Amidoamine) dendrimer-templated nanocomposites. 1. Synthesis of zerovalent copper nanoclusters, *J. Am. Chem. Soc.*, 120, 7355-7356 (DOI: 10.1021/ja980861w)
58. Esumi K., Suzuki A., Aihara N., Usui K., Torigoe K. (1998), Preparation of gold colloids with UV irradiation using dendrimers as stabilizer, *Langmuir*, 14, 3157-3159 (DOI: 10.1021/la980162x)
59. Esumi K., Isono R., Yoshimura T. (2004), Preparation of PAMAM-and PPI-metal (silver, platinum, and palladium) nanocomposites and their catalytic activities for reduction of 4-Nitrophenol, *Langmuir*, 20, 237-243 (DOI: 10.1021/la035440t)

Chapter 1

60. Wu L., Li B.-L., Huang Y.-Y., Zhou H. -F., He Y.-M., Fan Q. -H. (2006), Phosphine dendrimer-stabilized palladium nanoparticles, a highly active and recyclable catalyst for the Suzuki–Miyaura reaction and hydrogenation, *Org. Lett.*, 8, 3605-3608 (DOI: 10.1021/ol0614424)
61. Caló V., Nacci A., Monopoli A., Laera S., Cioffi N. (2003), Pd nanoparticles catalyzed stereospecific synthesis of β -aryl cinnamic esters in ionic liquids, *J. Org. Chem.*, 68, 2929-2933 (DOI: 10.1021/jo026877t)
62. Deshmukh R. R., Rajagopal R., Srinivasan K. V. (2001), Ultrasound promoted C–C bond formation: Heck reaction at ambient conditions in room temperature ionic liquids, *Chem. Commun.*, 1544-1545 (DOI: 10.1039/b104532f)
63. Somorjai G. A., Park J. Y. (2008), Molecular factors of catalytic selectivity, *Angew. Chem. Int. Ed.*, 47, 9212-9228 (DOI: 10.1002/anie.200803181)
64. Park J., Kang E., Son S. U., Park H. M., Lee M. K., Kim J., Kim K. W., Noh H. -J., Park J. -H., Bae C. J., Park J. -G., Hyeon T. (2005), Monodisperse nanoparticles of Ni and NiO: Synthesis, characterization, self-assembled superlattices, and catalytic applications in the Suzuki coupling reaction, *Adv. Mater.*, 17, 429-434 (DOI: 10.1002/adma.200400611)
65. Rampino L. D., Nord F. F. (1941), Preparation of palladium and platinum synthetic high polymer catalysts and the relationship between particle size and rate of hydrogenation, *J. Am. Chem. Soc.*, 63, 2745-2749 (DOI: 10.1021/ja01855a070)
66. Hutchings G. J. (2009), Heterogeneous catalysts-discovery and design, *J. Mater. Chem.*, 19, 1222-1235 (DOI: 10.1039/b812300b)
67. Reetz M. T., Westermann E. (2000), Phosphane-free palladium-catalyzed coupling reactions: The decisive role of Pd nanoparticles, *Angew. Chem. Int. Ed.*, 39, 165-168 (DOI: 10.1002/(SICI)1521-3773(2000103)39:1<165::AID-ANIE165>3.0.CO;2-B)
68. Reetz M. T., de Vries J. G. (2004), Ligand-free Heck reactions using low Pd-loading, *Chem. Commun.*, 1559-1563 (DOI: 10.1039/B406719N)

Chapter 1

69. Lewis L. N., Lewis N. (1986), Platinum-catalyzed hydrosilylation-colloid formation as the essential step, *J. Am. Chem. Soc.*, 108, 7228-7231 (DOI: 10.1021/ja00283a016)
70. Mirkin C. A. (2005), The beginning of a small revolution, *Small*, 1, 14-16 (DOI: 10.1002/smll.200400092)
71. Wang Y. -J., Wilkinson D. P., Zhang J.(2011), Noncarbon support materials for polymer electrolyte membrane fuel cell electrocatalysts, *Chem. Rev.*, 111, 7625–7651 (DOI: 10.1021/cr100060r)
72. Vernoux P., Lizarraga L., Tsampas M. N. *et al.* (2013), Ionically conducting ceramics as active catalyst supports, *Chem. Rev.*, 113, 8192–8260 (DOI: 10.1021/cr4000336)
73. Wang Y. -G., Yoon Y., Glezakou V. -A., Li J., Rousseau R. (2013), The role of reducible oxide-metal cluster charge transfer in catalytic processes: New insights on the catalytic mechanism of CO oxidation on Au/TiO₂ from ab Initio molecular dynamics, *J. Am. Chem. Soc.*, 135, 10673–10683 (DOI: 10.1021/ja402063v)
74. Kamat P. V. (2011), Graphene-based nanoassemblies for energy conversion, *J. Phys. Chem. Lett.*, 2, 242–251 (DOI: 10.1021/jz101639v)
75. Wang J., Trindade F. J., de Aquino C. B., Pieretti J. C., Domingues S. H., Ando R. A., Camargo P. H. C. (2015), Probing the catalytic activity of reduced graphene oxide decorated with Au nanoparticles triggered by visible light, *Chem. Eur. J.*, 21, 9889–9894 (DOI: 10.1002/chem.201500677)
76. Rodríguez-Reinoso F. (1998), The role of carbon materials in heterogeneous catalysis, *Carbon*, 36, 159-175 (DOI: 10.1016/S0008-6223(97)00173-5)
77. Rideal E. K., Wright W. M. (1925), CLXXXIV-Low temperature oxidation at charcoal surfaces. Part I. The behavior of charcoal in the absence of promoters, *J. Chem. Soc., Trans.*, 127, 1347-1357 (DOI: 10.1039/CT9252701347)
78. Serp P., Machado B., (2015) Carbon (Nano)materials for catalysis, *RSC catalysis series*, 23.

Chapter 1

79. Li B.; Xu Z. (2009), A non-metal catalyst for molecular hydrogen activation with comparable catalytic hydrogenation capability to noble metal catalyst, *J. Am. Chem. Soc.* 2009, 131, 16380-16382 (DOI: 10.1021/ja9061097)
80. Braun T., Wohlers M., Belz T., Nowitzke T., Wortmann G., Ushida Y., Pfander N., Schlögl R. (1997), Fullerene-based ruthenium catalysts: A novel approach for anchoring metal to carbonaceous supports. II. Hydrogenation activity, *Catal. Lett.*, 43, 167-173 (DOI: 10.1023/A:1018950925046)
81. Nagashima H., Kato Y., Yamagushi H., Kimura E., Kawanishi T., Kato M., Saito Y., Haga M., Itoh K. (1994), Synthesis and reactions of organoplatinum compounds of C₆₀, C₆₀Pt_n, *Chem. Lett.*, 23, 1207-1210 (DOI: 10.1246/cl.1994.1207)
82. Nagashima H., Nakaoka A., Saito Y., Kato M., Kawanishi T., Itoh K. (1992), C₆₀Pd_n: The first organometallic polymer of buckminsterfullerene, *J. Chem. Soc., Chem. Comm.*, 377-379 (DOI: 10.1039/C39920000377)
83. Mestl G., Maksimova N. I., Keller N., Roddatis V. V., Schlögl R. (2001), Carbon nanofilaments in heterogeneous catalysis: An industrial application for new carbon materials?, *Angew. Chem. Int. Ed.*, 40, 2066–2068 (DOI: 10.1002/1521-3773(20010601)40:11<2066::AID-ANIE2066>3.0.CO;2-I)
84. Zhang J., Liu X., Blume R., Zhang A., Schlögl R., Su D. S. (2008), Surface-modified carbon nanotubes catalyze oxidative dehydrogenation of n butane, *Science*, 322, 73-77 (DOI: 10.1126/science.1161916)
85. Basu P., Prakash P., Gravel E., Shah N., Bera K., Doris E., & Namboothiri I. N. N. (2016), Carbon nanotube–ruthenium hybrids for the partial reduction of 2-nitrochalcones: Easy access to quinoline N-oxides, *ChemCatChem*, 8, 1298-1302 (DOI: 10.1002/cctc.201600042)
86. Shah N., Gravel E., Jawale D. V., Doris E., Namboothiri I. N. N. (2015), Synthesis of quinoxalines by a carbon nanotube–gold nanohybrid-catalyzed cascade reaction of vicinal diols and keto alcohols with diamines, *ChemCatChem*, 7, 57-61 (DOI: 10.1002/cctc.201402782)

Chapter 1

87. Shah N., Gravel E., Jawale D. V., Doris E., Namboothiri I. N. N. (2014), Carbon nanotube–gold nanohybrid catalyzed N-formylation of amines by using aqueous formaldehyde, *ChemCatChem*, 6, 2201-2205 (DOI: 10.1002/cctc.201402225)
88. Pyun J. (2011), Graphene oxide as catalyst: Application of carbon materials beyond nanotechnology, *Angew. Chem., Int. Ed.*, 50, 46-48 (DOI: 10.1002/anie.201003897)
89. Mermin N. D. (1968), Crystalline order in two dimensions, *Phys. Rev.*, 176, 250 (DOI: 10.1103/PhysRev.176.250)
90. Zacharia R., Ulbricht H., Hertel T. (2004), Interlayer cohesive energy of graphite from thermal desorption of polyaromatic hydrocarbons, *Phys. Rev. B: Condens. Matter Mater. Phys.*, 69, 155406 (DOI: 10.1103/PhysRevB.69.155406)
91. Chen D., Tang L., Li J. (2010), Graphene-based materials in electrochemistry, *Chem. Soc. Rev.*, 39, 3157-3180 (DOI: 10.1039/B923596E)
92. Berger C., Song Z. M., Li X. B., Wu X. S., Brown N., Naud C., Mayou D., Li T. B., Hass J., Marchenkov A. N., Conrad E. H., First P. N., de Heer W. A. (2006), Electronic confinement and coherence in patterned epitaxial graphene, *Science*, 312, 1191-1196 (DOI: 10.1126/science.1125925)
93. Sutter P. W., Flege J. I., Sutter E. A. (2008), Epitaxial graphene on ruthenium, *Nat. Mater.*, 7, 406-411 (DOI: 10.1038/nmat2166)
94. Park S., Ruoff R. S. (2009), Chemical methods for the production of graphenes, *Nat. Nanotechnol.*, 4, 217-224 (DOI: 10.1038/nnano.2009.58)
95. Navalon S., Dhakshinamoorthy A., Alvaro M., Garcia H. (2014), Carbocatalysis by graphene-based materials, *Chem. Rev.*, 114, 6179-6212 (DOI: 10.1021/cr4007347)
96. Yang J. H., Sun G., Gao Y., Zhao H., Tang P., Tan J., Ma, D. (2013), Direct catalytic oxidation of benzene to phenol over metal-free graphene-based catalyst, *Energy Environ. Sci.*, 6, 793-798 (DOI: 10.1039/c3ee23623d)

Chapter 1

97. Dreyer D. R., Bielawski C. W. (2012), Graphite oxide as an olefin polymerization carbocatalyst: Applications in electrochemical double layer capacitors, *Adv. Funct. Mater.*, 22, 3247-3253 (DOI: 10.1002/adfm.201103152)
98. Dreyer D. R., Jia H. P., Bielawski C. W. (2010), Graphene oxide: A convenient carbocatalyst for facilitating oxidation and hydration reactions, *Angew. Chem. Int. Ed.*, 49, 6813 – 6816 (DOI: 10.1002/anie.201002160)
99. Song S., Yang H., Rao R., Liu H., Zhang A. (2010), Defects of multi-walled carbon nanotubes as active sites for benzene hydroxylation to phenol in the presence of H₂O₂, *Catal. Commun.*, 11, 783–787 (DOI: 10.1016/j.catcom.2010.02.015)
100. Albero J., Garcia H. (2015), Doped graphenes in catalysis, *J. Mol. Catal. A: Chem.*, 408, 296-309 (DOI: 10.1016/j.molcata.2015.06.011)
101. Cheng Y., Fan Y., Pei Y., Qiao M. (2015), Graphene-supported metal/metal oxide nanohybrids: Synthesis and applications in heterogeneous catalysis, *Catal. Sci. Technol.*, 5, 3903-3916 (DOI: 10.1039/C5CY00630A)
102. Ji J., Zhang G., Chen H., Wang S., Zhang G., Zhang F., Fan X. (2011), Sulfonated graphene as water-tolerant solid acid catalyst, *Chem. Sci.*, 2, 484-487 (DOI: 10.1039/C0SC00484G)
103. Tang P., Hu G., Li M., Ma D. (2016), Graphene-based metal-free catalysts for catalytic reactions in the liquid phase, *ACS Catal.*, 6, 6948-6958 (DOI: 10.1021/acscatal.6b01668)
104. Xue T., Jiang S., Qu Y., Su Q., Cheng R., Dubin S., Duan X. (2012), Graphene-supported hemin as a highly active biomimetic oxidation catalyst, *Angew. Chem. Int. Ed.*, 51, 3822-3825 (DOI: 10.1002/anie.201108400)
105. Gao Y., Tang P., Zhou H., Zhang W., Yang H., Yan N., Ma D. (2016), Graphene oxide catalyzed C–H bond activation: The importance of oxygen functional groups for biaryl construction, *Angew. Chem. Int. Ed.*, 55, 3124-3128 (DOI: 10.1002/anie.201510081)

Chapter 1

106. Hu F., Patel M., Luo F., Flach C., Mendelsohn R., Garfunkel E., Szostak M. (2015), Graphene-catalyzed direct Friedel–Crafts alkylation reactions: Mechanism, selectivity, and synthetic utility, *J. Am. Chem. Soc.*, 137, 14473–14480 (DOI: 10.1021/jacs.5b09636)
107. Devadoss A., Sudhagar P., Das S., Lee S. Y., Terashima C., Nakata K., Paik U. (2014), Synergistic metal–metal oxide nanoparticles supported electrocatalytic graphene for improved photo electrochemical glucose oxidation, *ACS Appl. Mater. Interfaces*, 6, 4864–4871 (DOI: 10.1021/am4058925)
108. Kou R., Shao Y., Mei D., Nie Z., Wang D., Wang C., Wang Y. (2011), Stabilization of electrocatalytic metal nanoparticles at metal-metal oxide-graphene triple junction points, *J. Am. Chem. Soc.*, 133, 8, 2541–2547 (DOI: 10.1021/ja107719u)
109. Kim H. K., Park S. H., Yoon S. B., Lee C. W., Jeong J. H., Roh K. C., Kim K. B. (2014), In situ synthesis of three-dimensional self-assembled metal oxide–reduced graphene oxide architecture, *Chem. Mater.*, 26, 4838–4843 (DOI: 10.1021/cm5020898)
110. Guo X. N., Jiao Z. F., Jin G. Q., Guo X. Y. (2015), Photocatalytic Fischer–Tropsch synthesis on graphene-supported worm-like ruthenium nanostructures, *ACS Catal.*, 5, 3836–3840 (DOI: 10.1021/acscatal.5b00697)
111. Singh G. P., Shrestha K. M., Nepal A., Klabunde K. J., Sorensen C. M. (2014), Graphene supported plasmonic photocatalyst for hydrogen evolution in photocatalytic water splitting, *Nanotechnology*, 25, 265701 (DOI: 10.1088/0957-4484/25/26/265701)
112. Song F. Z., Zhu Q. L., Tsumori N., Xu Q. (2015), Diamine-alkalized reduced graphene oxide: Immobilization of sub-2 nm palladium nanoparticles and optimization of catalytic activity for dehydrogenation of formic acid, *ACS Catal.*, 5, 5141–5144 (DOI: 10.1021/acscatal.5b01411)
113. Wang J., Kondrat S. A., Wang Y., Brett G. L., Giles C., Bartley J. K., Hutchings G. J. (2015), Au–Pd nanoparticles dispersed on composite titania/graphene oxide-supports as a highly active oxidation catalyst, *ACS Catal.*, 5, 3575–3587 (DOI: 10.1021/acscatal.5b00480)

Chapter 1

114. Scheuermann G. M., Rumi L., Steurer P., Bannwarth W., Mülhaupt R. (2009), Palladium nanoparticles on graphite oxide and its functionalized graphene derivatives as highly active catalysts for the Suzuki– Miyaura coupling reaction, *J. Am. Chem. Soc.*, 131, 8262-8270 (DOI: 10.1021/ja901105a)
115. Moussa S., Siamaki A. R., Gupton B. F., El-Shall M. S. (2012), Pd-partially reduced graphene oxide catalysts (Pd/PRGO): Laser synthesis of Pd nanoparticles supported on PRGO nanosheets for carbon–carbon cross coupling reactions, *ACS Catal.*, 2, 145-154 (DOI: 10.1021/cs200497e)
116. Zhu S., Song Y., Zhao X., Shao J., Zhang J., Yang B. (2015), The photoluminescence mechanism in carbon dots (graphene quantum dots, carbon nanodots, and polymer dots): Current state and future perspective, *Nano Res.*, 8, 355-381 (DOI: 10.1007/s12274-014-0644-3)
117. Hola K., Zhang Y., Wang Y., Giannelis E. P., Zboril R., Rogach A. L. (2014), Carbon dots-Emerging light emitters for bioimaging, cancer therapy and optoelectronics, *Nano Today*, 9, 590-603 (DOI: 10.1016/j.nantod.2014.09.004)
118. Qu S., Wang X., Lu Q., Liu X., Wang L. (2012), A biocompatible fluorescent ink based on water-soluble luminescent carbon nanodots, *Angew. Chem.*, 124, 12381–12384 (DOI: 10.1002/ange.201206791)
119. Baruah U., Konwar A., Chowdhury D. (2016), A sulphonated carbon dot–chitosan hybrid hydrogel nanocomposite as an efficient ion-exchange film for Ca^{2+} and Mg^{2+} removal, *Nanoscale*, 8, 8542-8546 (DOI: 10.1039/C6NR01129B)
120. Wang Y., Hu A. (2014), Carbon quantum dots: Synthesis, properties and applications, *J. Mater. Chem. C*, 2, 6921-6939 (DOI: 10.1039/C4TC00988F)
121. Das B., Dadhich P., Pal P., Srivas P. K., Bankoti K., Dhara S. (2014), Carbon nanodots from date molasses: New nanolights for the in vitro scavenging of reactive oxygen species, *J. Mater. Chem. B*, 2, 6839-6847 (DOI:10.1039/C4TB01020E)

Chapter 1

122. Lim S. Y., Shen W., Gao Z. (2015), Carbon quantum dots and their applications, *Chem. Soc. Rev.*, 44, 362-381 (DOI:10.1039/C4CS00269E)
123. Bhunia S. K., Saha A., Maity A. R., Ray S. C., Jana N.R. (2013), Carbon Nanoparticle-based Fluorescent Bio imaging Probes, *Sci. Rep.*, 3, 1473 (DOI:10.1038/srep01473)
124. Wang S., Chen Z.-G., Cole I., Li Q. (2015), Structural Evolution of Graphene Quantum Dots during Thermal Decomposition of Citric Acid and the Corresponding Photoluminescence, *Carbon*, 82, 304-313 (DOI:10.1016/j.carbon.2014.10.075)
125. Yang Y., Ji X., Jing M., Hou H., Zhu Y., Fang L., Banks C. E. (2015), Carbon dots supported upon N-doped TiO₂ nanorods applied into sodium and lithium ion batteries, *J. Mater. Chem. A*, 3, 5648-5655 (DOI:10.1039/c4ta05611f)
126. Hutton G. A., Reuillard B., Martindale B. C., Caputo C. A., Lockwood C. W., Butt J. N., Reisner E. (2016), Carbon dots as versatile photo sensitizers for solar-driven catalysis with redox enzymes, *J. Am. Chem. Soc.*, 138, 16722–16730 (DOI: 10.1021/jacs.6b10146)
127. Zheng X. T., Ananthanarayanan A., Luo K. Q., Chen P. (2015), Glowing graphene quantum dots and carbon dots: Properties, syntheses, and biological applications, *Small*, 11, 1620-1636 (DOI: 10.1002/smll.201402648)
128. Baptista F. R., Belhout S. A., Giordani S., Quinn S. J. (2015), Recent developments in carbon nanomaterial sensors, *Chem. Soc. Rev.*, 44, 4433-4453 (DOI:10.1039/C4CS00379A)
129. Zhang J., Yu S. H. (2016), Carbon dots: Large-scale synthesis, sensing and bioimaging, *Mater. Today*, 19, 382-393 (DOI:10.1016/j.mattod.2015.11.008)
130. Bourlinos A. B., Stassinopoulos A., Anglos D., Zboril R., Karakassides M., Giannelis E. P. (2008), Surface functionalized carbogenic quantum dots, *Small*, 4, 455-458 (DOI: 10.1002/smll.200700578)
131. Ye R., Xiang C., Lin J., Peng Z., Huang K., Yan Z., Ceriotti G. (2013), Coal as an abundant source of graphene quantum dots, *Nat. Commun.*, 4, 2943 (DOI:10.1038/ncomms3943)

Chapter 1

132. Wang J., Wang C. F., Chen S. (2012), Amphiphilic Egg - Derived Carbon Dots: Rapid Plasma Fabrication, Pyrolysis Process, and Multicolor Printing Patterns, *Angew. Chem. Int. Ed.*, 51, 9297-9301(DOI: 10.1002/anie.201204381)
133. Jiang J., He Y., Li S., Cui H. (2012), Amino acids as the source for producing carbon nanodots: Microwave assisted one-step synthesis, intrinsic photoluminescence property and intense chemiluminescence enhancement, *Chem. Commun.*, 48, 9634-9636 (DOI:10.1039/C2CC34612E)
134. Zhu S., Meng Q., Wang L., Zhang J., Song Y., Jin H., Yang B. *et al.* (2013), Highly photoluminescent carbon dots for multicolor patterning, sensors, and bio imaging, *Angew. Chem. Int. Ed.*, 52, 3953-3957 (DOI: 10.1002/anie.201300519)
135. Chai N. N., Wang H. X., Hu C. X., Wang Q., Zhang H. L. (2015), Well-controlled layer-by-layer assembly of carbon dot/CdS heterojunctions for efficient visible-light-driven photocatalysis, *J. Mater. Chem. A*, 3, 16613-16620 (DOI: 10.1039/C5TA03649F)
136. Xu X., Ray R., Gu Y., Ploehn H. J., Gearheart L., Raker K., Scrivens W. A. (2004), Electrophoretic analysis and purification of fluorescent single-walled carbon nanotube fragments, *J. Am. Chem. Soc.*, 126, 12736-12737 (DOI: 10.1021/ja040082h)
137. Liu H., Ye T., Mao C. (2007), Fluorescent carbon nanoparticles derived from candle soot, *Angew. Chem. Int. Ed.*, 46, 6473-6475 (DOI: 10.1002/anie.200701271)
138. Hens S. C., Lawrence W. G., Kumbhar A. S., Shenderova O. (2012), Photoluminescent Nanostructures from Graphite Oxidation, *J. Phys. Chem. C*, 116, 20015-20022 (DOI: 10.1021/jp303061e)
139. Wei J., Qiu J. (2014), Unveil the Fluorescence of Carbon Quantum Dots, *Adv. Eng. Mater.*, 17, 138-142 (DOI:10.1002/adem.201400146)
140. Hu S. L., Niu K. Y., Sun J., Yang J., Zhao N. Q., Du X.W. (2009), One step synthesis of fluorescent carbon nanoparticles by laser irradiation, *J. Mater. Chem.*, 19, 484-488 (DOI:10.1039/B812943F)

Chapter 1

141. Sahu S., Behera B., Maiti T. K., Mohapatra S. (2012), Simple one-step synthesis of highly luminescent carbon dots from orange juice: Application as excellent bio-imaging agents, *Chem. Commun.*, 48, 8835-8837 (DOI:10.1039/C2CC33796G)
142. Liang Q., Ma W., Shi Y., Li Z., Yang, X. (2013), Easy synthesis of highly fluorescent carbon quantum dots from gelatin and their luminescent properties and applications, *Carbon*, 60, 421-428 (DOI:10.1016/j.carbon.2013.04.055)
143. Sk M. P., Jaiswal A., Paul A., Ghosh S. S., Chattopadhyay A. (2012), Presence of amorphous carbon nanoparticles in food caramels, *Sci. Rep.*, 2, 383 (DOI:10.1038/srep0038)
144. Jiang C., Wu H., Song X., Ma X., Wang J., Tan M. (2014), Presence of photoluminescent carbon dots in Nescafe® original instant coffee: Applications to bio imaging, *Talanta*, 127, 68-74 (DOI:10.1016/j.talanta.2014.01.046)
145. Jaiswal A., Ghosh S. S., Chattopadhyay A. (2012), One step synthesis of C-dots by microwave mediated caramelization of poly (ethyleneglycol), *Chem. Commun.*, 48, 407-409 (DOI:10.1039/C1CC15988G)
146. Liu Y., Xiao N., Gong N., Wang H., Shi X., Gu W., Ye L. (2014), One step microwave-assisted polyol synthesis of green luminescent carbon dots as optical nanoprobe, *Carbon*, 68, 258-264 (DOI:10.1016/j.carbon.2013.10.086)
147. Wei W., Xu C., Wu L., Wang J., Ren J., Qu X. (2014), Non-enzymatic browning-reaction: A versatile route for production of nitrogen-doped carbon dots with tunable multicolor luminescent display, *Sci. Rep.*, 4, 3564 (DOI:10.1038/srep03564)
148. Luo P. G., Sahu S., Yang S. T., Sonkar S. K., Wang J., Wang H., Sun Y. P. (2013), Carbon “quantum” dots for optical bio imaging, *J. Mater. Chem. B*, 1, 2116-2127 (DOI: 10.1039/C3TB00018D)
149. Zheng M., Liu S., Li J., Qu D., Zhao H., Guan X., Sun Z. (2014), Integrating oxaliplatin with highly luminescent carbon dots: An unprecedented theranostic agent for personalized medicine, *Adv. Mater.*, 26, 3554-3560 (DOI: 10.1002/adma.201306192)

Chapter 1

150. Ding C., Zhu A., Tian Y. (2014), Functional surface engineering of C-dots for fluorescent biosensing and in vivo bio imaging, *Acc. Chem. Res.*, 47, 20-30 (DOI: 10.1021/ar400023s)
151. Linic S., Aslam U., Boerigter C., Morabito M. (2015), Photochemical transformations on plasmonic metal nanoparticles, *Nat. Mater.*, 14, 567-576 (DOI: 10.1038/nmat4281)
152. Han Y., Huang H., Zhang H., Liu Y., Han X., Liu R., Li H., Kang Z. (2014), Carbon quantum dots with photo enhanced hydrogen-bond catalytic activity in aldol condensations, *ACS Catal.*, 4, 781-787 (DOI: 10.1021/cs401118x)
153. Yang K. D., Ha Y., Sim U., An J., Lee C. W., Jin K., Kim Y., Park J., Hong J. S., Lee J. H., Lee H. -E., Jeong H. -Y., Kim H., Nam K. T.(2016), Graphene quantum sheet catalyzed silicon photocathode for selective CO₂ conversion to CO, *Adv. Funct. Mater.*, 26, 233-242 (DOI: 10.1002/adfm.201502751)
154. Baker S. N., Baker G. A. (2010), Luminescent carbon nanodots: Emergent nanolights, *Angew. Chem. Int. Ed.*, 49, 6726-6744 (DOI: 10.1002/anie.200906623)
155. Li H., He X., Kang Z., Huang H., Liu Y., Liu J., Lee S. T. (2010), Water-soluble fluorescent carbon quantum dots and photocatalyst design, *Angew. Chem. Int. Ed.*, 49, 4430-4434 (DOI: 10.1002/anie.200906154)
156. Karthik S., Saha B., Ghosh S. K., Singh N. P. (2013), Photo responsive quinoline tethered fluorescent carbon dots for regulated anticancer drug delivery, *Chem. Commun.*, 49, 10471-10473 (DOI: 10.1039/C3CC46078A)
157. Dey D., Bhattacharya T., Majumdar B., Mandani S., Sharma B., Sarma T. K.(2013), Carbon dot reduced palladium nanoparticles as active catalysts for carbon-carbon bond formation, *Dalton Trans.*, 42, 13821-13825, (DOI: 10.1039/c3dt51234g)
158. Liu R., Huang H., Li H., Liu Y., Zhong J., Li Y., Kang Z. (2014), Metal nanoparticle/carbon quantum dot composite as a photo catalyst for high-

Chapter 1

- efficiency cyclohexane oxidation, *ACS Catal.*, 4, 328-336 (DOI: 10.1021/cs400913h)
159. Behr A., Henze G., Schomäcker R. (2006), Thermo regulated liquid/liquid catalyst separation and recycling, *Adv. Synth. Catal.*, 348, 1485-1495 (DOI: 10.1002/adsc.200606094)
160. Teunissen W., Bol A. A., Geus J. W. (1999), Magnetic catalyst bodies, *Catal. Today*, 48, 329-336 (DOI: 10.1016/S0920-5861(98)00389-7)
161. Wang X., Zhuang J., Peng Q., Li Y. D. (2005), A general strategy for nanocrystal synthesis, *Nature*, 437, 121-124 (DOI: 10.1038/nature03968)
162. Suslick K. S., Fang M., Hyeon T. (1996), Sonochemical synthesis of iron colloids, *J. Am. Chem. Soc.*, 118, 11960-11961 (DOI: 10.1021/ja961807n)
163. Laurent S., Forge D., Port M., Roch A., Robic C., Vander Elst L., Muller R. N. (2008), Magnetic iron oxide nanoparticles: Synthesis, stabilization, vectorization, physicochemical characterizations, and biological applications, *Chem. Rev.*, 108, 2064-2110 (DOI: 10.1021/cr068445e)
164. Rabias I., Fardis M., Devlin E., Boukos N., Tsitrouli D., Papavassiliou G. (2008), No aging phenomena in ferrofluids: The influence of coating on interparticle interactions of maghemite nanoparticles, *ACS nano*, 2, 977-983 (DOI: 10.1021/nn700414w)
165. Shen X. C., Fang X. Z., Zhou Y. H., Liang H. (2004), Synthesis and characterization of 3-aminopropyltriethoxysilane-modified super paramagnetic magnetite nanoparticles, *Chem. Lett.*, 33, 1468-1469 (DOI: 10.1246/cl.2004.1468)
166. MasPOCH D., Ruiz-Molina D., Veciana J. (2004), Magnetic nanoporous coordination polymers, *J. Mater. Chem.*, 14, 2713-2723 (DOI: 10.1039/B407169G)
167. Baruwati B., Guin D., Manorama S. V. (2007), Pd on surface-modified NiFe₂O₄ nanoparticles: A magnetically recoverable catalyst for Suzuki and Heck reactions, *Org. Lett.*, 9, 5377-5380 (DOI: 10.1021/ol702064x)
168. Polshettiwar V., Baruwati B., Varma R. S. (2009), Self-assembly of metal oxides into three-dimensional nanostructures: Synthesis and

Chapter 1

- application in catalysis, *ACS Nano*, 3, 728- 736 (DOI: 10.1021/nn800903p)
169. Polshettiwar V., Baruwati B., Varma R. S. (2009), Nanoparticle-supported and magnetically recoverable nickel catalyst: A robust and economic hydrogenation and transfer hydrogenation protocol, *Green Chem.*, 11, 127-131 (DOI: 10.1039/B815058C)
170. Yoon T. -J., Lee W., Oh Y. -S., Lee J. -K. (2003), Magnetic nanoparticles as a catalyst vehicle for simple and easy recycling, *New. J. Chem.*, 27, 227-229 (DOI: 10.1039/B209391J)
171. Shi F., Tse M. K., Pohl M. M., Brückner A., Zhang S., Beller M. (2007), Tuning catalytic activity between homogeneous and heterogeneous catalysis: Improved activity and selectivity of free nano-Fe₂O₃ in selective oxidations, *Angew. Chem. Int. Ed.*, 46, 8866-8868 (DOI: 10.1002/anie.200703418)
172. Polshettiwar V., Varma R. S. (2009), Nanoparticle-supported and magnetically recoverable palladium (Pd) catalyst: A selective and sustainable oxidation protocol with high turnover number, *Org. Biomol. Chem.*, 7, 37-40 (DOI: 10.1039/B817669H)
173. Polshettiwar V., Baruwati B., Varma R. S. (2009), Magnetic nanoparticle-supported glutathione: A conceptually sustainable organocatalyst, *Chem. Commun.*, 1837-1839 (DOI: 10.1039/B900784A)
174. Kawamura M., Sato K. (2007), Magnetic nanoparticle-supported crown ethers, *Chem. Commun.*, 3404-3405 (DOI: 10.1039/B705640K)
175. Hu A., Yee G. T., Lin W. (2005), Magnetically recoverable chiral catalysts immobilized on magnetite nanoparticles for asymmetric hydrogenation of aromatic ketones, *J. Am. Chem. Soc.*, 127, 12486-12487 (DOI: 10.1021/ja053881o)
176. Luo S., Zheng X., Cheng J.-P. (2008), Asymmetric bifunctional primary aminocatalysis on magnetic nanoparticles, *Chem. Commun.*, 5719-5721 (DOI: 10.1039/B812958D)
177. Polshettiwar V., Varma R. S. (2009), Nanoparticle-supported and magnetically recoverable ruthenium hydroxide catalyst: Efficient

Chapter 1

hydration of nitriles to amides in aqueous medium, *Chem. Eur. J.*, 15, 1582-1586 (DOI: 10.1002/chem.200802264)

178. Phan N. T. S., Jones C.W. (2006), Highly accessible catalytic sites on recyclable organosilane-functionalized magnetic nanoparticles: An alternative to functionalized porous silica catalysts, *J. Mol. Catal. A Chemical*, 253, 123-131 (DOI: 10.1016/j.molcata.2006.03.019)

Chapter 1

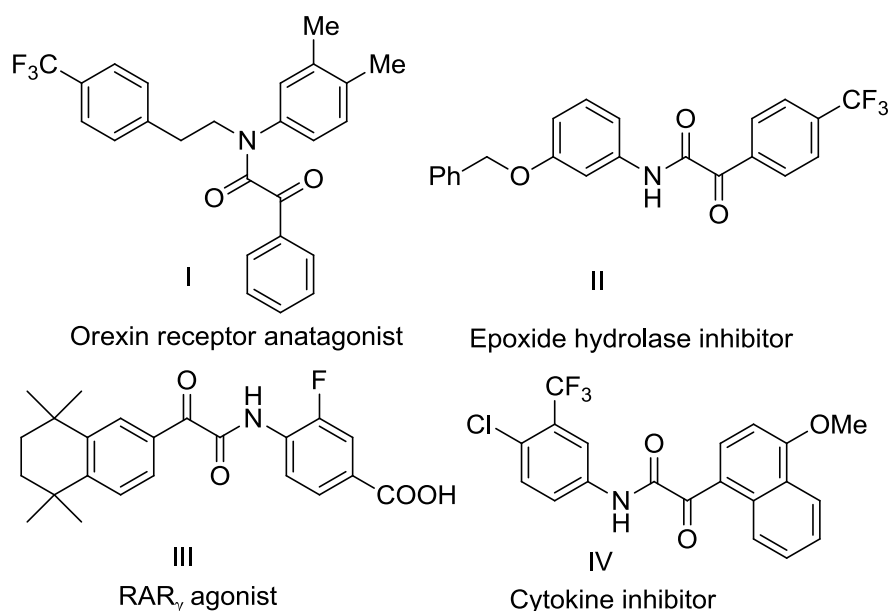
Chapter 2

Graphene Oxide as Metal-Free Catalyst in Oxidative Dehydrogenative C-N Coupling Leading to α -Ketoamides: Importance of Dual Catalytic Activity

Chapter 2

2.1 Introduction

Exploration of cost-effective, recyclable and environmental friendly metal-free catalysts for organic transformations is important in the green chemistry milieu. C-C and C-X (X= heteroatom) coupling reactions through cross-dehydrogenative coupling (CDC) pathway is an effective method towards construction of bio-molecules with a variety of pharmaceutical activity.^[1-16] α -ketoamides and their derivatives represent one of the important class of compounds with high biological and pharmacological activity viz. anti-viral, anti-HIV, anti-tumor, anti-inflammatory, anti-IBD, anti-bacterial, drugs and drug candidates (Scheme 2.1).^[17-20]

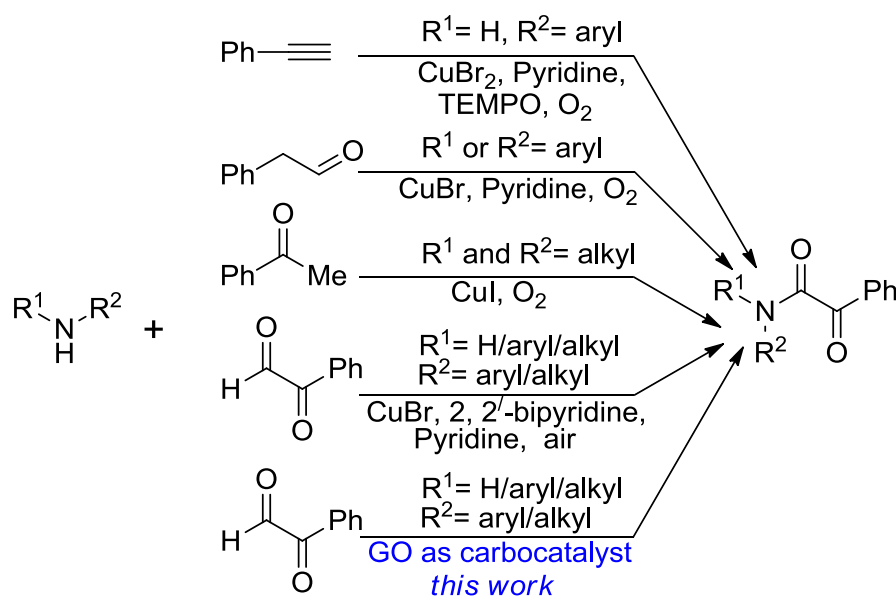


Scheme 2.1. Biologically active α -Ketoamides

They are also versatile and valuable intermediates and synthons in a variety of functional group transformations and total synthesis.^[21-25] Several approaches based on transition metal catalysts have been adopted towards the synthesis of the α -ketoamides. Although, these transition metal catalysts show excellent efficiency, a large number of them suffer from a variety of limitations: (1) N-unsubstituted anilines are required in the reaction of amidation diketonization of terminal alkynes;^[26] (2) aliphatic amines do not work in the reaction of aryl acetaldehydes with anilines^[27] and (3) only aliphatic secondary amines work in the coupling reaction of aryl methyl ketones with amines.^[28] Recently, DMSO

Chapter 2

mediated synthesis of α -ketoamides has been achieved, however the method is limited only up to secondary amines.^[29] A homogeneous copper catalyst could afford α -ketoamides with wide substrate scope through oxidative CDC reaction (Scheme 2.2).^[30] However, the separation and recycling of catalyst in these homogeneous catalytic systems remains a challenge. Therefore, there is a huge scope for the development of heterogeneous and metal-free pathway towards direct C-N coupling with the emphasis on the reduction in production cost and eliminating metal contamination.



Scheme 2.2. Synthetic methods for α -ketoamides

Recently, carbonaceous nanomaterials have received considerable impetus as non-metal alternatives for clean energy conversion as well as important organic transformations (carbocatalysis),^[31-34b] owing to their sustainability and affordability. Graphene oxide (GO), a two-dimensional nanomaterial with various oxyfunctionalized groups has shown very good activity as catalysts in organic transformations such as oxidation, hydration, alkylation reaction etc.^[35-43] Recently, the catalytic activity of GO was successfully harnessed for aryl-aryl coupling through C-H bond activation.^[44] Efficient catalytic activity of the base and acid treated graphene oxide in oxidative C-N coupling reaction was pioneered by Loh *et. al.*^[45] Although effective surface modification such as hole generation on the basal plane or heteroatom substitution on the carbon sites might be influential in high catalytic

activity,^[45-47] the presence of specific oxyfunctionalized groups in GO can also function as active sites for catalytic transformations.^[48-51] Herein, we show that GO can be employed as an effective heterogeneous catalyst for the CDC reaction of α -ketoaldehyde and amines leading to the formation of α -ketoamides with a large substrate scope under mild reaction conditions. The oxygen functionalities on the GO surface showed dual activity as both acid and oxidizing catalyst that was crucial in the formation of α -ketoamides. Further, we demonstrate that the amount of oxygenated groups connected to the carbon skeleton had a major impact on the catalytic reaction.

2.2 Results and Discussion

2.2.1 Synthesis and characterization of graphene oxide

We evaluated the catalytic activity of GO with high oxygen content as a metal-free heterogeneous carbocatalyst for C-N coupling through CDC pathway. Oxygen rich GO was synthesized by the modified Hummer's method and was extensively purified to remove any metal impurity. The transmission electron microscopy (TEM) indicated a layered structure of GO which was further supported by AFM studies revealing that the GO sample consist of two to three layers of graphene sheets (Fig. 2.1a and 2.1b). The X-ray diffraction (XRD) pattern showed a characteristic peak at 2θ value of 10.2° with d spacing of 0.865 nm (Fig. 2.1c). X-ray photoelectron spectroscopy (XPS) analysis showed C1s core level spectrum of GO (Fig. 2.1d), fitted into four components with binding energies (BEs) at about 284.5, 286.4, 287.6 and 288.9 eV which corresponds to C-C, C-O, C=O and O-C=O species respectively. UV-visible study showed two absorption peaks, a maximum at 230 nm corresponding to π - π^* transitions of aromatic C-C bonds and a shoulder at 305 nm attributed to n- π^* transitions of C=O bonds (Fig. 2.1e). FTIR spectrum of the synthesized GO showed the presence of various oxygen containing functional groups (Fig. 2.1f). In general, the surface of GO consists of four different oxy-functionalized groups on graphene sheets, namely hydroxyl (-OH), epoxide (C-O-C), carbonyl (C=O), and carboxylic acid (-C(O)OH) moieties. The majority of the oxygenated groups come from hydroxyl and epoxy moieties which are distributed over the

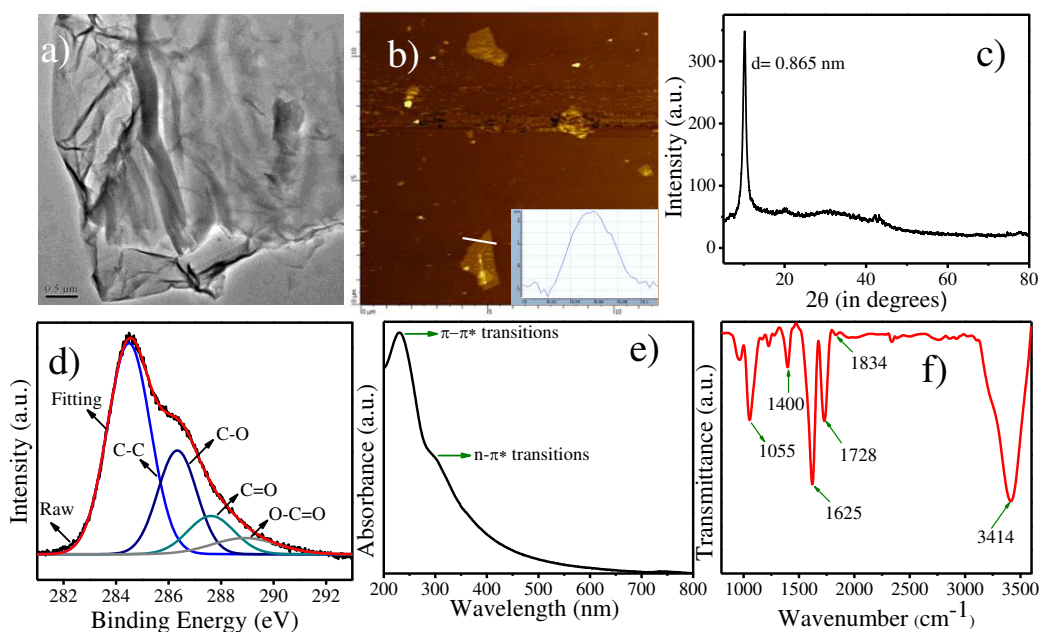
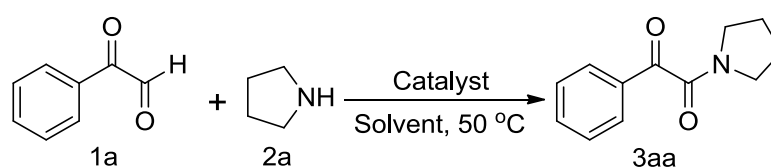


Figure 2.1. a) TEM image; scale bar 500 nm, b) AFM image (inset height profile of GO), c) Powder X-ray diffraction pattern, d) C1s core level XPS spectrum e) UV-visible spectrum and f) FTIR spectrum of GO

basal plane of the graphene surface and are electrophilic in nature. On the other hand, carbonyl and carboxylic acid groups are located at the edges of the graphene sheets and are nucleophilic in nature.^[44, 53] The vibrational modes in GO include contributions from ketonic groups such as anhydrides, lactones and pyrones (between 1,550–1,850 cm^{-1}), hydroxyls namely phenols and lactols (between 3,050–3,800 and 1,000–1,150 cm^{-1}), carboxyls at 1650–1750 cm^{-1} , C-OH vibrations (between 3,000–3,600 and 1,080 cm^{-1}), epoxides (C–O–C at 850 and 1,230–1,330 cm^{-1}), ethers (C–O at 800–1,200 cm^{-1}) and sp^2 -hybridized C=C (sp^2 -C, in-plane vibrations between 1,500–1600 cm^{-1}).^[45, 54]

2.2.2 Optimization studies and substrate scope

For the C-N coupling, initially we choose phenylglyoxal monohydrate and pyrrolidine as the model substrates (Table 2.1). No product formation was observed when the reaction was conducted at 100 °C in absence of catalyst (entry 1, Table 2.1). However, the coupling product α -ketoamide (3aa) was formed in 38% yield when a small amount (10 mg) of GO was added to the reaction at room temperature (entry 2, Table 2.1), indicating that oxygen functionalities on GO surface could function as potential active sites for the coupling reaction.

Table 2.1. Oxidative coupling of 1a with 2a under various conditions^a

Entry	Catalyst	Solvent	Yield (%) ^b
1 ^c	none	acetonitrile	trace
2 ^d	GO (10 wt%)	acetonitrile	38
3	GO (10 wt %)	acetonitrile	92
4 ^e	GO (10 wt%)	acetonitrile	85
5	Graphite (10 wt %)	acetonitrile	trace
6	Activated carbon (10 wt %)	acetonitrile	trace
7	CNT (10 wt %)	acetonitrile	trace
8	rGO (10 wt%)	acetonitrile	20%

^a Reaction conditions: 1a (0.25 mmol), 2a (0.375 mmol), cat. 10 wt%, 3.0 mL acetonitrile, Ar atmosphere, 50 °C, 4 h. ^b Yields of isolated product. ^c Reaction at 100 °C for 12 h. ^{d, e} Reaction was carried out at room temperature and 90 °C respectively. CNT= Carbon nanotube

The complete conversion of phenyl glyoxal and the formation of 3aa (92%) was achieved when the reaction temperature was increased to 50 °C (entry 3, Table 2.1). Further increase in reaction temperature proved to be unfavorable for yield of the desired product due to formation of other by-products (entry 4, Table 2.1). Variable catalyst loading as well as solvents was scrutinized in order to achieve optimal reaction conditions (Table 2.2). Interestingly, presence of air was found to be detrimental as several by-products were formed lowering the overall yield of the desired product (entry 10, Table 2.2). Other carbonaceous materials, such as graphite, activated carbon and CNT showed very less activity (entry 5-7, Table 2.1). Reduced GO obtained by reduction of GO with hydrazine hydrate afforded very less yield (20%) (entry 8, Table 2.1). The results clearly indicated that oxygen functionalities on GO surface were instrumental in catalyzing the formation of α -ketoamide.

Having achieved the optimized reaction conditions, we evaluated the substrate scope with a range of α -carbonyl aldehyde and secondary amines (Table 2.3). In general, both electronically activating and deactivating α -carbonyl aldehydes

Chapter 2

Table 2.2. Optimization studies of coupling reaction of 1a and 2a^a

Entry	Catalyst (wt %)	Solvent	Yield (%) ^b
1	GO (10 wt %)	Water	65
2	GO (10 wt %)	Acetonitrile	92
3	GO (10 wt%)	Ethanol	45
4	GO (10 wt%)	THF	trace
5	GO (10 wt%)	DMF	trace
6	GO (5 wt%)	Acetonitrile	65
7	GO (15 wt%)	Acetonitrile	90
8 ^c	Benzene filtrate	Acetonitrile	trace
9	MnSO ₄ (10 wt%)	Acetonitrile	trace
10 ^d	GO (10 wt%)	Acetonitrile	72

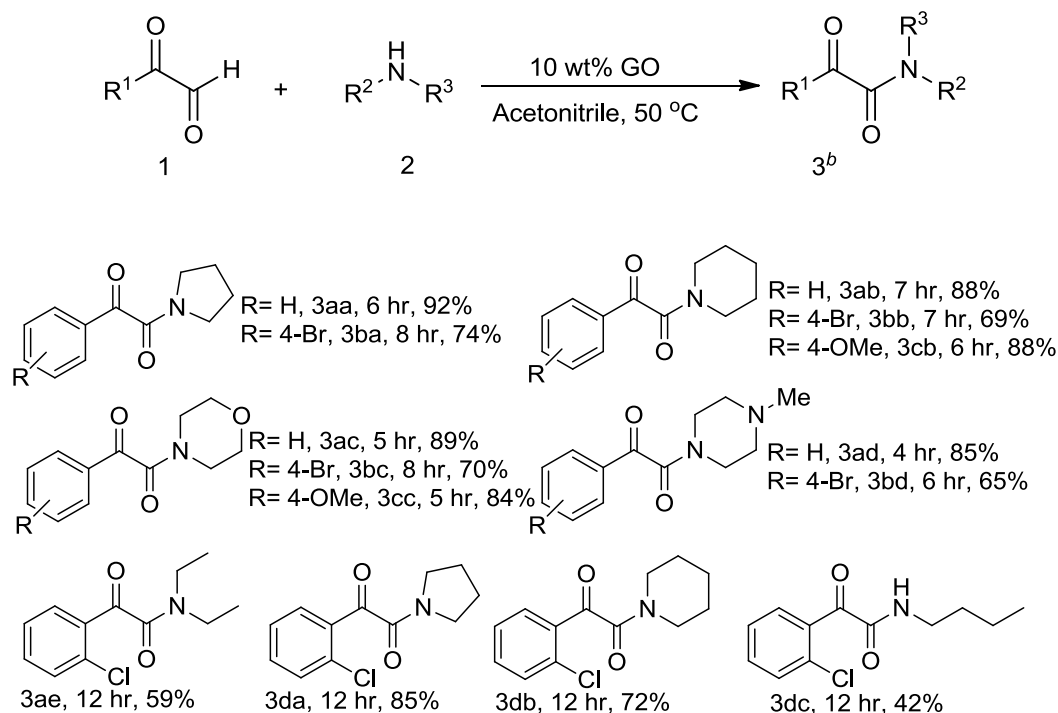
^a Reaction conditions: 1a (0.25 mmol), 2a (0.375 mmol), 3.0 mL solvent, Ar atmosphere, 50 °C, 4 h. ^bYields of isolated product. ^cGO catalyst was boiled in benzene and GO was filtered. The resultant benzene filtrate was taken as the catalyst. ^dReaction was carried out in presence of air

could be transformed into α -ketoamides with high yield. Moreover, substituents at different positions of the phenyl ring and their electronic nature did not affect the yield of the desired α -ketoamides. Various aliphatic secondary amines such as pyrrolidine, piperidine, morpholine, *N*-methylpiperazine and *N,N*-diethylamine afforded moderate to high yield of the desired product. Aliphatic primary amines also could be coupled under present reaction conditions, albeit with moderate yield (entry 3dc, Table 2.3).

On the other hand, when the coupling reaction was carried out using aromatic secondary amine *N*-methylaniline under the optimized conditions, it resulted in very poor yield. Moreover, very low yield of the desired product was obtained when aromatic primary amines were coupled with α -carbonyl aldehydes. This can be attributed to the participation of the nitrogen lone pair in aromaticity, thereby lowering the nucleophilic tendency of the amine group towards the aldehyde. To overcome this, we postulated that the presence of an external base can help in retaining the nucleophilic character of the amine group and thus favoring the reaction towards the desired coupling products. Therefore, the coupling between phenylglyoxal monohydrate and 4-aminobenzonitrile was

Chapter 2

Table 2.3. GO catalyzed oxidative coupling of variety of α -keto aldehydes and aliphatic secondary/primary amines.^a

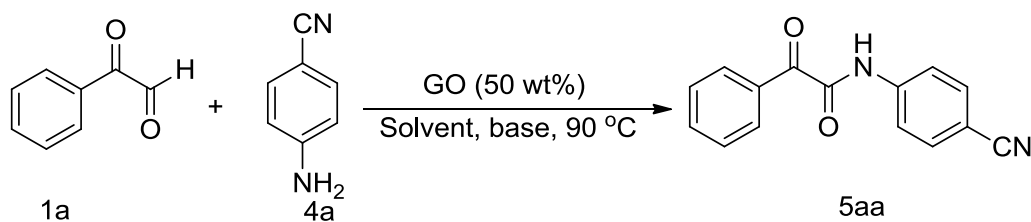


^a Reaction conditions: 1 (0.25 mmol), 2 (0.375 mmol), GO catalyst 10 wt%, acetonitrile 3.0 mL, Ar atmosphere, 50 °C for 4 h. ^b Yields of isolated product

studied in order to achieve the optimized condition suitable for primary amines (Table 2.4). It was observed that higher GO catalyst loading was required at elevated reaction temperature for effective coupling of primary amines as compared to secondary aliphatic amines. Although yield of ketoamide formed was low only in presence of GO (25%, entry 1, Table 2.4), the product formation was significantly enhanced in presence of an external base. Among various organic bases screened, DABCO was found to be most suitable, as the model coupling reaction resulted in excellent yield (65%, entry 2, Table 2.4). Inorganic bases such as K_2CO_3 and NaOH were found to be ineffective. Among the solvents toluene was found to be most suitable (entry 7-9, Table 2.4). From the optimization data, the best yield (75%) for the primary amine coupling was achieved when the reaction was performed using GO (50 wt %) at 90 °C under Ar environment (entry 15, Table 2.4).

Chapter 2

Table 2.4. Oxidative coupling of 1a and 4a under various reaction conditions^a



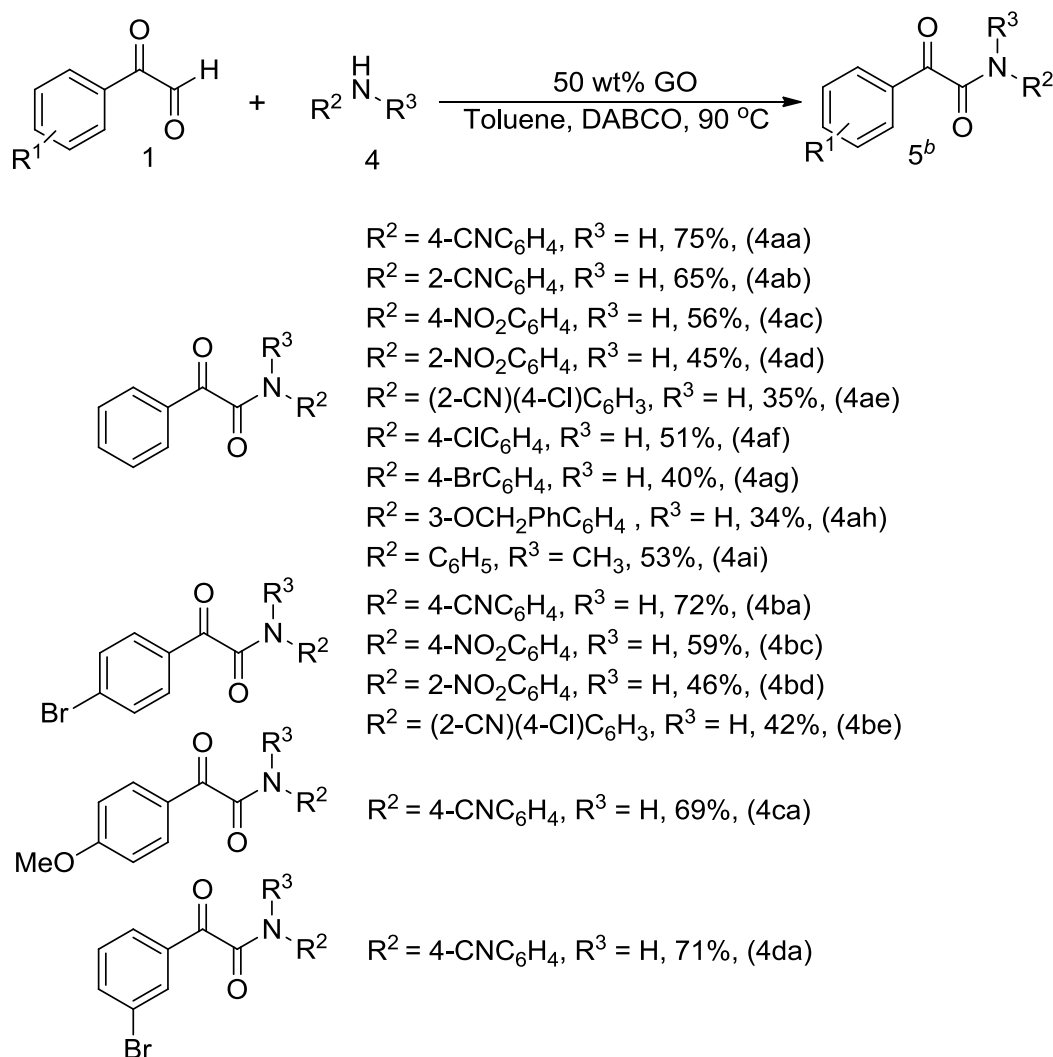
Entry	Catalyst	Solvent	Base (equiv)	Yield (%) ^b
1	GO (50 wt %)	Toluene	None	25
2	GO (50 wt%)	Toluene	DABCO (2.0)	65
3	GO (50 wt%)	Toluene	Pyridine (2.0)	57
4	GO (50 wt%)	Toluene	DIPEA (2.0)	trace
5	GO (50 wt%)	Toluene	K ₂ CO ₃ (2.0)	trace
6	GO (50 wt%)	Toluene	NaOH (2.0)	trace
7	GO (50 wt%)	CH ₃ CN	DABCO (2.0)	45
8	GO (50 wt%)	DMF	DABCO (2.0)	52
9	GO (50 wt%)	H ₂ O	DABCO (2.0)	31
10	GO (100 wt%)	Toluene	DABCO (2.0)	67
11 ^c	GO (50 wt %)	Toluene	DABCO (2.0)	42
12	GO (50 wt%)	Toluene	DABCO (3.0)	63
13	GO (10 wt%)	Toluene	DABCO (3.0)	38
14	GO (30 wt%)	Toluene	DABCO (3.0)	55
15 ^d	GO (50 wt%)	Toluene	DABCO (3.0)	75

^a Reaction conditions: 1a (0.375 mmol), 4a (0.25 mmol), GO catalyst, solvent 3.0 mL, Ar atmosphere, 90 °C, 12 h. ^b Yields of isolated product. ^c Reaction was carried out 60 °C. ^d Reaction was carried out in presence of molecular sieves (4 Å) (100 mg). DABCO = 1,4-Diazabicyclo[2.2.2]octane. DIPEA = *N*-diisopropylethylamine

Under these conditions, scope of the reaction with respect to various anilines was investigated. Both electron rich and electron deficient aniline could be inserted into the α -ketoamide skeleton (Table 2.5). Furthermore, substituents at different positions of the phenyl ring did not affect the yield of the product. Halo substituted α -carbonyl aldehydes were also well tolerated and

Chapter 2

Table 2.5. GO catalyzed oxidative coupling of different α -carbonyl aldehydes with variety of primary amines ^a



^a Reaction conditions: **1** (0.375 mmol), **4a** (0.25 mmol), GO catalyst 50 wt%, DABCO 2.0 equiv., 100 mg molecular sieves (4 Å), toluene 3.0 mL, Ar atmosphere, 90 °C, 12 h. ^b Yields of isolated product

corresponding α -ketoamides could be obtained with significant yield that can be used for further transformations. In addition, the coupling of aromatic secondary amine *N*-methylaniline with phenyl glyoxal monohydrate resulted in significant yield (53%, entry 4ai, Table 2.5) in presence of DABCO.

2.2.3 Conservation of mass and formation of byproducts

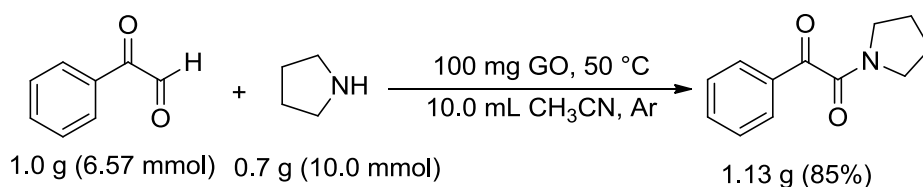
CO₂ formation is a readily observed phenomenon in oxidative coupling reactions, either due to over-oxidation of the reaction mass or volatile nature of

Chapter 2

the reaction components.^[55, 56] In the present case, no CO₂ formation was observed during the reaction, as 100% carbon mass balance was obtained. GC analysis showed the formation of mainly phenylglyoxylic acid, the oxidized form of phenylglyoxal as a by product along with amides during the reactions.^[57, 58]

2.2.4 Large scale synthesis

The present methodology using GO as a carbocatalyst could be applied for large scale synthesis, as we could obtained high yield of the ketoamide product for the model coupling reaction of phenylglyoxal and pyrrolidine (85%, Scheme 2.3).



Scheme 2.3. Gram scale synthesis for the coupling reaction of phenylglyoxal and pyrrolidine

2.2.5 Recovery and recyclability

The GO catalyst could be easily separated from the reaction mixture by simple filtration and it maintained 80% of its original activity, even after five

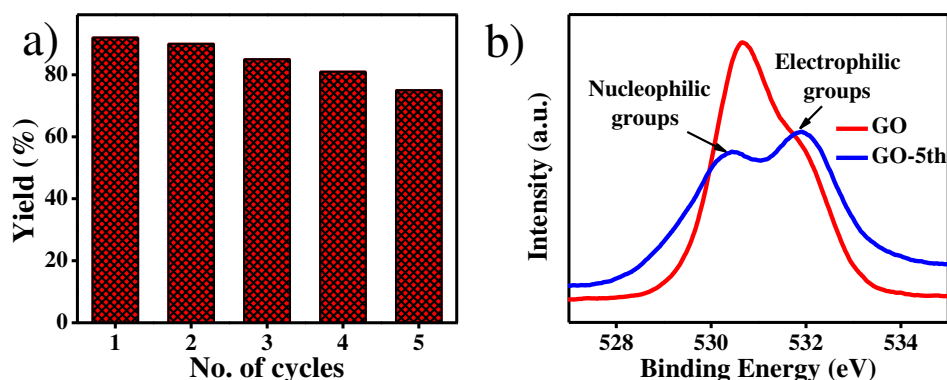
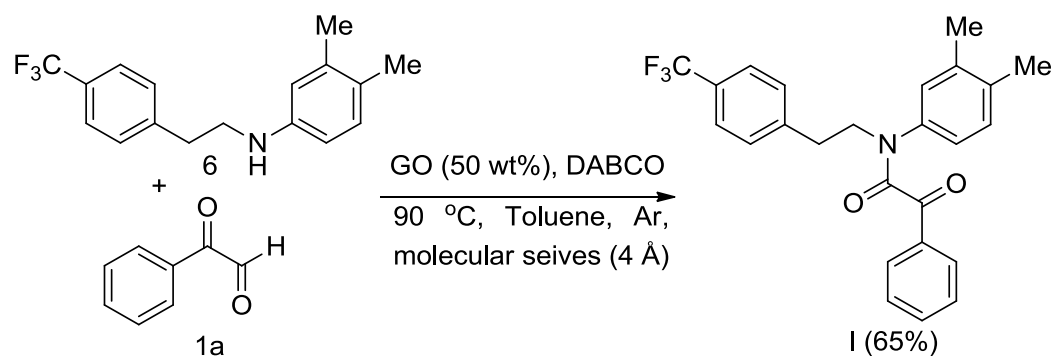


Figure 2.2. a) Product yield after different cycle of catalytic reactions using recovered GO after subsequent reactions as catalyst and b) XPS O1s core level spectrum of GO and GO recovered after 5th catalytic cycle for the model coupling reaction

cycles (Fig. 2.2a). This reduced activity may be attributed to decrease in nucleophilic oxygen groups in GO upon repeated catalytic run (Fig. 2.2b). The original activity could be regenerated by re-oxidation of the catalyst.

2.2.6 Synthesis of bioactive compound

Since α -ketoamides are ubiquitous structural motifs in many biologically active compounds such as drugs and precursors for other important compounds, the use of GO as an effective carbocatalyst gives a green and easily practical heterogenic protocol to construct bioactive compounds from readily available starting materials. We investigated the potential of GO towards the synthesis of orexin receptor antagonist (I), that could be easily synthesized from phenylglyoxal monohydrate and 6 to give I in 65% yield (Scheme 2.4).



Scheme 2.4. Synthesis of orexin receptor antagonist (I)

2.2.7 Mechanistic Investigation

In order to have an insight into the reaction pathway for the GO catalyzed C-N coupling reaction, we performed a time-dependent HPLC-MS study of the model reaction between phenyl glyoxal and pyrrolidine which clearly demonstrated the initial formation of the hemiaminal intermediate and its subsequent conversion to ketoamide (Fig. 2.3). The hemiaminal intermediate initially formed could be isolated and characterized by NMR and mass spectroscopy (Experimental Section). This suggested the dual activity of GO as both acid and oxidation catalyst. The formation of hemiaminal intermediate was governed by the acid catalytic activity of oxyfunctionalized groups on GO surface. The conversion of the hemiaminal intermediate to the corresponding

Chapter 2

ketoamide took place through an oxidative pathway. Even under Ar atmosphere the yield of the product did not suffer, thus ruling out the involvement of aerial oxidation in the second step.

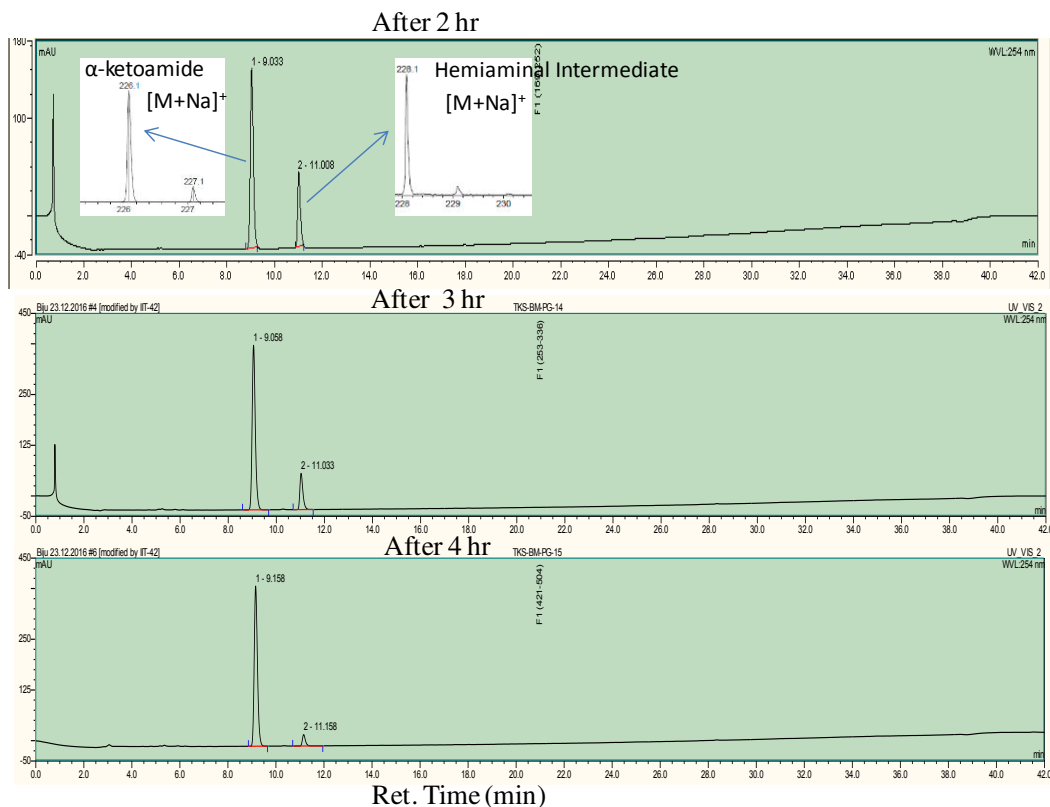
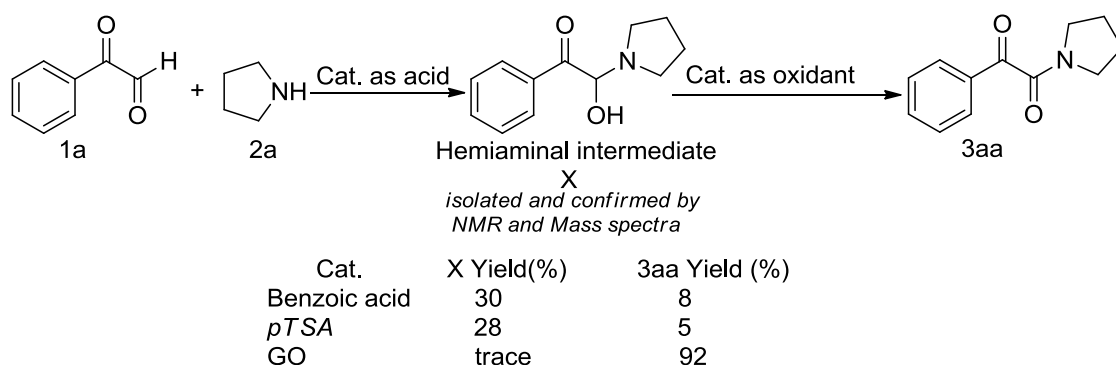


Figure 2.3. Time-dependent HPLC-MS analysis of the coupling reaction of phenyl glyoxal monohydrate and pyrrolidine with its corresponding ESI-MS

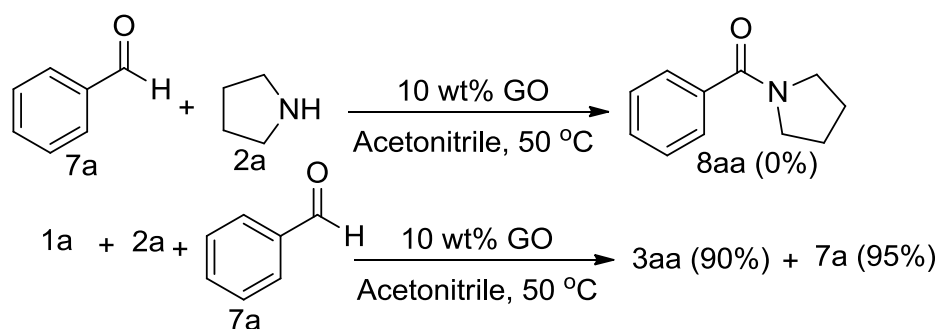
A few control experiments (Scheme 2.5) were carried out using benzoic acid and *p*-TSA as catalysts for the model coupling reaction. The use of these acid catalysts led to the formation of the hemiaminal form as the major product with a trace amount of ketoamide formation. As these catalysts do not possess oxidative catalytic capability, the formation of ketoamides was not favorable. On the other hand, formation of ketoamide using GO could take place efficiently due to the intrinsic acidic as well as oxidizing capability of GO, where the conversion from hemiaminal to ketoamide took place through oxidation pathway.

Chapter 2



Scheme 2.5. Formation of hemiaminal intermediate followed by α -ketoamide

It is worth mentioning that only benzaldehyde could not be coupled with amines using GO as a catalyst (Scheme 2.6). When phenylglyoxal monohydrate was reacted with pyrrolidine in presence of benzaldehyde, 3aa was obtained in 90% yield whereas 95% of benzaldehyde was recovered.



Scheme 2.6. Comparison of benzaldehyde and phenylglyoxal towards α -ketoamide formation

To explore the involvement of oxy-functionalized groups on the catalytic activity leading to the formation of α -ketoamides, we evaluated the performance of GO for the model reaction using samples annealed at different temperature. It is well known that GO contains various oxygen containing groups such as hydroxyl (-OH), epoxide (C-O-C), carbonyl (C=O) and carboxylic acid (-CO₂H) moieties on the basal plane and edges. Four different GO catalysts with different oxygen content were prepared by controlling the annealing temperature (200 °C, 400 °C, 600 °C and 800 °C). As shown in Fig. 2.4, the catalytic activity of GO decreased significantly with catalysts annealed at elevated temperature (Fig. 2.4a), which could be correlated to decreased oxygen content (Fig. 2.4a, inset). A decrease in relative oxygen content at various annealing temperature could be

Chapter 2

confirmed from XPS studies (Fig. 2.4b).^[44, 59] O1s core level XPS spectrum showed relative decrease in nucleophilic oxygen groups over the surface of GO upon annealing treatment which again confirmed the change in electronic nature in the GO surface (Fig. 2.4c).

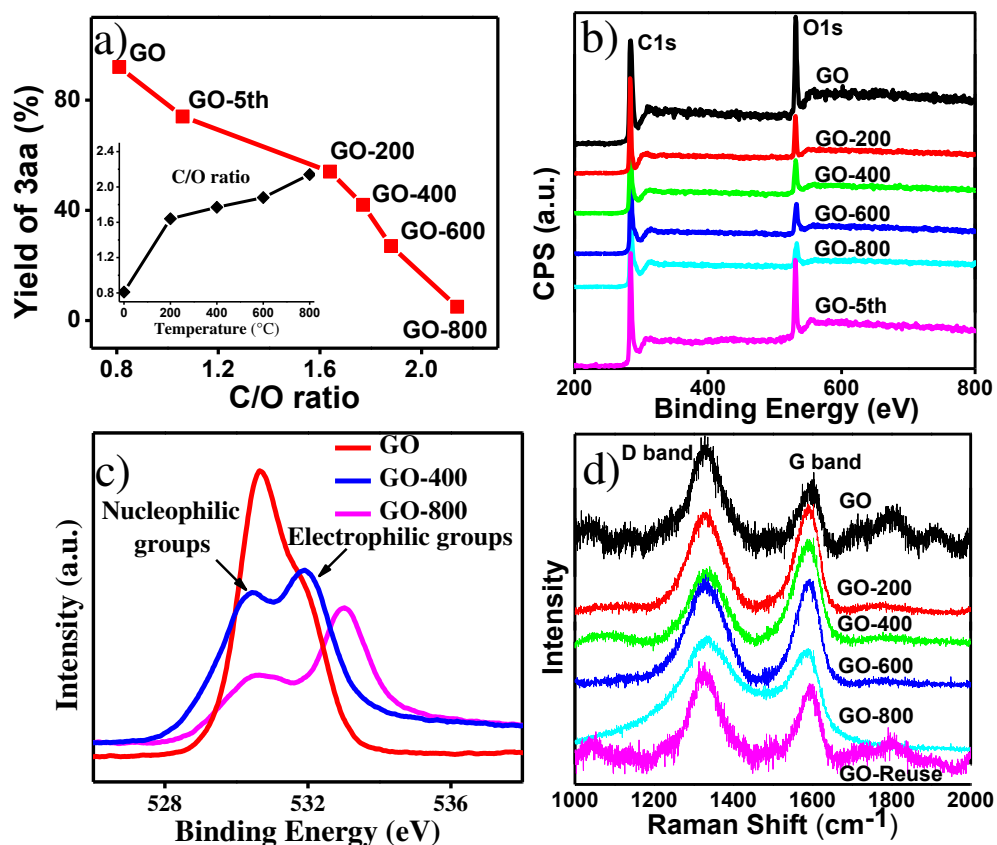


Figure 2.4. a) Catalytic activity (inset, relative C/O ratio with increasing temperature), GO-5th denotes the catalyst after 5th cycle, b) XPS survey spectra, c) O1s core level XPS spectra d) Raman spectra of GO annealed at different temperature

A gradual decrease in amount of oxygen containing functional groups and their relative distribution upon annealing treatment was obtained from the transmission infrared differential spectra (Fig. 2.5).^[45, 54] Zeta potential measurements also revealed the decrease in acidic functionality on GO surface at elevated temperature (Fig. 2.6). From Raman Spectra (Fig. 2.4d) and SEM images (Fig. 2.7) it was observed that in spite of removal of oxygen species, the annealing treatment did not have significant affect on structural aspects of GO. Surface area measurements showed that there were no significant changes in the surface area of pristine GO and its annealed analogues (Table 2.6).

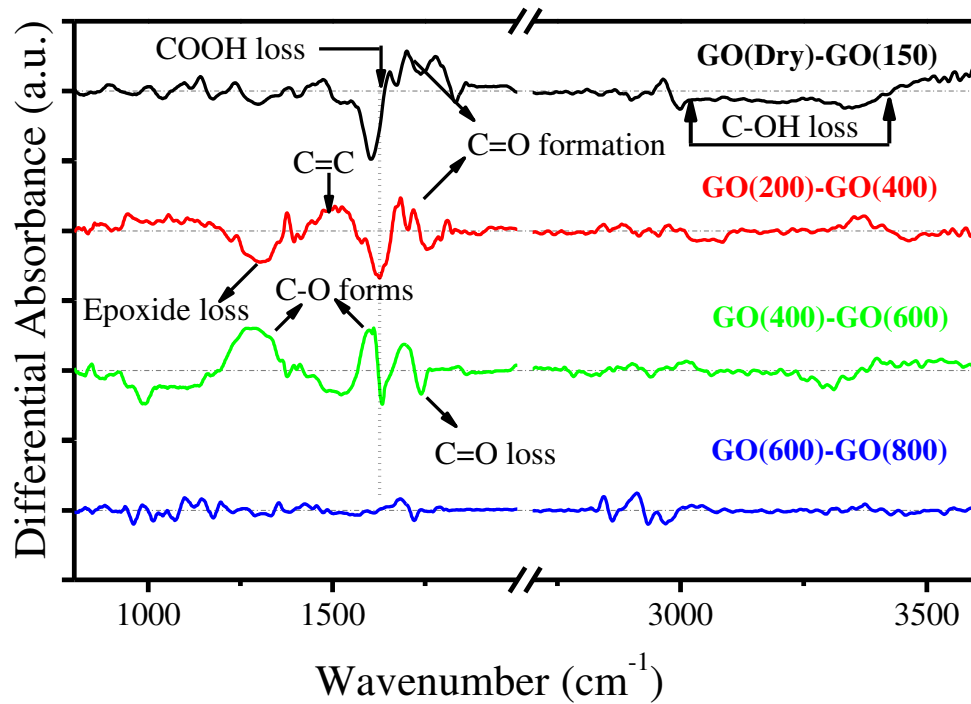


Figure 2.5. Transmission infrared differential spectra of GO showing relative amounts and distribution of oxygenated functional groups at different annealing temperature regime. It presents the changes in functional groups at various elevated temperature

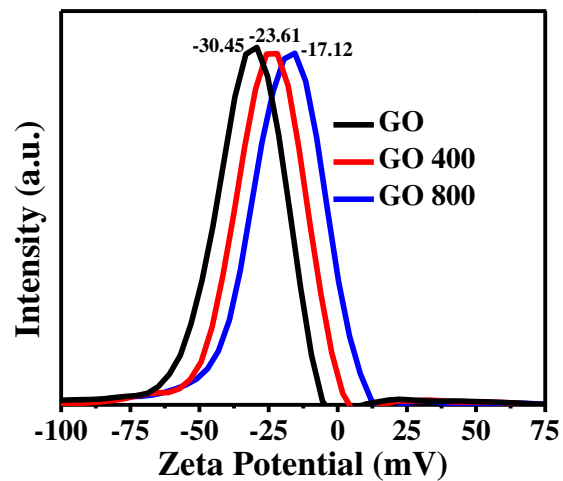


Figure 2.6. Zeta potential measurement of GO samples annealed at different temperature

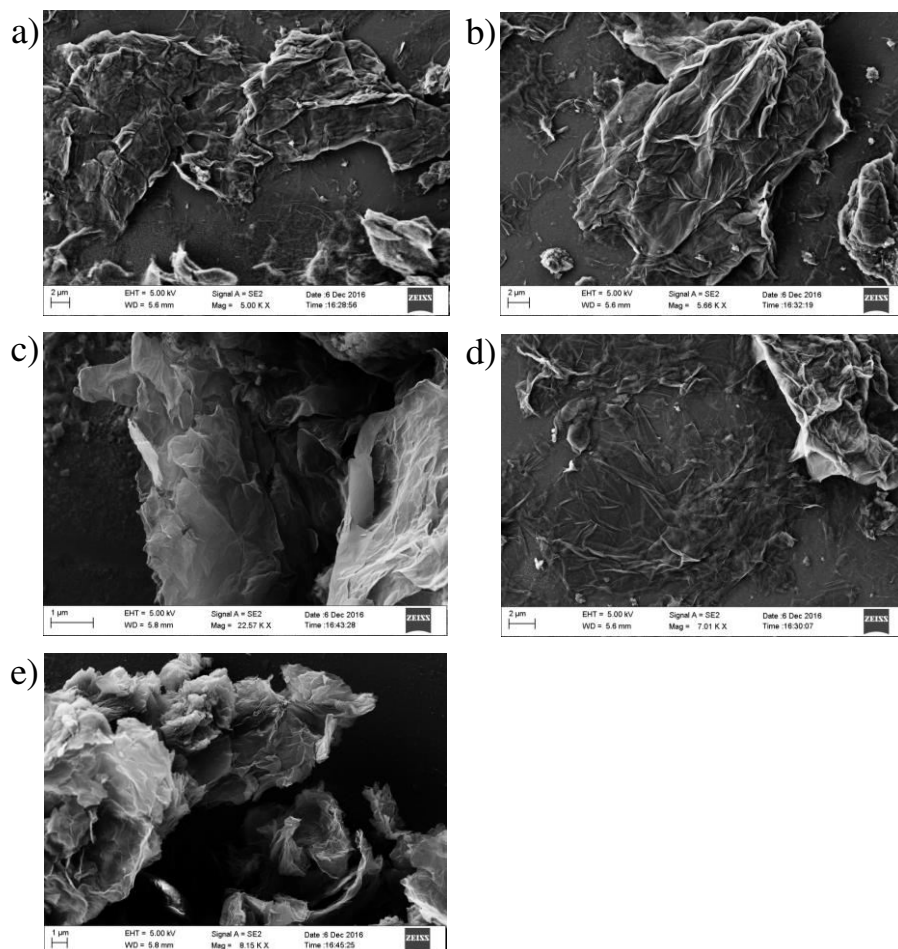


Figure 2.7. (a, b, c, d and e) SEM images of GO annealed at different temperature (pristine GO, 200, 400, 600 and 800 °C respectively) showing no apparent changes in surface morphology

Table 2.6. Surface area of Graphene Oxide annealed at different temperature

GO Annealing Temperature (°C)	Surface area (m ² /g)
Pristine GO	534
200	589
400	601
600	518
800	542

In order to verify the role of variable functional groups on GO surface responsible for the remarkable catalytic activity during the cross-dehydrogenative

C-N coupling reactions, the surface of GO was modified under various conditions following a reported procedure.^[45] GO surface consists of several acidic and basic oxygenated groups solvated by water molecules. Due to this amphiphilic nature, the surface property of GO can be tuned by base-acid treatments. The synthesized GO was first refluxed in presence of NaOH pellets to get the base treated GO (bGO).^[60, 61] Compared to GO, the FTIR intensity of hydroxyl band at $\sim 3000\text{-}3600\text{ cm}^{-1}$ in bGO decreased significantly (Fig. 2.8a). The intensity of -COOH groups also decreased due to deprotonation of the COOH group (1725 cm^{-1}) while that of $\text{sp}^2\text{ C=C}$ (1560 cm^{-1}) increased. This signifies that the carbon backbone now consist of extended $\pi\text{-}\pi^*$ network following the base treatment. The reduction of oxygen functionalities could be attributed to dehydration reaction driven by base mediated reflux.^[62] To further examine whether the affected functional groups in bGO can be retained, bGO was treated with a 0.1 M HCl solution (baGO). Interestingly, the peak intensity of the carboxyl group at 1725 cm^{-1} could be regenerated which may be attributed to reprotonation of the carboxyl group in presence of HCl. However, the peak intensity of hydroxyl and epoxy groups could not be recovered. Thus, after subsequent base and acid treatments of GO, the residual oxygen groups present in baGO mainly consisted of ketones, highly reduced epoxides and carboxylic acids. When the model reaction of phenyl glyoxal and pyrrolidine was carried out using

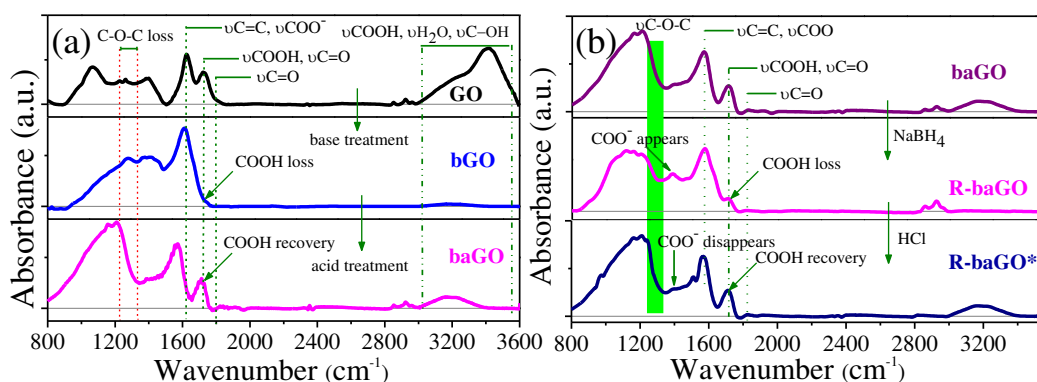


Figure 2.8. Transmission infrared absorption spectra for (a) GO (black), bGO (blue), baGO (magenta) and (b) baGO (purple), R-baGO(magenta) and R-baGO* (navy)

these modified GO (bGO and baGO), we observed decreased activity in case of bGO (20% yield), while baGO showed significant recovery in catalytic activity with 85% yield (entry 1 and 2, Table 2.7). This regeneration in catalytic activity

Chapter 2

may be originated either from ketone, carboxyls or epoxide functionality present on GO. Further evaluations were carried out with baGO reduced with NaBH₄ (RbaGO), during which ketones and epoxides are reduced along with deprotonation of carboxylic acid groups as observed by FTIR studies (Fig. 2.8b). Catalytic activity studies of RbaGO showed significantly reduced activity with 15% yield (entry 3, Table 2.7). Finally, a neutralization step using HCl resulted in recovery of the carboxylic acid group on GO surface that showed significant enhancement in catalytic activity with 81% yield (entry 4, Table 2.7).

Table 2.7. Catalytic activity of modified GO

Entry	Catalyst (10 wt%)	GC Yield (%)
1	bGO	20
2	baGO	85
3	RbaGO	15
4	RbaGO*	81
5	1-Pyrene-carboxylic acid	72
6	Pyrene	10

Reaction conditions: Phenyl glyoxal (0.25 mmol), pyrrolidine (0.375 mmol), 3.0 mL solvent, Ar atmosphere, 50 °C, 4 h. bGO= GO treated with NaOH, baGO= bGO neutralized with HCl, RbaGO= baGO reduced by NaBH₄, RbaGO= RbaGO neutralized by HCl*

During this neutralization step, neither ketone/epoxide could be reoxidized nor new oxygenated functionalities could be introduced. From these studies, it could be concluded that the catalytic activity of GO for the C-N coupling reaction was mainly due to the presence of COOH functionality on its surface.

To confirm the role of carboxylic acids in the catalytic reaction, 1-pyrene-carboxylic acid was used a model catalyst to mimic the graphene based material. Surprisingly, 1-pyrene-carboxylic acid also resulted in significant yield of the catalytic reaction (entry 5, Table 2.7). On the other hand, only the π conjugated system, such as pyrene could not afford appreciable yield during the reaction (entry 6, Table 2.7). Moreover only trace amount of product could be obtained when benzoic acid was used as the catalyst (Scheme 2.4). From these observations it can be concluded that both the carboxylic acid and the π - π^*

backbone in GO was influential in catalyzing the coupling reaction. Whereas the π carbon backbone helped in bringing the reactant molecules to the surface of GO, CO_2H participated in catalyzing the coupling reaction.

2.2.8 Leaching Test

Further, to ensure the degree of heterogeneity of GO, we performed a leaching test. No active species from the GO surface were found to be leached as we could observe no reaction by stopping the catalytic reaction after 2 hrs and continuing the reaction by removing the catalyst (Fig. 2.9).

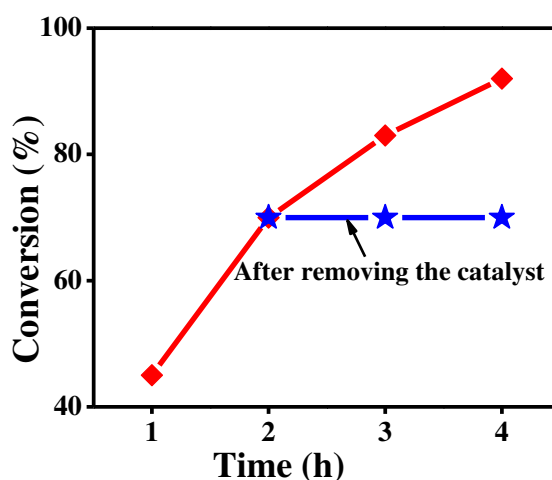


Figure 2.9. Formation of α -ketoamide as a function of time under standard conditions (red line) and removal of GO catalyst after 2 hour (blue line)

Thus, the oxygen functionality on GO surface acted as both acidic as well as oxidizing active sites for the coupling reaction. Low catalytic activity demonstrated by reduced GO also supported these results. Further, a control experiment was carried out to assess the role of trace Mn^{2+} ion that could be formed during oxidation of graphite to graphene oxide. The addition of MnSO_4 to the model coupling reaction of phenylglyoxal monohydrate and pyrrolidine did not have any influence on the reaction kinetics (entry 9, Table 2.2).^[63] Further, extraction of any metal impurity in GO through boiling in benzene and performing the model coupling reaction of phenylglyoxal monohydrate and pyrrolidine in the resultant benzene did not yield any product (entry 8, Table 2.2).^[44]

2.3 Conclusion

In conclusion, graphene oxide has been demonstrated as an efficient and heterogeneous carbocatalyst for the synthesis of α -ketoamides in high yields. The dual acidic and oxidizing catalytic activity of graphene oxide was instrumental in the C-N coupling reaction through a hemiaminal intermediate. Both primary and secondary amines were suitable for this transformation and could provide an attractive approach for the synthesis of biologically active compounds. A detailed mechanistic investigation, using graphene oxide modified under various conditions, such as base, acid and reducing agent treatment as well as annealing at variable temperature demonstrated the involvement of carboxylic acid functionality on the surface in catalyzing the cross-dehydrogenative C-N coupling reactions. The correlation between oxyfunctionalized groups on the layered two dimensional nanocarbon surface and activity could provide insights towards the development of carbonaceous catalytic systems for important coupling reactions.

2.4 Experimental Section

2.4.1 General Information

The powder XRD measurements were carried out by using a Bruker D8 Advance X-ray diffractometer with CuK α source (wavelength= 0.154 nm). TEM images were obtained by using a JEOL JEM- 2100 microscope operated at 200 kV. Atomic force microscopy was carried out by using an AIST-NT instrument (model SMART SPM 10000, Tapping mode), the samples were prepared by drop casting a water dispersion on mica. FTIR spectra were recorded with KBr pellets by using a Bruker Tensor 27 instrument. The zeta potential studies were done on a Micromeritics Nanoplus 3 instrument. XPS spectra were recorded by using an ESCA instrument, VSW of UK make. ^1H and ^{13}C NMR spectra were recorded with Bruker Advance (III) 400 MHz or 100 MHz spectrometers, respectively. Data for ^1H NMR spectra are reported as chemical shift (δ ppm), multiplicity (s=singlet, d = doublet, t = triplet, m = multiplet), coupling constant (J Hz) and integration and assignment data for ^{13}C NMR spectra are reported as a chemical

shift. High resolutions mass spectral analyses (HRMS) were carried out using ESI- TOF-MS.

2.4.2 Materials

Graphene oxide was synthesized from natural graphite by the modified hummer's method.⁵²

2.4.3 Reaction procedure for the synthesis of α -ketoamide

In a 10 mL Teflon sealed glass tube, 0.25 mmol α -carbonyl aldehyde, 0.375 mmol amine, 3.0 ml acetonitrile and 10 mg GO was taken and the mixture was heated at 50 °C for the specified time. After cooling, the catalyst was filtered, the crude reaction mixture was extracted with ethyl acetate and washed with 0.5 N HCL and NaHCO₃. The crude reaction mixture was further evaporated in reduced vaccum and purified by column chromatography using 5-10% ethyl acetate/hexane solvent system. For primary amines, 0.25 mmol of amine, 0.375 mmol α -carbonyl aldehyde, 2.0 equiv. DABCO, 30 mg GO, 100 mg molecular sieves (4 Å) and 3.0 mL toluene were mixed and heated in Teflon sealed glass tube at 90 °C.

2.4.4 Isolation of hemiaminal intermediate

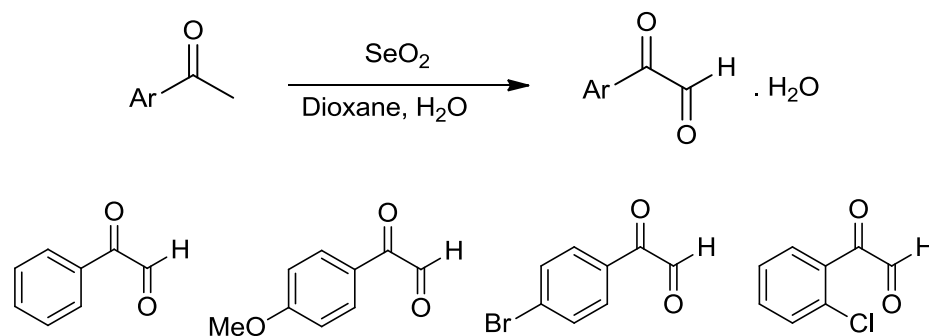
2-hydroxy-1-phenyl-2-(pyrrolidin-1-yl)ethanone (x). 30 mg GO, 1.0 mmol of phenylglyoxal monohydrate (152 mg) and 1.0 mmol pyrrolidine were mixed in CH₃CN solvent and stirred at 60 °C. The reaction was stopped after 0.5 hr and the organic compounds were extracted using ethyl acetate and water. The crude reaction mixture was dried over anhydrous Na₂SO₄ and the solvent was evaporated under reduced pressure. Finally, the hemiaminal intermediate was purified by column chromatography using 5-10% ethyl acetate/hexane solvent system in silica to give colourless solid.

2.4.6 HPLC analysis

A Dionex HPLC-Ultimate 3000 (High Performance Liquid Chromatography) pump was used to analyse products. 20 μL of sample was injected onto a Dionex Acclaim $\text{\textcircled{R}}$ 120 C18 column of 250 mm length with an internal diameter of 4.6 mm and 5 μm fused silica particles at a flow rate of 1 mL min^{-1} (linear gradient of 40 % v/v acetonitrile in water for 35 min, gradually rising to 100 % (v/v) acetonitrile in water at 35 min). This concentration was kept constant until 40 min when the gradient was decreased to 40 % (v/v) acetonitrile in water at 42 min. The sample preparation involved mixing of 100 μL reaction mixture in 900 μL acetonitrile-water (50: 50 mixture) solution containing 0.1 % trifluoroacetic acid. The samples were then filtered through a 0.45 μm syringe filter (Whatman, 150 units, 13 mm diameter, 2.7 mm pore size) prior to injection. The products were identified by using Ultimate 3000 RS Variable Wavelength Detector at 280 nm.

2.4.7 Preparation of arylglyoxal

All arylglyoxal substrates were prepared by a reported procedure.^[64]



2.4.8 Characterisation data

2.4.8.1 Characterization data for hemiaminal intermediate

2-hydroxy-1-phenyl-2-(pyrrolidin-1-yl)ethanone (x): ^1H NMR (CDCl_3 , 400 MHz): δ = 8.02 (d, J = 7.28 Hz, 1H), 7.86 (d, J = 7.28 Hz, 1H), 7.55-7.33 (m, 3H, OH), 5.91 (s, 1H), 3.55-3.05 (m, 4H), 2.07-1.80(m, 4H); ^{13}C NMR (CDCl_3 , 100 MHz): δ = 186.4, 135.1, 133.2, 131.2, 128.9, 128.2, 128.0, 127.6, 93.0, 48.9,

29.6, 25.6, 24.5. Mass: 205.2530, HRMS (ESI): calcd for $[\text{C}_{12}\text{H}_{15}\text{NO}_2^+ + \text{Na}^+]$ 228.0995, found 228.1017.

2.4.8.2 Characterization data for α -ketoamides

1-Phenyl-2-(pyrrolidin-1-yl)ethane-1,2-dione (3aa):²⁹ Yellow wax, ^1H NMR (CDCl_3 , 400 MHz): $\delta = 7.99$ (d, $J = 7.24$ Hz, 2H), 7.64-7.60 (t, $J = 7.28$ Hz, 1H), 7.51-7.47 (t, $J = 7.76$ Hz, 2H), 3.66-3.63 (t, $J = 6.52$ Hz, 2H), 3.43-3.40 (t, $J = 6.52$ Hz, 2H), 1.97-1.91 (m, 4H); ^{13}C NMR (CDCl_3 , 100 MHz): $\delta = 191.5$, 164.9, 134.5, 132.9, 129.8, 128.9, 46.6, 45.2, 25.9, 24.0. Mass: 203.2371, HRMS (ESI): calcd for $[\text{C}_{12}\text{H}_{13}\text{NO}_2^+ + \text{Na}^+]$ 226.0838, found 226.0849.

1-(4-bromophenyl)-2-(pyrrolidin-1-yl)ethane-1,2-dione (3ba):³⁰ Yellow gummy solid, ^1H NMR (CDCl_3 , 400 MHz): $\delta = 7.88$ (d, $J = 8.8$ Hz, 2H), 7.63 (d, $J = 8.4$ Hz, 2H), 3.64 (t, $J = 5.52$ Hz, 2H), 3.42 (t, $J = 5.28$ Hz, 2H), 1.95 (m, 4H); ^{13}C NMR (CDCl_3 , 100 MHz): $\delta = 190.2$, 164.1, 132.2, 131.7, 131.3, 130.0, 128.0, 127.6, 46.7, 45.3, 25.9, 23.9. Mass: 282.1332, HRMS (ESI): calcd for $[\text{C}_{12}\text{H}_{12}\text{BrNO}_2^+ + \text{Na}^+]$ 303.9944, found 303.9959.

1-phenyl-2-(piperidin-1-yl)ethane-1,2-dione (3ab):⁶⁵ Light yellow solid, m.p. 106-109 °C; ^1H NMR (CDCl_3 , 400 MHz): $\delta = 7.95$ (d, $J = 7.76$ Hz, 2H), 7.62 (t, $J = 7.24$ Hz, 1H), 7.50 (t, $J = 7.52$ Hz, 2H), 3.69 (br, 2H), 3.28 (t, $J = 5.28$ Hz, 2H), 1.69 (br, 4H), 1.54 (br, 2H); ^{13}C NMR (CDCl_3 , 100 MHz): $\delta = 191.0$, 165.1, 132.6, 132.3, 131.2, 130.4, 47.3, 42.5, 26.5, 25.7, 24.6. Mass: 217.2637, HRMS (ESI): calcd for $[\text{C}_{13}\text{H}_{15}\text{NO}_2^+ + \text{Na}^+]$ 240.0995, found 240.1006.

1-(4-bromophenyl)-2-(piperidin-1-yl)ethane-1,2-dione (3bb):⁶⁶ Yellow oil, ^1H NMR (CDCl_3 , 400 MHz): $\delta = 7.81$ (d, $J = 8.52$ Hz, 2H), 7.65 (d, $J = 8.52$ Hz, 2H), 3.68 (t, $J = 4.24$ Hz, 2H), 3.27 (t, $J = 5.76$ Hz, 2H), 1.69-1.66 (m, 4H), 1.57-1.51 (m, 2H); ^{13}C NMR (CDCl_3 , 100 MHz): $\delta = 190.6$, 164.8, 132.3, 132.0, 130.9, 130.1, 47.0, 42.2, 26.2, 25.4, 24.3. Mass: 296.1598, HRMS (ESI): calcd for $[\text{C}_{13}\text{H}_{14}\text{BrNO}_2^+ + \text{Na}^+]$ 318.0100, found 318.0122.

1-(4-methoxyphenyl)-2-(piperidin-1-yl)ethane-1,2-dione (3cb):⁶⁶ Yellow wax, ^1H NMR (CDCl_3 , 400 MHz): $\delta = 7.91$ (d, $J = 8.8$ Hz, 2H), 6.97 (d, $J = 8.76$ Hz, 2H), 3.87 (s, 3H), 3.69-3.67 (m, 2H), 3.29-3.26 (m, 2H), 1.68-1.67 (m, 4H), 1.55-

1.51 (m, 2H); ^{13}C NMR (CDCl_3 , 100 MHz): $\delta = 190.6, 165.7, 164.7, 131.9, 126.3, 114.2, 55.5, 47.0, 42.0, 26.1, 25.4, 24.3$. Mass: 247.2897, HRMS (ESI): calcd for $[\text{C}_{14}\text{H}_{17}\text{NO}_3^+ + \text{Na}^+]$ 270.1101, found 270.1115.

1-morpholino-2-phenylethane-1,2-dione (3ac):³⁰ Yellow liquid, ^1H NMR (CDCl_3 , 400 MHz): $\delta = 7.96$ (d, $J = 7.0$ Hz, 2H), 7.65 (t, $J = 7.56$ Hz, 1H), 7.51 (t, $J = 7.52$ Hz, 2H), 3.78 (s, 4H), 3.65 (t, $J = 4.8$ Hz, 2H), 3.37 (t, $J = 4.52$ Hz, 2H); ^{13}C NMR (CDCl_3 , 100 MHz): $\delta = 191.1, 165.4, 134.9, 133.0, 129.6, 129.0, 66.7, 66.6, 46.2, 41.6$. Mass: 219.2365, HRMS (ESI): calcd for $[\text{C}_{12}\text{H}_{13}\text{NO}_3^+ + \text{Na}^+]$ 242.0788, found 242.0799.

1-(4-bromophenyl)-2-morpholinoethane-1,2-dione (3bc):⁶⁵ Yellow gummy solid, ^1H NMR (CDCl_3 , 400 MHz): $\delta = 7.83$ (d, $J = 8.52$ Hz, 2H), 7.67 (d, $J = 8.52$ Hz, 2H), 3.80-3.75 (br, 4H), 3.65 (t, $J = 5.00$ Hz, 2H), 3.37 (t, $J = 4.52$ Hz, 2H); ^{13}C NMR (CDCl_3 , 100 MHz): $\delta = 189.8, 164.8, 132.4, 131.8, 131.0, 130.4, 66.7, 66.6, 46.2, 41.7$. Mass: 298.1326, HRMS (ESI): calcd for $[\text{C}_{12}\text{H}_{12}\text{BrNO}_3^+ + \text{Na}^+]$ 319.9893, found 319.9910.

1-(4-methoxyphenyl)-2-morpholinoethane-1,2-dione (3cc):⁶⁵ Yellow oil, ^1H NMR (CDCl_3 , 400 MHz): $\delta = 7.93$ (d, $J = 8.76$ Hz, 2H), 6.98 (d, $J = 9.04$ Hz, 2H), 3.88 (s, 3H), 3.77 (br, 4H), 3.64 (t, $J = 5.0$ Hz, 2H), 3.37 (t, $J = 4.76$ Hz, 2H); ^{13}C NMR (CDCl_3 , 100 MHz): $\delta = 190.6, 165.7, 164.7, 132.0, 126.3, 114.2, 55.6, 47.0, 42.0$. Mass: 249.2625, HRMS (ESI): calcd for $[\text{C}_{13}\text{H}_{15}\text{NO}_4^+ + \text{Na}^+]$ 272.0893, found 272.0899.

1-(4-methylpiperazin-1-yl)-2-phenylethane-1,2-dione (3ad):³⁰ Yellow gummy solid, ^1H NMR (CDCl_3 , 400 MHz): $\delta = 7.95$ (d, $J = 8.04$ Hz, 2H), 7.64 (t, $J = 7.28$ Hz, 1H), 7.52 (d, $J = 7.0$ Hz, 2H), 3.82-3.76 (m, 2H), 3.39-3.34 (m, 2H), 2.54-2.49 (m, 2H), 2.40-2.35 (m, 2H), 2.31 (s, 3H); ^{13}C NMR (CDCl_3 , 100 MHz): $\delta = 191.4, 165.3, 134.7, 133.0, 129.6, 128.9, 54.8, 54.3, 45.8, 45.6, 41.0$. Mass: 232.2783, HRMS (ESI): calcd for $[\text{C}_{13}\text{H}_{16}\text{N}_2\text{O}_2^+ + \text{Na}^+]$ 255.1104, found 255.1126

1-(4-bromophenyl)-2-(4-methylpiperazin-1-yl)ethane-1,2-dione (3bd):⁶⁵ Yellow gummy solid, ^1H NMR (CDCl_3 , 400 MHz): $\delta = 7.82$ (d, $J = 7.76$ Hz, 2H), 7.66 (d, $J = 8.04$ Hz, 2H), 3.80-3.75 (m, 2H), 3.39-3.34 (m, 2H), 2.53-2.47 (m,

Chapter 2

2H), 2.40-2.35 (m, 2H), 2.31 (s, 3H); ^{13}C NMR (CDCl_3 , 100 MHz): $\delta = 190.1$, 164.7, 132.4, 131.9, 131.0, 130.3, 128.0, 127.6, 54.8, 54.3, 45.9, 45.7, 41.1. Mass: 311.1744, HRMS (ESI): calcd for $[\text{C}_{13}\text{H}_{15}\text{BrN}_2\text{O}_2^+ + \text{Na}^+]$ 333.0209, found 333.0230.

2-(2-chlorophenyl)-*N*, *N*-diethyl-2-oxoacetamide (3ae):⁶⁸ Colourless gummy solid, ^1H NMR (CDCl_3 , 400 MHz): $\delta = 7.88$ (d, $J = 7.28$ Hz, 1H), 7.48 (t, $J = 8.0$ Hz, 1H), 7.43-7.36 (m, 2H), 3.53-3.48 (q, 2H), 3.37-3.32 (q, 2H), 1.53 (br, 6H). Mass: 239.6981, HRMS (ESI): calcd for $[\text{C}_{12}\text{H}_{14}\text{ClNO}_2^+ + \text{Na}^+]$ 262.0605, found 262.0627.

1-(2-chlorophenyl)-2-(pyrrolidin-1-yl)ethane-1,2-dione (3da):⁶⁹ Yellow gummy solid, ^1H NMR (CDCl_3 , 400 MHz): $\delta = 7.83$ (d, $J = 8.04$ Hz, 1H), 7.48 (t, $J = 7.04$ Hz, 1H), 7.42-7.36 (m, 2H), 3.59 (br, 4H), 1.97 (br, 4H); ^{13}C NMR (CDCl_3 , 100 MHz): $\delta = 190.7$, 164.4, 133.9, 132.0, 130.5, 127.2, 46.8, 45.7, 25.8, 23.9. Mass: 237.6822, HRMS (ESI): calcd for $[\text{C}_{12}\text{H}_{12}\text{ClNO}_2^+ + \text{Na}^+]$ 260.0449, found 260.0467.

1-(2-chlorophenyl)-2-(piperidin-1-yl)ethane-1,2-dione (3db):⁷⁰ Yellow gummy solid, ^1H NMR (CDCl_3 , 400 MHz): $\delta = 7.88$ (d, $J = 7.52$ Hz, 1H), 7.48 (t, $J = 7.28$ Hz, 1H), 7.43-7.36 (m, 2H), 3.64 (br, 2H), 3.41 (br, 2H), 1.68-1.58 (br, 6H); ^{13}C NMR (CDCl_3 , 100 MHz): $\delta = 190.0$, 165.3, 134.2, 133.8, 133.2, 132.3, 130.8, 127.2, 46.9, 42.4, 25.5, 25.0, 24.4. Mass: 251.0713, HRMS (ESI): calcd for $[\text{C}_{13}\text{H}_{14}\text{ClNO}_2^+ + \text{Na}^+]$ 274.0605, found 274.0628.

***N*-butyl-2-(2-chlorophenyl)-2-oxoacetamide (3dc):**⁶⁷ Yellow liquid, ^1H NMR (CDCl_3 , 400 MHz): $\delta = 7.67$ (d, $J = 7.04$ Hz, 1H), 7.44-7.33 (m, 3H), 6.94 (br, 1H), 3.41-3.36 (m, 2H), 1.63-1.58 (m, 2H), 1.45-1.36 (m, 2H), 0.97-0.93 (m, 3H). Mass: 239.6981, HRMS (ESI): calcd for $[\text{C}_{12}\text{H}_{14}\text{ClNO}_2^+ + \text{Na}^+]$ 262.0605, found 262.0618.

***N*-(4-cyanophenyl)-2-oxo-2-phenylacetamide (4aa):**²⁹ Colourless solid, ^1H NMR (CDCl_3 , 400 MHz): $\delta = 9.14$ (br, 1H), 8.42 (d, $J = 8.0$ Hz, 2H), 7.85 (d, $J = 8.8$ Hz, 2H), 7.70-7.66 (m, 3H), 7.52 (t, $J = 8.0$ Hz, 2H); ^{13}C NMR (CDCl_3 , 100 MHz): $\delta = 186.3$, 158.8, 140.5, 135.0, 133.4, 132.6, 131.5, 128.7, 119.9, 118.5,

108.4. Mass: 250.2521, HRMS (ESI): calcd for $[\text{C}_{15}\text{H}_{10}\text{N}_2\text{O}_2^+ + \text{Na}^+]$ 273.0634, found 273.0651.

***N*-(2-cyanophenyl)-2-oxo-2-phenylacetamide (4ab):**²⁹ Yellow solid, ¹H NMR (CDCl₃, 400 MHz): $\delta = 9.53$ (br, 1H), 8.52 (d, $J = 8.04$ Hz, 1H), 8.43 (d, $J = 7.28$ Hz, 2H), 7.69-7.65 (m, 3H), 7.52 (t, $J = 8.04$ Hz, 2H), 7.27 (t, $J = 7.52$ Hz, 1H); ¹³C NMR (CDCl₃, 100 MHz): $\delta = 185.8, 158.9, 139.0, 134.9, 134.1, 132.7, 132.6, 131.5, 128.6, 125.2, 120.9, 115.7, 103.3$. Mass: 250.2521, HRMS (ESI): calcd for $[\text{C}_{15}\text{H}_{10}\text{N}_2\text{O}_2^+ + \text{Na}^+]$ 273.0634, found 273.0655.

***N*-(4-nitrophenyl)-2-oxo-2-phenylacetamide (4ac):**²⁹ Yellow solid, m.p. 202-205 °C; ¹H NMR (CDCl₃, 400 MHz): $\delta = 9.25$ (br, 1H), 8.43 (d, $J = 7.8$ Hz, 2H), 8.30 (d, $J = 9.04$ Hz, 2H), 7.90 (d, $J = 8.52$ Hz, 2H), 7.69 (t, $J = 7.28$ Hz, 1H), 7.53 (t, $J = 7.28$ Hz, 2H); ¹³C NMR (CDCl₃, 100 MHz): $\delta = 186.2, 158.8, 144.3, 142.2, 135.1, 132.5, 131.5, 128.7, 125.2, 119.5$. Mass: 270.2402, HRMS (ESI): calcd for $[\text{C}_{14}\text{H}_{10}\text{N}_2\text{O}_4^+ + \text{Na}^+]$ 293.0533, found 293.0545.

***N*-(2-nitrophenyl)-2-oxo-2-phenylacetamide (4ad):** Yellow solid, ¹H NMR (CDCl₃, 400 MHz): $\delta = 11.86$ (br, 1H), 8.90 (d, $J = 8.52$ Hz, 1H), 8.41 (d, $J = 7.8$ Hz, 2H), 8.31 (d, $J = 8.52$ Hz, 1H), 7.73 (t, $J = 7.24$ Hz, 1H), 7.67 (t, $J = 7.52$ Hz, 1H), 7.52 (t, $J = 7.76$ Hz, 2H), 7.29 (t, $J = 7.52$ Hz, 1H); ¹³C NMR (CDCl₃, 100 MHz): $\delta = 186.0, 159.8, 137.2, 135.8, 134.8, 133.3, 132.7, 131.4, 128.6, 126.1, 124.4, 121.9$. Mass: 270.2402, HRMS (ESI): calcd for $[\text{C}_{14}\text{H}_{10}\text{N}_2\text{O}_4^+ + \text{Na}^+]$ 293.0533, found 293.0542.

***N*-(4-chloro-2-cyanophenyl)-2-oxo-2-phenylacetamide (4ae):** Colourless solid, ¹H NMR (CDCl₃, 400 MHz): $\delta = 9.56$ (br, 1H), 8.52 (t, $J = 8.04$ Hz, 1H), 8.42 (t, $J = 8.28$ Hz, 2H), 7.72-7.62 (m, 3H), 7.57-7.51 (m, 2H); ¹³C NMR (CDCl₃, 100 MHz): $\delta = 185.5, 158.8, 137.7, 135.1, 134.4, 132.4, 132.0, 131.5, 130.4, 128.7, 122.1, 104.6$. Mass: 284.6972, HRMS (ESI): calcd for $[\text{C}_{15}\text{H}_9\text{ClN}_2\text{O}_2^+ + \text{Na}^+]$ 307.0245, found 307.0258.

***N*-(4-chlorophenyl)-2-oxo-2-phenylacetamide (4af):**²⁹ Yellow solid, ¹H NMR (CDCl₃, 400 MHz): $\delta = 8.95$ (br, 1H), 8.42 (d, $J = 8.04$ Hz, 2H), 7.68-7.64 (m, 3H), 7.51 (t, $J = 7.52$ Hz, 2H), 7.37 (d, $J = 8.76$ Hz, 2H); ¹³C NMR (CDCl₃, 100 MHz): $\delta = 187.0, 158.7, 135.2, 134.7, 132.9, 131.4, 130.4, 129.3, 128.6, 121.1$.

Chapter 2

Mass: 259.6877, HRMS (ESI): calcd for $[\text{C}_{14}\text{H}_{10}\text{ClNO}_2^+ + \text{Na}^+]$ 282.0292, found 282.0299.

***N*-(4-bromophenyl)-2-oxo-2-phenylacetamide (4ag):**²⁹ Yellow solid, ^1H NMR (CDCl_3 , 400 MHz): $\delta = 8.95$ (br, 1H), 8.41 (d, $J = 7.8$ Hz, 2H), 7.66 (t, $J = 7.24$ Hz, 1H), 7.61 (d, $J = 8.52$ Hz, 2H), 7.53-7.49 (m, 4H); ^{13}C NMR (CDCl_3 , 100 MHz): $\delta = 186.9, 158.7, 135.6, 134.7, 132.9, 132.2, 131.4, 128.6, 121.4, 118.0$. Mass: 304.1387, HRMS (ESI): calcd for $[\text{C}_{14}\text{H}_{10}\text{BrNO}_2^+ + \text{Na}^+]$ 325.9787, found 325.9799.

***N*-(3-(benzyloxy)phenyl)-2-oxo-2-phenylacetamide (4ah):** Yellow gummy solid, ^1H NMR (CDCl_3 , 400 MHz): $\delta = 8.91$ (br, 1H), 8.41 (d, $J = 7.8$ Hz, 2H), 7.65 (t, $J = 7.24$ Hz, 1H), 7.55 (s, 1H), 7.51 (t, $J = 7.76$ Hz, 2H), 7.46 (d, $J = 7.28$ Hz, 1H), 7.38 (t, $J = 7.52$ Hz, 2H), 7.34 (d, $J = 6.76$ Hz, 1H), 7.28 (t, $J = 8.04$ Hz, 2H), 7.17 (d, $J = 7.52$ Hz, 1H), 6.82 (d, $J = 6.04$ Hz, 1H), 5.10 (s, 2H); ^{13}C NMR (CDCl_3 , 100 MHz): $\delta = 187.3, 159.4, 158.8, 137.7, 136.7, 134.6, 134.4, 133.6, 133.0, 131.4, 129.9, 128.7, 128.5, 128.1, 128.0, 127.6, 127.5, 112.4, 112.1, 106.4, 70.0$. Mass: 331.3646, HRMS (ESI): calcd for $[\text{C}_{21}\text{H}_{17}\text{NO}_3^+ + \text{Na}^+]$ 354.1101, found 354.1115.

***N*-methyl-2-oxo-*N*, 2-diphenylacetamide (4ai):**²⁷ Yellow wax, ^1H NMR (CDCl_3 , 400 MHz): $\delta = 7.85$ (d, $J = 7.76$ Hz, 2H), 7.56 (t, $J = 7.52$ Hz, 1H), 7.42 (t, $J = 7.8$ Hz, 2H), 7.23-7.19 (m, 3H), 7.13 (d, $J = 7.28$ Hz, 2H), 3.48 (s, 3H); ^{13}C NMR (CDCl_3 , 100 MHz): $\delta = 190.7, 167.0, 141.1, 134.2, 133.5, 129.5, 129.3, 128.7, 128.0, 126.7, 36.2$. Mass: 239.2692, HRMS (ESI): calcd for $[\text{C}_{15}\text{H}_{13}\text{NO}_2^+ + \text{Na}^+]$ 262.0838, found 262.0845.

2-(4-bromophenyl)-*N*-(4-cyanophenyl)-2-oxoacetamide (4ba):²⁷ Yellow solid, ^1H NMR (DMSO-d_6 , 400 MHz): $\delta = 11.36$ (br, 1H), 8.03 (d, $J = 8.52$ Hz, 2H), 7.97 (d, $J = 8.8$ Hz, 2H), 7.88 (d, $J = 8.56$ Hz, 2H), 7.85 (d, $J = 8.56$ Hz, 2H); ^{13}C NMR (DMSO-d_6 , 100 MHz): $\delta = 187.5, 166.9, 162.7, 141.8, 133.3, 132.1, 132.0, 131.5, 131.4, 129.2, 128.1, 127.3, 125.7, 120.3, 106.5$. Mass: 329.1482, HRMS (ESI): calcd for $[\text{C}_{15}\text{H}_9\text{BrN}_2\text{O}_2^+ + \text{Na}^+]$ 350.9740, found 350.9758.

2-(4-bromophenyl)-N-(4-nitrophenyl)-2-oxoacetamide (4bc): Yellow liquid, ^1H NMR (CDCl_3 , 400 MHz): $\delta = 9.24$ (br, 1H), 8.34 (d, $J = 8.28$ Hz, 2H), 8.30 (d, $J = 9.04$ Hz, 2H), 7.89 (d, $J = 9.04$ Hz, 2H), 7.69 (d, $J = 8.76$ Hz, 2H); ^{13}C NMR (CDCl_3 , 100 MHz): $\delta = 187.3, 162.7, 143.6, 143.2, 132.1, 132.0, 131.4, 129.2, 124.9, 120.1$. Mass: 349.1363, HRMS (ESI): calcd for $[\text{C}_{14}\text{H}_9\text{BrN}_2\text{O}_4^+ + \text{Na}^+]$ 370.9638, found 370.9657.

2-(4-bromophenyl)-N-(2-nitrophenyl)-2-oxoacetamide (4bd): Yellow liquid, ^1H NMR (CDCl_3 , 400 MHz): $\delta = 11.88$ (br, 1H), 8.88 (d, $J = 8.28$ Hz, 1H), 8.32 (d, $J = 8.52$ Hz, 3H), 7.73 (t, $J = 8.52$ Hz, 1H), 7.68 (d, $J = 8.52$ Hz, 2H), 7.30 (t, $J = 8.28$ Hz, 1H); ^{13}C NMR (CDCl_3 , 100 MHz): $\delta = 185.0, 159.5, 135.8, 133.2, 132.8, 132.0, 131.5, 130.7, 126.1, 124.6, 121.9$. Mass: 349.1363, HRMS (ESI): calcd for $[\text{C}_{14}\text{H}_9\text{BrN}_2\text{O}_4^+ + \text{Na}^+]$ 370.9638, found 370.9653.

2-(4-bromophenyl)-N-(4-chloro-2-cyanophenyl)-2-oxoacetamide (4be): Yellow solid, ^1H NMR (CDCl_3 , 400 MHz): $\delta = 9.55$ (br, 1H), 8.49 (d, $J = 7.56$ Hz, 1H), 8.33 (d, $J = 8.8$ Hz, 2H), 7.68-7.60 (m, 4H). Mass: 363.5932, HRMS (ESI): calcd for $[\text{C}_{15}\text{H}_8\text{BrClN}_2\text{O}_2^+ + \text{Na}^+]$ 384.9350, found 384.9361.

N-(4-cyanophenyl)-2-(4-methoxyphenyl)-2-oxoacetamide (4ca):²⁹ Yellow solid, ^1H NMR (CDCl_3 , 400 MHz): $\delta = 9.22$ (br, 1H), 8.50 (d, $J = 9.00$ Hz, 2H), 7.83 (d, $J = 8.76$ Hz, 2H), 7.69 (d, $J = 8.56$ Hz, 2H), 6.99 (d, $J = 9.04$ Hz, 2H), 3.91 (s, 3H); ^{13}C NMR (CDCl_3 , 100 MHz): $\delta = 187.1, 164.6, 163.9, 141.9, 133.3, 132.6, 125.0, 120.2, 118.8, 114.5, 106.3, 55.8$. Mass: 380.2781, HRMS (ESI): calcd for $[\text{C}_{16}\text{H}_{12}\text{N}_2\text{O}_3^+ + \text{Na}^+]$ 303.0740, found 303.0762.

2-(3-bromophenyl)-N-(4-cyanophenyl)-2-oxoacetamide (4da): Yellow solid, ^1H NMR (CDCl_3 , 400 MHz): $\delta = 9.12$ (br, 1H), 8.54 (s, 1H), 8.39 (d, $J = 7.8$ Hz, 1H), 7.84-7.79 (m, 3H), 7.70 (d, $J = 8.8$ Hz, 2H), 7.41 (t, $J = 8.0$ Hz, 1H); ^{13}C NMR (CDCl_3 , 100 MHz): $\delta = 185.1, 158.3, 140.2, 137.8, 134.2, 133.4, 130.2, 130.1, 122.8, 119.9, 118.4, 108.6$; Mass: 329.1482, HRMS (ESI): calcd for $[\text{C}_{15}\text{H}_9\text{BrN}_2\text{O}_2^+ + \text{Na}^+]$ 350.9740, found 350.9749.

N-(3,4-dimethylphenyl)-2-oxo-2-phenyl-N-(4-(trifluoromethyl)phenethyl)acetamide (I):²⁷ Yellow wax, ^1H NMR (CDCl_3 , 400 MHz): $\delta = 7.63$ (s, 1H), 7.53 (d, $J = 7.04$ Hz, 2H), 7.36 (d, $J = 7.28$ Hz, 2H),

Chapter 2

7.22-7.15 (m, 4H), 7.08 (m, 2H), 6.50 (s, 1H), 4.44 (s, 1H), 3.70-3.63 (m, 1H), 3.23 (s, 1H), 3.04 (s, 1H), 2.19 (s, 3H), 2.12 (s, 3H); ^{13}C NMR (CDCl_3 , 100 MHz): $\delta = 188.3, 167.4, 138.28, 138.27, 136.9, 134.7, 132.8, 129.6, 129.4, 125.65, 125.61, 125.57, 125.54, 125.0, 121.0, 117.1, 44.0, 33.6, 19.4, 18.8$. Mass: 425.4429, HRMS (ESI): calcd for $[\text{C}_{25}\text{H}_{22}\text{F}_3\text{NO}_2^+ + \text{Na}^+]$ 448.1495, found 448.151.

***N*-(3,4-dimethylphenyl)-2-(4-(trifluoromethyl)phenyl)acetamide (A):**²⁷ Brown solid, ^1H NMR (CDCl_3 , 400 MHz): $\delta = 7.64$ (d, $J = 7.76$ Hz, 2H), 7.47 (d, $J = 7.8$ Hz, 2H), 7.21 (s, 1H), 7.15 (d, $J = 7.52$ Hz, 1H), 7.04 (d, $J = 7.56$ Hz, 1H), 6.93 (br, 1H), 3.75 (s, 2H), 2.20 (s, 3H), 2.19 (s, 3H); ^{13}C NMR (CDCl_3 , 100 MHz): $\delta = 167.7, 138.5, 137.2, 135.0, 133.1, 129.9, 129.7, 125.9, 125.8, 121.3, 117.4, 44.3, 19.8, 19.1$. Mass: 307.3102, HRMS (ESI): calcd for $[\text{C}_{17}\text{H}_{16}\text{F}_3\text{NO}^+ + \text{Na}^+]$ 330.1076, found 330.1082.

3,4-dimethyl-*N*-(4-(trifluoromethyl)phenethyl)aniline (6):²⁷ Yellow liquid, ^1H NMR (CDCl_3 , 400 MHz): $\delta = 7.56$ (d, $J = 7.8$ Hz, 2H), 7.32 (d, $J = 7.76$ Hz, 2H), 6.95 (d, $J = 7.8$ Hz, 1H), 6.45 (s, 1H), 6.42 (d, $J = 7.8$ Hz, 1H), 3.39 (t, $J = 7.0$ Hz, 2H), 2.95 (t, $J = 6.76$ Hz, 2H), 2.18 (s, 3H), 2.15 (s, 3H); ^{13}C NMR (CDCl_3 , 100 MHz): $\delta = 145.6, 143.6, 137.4, 130.3, 129.1, 125.9, 125.50, 125.46, 125.42, 125.38, 115.0, 110.6, 45.2, 35.4, 20.0, 18.6$. Mass: 293.3267, HRMS (ESI): calcd for $[\text{C}_{17}\text{H}_{18}\text{F}_3\text{N} + \text{H}^+]$ 294.1464, found 294.1480.

2.5 References

1. Bariwal J., Eycken E. V. D. (2013), C–N bond forming cross-coupling reactions: an overview, *Chem. Soc. Rev.*, 42, 9283-9303 (DOI: 10.1039/c3cs60228a)
2. Beccalli E. M., Broggini G., Martinelli M., Sottocornola S. (2007), C-C, C-O, C-N bond formation on sp^2 carbon by Pd(II)-catalyzed reactions involving oxidant agents, *Chem. Rev.*, 107, 5318–5365 (DOI: 10.1021/cr068006f)

Chapter 2

- Lyons T. W., Sanford M. S. (2010), Palladium-catalyzed ligand-directed C-H functionalization reactions, *Chem. Rev.*, 110, 1147–1169 (DOI: 10.1021/cr900184e)
- Li Z., Bohle D. S., Li C. –J. (2006), Cu-catalyzed cross-dehydrogenative coupling: A versatile strategy for C-C bond formations via the oxidative activation of sp^3 C-H bonds, *Proc. Natl. Acad. Sci. USA*, 103, 8928–8933 (DOI: 10.1073/pnas.0601687103)
- Wu K., Huang Z., Qi X., Li Y., Zhang G., Liu C., Yi H., Meng L., Bunel E. E., Miller J. T., Pao C. –W., Lee J. –F., Lan Y., Lei A. (2015), Copper-catalyzed aerobic oxidative coupling: From ketone and diamine to pyrazine, *Sci. Adv.*, 1, e1500656 (DOI: 10.1126/sciadv.1500656)
- Sun C. –L., Shi Z. –J. (2014), Transition-metal-free coupling reactions, *Chem. Rev.*, 114, 9219–9280 (DOI: 10.1021/cr400274j)
- Davies H. M. L., Long M. S. (2005), Recent advances in catalytic intramolecular C-H aminations, *Angew. Chem. Int. Ed.*, 44, 3518 –3520 (DOI: 10.1002/anie.200500554)
- Collet F., Dodd R. H., Dauban P. (2009), Catalytic C-H amination: recent progress and future directions, *Chem. Commun.*, 5061–5074 (DOI: 10.1039/b905820f)
- Espino C. G., Wehn P. M., Chow J., Bois J. D. (2001), Synthesis of 1,3-difunctionalized amine derivatives through selective C-H bond oxidation, *J. Am. Chem. Soc.*, 123, 6935–6936 (DOI: 10.1021/ja011033x)
- Liu X., Zhang Y., Wang L., Fu H., Jiang Y., Zhao Y. (2008), General and efficient copper-catalyzed amidation of saturated C-H bonds using *N*-Halosuccinimides as the oxidants, *J. Org. Chem.*, 73, 6207–6212 (DOI: 10.1021/jo800624m)
- Evans R. W., Zbieg J. R., Zhu S., Li W., Macmillan D. W. C. (2013), Simple catalytic mechanism for the direct coupling of α -carbonyls with functionalized amines: A one-step synthesis of plavix, *J. Am. Chem. Soc.*, 135, 16074–16077 (DOI: 10.1021/ja4096472)

Chapter 2

12. Sun C.-L., Li B.-J., Shi Z.-J. (2010), Pd-catalyzed oxidative coupling with organometallic reagents *via* C-H activation, *Chem. Commun.*, 46, 677–685 (DOI: 10.1039/b908581e)
13. Liu C., Zhang H., Shi W., Lei A. (2011), Bond formations between two nucleophiles: Transition metal catalyzed oxidative cross-coupling reactions, *Chem. Rev.*, 111, 1780-1824 (DOI: 10.1021/cr100379j)
14. Li C. -J. (2009), Cross-dehydrogenative coupling (CDC): Exploring C-C bond formations beyond functional group transformations, *Acc. Chem. Res.*, 42, 335-344 (DOI: 10.1021/ar800164n)
15. Yeung C. S., Dong V. M. (2011), Catalytic dehydrogenative cross-coupling: Forming carbon-carbon bonds by oxidizing two carbon-hydrogen bonds, *Chem. Rev.*, 111, 1215-1292 (DOI: 10.1021/cr100280d)
16. Liu Y., Ge H. (2017), Site-selective C-H arylation of primary aliphatic amines enabled by a catalytic transient directing group, *Nature Chem.*, 9, 26-32 (DOI: 10.1038/nchem.2606)
17. Knust, H.; Nettekoven, M.; Pinard, E.; Roche, O.; Rogers- Evans, M. (2009), Monoamide derivatives as orexin receptor antagonists, *PCT Int. Appl. WO 2009016087*.
18. Crowley, C. A.; Delaet, N. G. J.; Ernst, J.; Grove, C. G.; Hepburn, B.; King, B.; Larson, C. J.; Miller, S.; Pryor, K.; Shuster, L. J. (2007), Therapy using cytokine inhibitors, *PCT Int. Appl. WO 2007146712*.
19. Álvarez S., Álvarez R., Khanwalkar H., Germain P., Lemaire G., Rodríguez-Barrios F., Gronemeyer H., de Lera A. R. (2009), Retinoid receptor subtype-selective modulators through synthetic modifications of RAR γ agonists, *Bioorg. Med. Chem.*, 17, 4345-4359 (DOI: 10.1016/j.bmc.2009.05.035)
20. Aavula, B. R.; Anandan, S. K.; Gless, R. D. J.; Patel, D. V.; Webb, H. H. K. (2008), Soluble epoxide hydrolase inhibitors, *PCT Int. Appl. WO 2008073623*

Chapter 2

21. Tanaka H., Kuroda A., Marusawa H., Hatanaka H., Kino T., Goto T., Hashimoto M., Taga, T. (1987), Structure of FK506, a novel immunosuppressant isolated from streptomyces, *J. Am. Chem. Soc.*, 109, 5031-5033 (DOI: 10.1021/ja00250a050)
22. Jesuraj J. L., Sivaguru J. (2010), Photo chemical type II reaction of atropchiral benzoylformamides to point chiral oxazolidin-4-ones. Axial chiral memory leading to enantiomeric resolution of photoproducts, *Chem. Commun.*, 46, 4791-4793 (DOI: 10.1039/c0cc00470g)
23. Qian J., Cuerrier D., Davies P. L., Li Z., Powers J. C., Campbell R. L. (2008), Cocrystal structures of primed side-extending α -ketoamide inhibitors reveal novel calpain-inhibitor aromatic interactions, *J. Med. Chem.*, 51, 5264-5270 (DOI: 10.1021/jm800045t)
24. Tomita D., Yamatsugu K., Kanai M., Shibasaki M. (2009), Enantioselective synthesis of SM-130686 based on the development of asymmetric Cu(I)F catalysis to access 2-oxindoles containing a tetrasubstituted carbon, *J. Am. Chem. Soc.*, 131, 6946-6948 (DOI: 10.1021/ja901995a)
25. Yang L., Wang D. -X., Huang Z. -T., Wang M. -X. (2009), Cr(III)(salen)Cl catalyzed enantioselective intramolecular addition of tertiary enamides to ketones: A general access to enantioenriched 1*H*-Pyrrol-2(3*H*)-one derivatives bearing a hydroxylated quaternary carbon atom, *J. Am. Chem. Soc.*, 131, 10390-10391 (DOI: 10.1021/ja904534t)
26. Zhang C., Jiao N. (2010), Dioxygen activation under ambient conditions: Cu-catalyzed oxidative amidation-diketonization of terminal alkynes leading to α -ketoamides, *J. Am. Chem. Soc.*, 132, 28-29 (DOI: 10.1021/ja908911n)
27. Zhang C., Xu Z., Zhang L., Jiao N. (2011), Copper-catalyzed aerobic oxidative coupling of aryl acetaldehydes with anilines leading to α -ketoamides, *Angew. Chem. Int. Ed.*, 50, 11088-11092 (DOI: 10.1002/anie.201105285)

Chapter 2

28. Du F. -T., Ji J. -X. (2012), Copper-catalyzed direct oxidative synthesis of α -ketoamides from aryl methyl ketones, amines and molecular oxygen, *Chem. Sci.*, 3, 460-465 (DOI: 10.1039/c1sc00312g)
29. Zhang C., Zong X., Zhang L., Jiao N. (2012), Copper-catalyzed aerobic oxidative cross-dehydrogenative coupling of amine and α -carbonyl aldehyde: A practical and efficient approach to α -ketoamides with wide substrate scope, *Org. Lett.*, 14, 3280-3283 (DOI: 10.1021/ol301130u)
30. Mupparapu N., Khan S., Battula S., Kushwaha M., Gupta A. P., Ahmed Q. N., Vishwakarma R. A. (2014), Metal-free oxidative amidation of 2-oxoaldehydes: A facile access to α -ketoamides, *Org. Lett.*, 16, 1152–1155 (DOI: 10.1021/ol5000204)
31. Yu H., Peng F., Tan J., Hu X., Wang H., Yang J., Zheng W. (2011), Selective catalysis of the aerobic oxidation of cyclohexane in the liquid phase by carbon nanotubes, *Angew. Chem. Int. Ed.*, 50, 3978-3982 (DOI: 10.1002/anie.201007932)
32. Wen G., Wu S., Li B., Dai C., Su D. S. (2015), Active sites and mechanisms for direct oxidation of benzene to phenol over carbon catalysts, *Angew. Chem. Int. Ed.*, 54, 4105-4109 (DOI: 10.1002/anie.201410093)
33. Zhang J., Su D., Zhang A., Wang D., Schlögl R., Hébert C. (2007), Nanocarbon as robust catalyst: Mechanistic insight into carbon mediated catalysis, *Angew. Chem. Int. Ed.*, 46, 7319-7323 (DOI: 10.1002/anie.200702466)
34. Su D. S., Wen G., Wu S., Peng F., Schlögl R. (2017), Carbocatalysis in liquid-phase reactions, *Angew. Chem. Int. Ed.*, 56, 936-964 (DOI: 10.1002/anie.201600906)
35. Dreyer D. R., Bielawski C. W. (2011), Carbocatalysis: Heterogeneous carbons finding utility in synthetic chemistry, *Chem. Sci.*, 2, 1233–1240 (DOI: 10.1039/c1sc00035g)
36. Machado B. F., Serp P. (2012), Graphene-based materials for catalysis, *Catal. Sci. Technol.*, 2, 54–75 (DOI: 10.1039/c1cy00361e)

Chapter 2

37. Su C., Loh K. P. (2013), Carbocatalysts: Graphene oxide and its derivatives, *Acc. Chem. Res.*, 46, 2275-2285 (DOI: 10.1021/ar300118v)
38. Navalon S., Dhakshinamoorthy A., Alvaro M., Garcia H. (2014), Carbocatalysis by graphene-based materials, *Chem. Rev.*, 114, 6179-6212 (DOI: 10.1021/cr4007347)
39. Hu F., Patel M., Luo F., Flach C., Mendelsohn R., Garfunkel E., He H., Szostak M. (2015), Graphene-catalyzed direct Friedel-Crafts alkylation reactions: Mechanism, selectivity and synthetic utility, *J. Am. Chem. Soc.*, 137, 14473-14480 (DOI: 10.1021/jacs.5b09636)
40. Dreyer D. R., Jia H. -P., Bielawski C. W. (2010), Graphene oxide: A convenient carbocatalyst for facilitating oxidation and hydration reactions, *Angew. Chem. Int. Ed.*, 49, 6813-6816 (DOI: 10.1002/anie.201002160)
41. Su C., Tandiana R., Balapanuru J., Tang W., Pareek K., Nai C. T., Hayashi T., Loh K. P. (2015), Tandem catalysis of amines using porous graphene oxide, *J. Am. Chem. Soc.*, 137, 685-690 (DOI: 10.1021/ja512470t)
42. Primo A., Neatu F., Florea M., Parvulescu V., Garcia H. (2014), Graphenes in the absence of metals as carbocatalysts for selective acetylene hydrogenation and alkene hydrogenation, *Nat. Commun.*, 5, 5291-5299 (DOI: 10.1038/ncomms6291)
43. Tang P., Hu G., Li M., Ma D. (2016), Graphene-based metal-free catalysts for catalytic reactions in the liquid phase, *ACS Catal.*, 6, 6948-6958 (DOI: 10.1021/acscatal.6b01668)
44. Gao Y., Tang P., Zhou H., Zhang W., Yang H., Yan N., Hu G., Mei D., Wang J., Ma D. (2016), Graphene oxide catalyzed C-H bond activation: The importance of oxygen functional groups for biaryl construction, *Angew. Chem. Int. Ed.*, 55, 3124-3128 (DOI: 10.1002/anie.201510081)
45. Su C., Acik M., Takai K., Lu J., Hao S. -J., Zheng Y., Wu P., Bao Q., Enoki T., Chabal Y. J., Loh K. P. (2012), Probing the catalytic activity of porous graphene oxide and the origin of this behaviour, *Nat. Commun.*, 3, 1298-1306 (DOI: 10.1038/ncomms2315)

Chapter 2

46. Primo A., Parvulescu V., Garcia H. (2017), Graphenes as metal-free catalysts with engineered active sites, *J. Phys. Chem. Lett.*, 8, 264-278 (DOI: 10.1021/acs.jpcclett.6b01996)
47. Long J., Xie X., Xu J., Gu Q., Chen L., Wang X. (2012), Nitrogen-doped graphene nanosheets as metal-free catalysts for aerobic selective oxidation of benzylic alcohols, *ACS Catal.*, 2, 622-631 (DOI: 10.1021/cs3000396)
48. Verma S., Mungse H. P., Kumar N., Choudhary S., Jain S. L., Sain B., Khatri O. P. (2011), Graphene oxide: an efficient and reusable carbocatalyst for aza-Michael addition of amines to activated alkenes, *Chem. Commun.*, 47, 12673-12675 (DOI: 10.1039/c1cc15230k)
49. Dhakshinamoorthy A., Alvaro M., Concepción P., Fornés V., Garcia H. (2012), Graphene oxide as an acid catalyst for the room temperature ring opening of epoxides, *Chem. Commun.*, 48, 5443-5445 (DOI: 10.1039/c2cc31385e)
50. Kumar A. V., Rao K. R. (2011), Recyclable graphite oxide catalyzed Friedel-Crafts addition of indoles to α , β -unsaturated ketones, *Tetrahedron Lett.*, 52, 5188-5191 (DOI: 10.1016/j.tetlet.2011.08.002)
51. Bhattacharya T., Majumdar B., Dey D., Sarma, T. K. (2014), Ultrasound mediated synthesis of α -aminophosphonates and 3,4-dihydropyrimidin-2-ones using graphene oxide as a recyclable catalyst under solvent-free conditions, *RSC Adv.*, 4, 45831-45837 (DOI: 10.1039/c4ra08533g)
52. Marcano D. C., Kosynkin D. V., Berlin J. M., Sinitskii A., Sun Z., Slesarev A., Alemany L. B., Lu W., Tour J. M. (2010), Improved synthesis of graphene oxide, *ACS Nano*, 4, 4806-4814 (DOI: 10.1021/nn1006368)
53. Frank B., Blume R., Rinaldi A., Trunschke A., Schlögl R. (2011), Oxygen insertion catalysis by sp^2 carbon, *Angew. Chem. Int. Ed.*, 50, 10226– 10230 (DOI: 10.1002/anie.201103340)
54. Acik M., Lee G., Mattevi C., Chhowalla M., Cho K., Chabal Y. J. (2010), Unusual infrared-absorption mechanism in thermally reduced graphene oxide, *Nat. Mater.*, 9, 840-845 (DOI: 10.1038/nmat2858)

Chapter 2

55. Majumdar B., Bhattacharya T., Sarma T. K. (2016), Gold nanoparticle-polydopamine-reduced graphene oxide ternary nanocomposite as an efficient catalyst for selective oxidation of benzylic C(sp³)-H bonds under mild conditions, *ChemCatChem*, 8, 1825-1835 (DOI: 10.1002/cctc.201600136)
56. Kesavan L., Tiruvalam R., Ab Rahim M. H., bin Saiman M. I., Enache D. I., Jenkins R. L., Dimitratos N., Sanchez J. A. L., Taylor S. H., Knight D. W., Kiely C. J., Hutchings G. J. (2011), Solvent-free oxidation of primary carbon-hydrogen bonds in toluene using Au-Pd alloy nanoparticles, *Science*, 331, 195–199 (DOI: 10.1126/science.1198458)
57. Risi C. D., Pollini G. P., Zanirato V. (2016), Recent developments in general methodologies for the synthesis of α -ketoamides, *Chem. Rev.*, 116, 3241–3305 (DOI: 10.1021/acs.chemrev.5b00443)
58. Kumar D., Vemula S. R., Cook G. R. (2016), Recent advances in the catalytic synthesis of α -ketoamides, *ACS Catal.*, 6, 4920–4945 (DOI: 10.1021/acscatal.6b01116)
59. Tang P., Hu G., Gao Y., Li W., Yao S., Liu Z., Ma D. (2014), The microwave adsorption behavior and microwave-assisted heteroatoms doping of graphene-based nano-carbon materials, *Sci. Rep.*, 4, 5901-5907 (DOI: 10.1038/srep05901)
60. He W., Lu L., (2012), Revisiting the structure of graphene oxide for preparing new-style graphene-based ultraviolet absorbers, *Adv. Funct. Mater.*, 22, 2542-2549 (DOI: 10.1002/adfm.201102998)
61. Rourke J. P., Pandey P. A., Moore J. J., Bates M., Kinloch I. A., Young R. J., Wilson N. R. (2011), The real graphene oxide revealed: Stripping the oxidative debris from the graphene-like sheets, *Angew. Chem. Int. Ed.*, 50, 3173–3177 (DOI: 10.1002/anie.2011007520)
62. Liao K. -H., Mittal A., Bose S., Leighton C., Mkhoyan K. A., Macosko C. W. (2011), Aqueous only route toward graphene from graphite oxide, *ACS Nano*, 5, 1253-1258 (DOI: 10.1021/nn1028967)

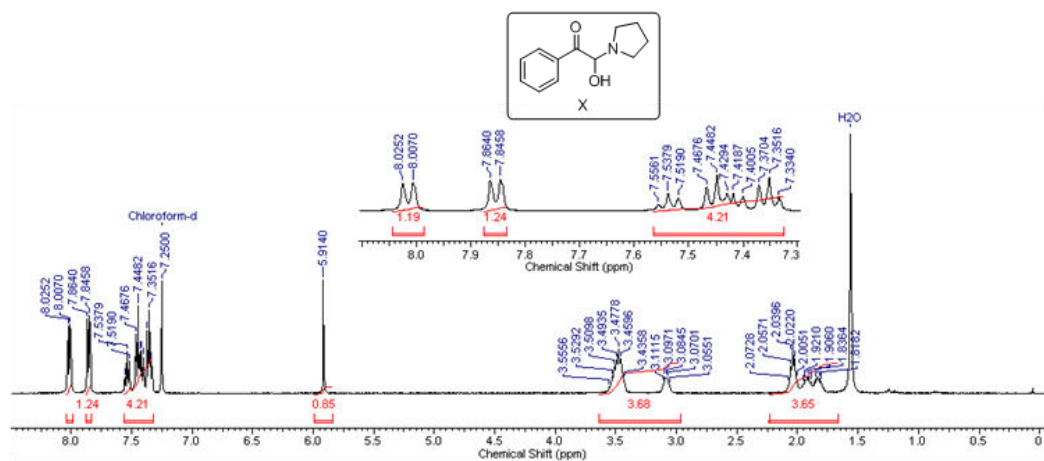
Chapter 2

63. Espinosa J. C., Navalón S., Álvaro M., Garcia H. (2016), Reduced graphene oxide as a metal-free catalyst for the light-assisted Fenton-like reaction, *ChemCatChem*, 8, 2642-2648 (DOI: 10.1002/cctc.201600364)
64. Shi M. Sc. S., Wang M. Sc. T., Weingand V., Rudolph M., Hashmi A. S. K. (2014), Gold(I)-catalyzed diastereoselective hydroacylation of terminal alkynes with glyoxals, *Angew. Chem. Int. Ed.*, 53, 1148-1151 (DOI: 10.1002/anie.201307685)
65. Zhang X., Wang M., Zhang Y., Wang L. (2013), A novel and metal-free approach towards α -ketoamides using a TBHP/I₂-promoted tandem reaction of amines with β -diketones via C-C bond cleavage, *RSC Adv.*, 3, 1311–1316 (DOI: 10.1039/c2ra22116k)
66. Zhang X., Wang L. (2012), TBHP/I₂-promoted oxidative coupling of acetophenones with amines at room temperature under metal-free and solvent-free conditions for the synthesis of α -ketoamides, *Green Chem.*, 14, 2141–2145 (DOI: 10.1039/C2GC35489F)
67. Zhang Z., Su J., Zha Z., Wang Z. (2013), A novel approach for the one-pot preparation of α -ketoamides by anodic oxidation, *Chem. Commun.*, 49, 8982-8984 (DOI: 10.1039/C3CC43685C)
68. Zhang X., Yang W., Wang L. (2013), Silver-catalyzed amidation of benzoylformic acids with tertiary amines via selective carbon–nitrogen bond cleavage, *Org. Biomol. Chem.*, 11, 3649-3654 (DOI: 10.1039/C3OB40619A)
69. Deshidi R., Devari S., Shah B. A. (2015), Iodine-promoted oxidative amidation of terminal alkenes-synthesis of α -ketoamides, benzothiazoles, and quinazolines, *Eur. J. Org. Chem.*, 2015, 1428–1432 (DOI: 10.1002/ejoc.201403547)
70. Shao Y., Wu Z., Miao C., Liu L. (2014), Mild gold-catalyzed aerobic dehydrogenative coupling of amines and phenylglyoxal derivatives, *J. Organomet. Chem.*, 767, 60-64 (DOI: 10.1016/j.jorganchem.2014.05.017)

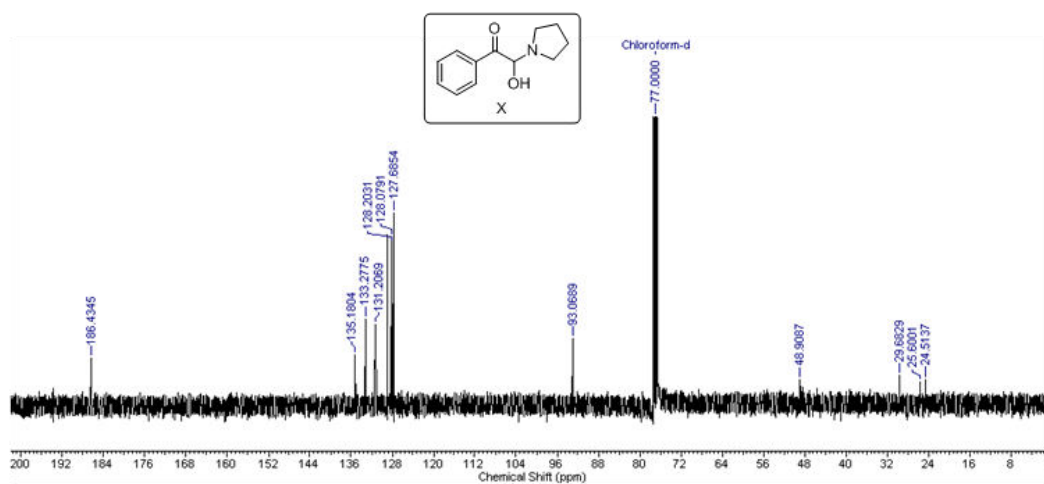
Appendix-Chapter 2

*^1H and ^{13}C NMR Spectra of Hemiaminal
Intermediate and α -Ketoamides*

Chapter 2



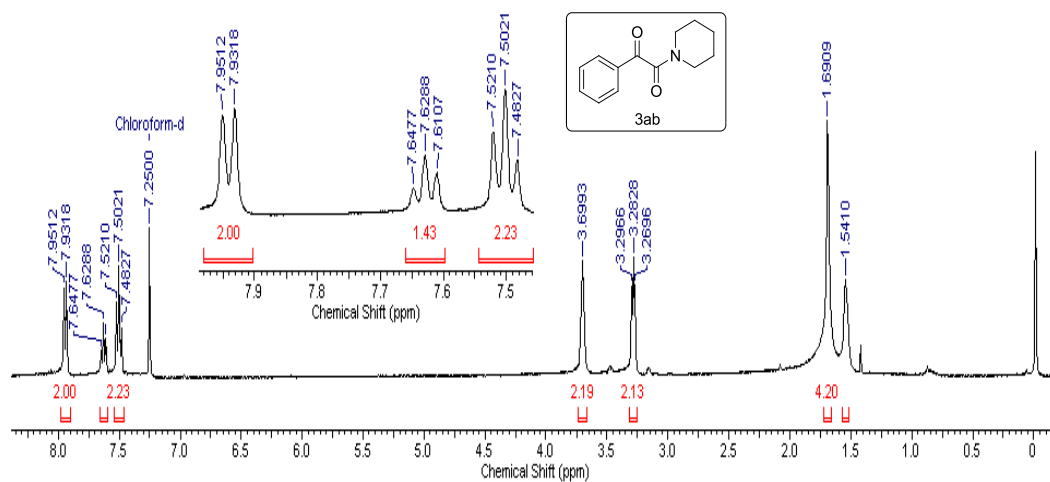
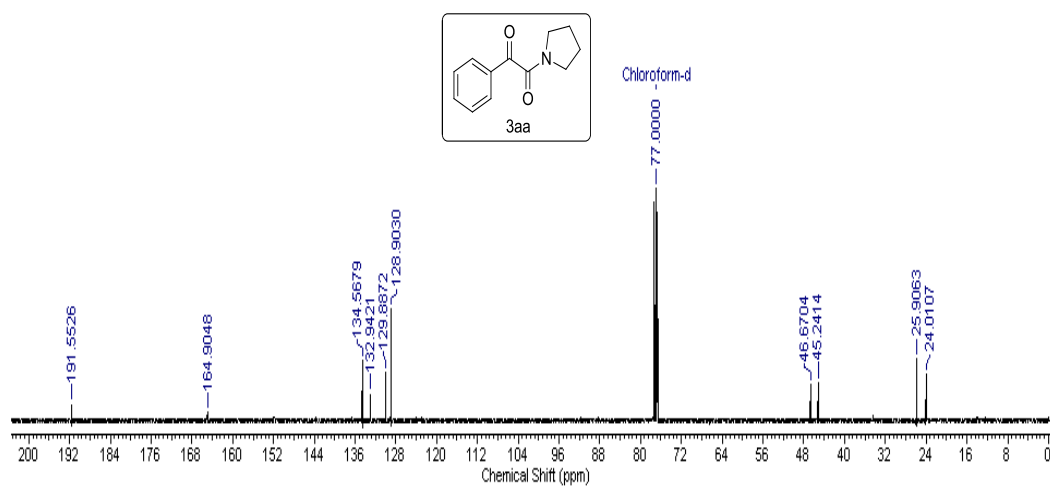
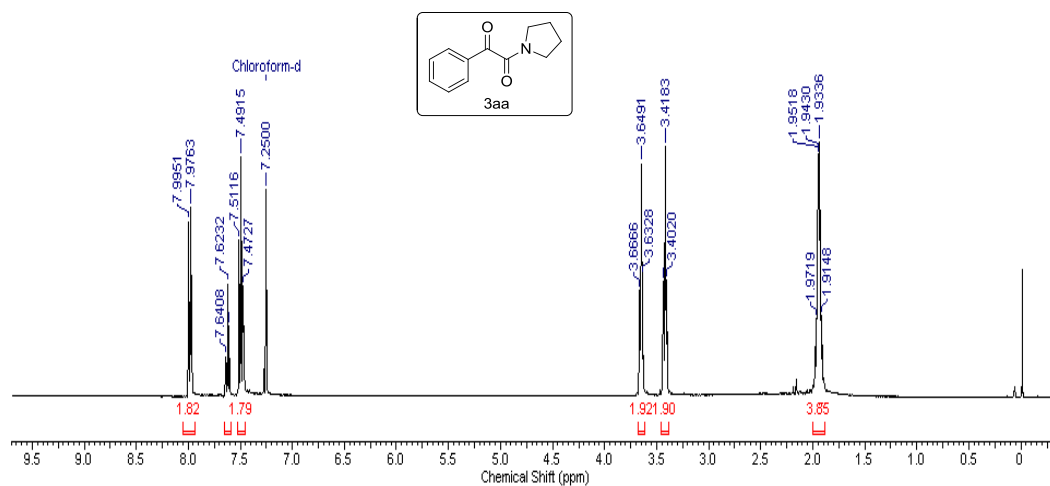
¹H NMR of hemimainal intermediate



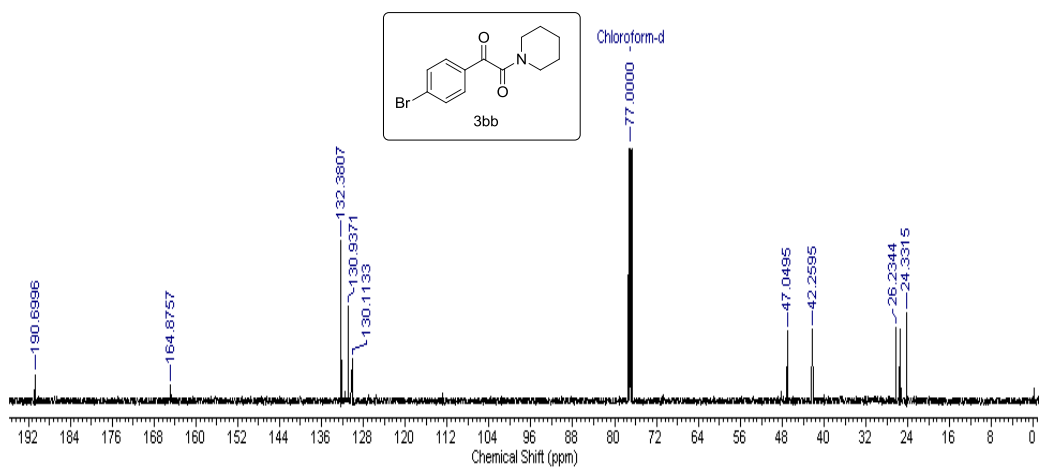
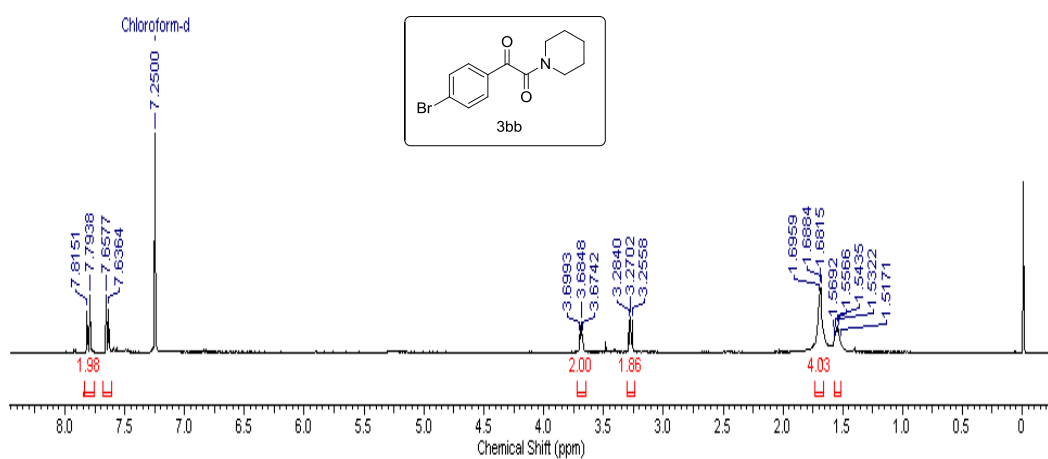
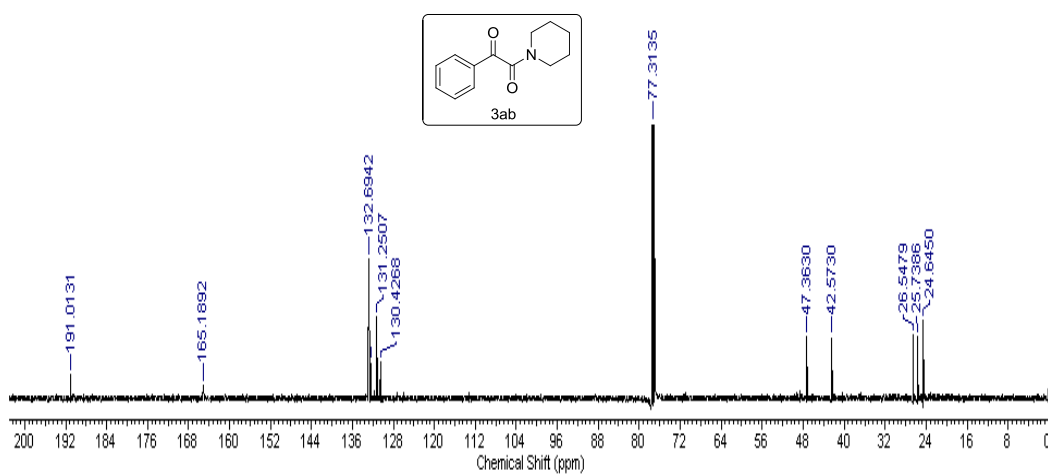
¹³C NMR of hemimainal intermediate

Chapter 2

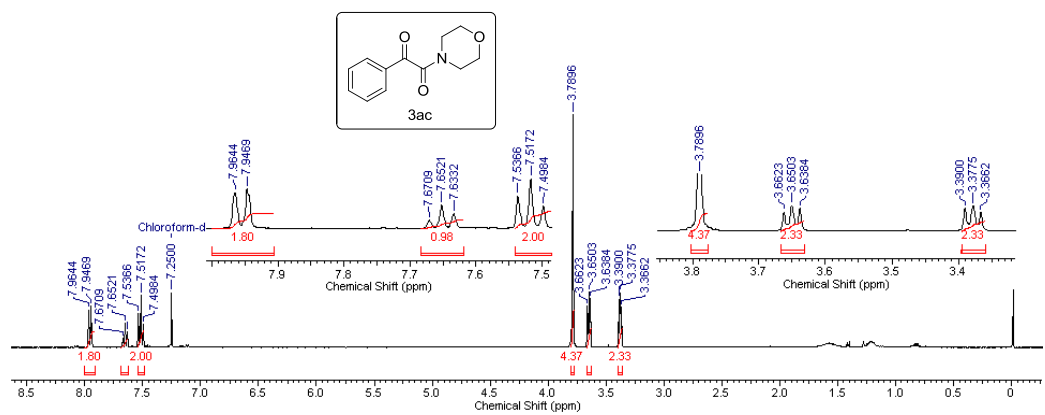
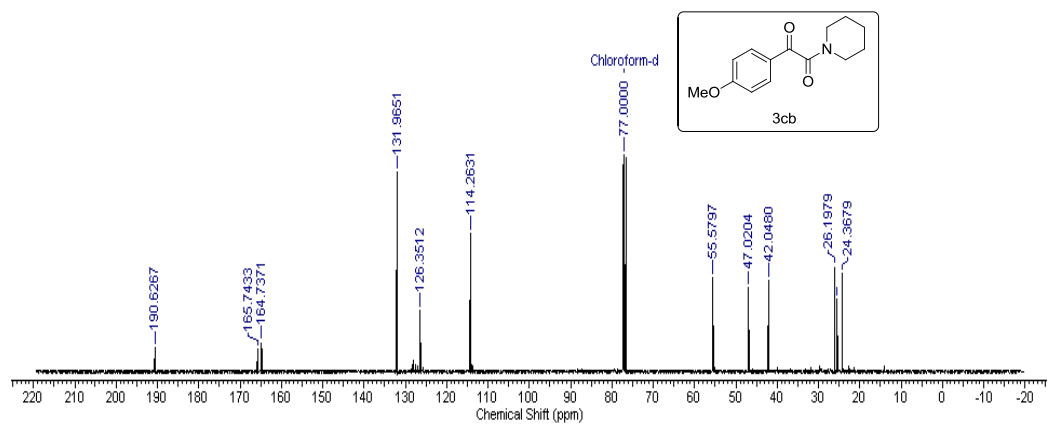
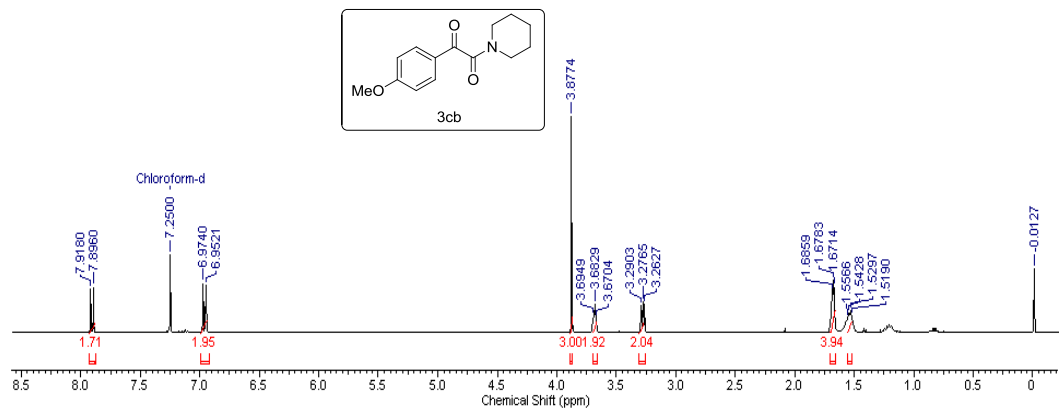
^1H and ^{13}C NMR spectra of α -Ketoamides



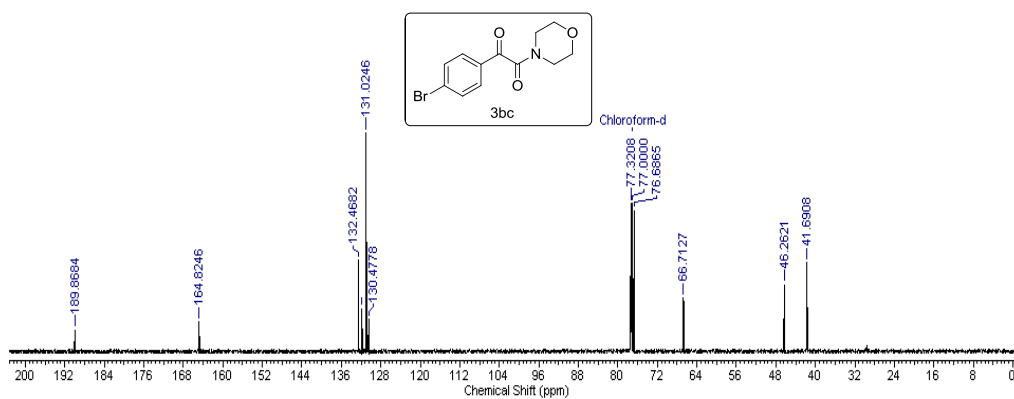
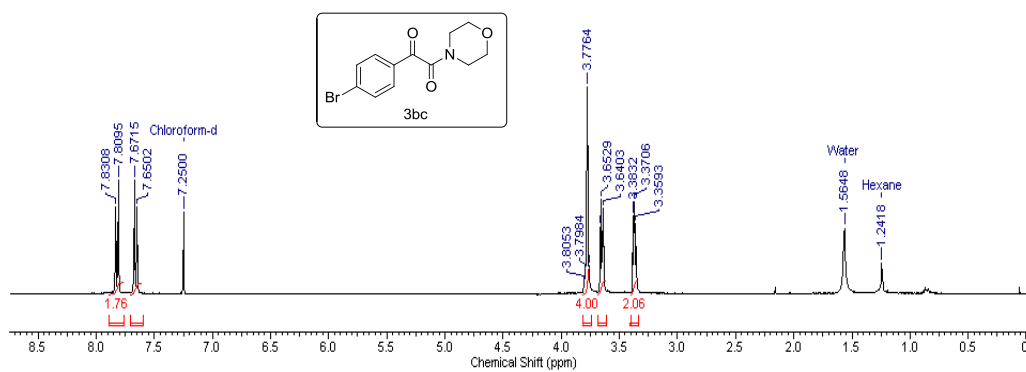
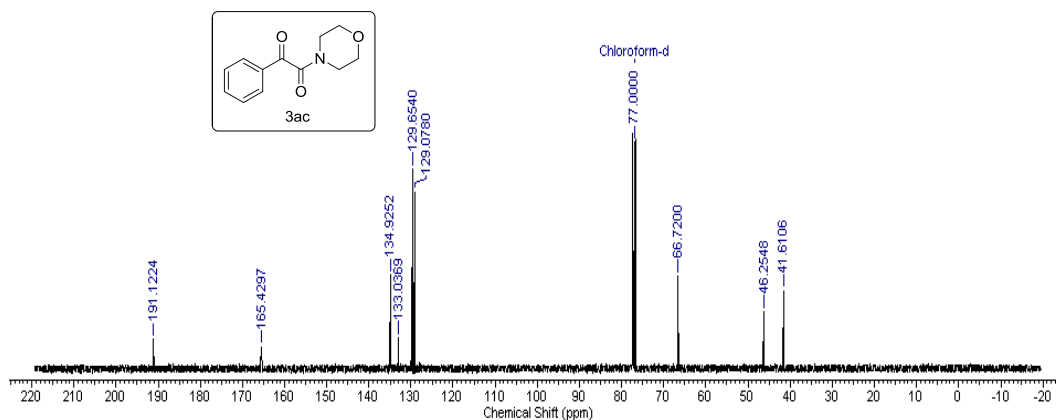
Chapter 2



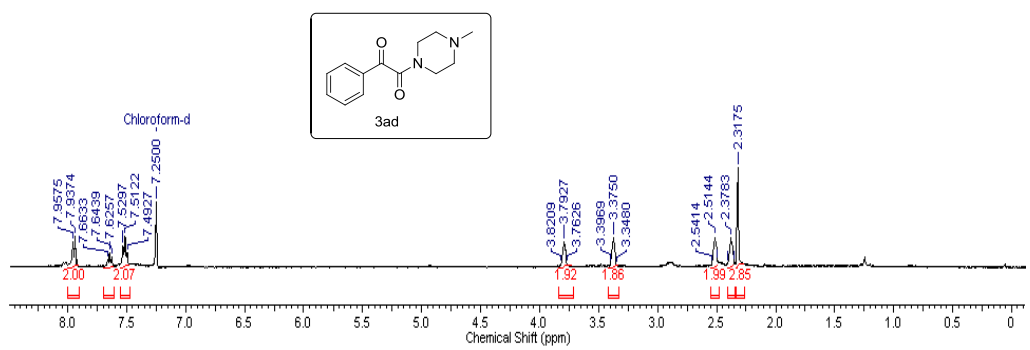
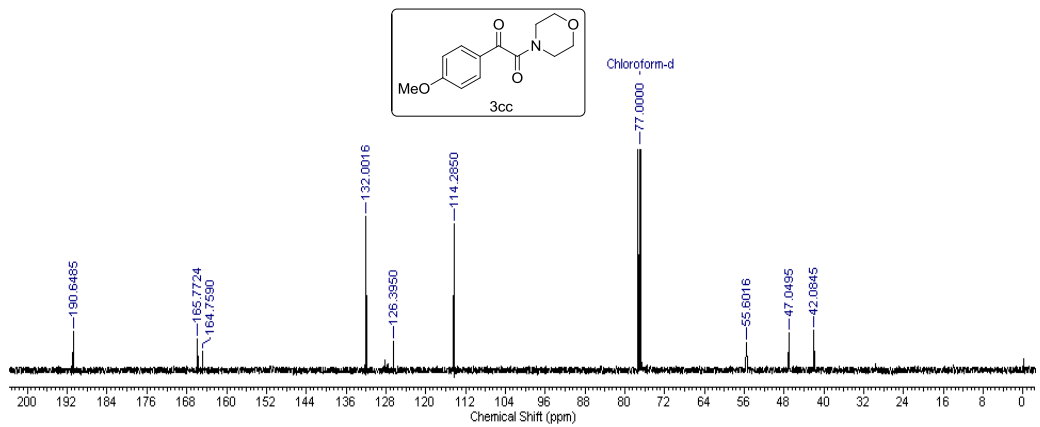
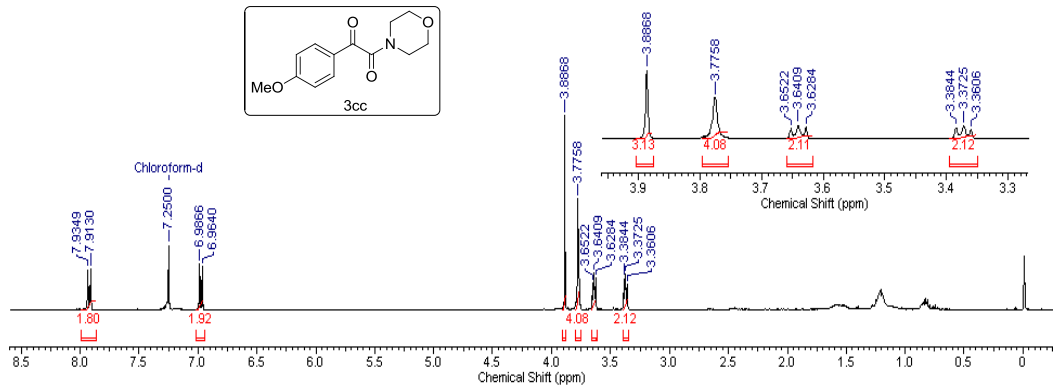
Chapter 2



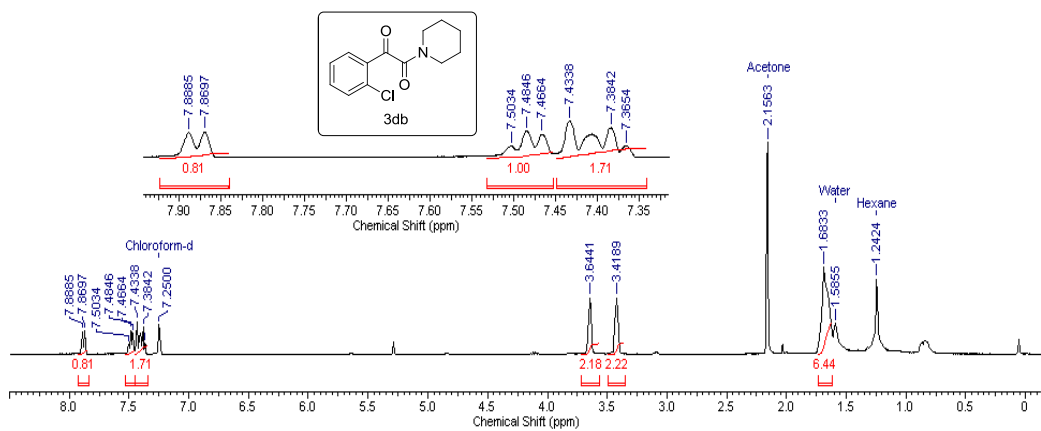
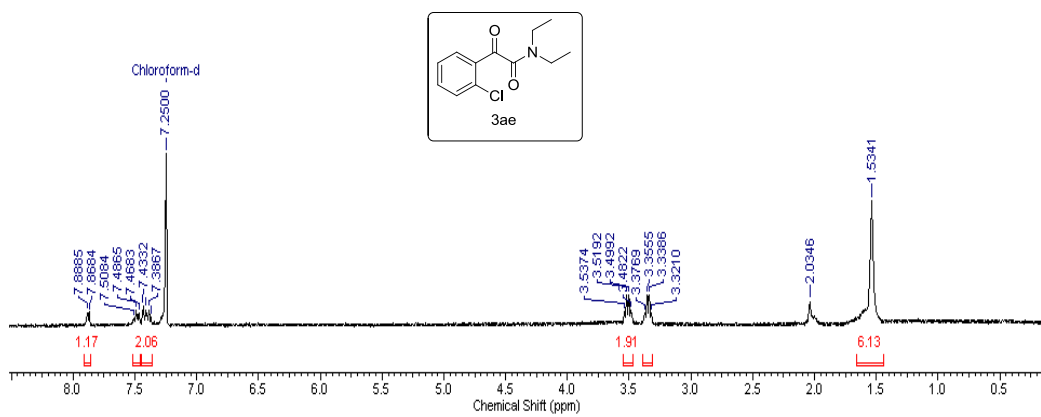
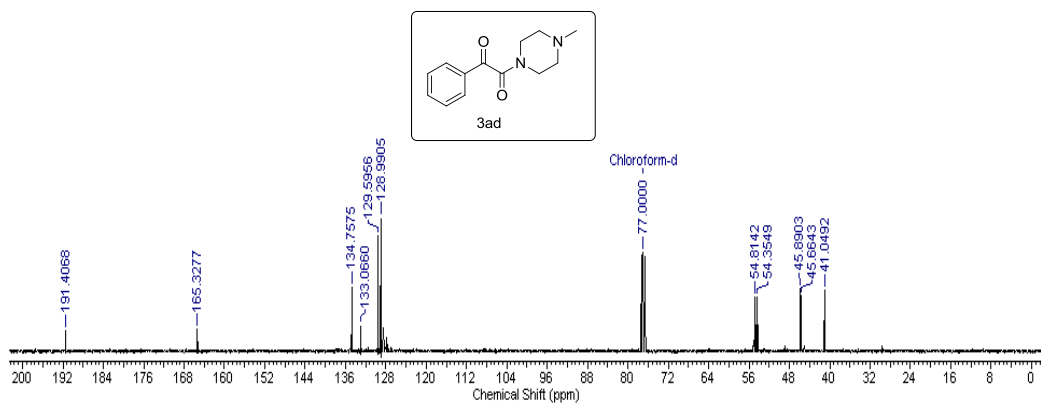
Chapter 2



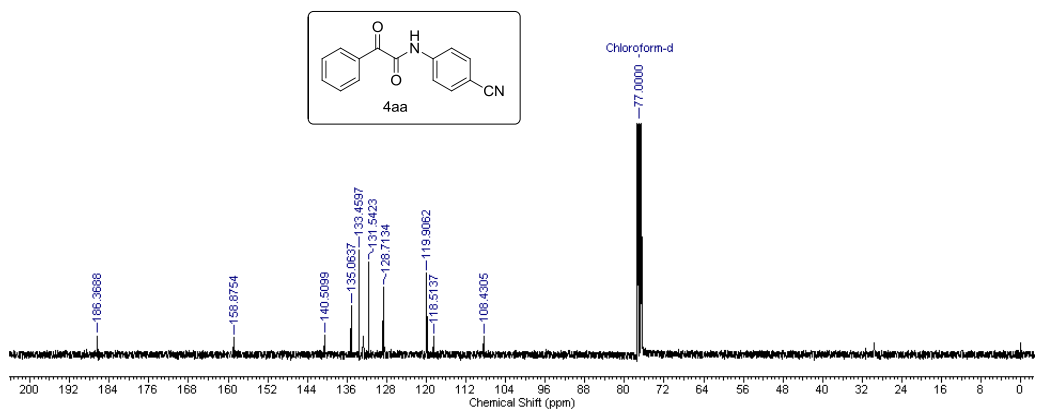
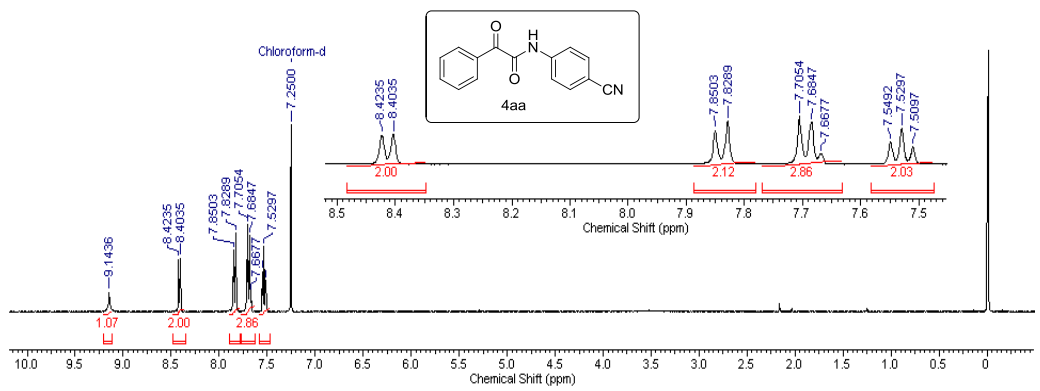
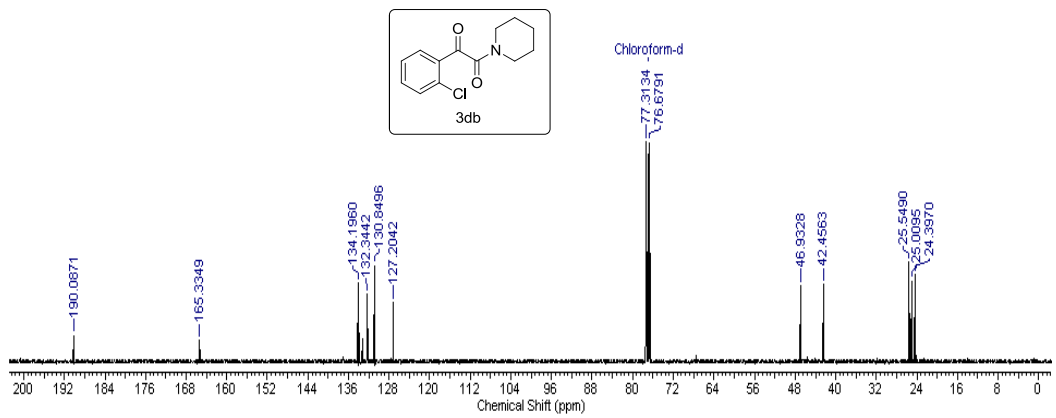
Chapter 2



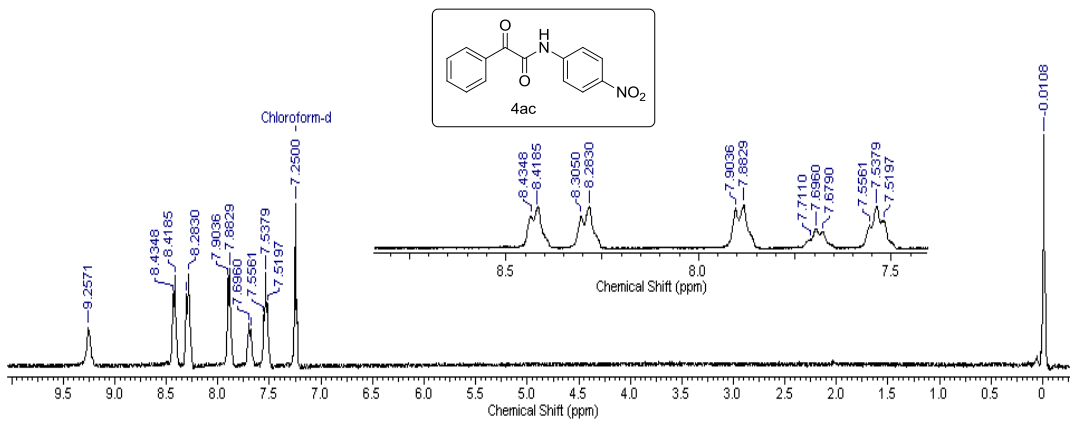
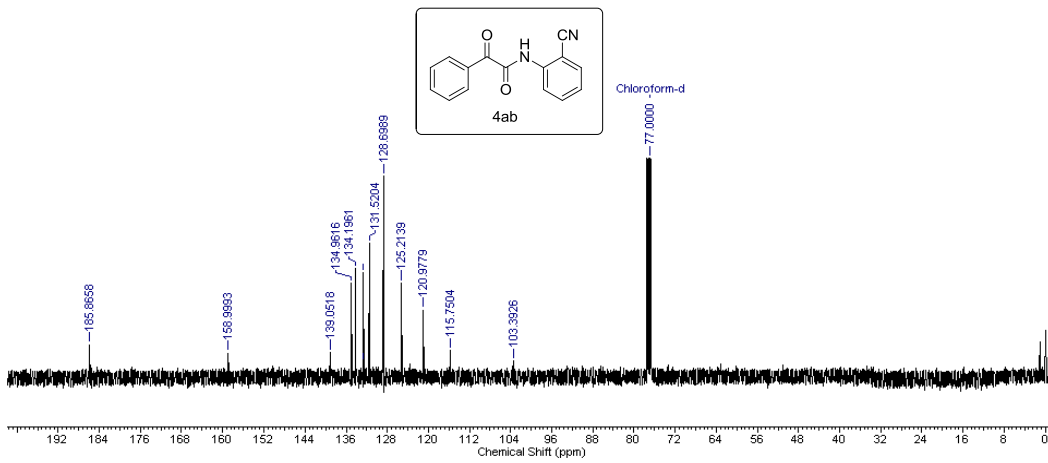
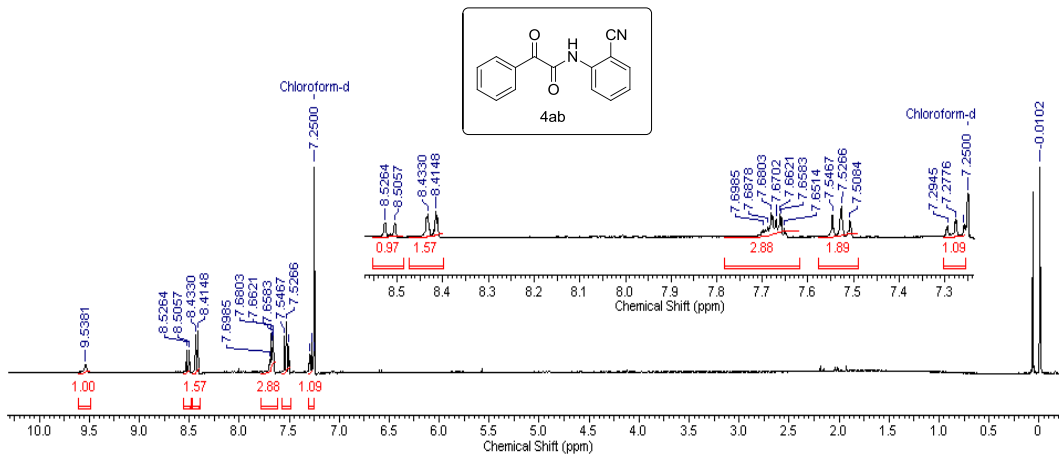
Chapter 2



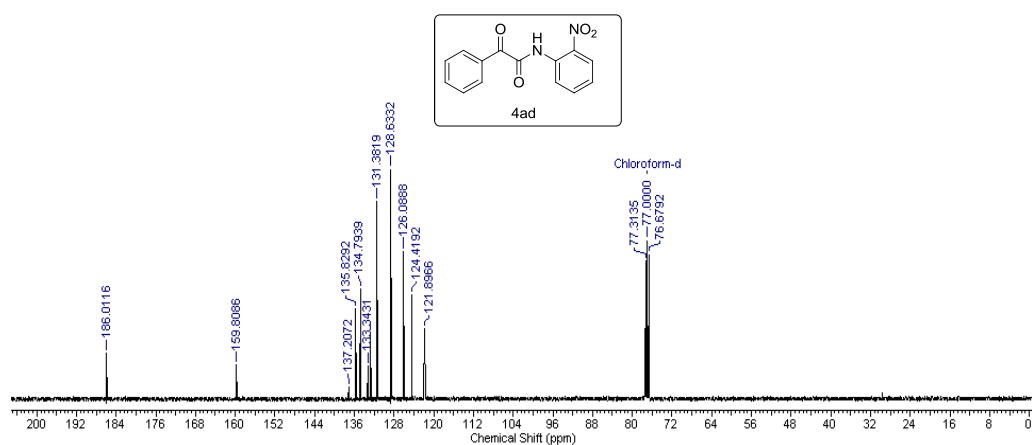
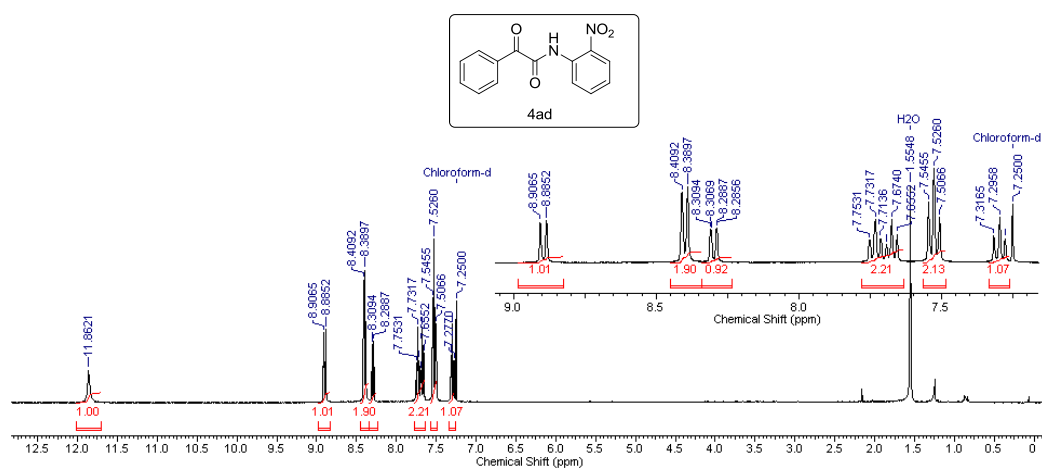
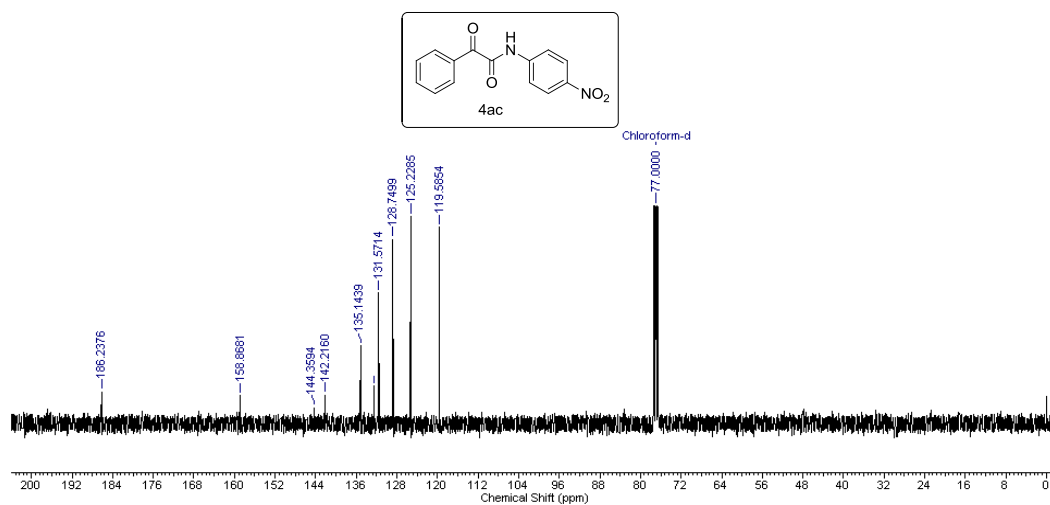
Chapter 2



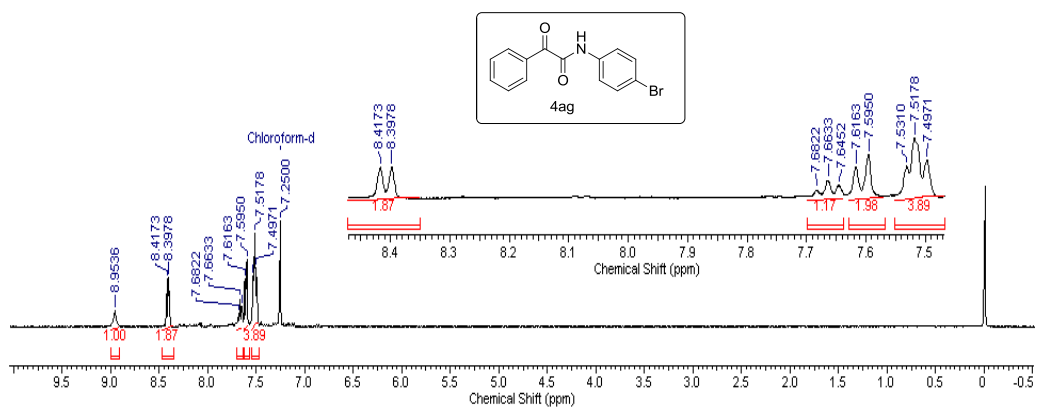
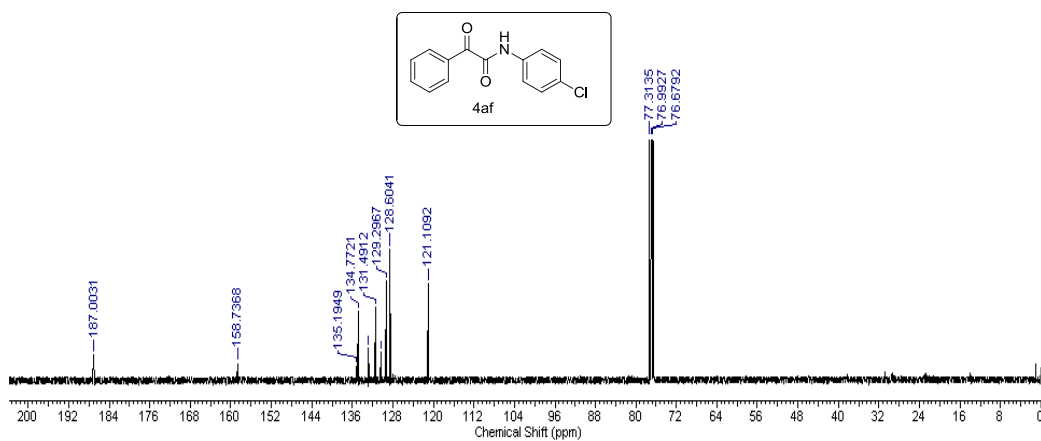
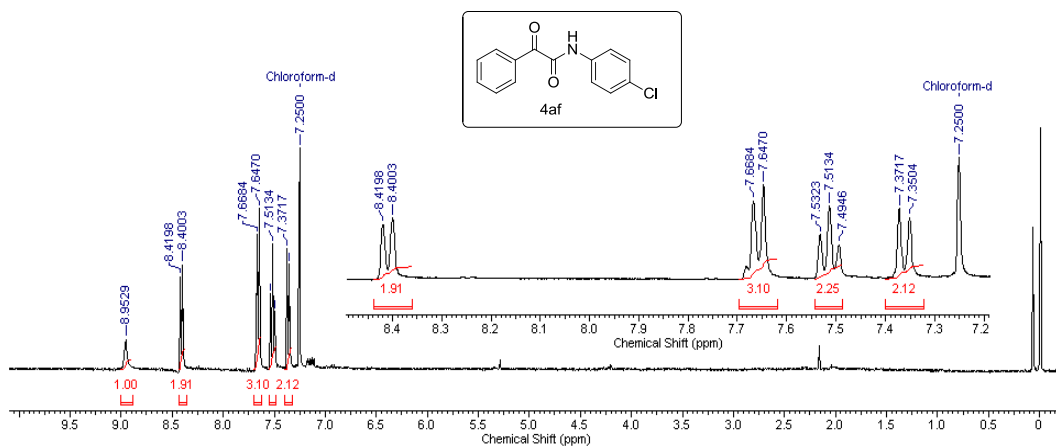
Chapter 2



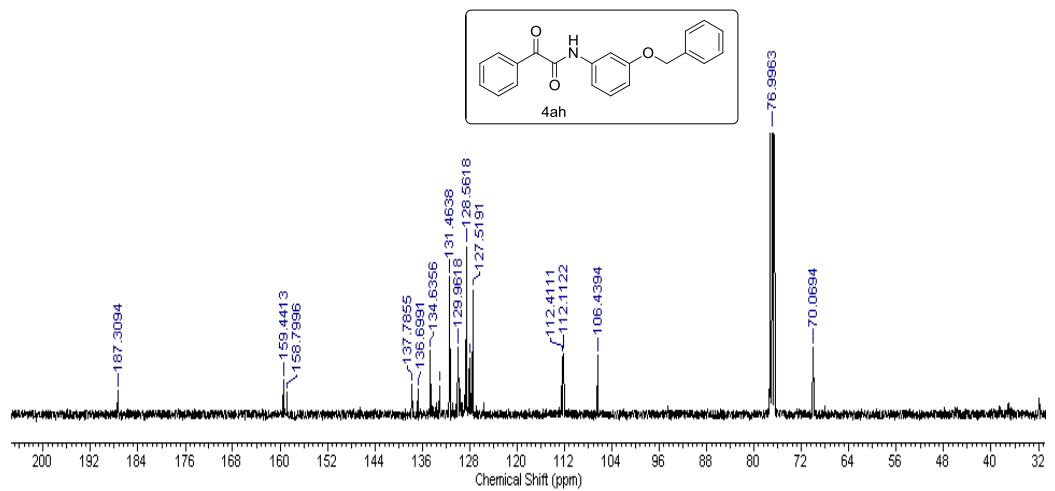
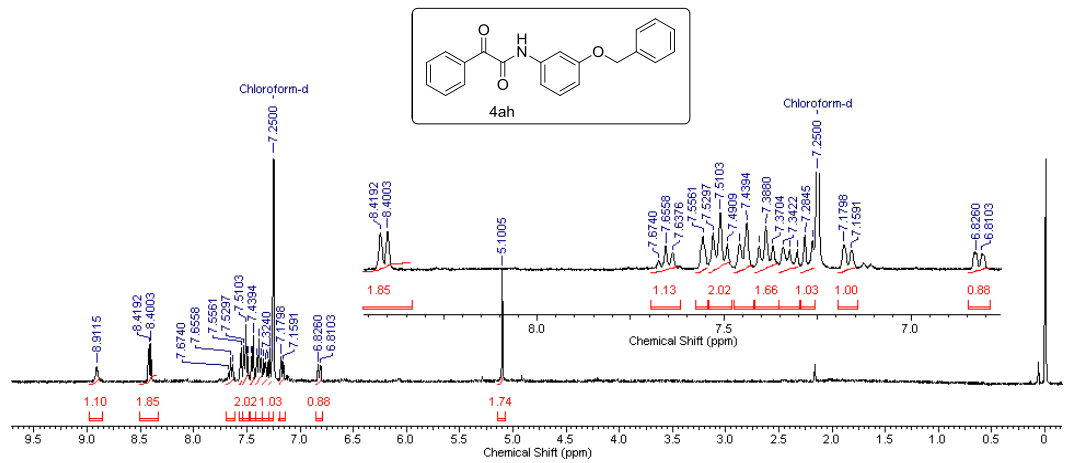
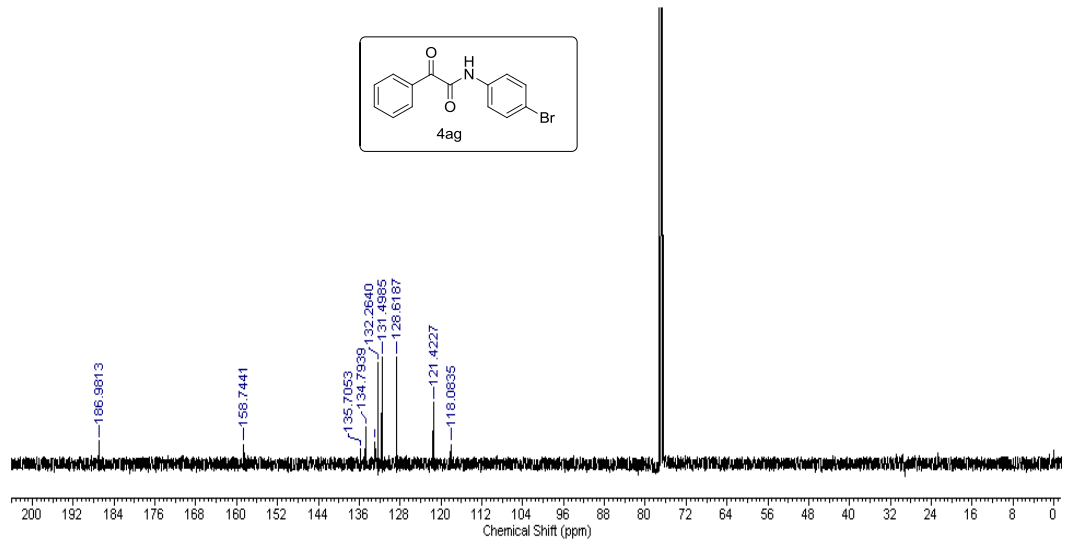
Chapter 2



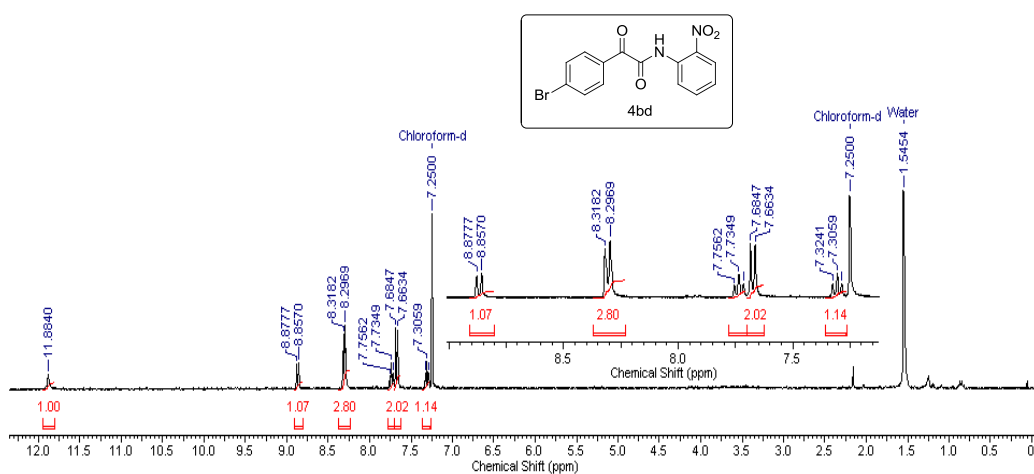
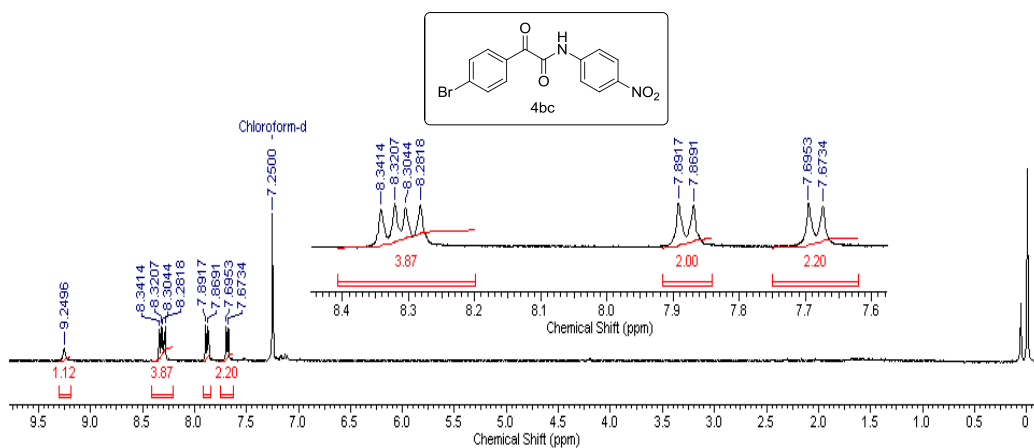
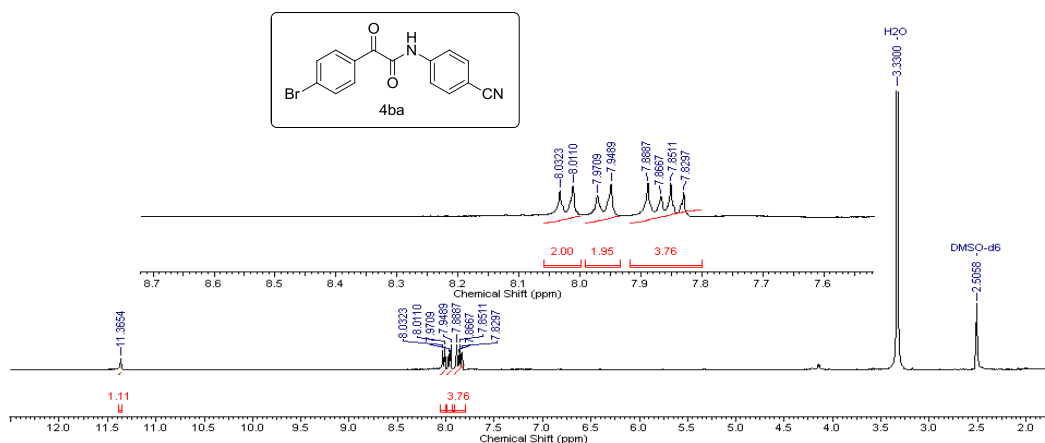
Chapter 2



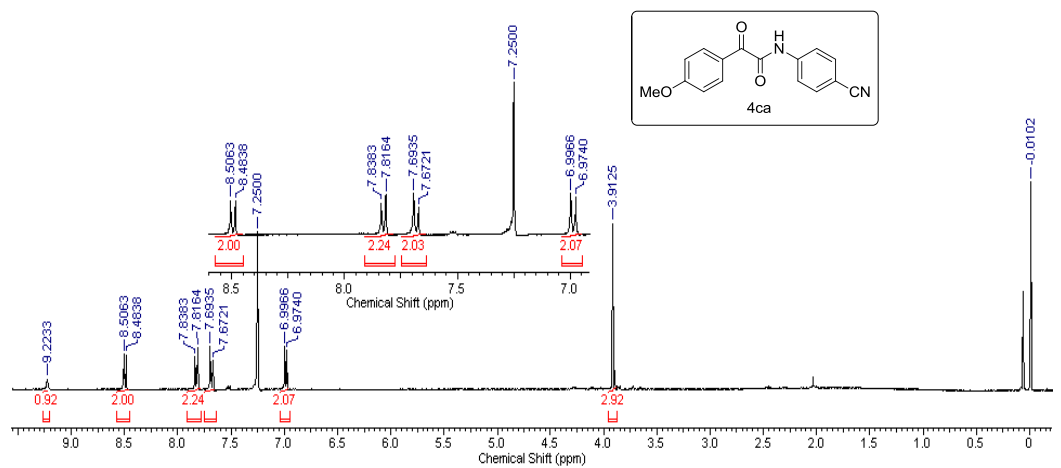
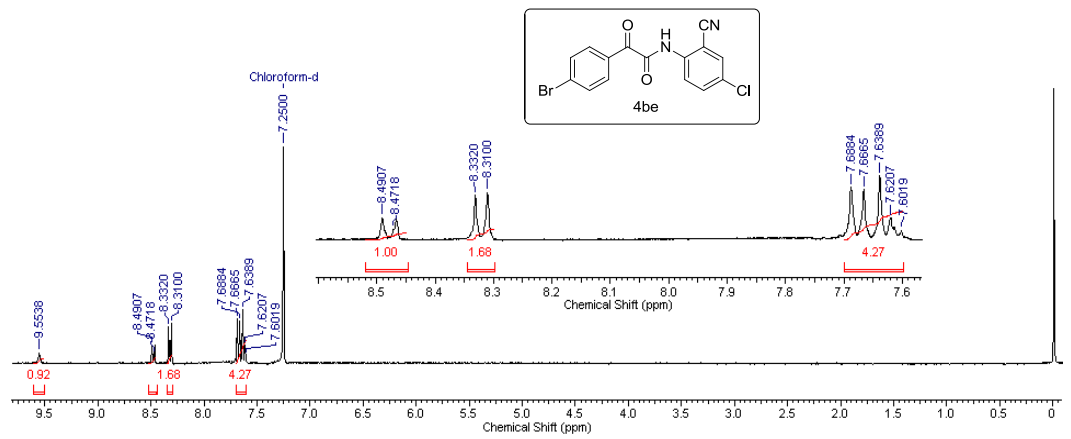
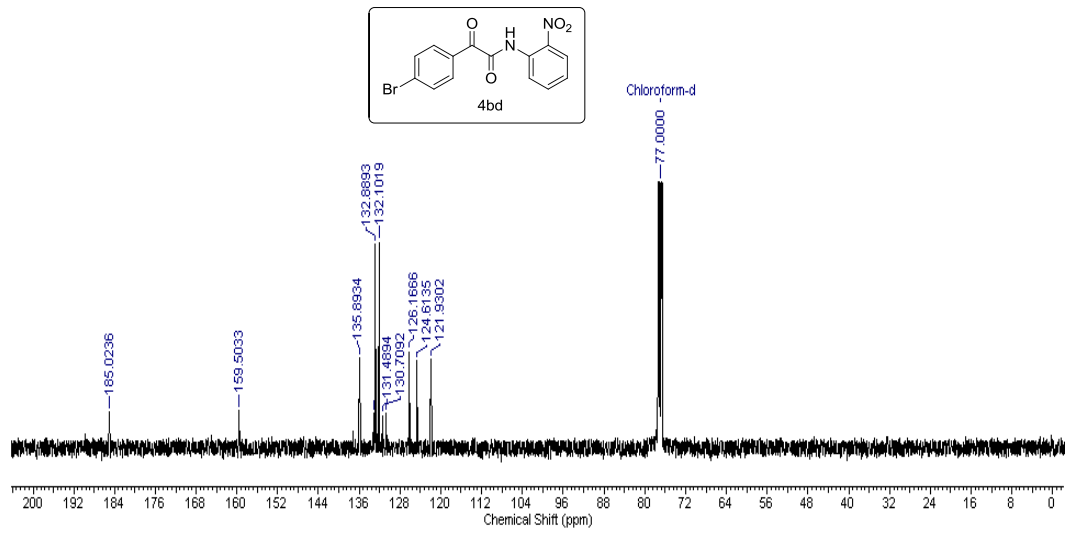
Chapter 2



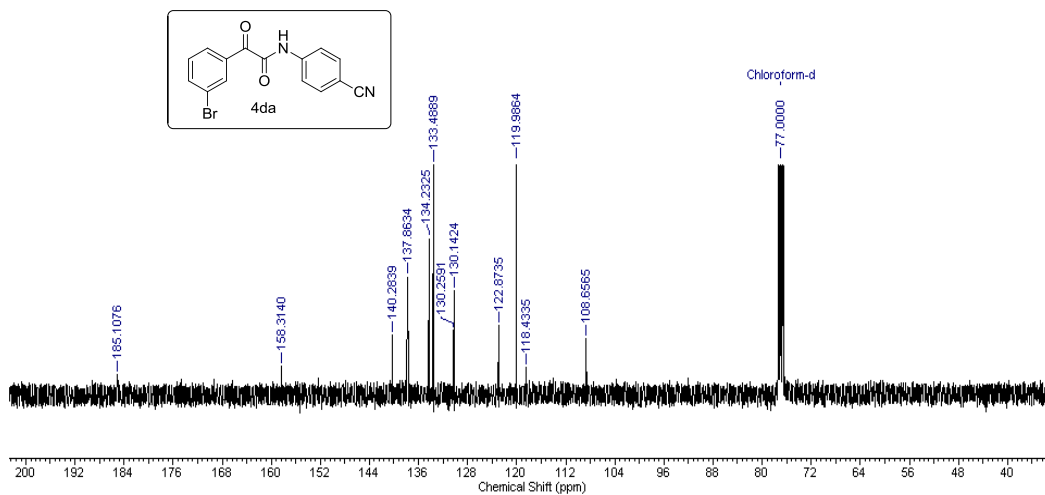
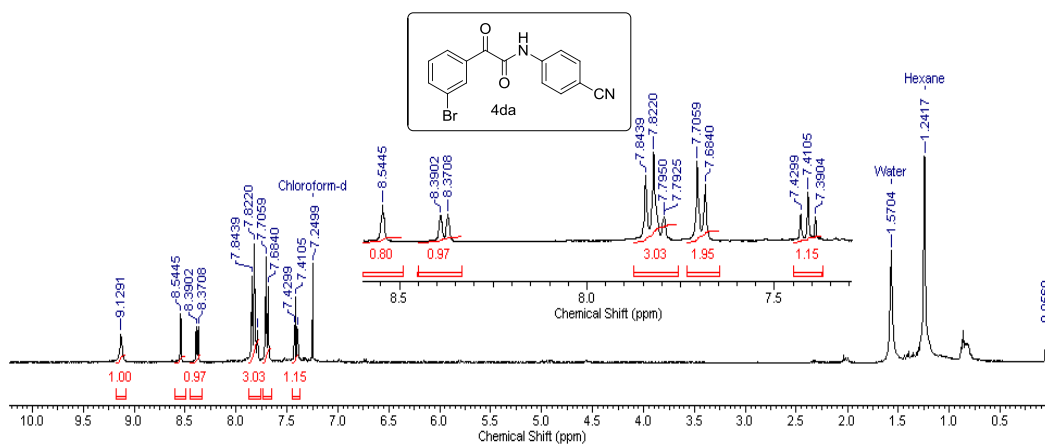
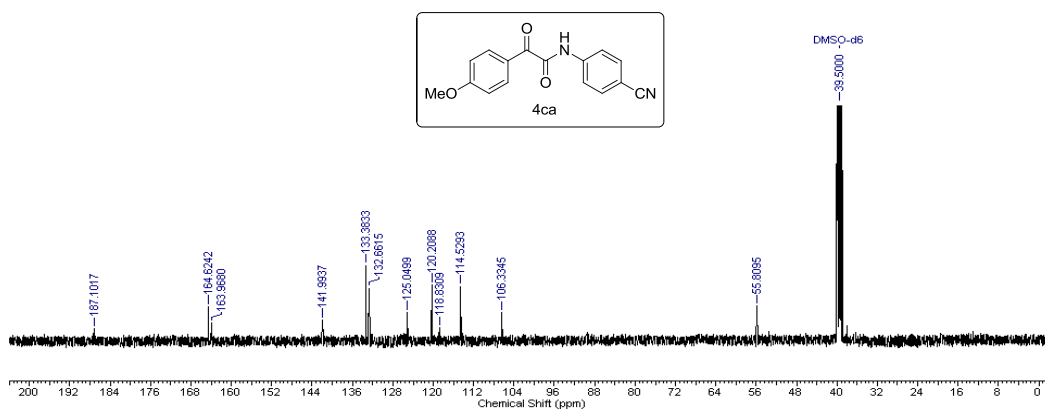
Chapter 2



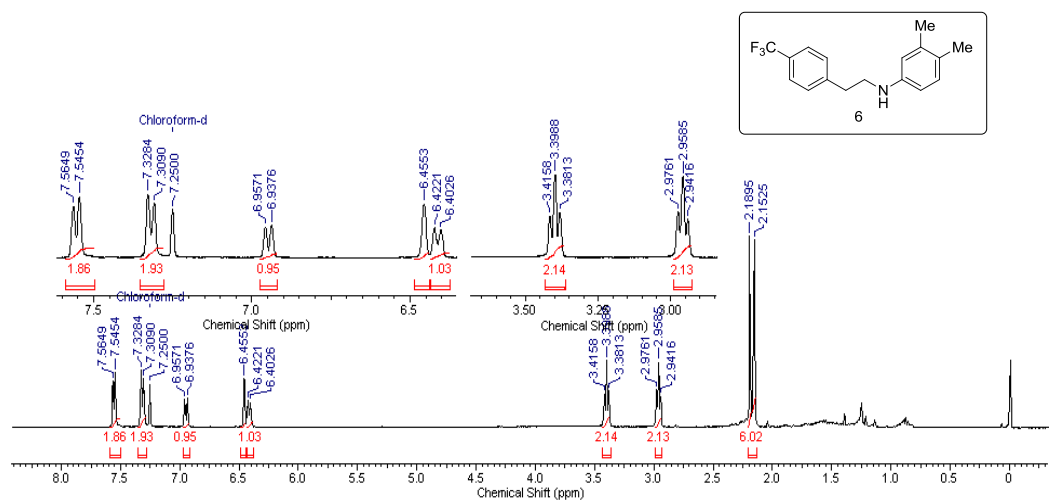
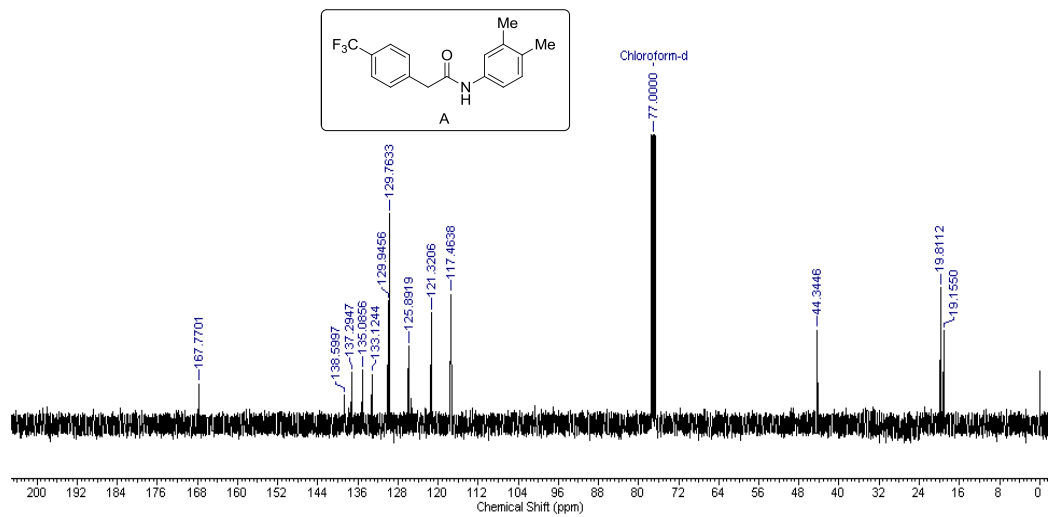
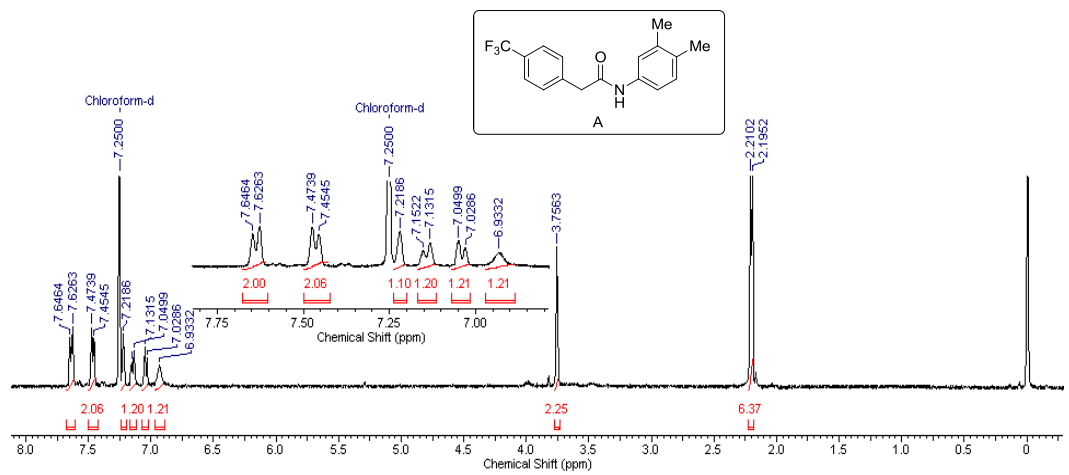
Chapter 2



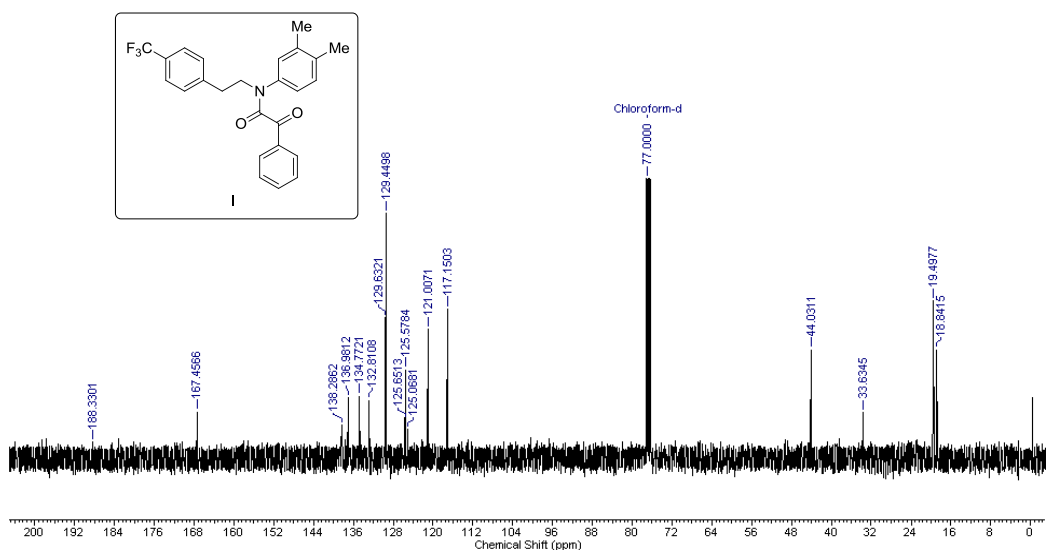
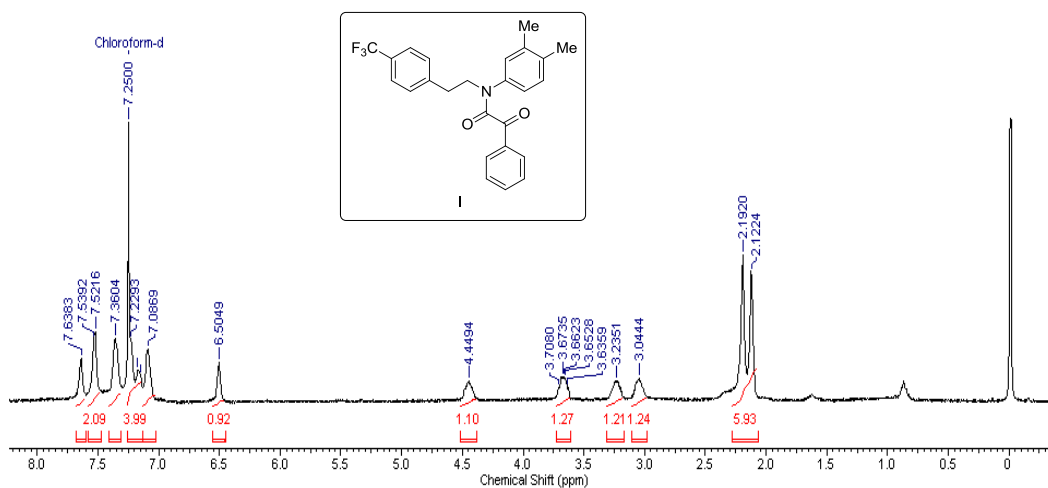
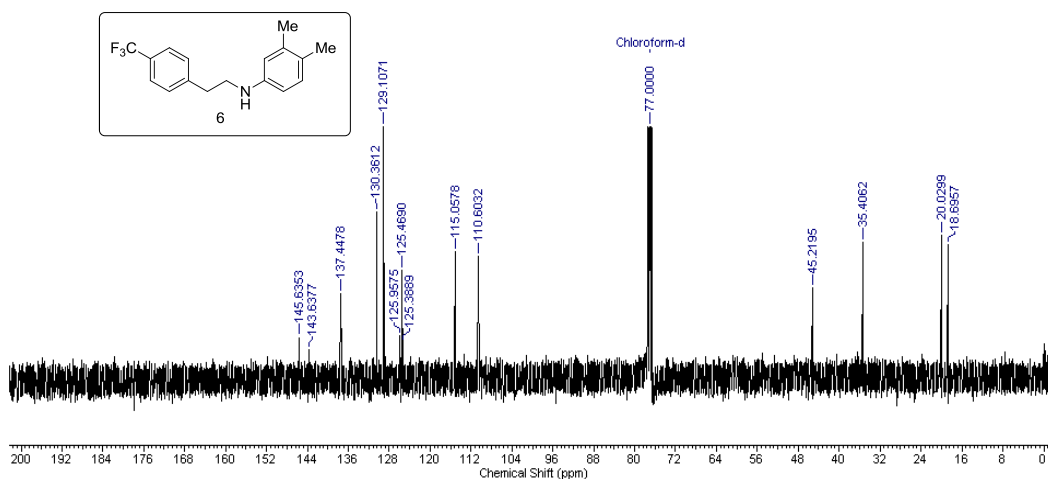
Chapter 2



Chapter 2



Chapter 2



Chapter 3

Probing Carbocatalytic Activity of Carbon Nanodots for the Synthesis of Biologically Active Dihydro/Spiro/Glyco Quinazolinones and Aza-Michael Adducts

Chapter 3

3.1 Introduction

Acid catalyzed processes play a key role in modern organic synthesis.^[1-2] Traditional acid catalysts including mineral acids such as sulphuric acid and organic acids such as *p*-toluenesulphonic acid give rise to serious disadvantages like corrosion, toxicity, separation of catalysts from homogeneous reaction mixtures and necessity of neutralization of waste streams which impedes their commercialization.^[3-4] Development of solid acid catalysts with a possibility to tune the surface properties including acidic functionalities might be important in controlling the yield and selectivity of the products. Carbonaceous materials such as carbon nanotube and graphene oxide have been extensively used as carbocatalysts or as supports for immobilization of catalytically active species.^[5-7] With the emphasis on catalytic materials with extensive environmental footprint towards green and sustainable chemistry, the exploitation of the inherent catalytic activity induced by the surface functionality of the carbonaceous materials is of continuous quest to afford a highly benign and affordable synthesis.^[8-11] For example, the carboxylic acid and epoxide functionalities on graphene oxide (GO) have been exploited as catalytic sites for important organic transformations such as oxidation and hydration reactions,^[12] aza-Michael addition reaction,^[13] ring-opening reactions,^[14-15] Friedel-Crafts reaction,^[16] multi-component coupling reactions^[17] etc. However, harsh reaction conditions involving use of strong oxidizing agents such as conc. H₂SO₄ and KMnO₄ in the synthesis of GO and possible involvement of trace metals on GO surfaces during catalytic reactions demands designing more environmentally benign alternative carbocatalysts.^[18] Carbon nanodots (CND), a fluorescent form of carbon, have attracted tremendous research activities in recent years owing to their ease of synthesis through a metal-free pathway, tunable emission properties, biocompatibility, water-solubility and easy surface functionalization.^[19-20] Depending on the carbon source used for the synthesis of CNDs, tailored surface functionality can be achieved.^[21] The presence of –CO₂H functionality on the CND surface can be exploited for the acid catalyzed organic transformations in a recyclable pathway to achieve an efficient and sustainable synthesis of organic feedstocks following green protocols. The photocatalytic activity of CNDs has been exploited for environmental remediation, H₂ production, CO₂ reduction and

Chapter 3

organic synthesis.^[22-25] CNDs have also been used as surface stabilizing agents for nanoparticles for effective catalytic activities.^[26] However, few studies have focussed on exploring the surface functionality on CNDs as catalytic sites for important organic transformations.^[27]

2,3-Dihydroquinazolinones and aza-Michael adducts are important classes of organic compounds as potent building blocks for important natural products and as probes in biological applications.^[28-33] These compounds display wide range of biological activities as antitumor, antidefibrillatory, antidepressant, analgesic, diuretic, antihistamine, vasodilating agent, antihypertensive, CNS stimulant, tranquilizer and antianxiotic.^[28-31] Several acid catalysts such as β -cyclodextrin,^[34-35] ionic liquids,^[36] quaternary ammonium salts,^[37] silica sulfuric acid,^[38] montmorillonite K-10,^[39] cyanuric chloride,^[28] β -cyclodextrin-SO₃H,^[40] Cu-CNTs^[41] etc. have been developed for generating carbon-heteroatom bonds in aza-Michael adducts and quinazolinones. Although, these catalysts have shown efficacy with respect to yield of the products but several of these catalytic systems suffer from certain disadvantages such as tedious catalyst preparation involving laborious surface modifications, high reaction temperature, prolonged reaction time and extensive work-up procedures. In some cases, catalysts had to be surface passivated using strong acids such as conc. H₂SO₄ to obtain milder reaction conditions. Although carbonaceous nanomaterials such as GO have shown high activity towards acid-catalyzed organic transformations, the catalytic activity of their zero-dimensional counterpart CNDs has not been explored yet. This prompted us to investigate the inherent catalytic ability of –COOH surface functionalized CNDs towards carbon-heteroatom bond formation. β -carotene was employed as the carbon source to generate CNDs. The prime motive to use β -carotene was that unlike most of the carbon sources used to make CNDs,^[42] β -carotene doesn't have any oxygen functionality present in it. The catalytic activity of the CNDs is driven only by the surface –COOH groups generated during the carbonization of β -carotene. The ease of synthesis of CNDs from easily available carbon sources through simple microwave or hydrothermal treatment and with their non-toxic and biocompatible properties, CNDs can overcome numerous intricacies associated with other catalytic systems towards the synthesis of 2, 3-Dihydroquinazolinones and aza-Michael adducts through a

mild reaction pathway. Recently, Li *et al.* have shown the photocatalytic activity of sulphated graphene quantum dots in visible light induced ring opening reactions.^[43] The efficient catalytic activity of carboxylic acid functionalized CNDs, as reported herein, towards the synthesis of biologically active dihydro/spiroquinazolinones and quinazolinone-glyco- conjugates along with aza-Michael adducts demonstrate the potential of this carbonaceous nanodots as a non-toxic, biocompatible and recyclable acid catalyst for organic transformations of biological relevance.

3.2 Results and Discussion

3.2.1 Synthesis and characterization of CNDs

The CNDs were synthesized by a hydrothermal treatment of β -carotene in water (details in experimental section). It is worth mentioning that β -carotene is totally insoluble in water. However, upon hydrothermal treatment, it resulted in a yellow dispersion of carbon dots. The solution exhibited strong fluorescence

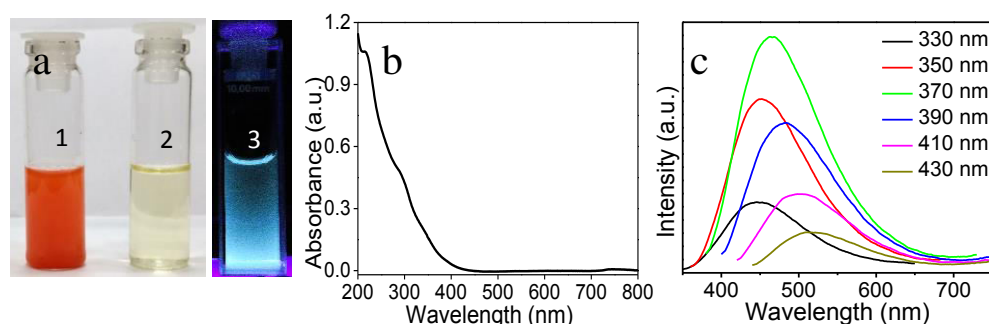


Figure 3.1. a) Digital images of (1) β -carotene dispersed in water, (2) CNDs hydrothermally obtained in daylight and (3) C-dot solution showing blue fluorescence under UV light ($\lambda_{\text{ex}} = 365$ nm), b) UV-visible spectrum and c) Excitation dependent emission spectrum of CNDs

under UV light ($\lambda_{\text{ex}} = 365$ nm) (Fig. 3.1a). The absorption spectrum of C-dots (Fig. 3.1b) showed a narrow peak at 280 nm assigned to the $\pi \rightarrow \pi^*$ transition of nanocarbon. The as synthesized CNDs exhibited maximum emission at 468 nm when excited at 370 nm and photoluminescence shifted to longer wavelengths with increasing excitation wavelengths, a typical behaviour of CNDs (Fig. 3.1c). Transmission electron microscopy (TEM) images showed the formation of well-

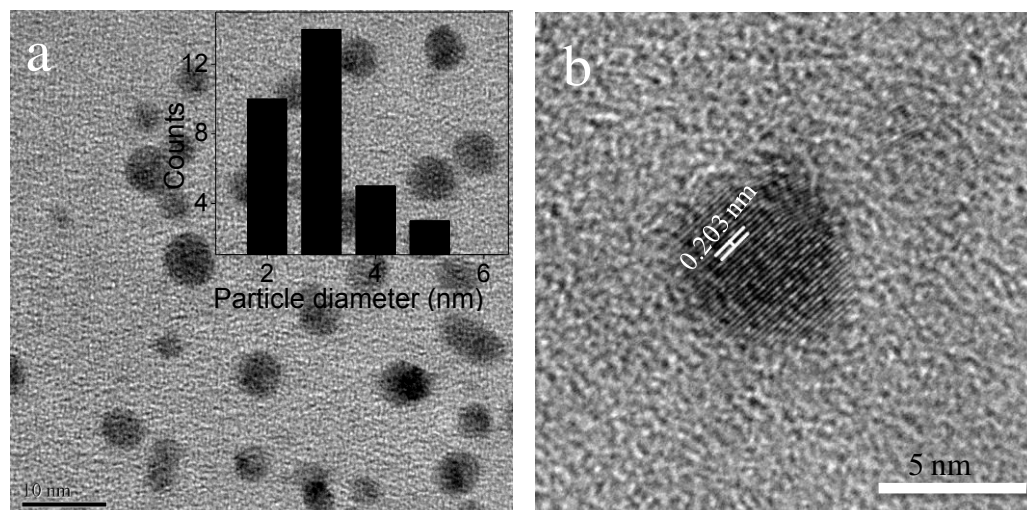


Figure 3.2. a) TEM image of CNDs (scale bar 10 nm), particle size distribution histogram (inset a) and b) High resolution transmission electron microscopy image of CNDs

dispersed spherical nanoparticles with average particle diameter of 3.5 ± 0.8 nm (Fig.3.2a). High resolution TEM image showed the formation of highly crystalline CNDs as evidenced by the appearance of lattice fringes signifying the (102) lattice plane of graphitic (sp^2) carbon (Fig. 3.2b). AFM studies validated the formation of CNDs with particle sizes in the range of 3.5-5.5 nm and their contour heights between 1 and 2 nm (Fig. 3.3a). Powder X-ray diffraction spectra of CNDs showed a broad peak at $2\theta = 23^\circ$, corresponding to a d-spacing of 3.8 \AA (Fig. 3.3b). Further, X-ray photoelectron spectroscopy (XPS) measurements revealed the structural features of CNDs. The C1s core level spectrum of CNDs was fitted into four components with binding energies (BEs) at about 285.1, 286.8, 287.8 and 289.0 eV, which correspond to C-C, C-OH, C=O and O-C=O respectively (Fig. 3.4a). The presence of hydroxyl and carboxylic acid functionality on CND surface was further confirmed by FTIR studies (Fig. 3.4b)

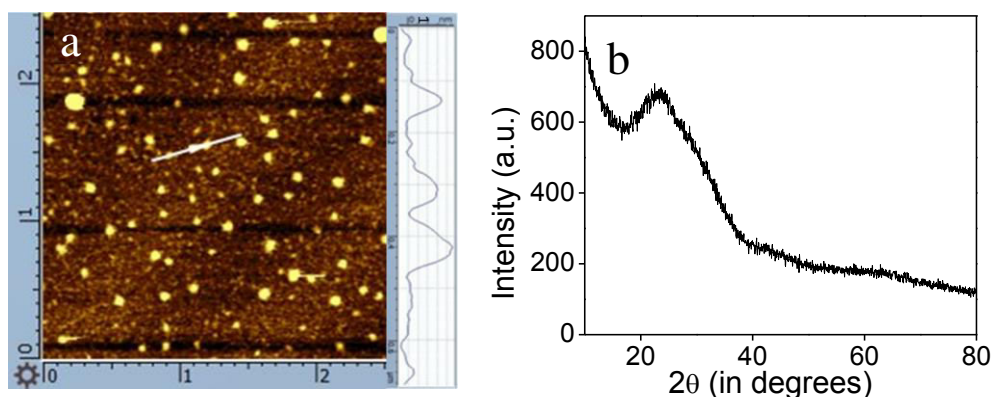


Figure 3.3. a) AFM image and b) powder X-ray diffraction pattern of CNDs

To quantify the hydroxyl and carboxyl groups present on the surface of CNDs, base titrations were performed (details in experimental section).

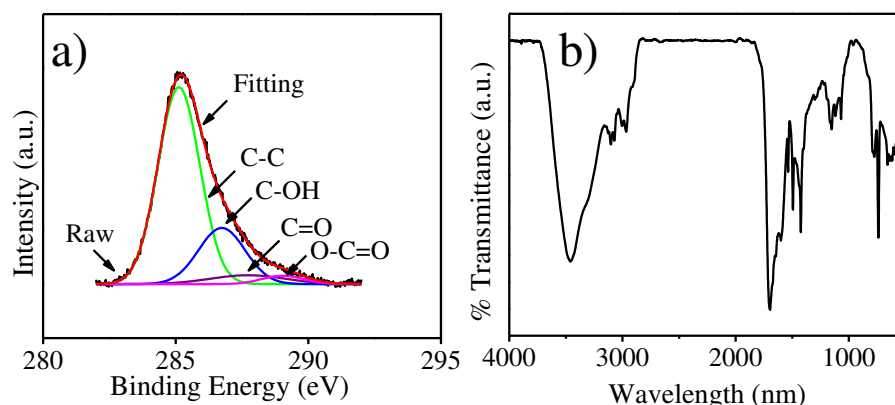
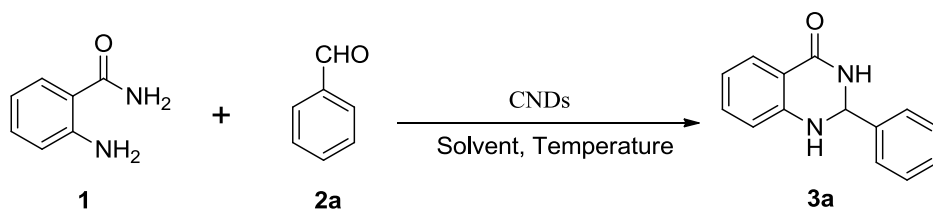


Figure 3.4. a) C1s XPS and b) FTIR spectrum of CNDs

3.2.2 Catalytic activity of carbon nanodots towards cyclocondensation reaction

The activity of $-\text{CO}_2\text{H}$ functionalized CNDs in acid catalyzed organic transformations was studied for the cyclocondensation reaction between 2-aminobenzamide and aldehydes leading to the formation of 2,3-dihydroquinazolinon-4(1H)-one (Scheme 3.1). The model reaction of condensation between 2-aminobenzamide and benzaldehyde was studied with respect to temperature, catalyst loading and solvent variation in order to achieve



Scheme 3.1. Model cyclocondensation reaction leading to the formation of 2,3-dihydroquinazolinon-4(1H)-one

the optimized reaction condition (Table 3.1 and Table 3.2). The reaction was highly dependent on catalyst loading, as higher conversion was observed with increasing concentration of CNDs.

3.2.2.1 Optimization with respect to catalyst loading, temperature, co-solvents and various acid catalysts

Table 3.1. Optimization with respect to catalyst loading and temperature^a

Entry	Catalyst loading (mg)	Temp. (°C)	Time (min)	Yield (%) ^b
1	0	25	150	45
2	1.0	25	120	62
3	3.0	25	90	65
4	5.0	25	70	76
5	5.0	40	55	97
6	7.0	40	50	97
7	5.0	40	40	79
8	5.0	40	120	^c 55
9	5.0	40	55	^d 95

^aAll the reactions were carried out using 2-aminobenzamide 1 (1.0 mmol), benzaldehyde 2a (1.0 mmol), in water-acetonitrile (9:1) mixture as solvent (11 ml). The amount of CND in the reaction medium was varied by using a parent solution of 0.6 mgmL⁻¹ concentration in water. ^bIsolated yields. ^cThe reaction was carried out by using 5 mg rCNDs. ^dThe reaction was performed under dark environment

Although the conversion was moderate at room temperature, increasing the reaction temperature to 40 °C resulted in high yield of the desired product. Further increase in temperature was detrimental for the reaction as several by-

Chapter 3

Table 3.2. Optimization with respect to co-solvents^a

Entry	Co-solvent (mL)	Time (min)	Yield (%) ^b
1	-	75	68 ^c
2	Ethanol	85	90
3	Methanol	90	88
4	Acetonitrile	55	97
5	Toluene	120	65
6	THF	60	85
7	DCM	80	81

^aAll the reactions were carried out using 10 mL of carbon dot solution in water (0.5 mgmL⁻¹) with co-solvent (1 mL), 2-aminobenzamide 1 (1.0 mmol), benzaldehyde 2a (1.0 mmol) at 40 °C.

^bIsolated yields. ^cReaction was performed in aqueous carbon dot solution

products were observed. Although the reaction proceeded well using water as the solvent, longer reaction time was required. This can be attributed to the low solubility of the substrates in water. Addition of a small amount of an organic solvent enhanced the yield minimizing the reaction time. Among different co-solvents screened, acetonitrile was found to be most suitable (Table 3.2). From these optimization studies, the best condition for this condensation reaction was found to be 10 mL of CND solution with 0.5 mgmL⁻¹ concentration at 40 °C using acetonitrile as a co-solvent. Reduced CNDs resulted in less yield of the desired product even after prolonged reaction time, suggesting the role of -CO₂H functionality on CNDs in catalyzing the reaction (Table 3.1, entry 8). Further, the model reaction was performed under a dark environment to ensure that the catalytic activity is due to the surface acidity of the CNDs and not induced by exposed daylight. Indeed, we found excellent result even when the reaction was carried out in dark (Table 3.1, entry 9). A comparative study was carried out using other carbonaceous materials such as graphene oxide, graphite, multiwall carbon nanotubes and β-cyclodextrin (Table 3.3) under the optimized reaction condition. The results clearly demonstrated the comparable catalytic activity of CNDs with GO, whereas the others gave moderate yield. For further comparison the model reaction was performed with some common acid catalysts such as conc. H₂SO₄, pTSA, benzoic acid and glacial acetic acid (Table 3.3) where conc.

Chapter 3

H₂SO₄ and *p*TSA were found to give excellent yields. Although from this comparative study we found GO, conc. H₂SO₄ and *p*TSA to be effective with respect to the product yield, the disadvantages associated with these catalysts as discussed earlier make CNDs a viable alternative for acid-catalyzed reactions.

Table 3.3. Catalytic activity of different carbon based catalysts and acid catalysts^a

Entry	Catalysts	Yield (%) ^b
1	Graphene Oxide	98
2	Graphite	64
3	MWCNT	55
4	β -Cyclodextrin	66
5	CNDs	97
6	Conc. H ₂ SO ₄	92
7	<i>p</i> -CH ₃ -C ₆ H ₄ -SO ₃ H	91
8	C ₆ H ₅ -COOH	59
9	CH ₃ COOH	57

^aAll the reactions were carried out using 2-aminobenzamide **1** (1.0 mmol), benzaldehyde **2a** (1.0 mmol), 5 mg catalyst in water-acetonitrile solvent (11 ml) at 40 °C. ^bIsolated yields

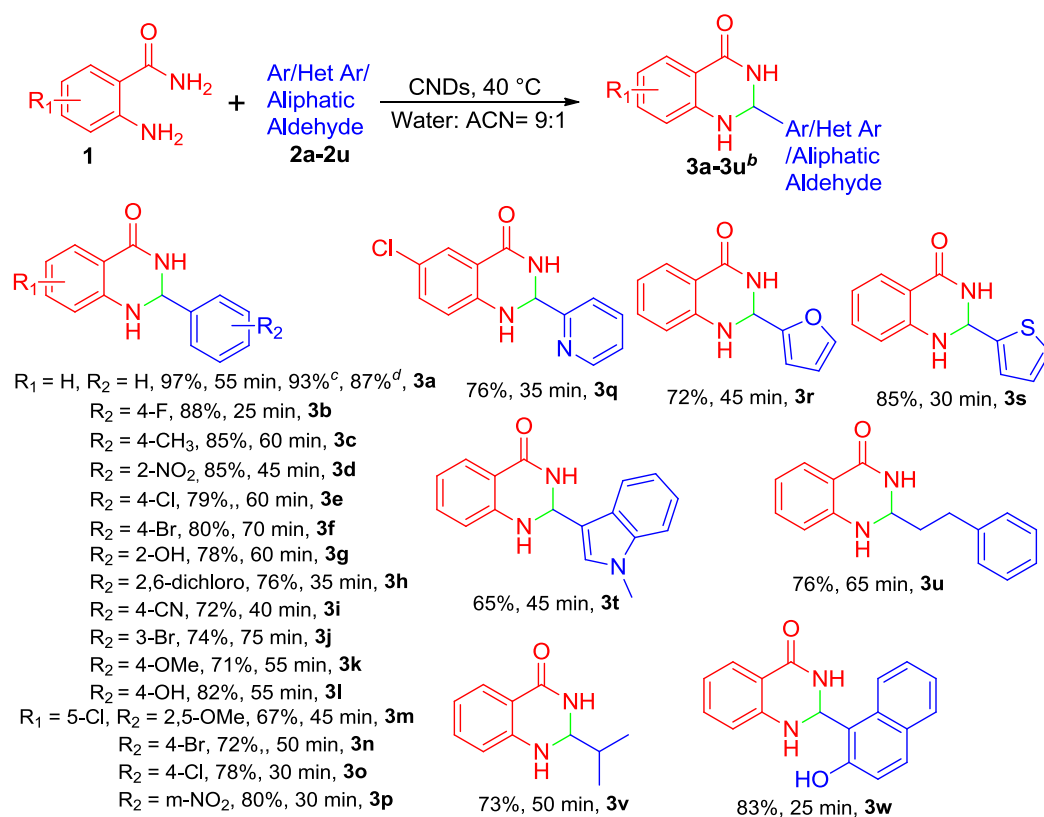
3.2.2.2 Substrate scope for the cyclocondensation reaction

After the initial assessment of the optimal reaction conditions, we investigated the scope of the reaction by condensing 2-aminobenzamide with various commercially available aromatic aldehydes having different electronically activating or deactivating substituents to form a series of dihydroquinazolines (Table 3.4). It was found that aldehydes with electron withdrawing substituents resulted in better yields compared to the ones with electron donating substituents. This can be attributed to the increased electrophilicity of the carbonyl moiety in the aldehydes with electron-withdrawing substituents. It was observed that heterocyclic aldehydes having pyridine, furan, thiophene and indole moiety (entry 3q-3t, Table 3.4) were equally compatible with the catalytic system and were easily introduced to the dihydroquinazolinone skeleton with excellent yields. The feasibility of the reaction was also investigated with aliphatic aldehydes that resulted in considerable formation of the dihydroquinazoline derivative (entry 3v, Table

Chapter 3

3.4). Aldehydes with fused ring systems were also found to be active under the set of reaction conditions and resulted in adequate yield (entry 3w, Table 3.4). To further expand the scope of the reaction, we performed the condensation reaction of aldehydes with 2-amino-5-chlorobenzamide and the yield of the dihydroquinazoline product was found to be excellent showing the efficient activity of CNDs with substituted 2-aminobenzamide as well.

Table 3.4. Substrate scope of the cyclocondensation reaction with various aromatic/heteroaromatic/aliphatic aldehydes^a

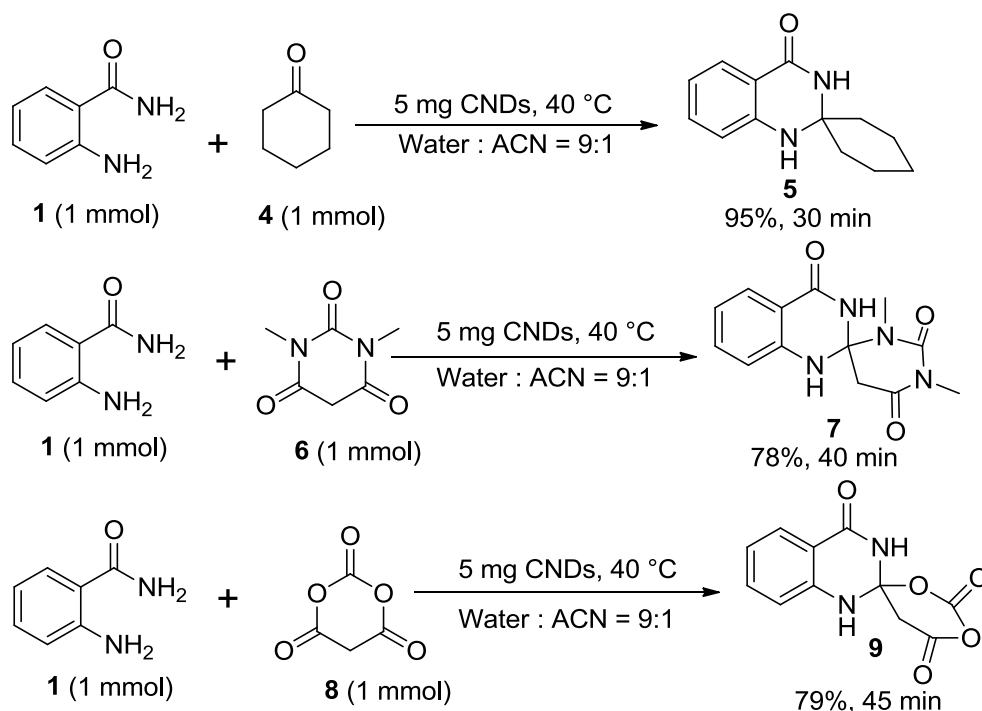


^aAll the reactions were carried out using **1** (1.0 mmol), aldehyde **2a-2u** (1.0 mmol), CND dispersion in water (10 ml)(0.5 mgmL⁻¹) and acetonitrile (1 mL) at 40 °C. ^b Isolated yields. ^{c,d}2nd and 3rd cycle respectively performed for 1 hr

After the successful exploration of CND catalysis for the condensation reaction with aromatic, aliphatic and heteroaromatic aldehydes, the methodology was further extended for cyclic ketones and cyclic heterocyclic ketones. It was observed that cyclohexanone and heterocyclic ketones 1, 3-dimethylbarbituric acid and 2, 2-dimethyl-1,3-dioxane-4,5-dione (Meldrum's acid) were easily introduced in the spirocyclized product with considerable yields (Scheme 3.2). It

Chapter 3

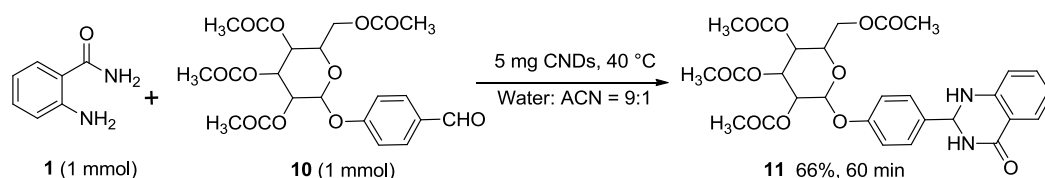
is worth mentioning that 1, 3-dimethylbarbituric acid and meldrum's acid are highly unstable under acidic or basic environment as they are prone to hydrolysis. However, due to mild acidic behavior of CNDs, the hydrolysis did not take place and we could obtain high yield of the spirocyclized product without any noticeable formation of hydrolysed by-products. Thus, the mild acidic behavior



Scheme 3.2. Synthesis of spirocyclized quinazolinones

of CND surface could be used as an effective catalyst for structurally perplexing substrates such as spirocyclized products under mild reaction conditions.

Further, we explored the possibility of using CNDs as catalysts for glycosidic bond formation. It is well known that due to high chemical sensitivity of the *O*-glycosidic linkages, synthesis of *O*-aryl glycosides is a challenging task. When 2-aminobenzamide was condensed with the glycoconjugate **10** (4-Formylphenyl 2,3,4,6-tetra-*O*-acetyl- β -D-galactopyranoside) using CNDs as a catalyst, the desired dihydroquinazolinone derivative with glycoside moiety was obtained with a significant isolated yield (Scheme 3.3). The glycosidic aldehyde **10** synthesized by a reported protocol (experimental section) and glycosidic dihydroquinazolinone **11** were characterised by NMR and Mass spectroscopy.

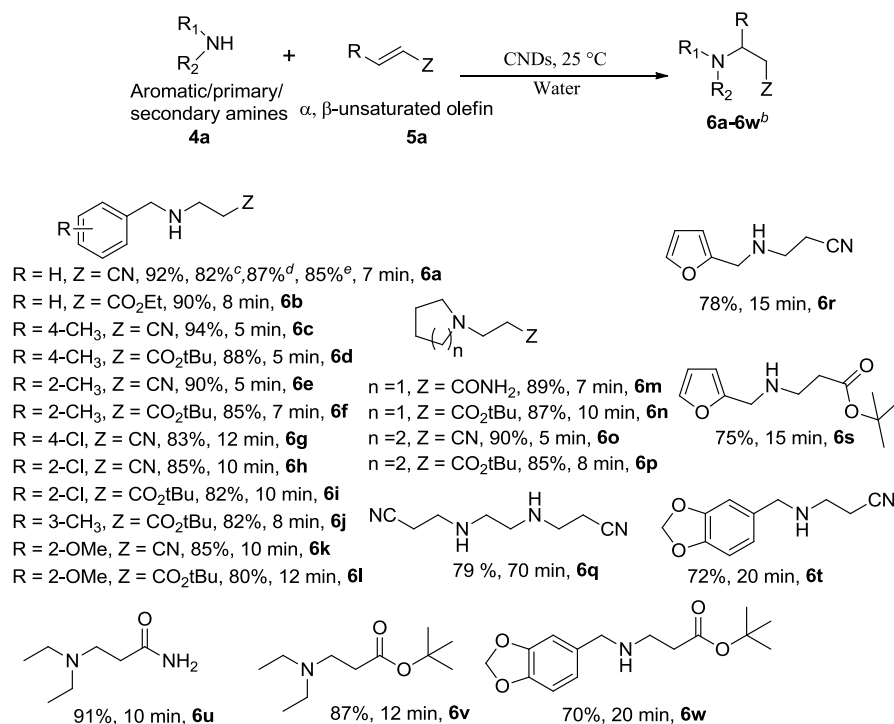


Scheme 3.3. Synthesis of Glycosidic bond

The catalytic applicability of the carboxylic acid functionalized CNDs for condensation reactions were further evaluated for the aza-Michael addition reaction between benzylamine and acrylonitrile at room temperature. In absence of any catalyst, the reaction required almost an hour to get completed in aqueous medium, as also reported by S. Verma *et al.*^[13] However, in presence of a catalytic amount of CNDs, the rate of this reaction enhanced tremendously as the reaction was completed within a short time (7 min). We extended the substrate scope using a wide range of amines with various α , β -unsaturated electron deficient systems including ethyl acrylate, acrylamide, tert-butylacrylate (Table 3.5).

3.2.3 Activity of CNDs towards aza-Michael addition reaction

Table 3.5. Aza-Michael addition of Amines and α , β -unsaturated compounds using CNDs^a



Chapter 3

^aAll reactions were carried out using 1.0 mmol of amine and 1.2 mmol of α , β -unsaturated compound, catalyst: 10 mL CNDS in water (0.5 mg mL^{-1}). ^bIsolated yields. ^cthe reaction was carried out for 55 min in water without any catalyst. ^{d,e}2nd and 3rd cycle of reaction respectively carried out for 7 min

A variety of amines including secondary amines, aromatic amines both with electronically activating and deactivating groups as well as aliphatic amines were compatible with the catalytic system and afforded the aza-Michael adducts in excellent yields. As reported in Table 3.5, most of the reactions got completed in a short reaction time (5-20 min), except for ethylenediamine (entry 6q, Table 3.5), where the reaction took prolonged time (70 min) for completion.

3.2.4 Recovery and recyclability

For industrial applications through a green chemistry approach, recyclability of the catalysts is highly desirable. We evaluated the reusability of the CNDS for both of the model reactions of 2, 3-dihydroquinazolinone and aza-Michael adducts. The CNDS could be readily recovered and reused for at least three runs without any significant impact on the yield of the products. Most important of all, the catalyst in the aqueous layer could be reused directly after the products were extracted in organic phase without any treatment. The recovered CNDS after the third cycle of reaction did not show any significant morphological or structural changes as observed by TEM (Fig. 3.5a) and other spectroscopic studies. C1s core level spectra of the recovered CNDS showed similar features of functional groups as that of the pristine catalyst showing no appreciable surface modification (Fig. 3.5b). The surface functional groups present on CNDS have been reported to influence the luminescence as they act as surface energy traps.^[44] In our case, we did not observe any shift in the emission peak in the fluorescence spectra of CNDS suggesting that the surface functional groups did not get modified during catalysis (Fig. 3.5c). This was further confirmed by zeta potential measurements, as the zeta potential value of CNDS before and after reaction did not change significantly (Fig. 3.5d). This further validates the activity of CNDS as a mere acid catalyst without undergoing any chemical modifications themselves.^[15]

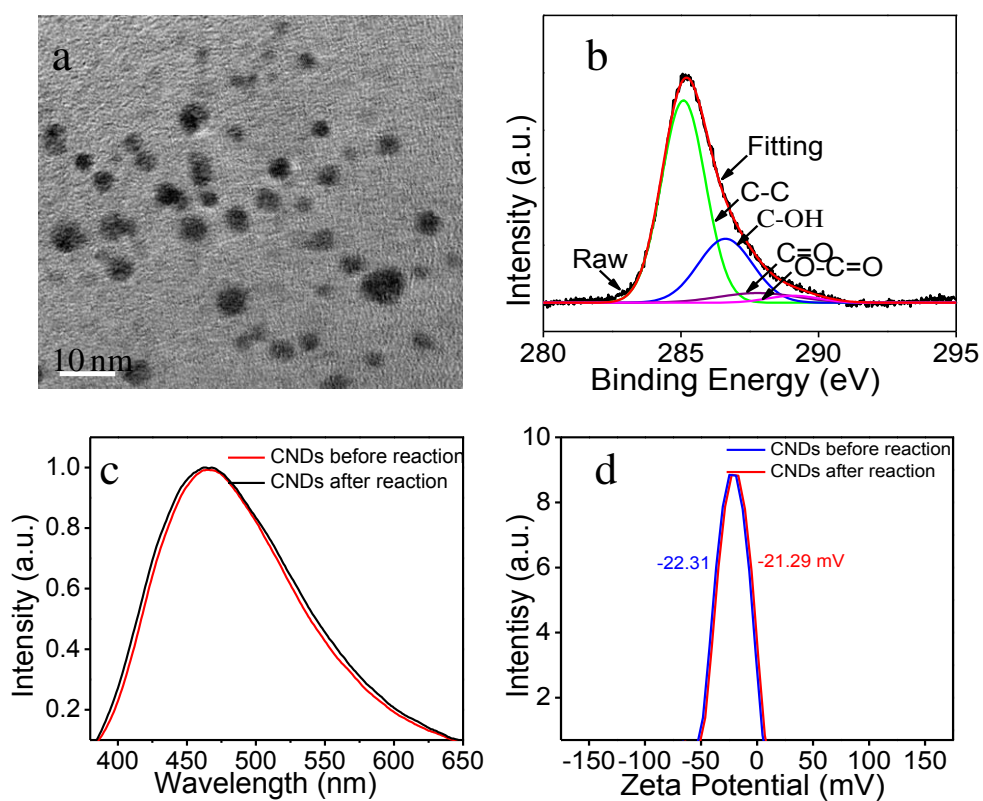
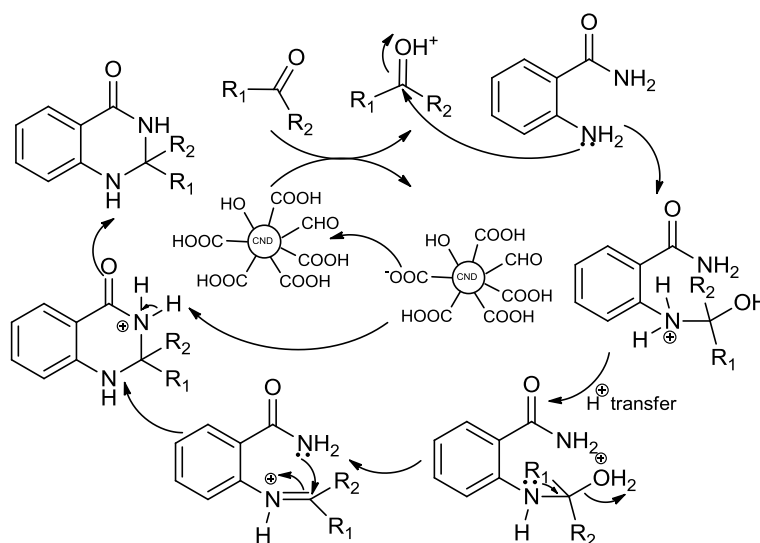


Figure 3.5. a) Transmission electron microscopy image and b) X-ray photoelectron spectroscopy study of C1s core level of CNDs recovered after 3rd cycle of reaction, c) Normalized fluorescence spectra and d) Zeta potential values of CNDs before and after reaction

3.2.5 Mechanism



Scheme 3.4. Plausible mechanism for CNDs catalyzed cyclocondensation reaction of carbonyl compound and 2-aminobenzamide

Chapter 3

A plausible mechanism for the formation of 2, 3-dihydroquinazolinone derivatives is shown below (Scheme 3.4). The inherent surface acidity of CNs first activates the carbonyl carbon making the carbon centre highly electrophilic for nucleophilic addition of 2-aminobenzamide. Hydrogen transfer resulted in protonated N, O-hemiketal followed by anchimeric assistance by the $-NH_2$ group to give an imine which further undergoes intramolecular cyclization and deprotonation to give the desired quinazolinone product.

3.3 Conclusion

In conclusion, carboxylic acid functionalized carbon nanodots can effectively catalyze condensation between 2-aminobenzamide and aldehydes/cyclic ketones leading to biologically relevant dihydro/spiroquinazolinones under mild reaction conditions. The mildly acidic surface behaviour of these dots could be extended towards the catalytic formation of aza-Michael adducts. The proficient catalytic activity of the nanodots for condensation reactions will definitely add up to the already established versatile applicability of these water-soluble, non-toxic and biocompatible fluorescent nanodots in biological, photocatalysis and opto-electronic device applications. Mild reaction conditions, easy work up and good recyclability may fortify carbon nanodots as effective acid catalyst for important organic transformations in a metal-free and green pathway.

3.4 Experimental Section

3.4.1 General Information

The powder XRD measurements were carried out by using a Bruker D8 Advance X-ray diffractometer with $CuK\alpha$ source (wavelength= 0.154 nm). TEM images were obtained by using a JEOL JEM- 2100 microscope operated at 200 kV. Atomic force microscopy was carried out by using an AIST-NT instrument (model SMART SPM 10000, Tapping mode), the samples were prepared by drop casting a water dispersion on mica. UV/Visible measurements were performed by using a Varian Cary 100 Bio Spectrophotometer. FTIR spectra were recorded with KBr pellets by using a Bruker Tensor 27 instrument. Emission spectra were recorded using a fluoromax-4p fluorometer from Horiba (Model: FM-100). The

time resolved fluorescence studies were performed on Horiba Yvon (model: Fluorocube-01-NL), a nanosecond time correlated single photon counting (TCSPC) system. The zeta potential studies were done on a Micromeritics Nanoplus 3 instrument. XPS spectra were recorded by using an ESCA instrument, VSW of UK make. ^1H and ^{13}C NMR spectra were recorded with Bruker Advance (III) 400 MHz or 100 MHz spectrometers, respectively. Data for ^1H NMR spectra are reported as chemical shift (δ ppm), multiplicity (s=singlet, d = doublet, t = triplet, m = multiplet), coupling constant (J Hz) and integration and assignment data for ^{13}C NMR spectra are reported as a chemical shift. High resolutions mass spectral analyses (HRMS) were carried out using ESI- TOF-MS.

3.4.2 Materials and Methods

The naturally occurring carbon source β -Carotene was purchased from Sisco Research Laboratory (SRL), India. Starting materials for organic reactions were purchased from Alfa Aesar and Sigma Aldrich. Acetobromo- α -D-galactose was purchased from Sigma Aldrich. All these chemicals were used without further purification. Milli-Q water was used throughout the experiments.

3.4.3 Synthesis of carbon nanodots (CNDs)

30 mg of natural carbon source β -carotene was dispersed in 30 mL Mili-Q water by sonication for 5 minutes and then the mixture was transferred to a 50 mL teflon coated autoclave. The heterogeneous mixture was then subjected to hydrothermal treatment at 180 °C for 3 hrs. This resulted in a pale-yellow dispersion of luminescent carbon nanodots after filtration. The concentration of CNDs in this dispersion was found to be 0.6 mgmL⁻¹. For the reduction of the CNDs (rCNDs), a similar procedure was followed which has been reported for reduction of grapheme oxide.^[45] Briefly, a 20 mL CND dispersion (0.6 mgmL⁻¹) was taken in a round bottom flask. Hydrazine hydrate (0.5 mL, 10 mmol) was then added and the mixture was heated under reflux conditions in an oil bath at 100 °C for 4 hours. The resultant solution was dialyzed against Milli-Q water for 48 hours to remove excess of reducing agent.

Chapter 3

3.4.4 Quantum yield of CNDs

Quantum yield of CNDs at an excitation wavelength of 350 nm was calculated using the following equation

$$\Phi = \Phi_R \times I/I_R \times OD_R/OD \times \eta^2/\eta_R^2 \quad (1)$$

Where Φ and I are the quantum yield and measured integrated emission intensity, η refractive index and OD the optical density. The subscript R refers to the reference fluorophore (Quinine sulphate, $\Phi_R = 0.54$) of known quantum yield. The quinine sulphate was dissolved in 0.1 M H_2SO_4 and CNDs was dispersed in Millipore water ($\eta = 1.33$).

Table 3.6. Quantum yield of quinine sulphate and CNDs

Substance	Absorbance at 350 nm	Area	Refractive Index	Quantum yield
Quinine sulphate	0.0769	2.26×10^8	1.33	0.54
CNDs	0.0809	8.91×10^6	1.33	0.02

3.4.5 The measurement of quantity of total functional groups (-OH and -CO₂H groups)

The quantitative assessment of -OH and -CO₂H functional groups on CND surface was carried out following a literature procedure.^[46] A CND dispersion (5 mL, 0.5 mg/mL) was first purged with argon for 30 minutes. Then it was titrated with aliquots of sodium hydroxide aqueous solution (0.05 mol/L). The mixture was stirred continuously and the pH was monitored using a pH meter. The titration was carried out until a pH of 10.41 was obtained. The total number of functional groups was calculated from the inflection point of the titration curve which was determined by plotting the ratio $\Delta pH/\Delta V$ against the volume of NaOH added. The experiment was repeated thrice to get precise values. The concentration of functional groups calculated using the equation $N_1V_1 = N_2V_2$ was found to be 1.96×10^{-3} mol/L.

3.4.6 The measurement of quantity of –CO₂H functional groups

A CND dispersion (5 mL, 0.5 mg/mL) was first purged with Ar for 30 minutes. Titration was carried out with aliquots of sodium bicarbonate aqueous solution (0.05 mol/L). The mixture was stirred continuously and the pH was monitored using a pH meter. The titration was carried out until a pH of 8.10 was reached. The acidity was calculated from the inflection point of the titration curve which was determined by plotting the ratio $\Delta\text{pH}/\Delta V$ against the volume of NaHCO₃ added. The experiment was repeated thrice to get precise values. The concentration of –CO₂H functional groups calculated to be 1.45×10^{-4} mol/L.

3.4.7 General method of synthesis of 2, 3-dihydroquinazolinones

In a typical reaction, 1.0 mmol of 2-aminobenzamide/5-chloro-2-aminobenzamide and 1.0 mmol of aldehydes/cyclic ketones were taken in a 15 mL of reaction vial with 10 mL of CNDs and 1 mL of acetonitrile. The mixture was stirred (900 rpm) at 40 °C for a period of time as mentioned in Table 3.4. The progress of the reactions was monitored by TLC using 25% ethyl acetate and hexane as eluent. After completion of the reaction, the reaction mixture was brought to room temperature where crystallized products were obtained. The crystallized products were filtered and further washed by hexane, dried and evaluated by spectral analysis. Any remaining products in the reaction mixture were further extracted using a hexane/ethyl acetate solvent mixture and subsequent evaporation under reduced pressure.

3.4.8 General method of synthesis of aza-Michael adducts

In a typical reaction, 1.0 mmol of amine and 1.2 mmol of α , β -unsaturated compound were mixed with 5 mg CND solution in water (10 mL) and stirred at room temperature for specified time as mentioned in Table 3.5. The progress of the reaction was monitored by TLC using 2% methanol-dichloromethane mixture as eluent. After completion of the reaction, the resulting products were extracted using hexane/ethyl acetate solvent mixture. The organic layer was dried over anhydrous sodium sulphate and evaporation of the solvent under reduced pressure gave the final product. The product was further dried under high vacuum and submitted for spectral analysis.

3.4.9 Reusability of the catalyst

After removing the crystallized organic products from the reaction mixture by filtration, the filtrate was further extracted with hexane/ethyl acetate solvent mixture (3 times) to remove any organic products present. The aqueous layer containing the carbon nanodots was further used for the next cycles of reaction.

3.4.10 Synthesis of 4-formylphenyl 2,3,4,6-tetra-O-acetyl- β -D-galactopyranoside

Acetobromo- α -D-galactose (0.5 g) and 4-hydroxybenzaldehyde (0.25g) were dissolved in 2.5 mL chloroform. An aqueous solution (2 mL) of sodium carbonate (0.3 g) and TBAB (tetrabutylammoniumbromide) (0.1 g) were added to the mixture.^[47] The mixture was heated to reflux under vigorous stirring overnight. The mixture was cooled, ethyl acetate was added and the organic layer was washed with 1 N NaOH solution to remove remaining phenol. Further, the organic layer was dried over sodium sulphate and evaporation of the solvent under reduced pressure. Repeated washing with ethanol and hexane gave the purified target product in 65% yield (0.38 g).

3.4.11 Characterisation data

2-phenyl-2,3-dihydroquinazolin-4(1H)-one (3a):⁴⁰ Colorless crystal (217 mg, 97%), m.p. 217-220 °C; ¹H NMR (400 MHz, CDCl₃): δ 7.94 (d, J = 7.76 Hz, 1H), 7.60 (m, 2H), 7.44 (m, 3H), 7.33 (t, J = 7.52 Hz, 1H), 6.90 (t, J = 7.76 Hz, 1H), 6.67 (d, J = 8.04 Hz, 1H), 5.90 (s, 1H), 5.88 (br, 1H, NH), 4.35 (br, 1H, NH), ¹³C NMR (100 MHz, DMSO-*d*₆): δ 164.0, 148.3, 142.1, 133.8, 128.9, 128.8, 127.8, 127.3, 117.6, 115.4, 114.8, 67.0. Mass: 224.00. HRMS (ESI): calcd for [C₁₄H₁₂N₂O + Na⁺] 247.0842, found 247.0864.

2-(4-fluorophenyl)-2,3-dihydroquinazolin-4(1H)-one (3b):⁴¹ Colorless crystal (212 mg, 88%), m.p. 199-202 °C; ¹H NMR (400 MHz, DMSO-*d*₆): δ 8.19 (br, 1H, NH), 7.67 (d, J = 7.56 Hz, 1H), 7.58 (m, 2H), 7.46-7.50 (m, 1H), 7.38 (s, 1H), 7.16 (t, J = 8.52 Hz, 1H), 6.97 (t, J = 8.8 Hz, 1H), 6.65 (d, J = 8.0 Hz, 2H), 5.74 (s, 1H, NH), ¹³C NMR (100 MHz, CDCl₃ + DMSO-*d*₆): δ 164.6, 148.0, 133.6, 129.3, 129.2, 127.8, 118.0, 115.5,

Chapter 3

115.28, 115.20, 114.8, 67.3. Mass: 242.2483, HRMS (ESI): calcd for [C₁₄H₁₁FN₂O + Na⁺] 265.0748, found 265.0771.

2-(*p*-tolyl)-2,3-dihydroquinazolin-4(1H)-one (3c):²⁸ Colorless crystal (202 mg, 85%), m.p. 232-235 °C; ¹H NMR (400 MHz, DMSO-*d*₆): δ 8.20 (br, 1H, NH), 7.57(d, *J* = 7.8 Hz, 1H), 7.34 (d, *J* = 7.76 Hz, 2H), 7.22 (t, *J* = 7.52 Hz, 1H), 7.16 (d, *J* = 7.8 Hz, 2H), 7.03 (s, 1H), 6.71 (d, *J* = 8.28 Hz, 1H), 6.65 (t, *J* = 7.52 Hz, 1H), 5.69 (s, 1H, NH), 2.28 (s, 3H), ¹³C NMR (100 MHz, DMSO-*d*₆): δ 164.1, 148.4, 139.1, 138.2, 133.7, 129.7, 129.3, 128.1, 127.8, 127.2, 117.5, 115.4, 114.8. Mass: 238.2845, HRMS (ESI): calcd for [C₁₅H₁₄N₂O + Na⁺] 261.0998, found 261.1016.

2-(2-nitrophenyl)-2,3-dihydroquinazolin-4(1H)-one (3d):⁵⁰ Orange crystal (228 mg, 85%), m.p. 193-196 °C; ¹H NMR (400 MHz, DMSO-*d*₆): δ 8.82 (1H, NH), 8.13-8.16 (m, 2H), 7.88-7.92 (m, 2H), 7.78-7.82 (m, 2H), 7.53-7.57 (m, 2H), 7.36 (t, *J* = 7.28 Hz, 1H), 7.17 (d, *J* = 7.76 Hz, 1H), ¹³C NMR (100 MHz, DMSO-*d*₆): δ 168.0, 158.7, 149.7, 149.2, 134.4, 132.8, 132.2, 130.3, 130.2, 129.9, 129.7, 127.0, 125.1, 119.7, , Mass: 269.2554, HRMS (ESI): calcd for [C₁₄H₁₁N₃O₃ + Na⁺] 292.0693, found 292.0715.

2-(4-chlorophenyl)-2,3-dihydroquinazolin-4(1H)-one (3e):⁴⁰ Colorless crystal (203 mg, 79%), m.p. 203-206 °C; ¹H NMR (400 MHz, DMSO-*d*₆): δ 8.33 (s, 1H, NH), 7.61 (d, *J* = 6.76 Hz, 1H), 7.45-7.52 (m, 4H), 7.26 (t, *J* = 8.28 Hz, 1H), 7.14 (s, 1H), 6.74 (d, *J* = 8.04 Hz, 1H), 6.69 (t, *J* = 7.24 Hz, 1H), 5.78 (s, 1H, NH), ¹³C NMR (100 MHz, DMSO-*d*₆): δ 163.9, 148.1, 141.1, 133.9, 133.4, 129.2, 128.7, 127.8, 117.7, 115.4, 114.9, 66.2.

2-(4-bromophenyl)-2,3-dihydroquinazolin-4(1H)-one (3f):⁴⁸ Colorless crystal (241 mg, 80%), m.p. 196-200 °C; ¹H NMR (400 MHz, DMSO-*d*₆): δ 8.26 (br, s, 1H, NH), 7.60 (d, *J* = 7.52 Hz, 1H), 7.52 (d, *J* = 8.52 Hz, 2H), 7.41 (d, *J* = 8.28 Hz, 2H), 7.20 (t, *J* = 7.0 Hz, 1H), 7.06 (s, 1H), 6.7 (d, *J* = 8.0 Hz, 1H), 6.63 (t, *J* = 7.28 Hz, 1H), 5.72 (s, 1H), ¹³C NMR (100 MHz, CDCl₃ + DMSO-*d*₆): δ 163.9, 148.0, 141.4, 133.7, 131.6, 129.4, 127.8, 122.0, 117.6, 115.3, 114.9, 66.4, Mass: 303.1539, HRMS (ESI): calcd for [C₁₄H₁₁BrN₂O + Na⁺] 324.9947 & 326.9927, found 324.9965 & 326.9951.

2-(2-hydroxyphenyl)-2,3-dihydroquinazolin-4(1H)-one (3g):⁴⁸ Colorless solid (187 mg, 78%), m.p. 222-225 °C; ¹H NMR (400 MHz, DMSO-*d*₆): δ 9.83 (s, 1H), 7.90 (s, 1H, NH), 7.59 (d, *J* = 7.76 Hz, 1H), 7.31 (d, *J* = 7.8 Hz, 1H), 7.20 (t, *J* = 7.04 Hz, 1H), 7.13 (t, *J* = 6.76 Hz, 1H), 6.83 (d, *J* = 8.04 Hz, 1H), 6.78 (d, *J* = 7.52 Hz, 1H), 6.75 (t, *J* = 8.28 Hz, 1H), 6.71 (s, 1H), 6.64 (t, *J* = 7.52 Hz, 1H), 5.98 (s, 1H), ¹³C NMR (100 MHz, DMSO-*d*₆): δ 164.4, 155.0, 148.5, 133.6, 129.7, 127.7, 127.68, 127.63, 119.2,

Chapter 3

117.4, 115.8, 115.2, 115.0, 61.6. Mass: 240.2573, HRMS (ESI): calcd for [C₁₄H₁₂N₂O₂ + Na⁺] 263.0791, found 263.0803.

2-(2,6-dichlorophenyl)-2,3-dihydroquinazolin-4(1H)-one (3h):⁵⁷ Pale-yellow crystal (221 mg, 76%), m.p. 166-168 °C; ¹H NMR (400 MHz, DMSO-*d*₆): δ 8.81 (s, 1H), 8.14 (br, 1H, NH), 7.91 (d, *J* = 7.24 Hz, 1H), 7.52-7.64 (m, 5H), 7.41 (t, *J* = 7.28 Hz, 1H), 7.24 (d, *J* = 7.76 Hz, 1H), ¹³C NMR (100 MHz, DMSO-*d*₆): δ 167.2, 158.8, 134.7, 133.0, 132.6, 131.6, 130.4, 130.0, 128.7, 127.5, 119.6, 97.9. . Mass: 293.1480, HRMS (ESI): calcd for [C₁₄H₁₀Cl₂N₂O + Na⁺] 315.0062, found 315.0080.

4-(4-oxo-1,2,3,4-tetrahydroquinazolin-2yl)benzotrile (3i):²⁸ Pale-yellow crystal (179 mg, 72%), m.p. 249-252 °C; ¹H NMR (400 MHz, DMSO-*d*₆): δ 8.45 (br, s, 1H, NH), 7.84 (d, *J* = 8.28 Hz, 2H), 7.63 (d, *J* = 8.04 Hz, 2H), 7.58 (d, *J* = 7.52 Hz, 1H), 7.26 (s, 1H), 7.23 (t, *J* = 7.28 Hz, 1H), 6.73 (d, *J* = 8.04 Hz, 1H), 6.67 (t, *J* = 7.28 Hz, 1H), 5.83 (s, 1H, NH), ¹³C NMR (100 MHz, DMSO-*d*₆): δ 163.8, 147.8, 147.7, 134.0, 132.8, 128.1, 127.8, 117.9, 115.3, 114.9, 111.5, 65.9. Mass: 249.2673, HRMS (ESI): calcd for [C₁₅H₁₁N₃O + Na⁺] 272.0794, found 272.0811.

2-(3-bromophenyl)-2,3-dihydroquinazolin-4(1H)-one (3j):²⁸ Colorless crystal (223 mg, 74%), m.p. 173-176 °C; ¹H NMR (400 MHz, DMSO-*d*₆): δ 8.36 (br, s, 1H, NH), 7.65 (s, 1H), 7.58 (d, *J* = 7.0 Hz, 1H), 7.51 (d, *J* = 8.04 Hz, 1H), 7.45 (d, *J* = 7.76 Hz, 1H), 7.33 (t, *J* = 8.00 Hz, 1H), 7.24 (t, *J* = 8.56 Hz, 1H), 7.19 (s, 1H), 6.73 (d, *J* = 8.04 Hz, 1H), 6.67 (t, *J* = 7.52 Hz, 1H), 5.75 (1H, NH), ¹³C NMR (100 MHz, DMSO-*d*₆): δ 163.8, 147.9, 145.1, 133.9, 131.6, 131.0, 130.1, 127.8, 126.2, 122.0, 117.8, 115.3, 114.9, 65.9. Mass: 303.1539, HRMS (ESI): calcd for [C₁₄H₁₁BrN₂O + Na⁺] 324.9947, found 324.9961.

2-(4-methoxyphenyl)-2,3-dihydroquinazolin-4(1H)-one (3k):²⁸ Colorless crystal (180 mg, 71%), m.p. 191-194 °C; ¹H NMR (400 MHz, DMSO-*d*₆): δ 8.16 (s, 1H, NH), 7.58 (d, *J* = 6.76 Hz, 1H), 7.38 (d, *J* = 8.72 Hz, 2H), 7.22 (t, *J* = 7.04 Hz, 1H), 6.98 (s, 1H), 6.92 (d, *J* = 8.8 Hz, 2H), 6.71 (d, *J* = 8.04 Hz, 1H), 6.65 (t, *J* = 7.24 Hz, 1H), 5.68 (s, 1H, NH), 3.73 (s, 3H), ¹³C NMR (100 MHz, DMSO-*d*₆): δ 164.1, 159.9, 148.4, 133.9, 133.7, 128.6, 127.8, 117.5, 115.4, 114.8, 114.1, 66.7, 55.6. Mass: 254.2839, HRMS (ESI): calcd for [C₁₅H₁₄N₂O₂ + Na⁺] 277.0947, found 277.0974.

2-(4-hydroxyphenyl)-2,3-dihydroquinazolin-4(1H)-one (3l):⁴⁸ Brown solid (196 mg, 82%), m.p. 278-281 °C; ¹H NMR (400 MHz, DMSO-*d*₆): δ 9.49 (s, 1H, -OH), 8.06 (s, 1H, NH), 7.58 (d, *J* = 7.0 Hz, 1H), 7.27 (d, *J* = 8.52 Hz, 2H), 7.21 (t, *J* = 6.76 Hz, 1H), 6.91 (s, 1H), 6.73 (d, *J* = 8.52 Hz, 2H), 6.70 (d, *J* = 8.28 Hz, 1H), 6.65 (t, *J* = 7.52 Hz,

1H), 5.63 (s, 1H, NH), ¹³C NMR (100 MHz, DMSO-*d*₆): δ 164.2, 158.1, 148.6, 133.6, 132.0, 128.7, 127.8, 117.5, 115.42, 115.40, 114.8, 67.1. Mass: 240.2573, HRMS (ESI): calcd for [C₁₄H₁₂N₂O₂ + Na⁺] 263.0791, found 263.0813.

6-chloro-2-(2,5-dimethoxyphenyl)-2,3-dihydroquinazolin-4(1H)-one (3m): Colorless solid (213 mg, 67%), ¹H NMR (400 MHz, DMSO-*d*₆): δ 8.19 (br, 1H, NH), 7.53 (d, 1H), 7.23-7.26 (dd, 1H), 7.01 (s, 1H), 6.96 (m, 1H), 6.89 (s, 1H), 6.86-6.90 (m, 1H), 6.77 (d, 1H), 5.97 (s, 1H), 3.76 (s, 3H), 3.65 (s, 3H), ¹³C NMR (100 MHz, DMSO-*d*₆): δ 163.1, 153.3, 150.9, 147.1, 133.5, 129.9, 126.8, 121.1, 116.9, 116.2, 114.1, 113.8, 112.7, 61.4, 56.5, 55.8. Mass: 318.7549, HRMS (ESI): calcd for [C₁₆H₁₅ClN₂O₃ + Na⁺] 341.0663, found 341.0678.

2-(4-bromophenyl)-6-chloro-2,3-dihydroquinazolin-4(1H)-one (3n):⁵¹ Pale-yellow solid (241 mg, 72%), m.p. 203-206 °C; ¹H NMR (400 MHz, DMSO-*d*₆): δ 8.59 (s, 1H), 8.11 (br, 1H, NH), 7.87 (d, *J* = 8.52 Hz, 2H), 7.79 (d, 1H), 7.75 (d, *J* = 8.28 Hz, 2H), 7.73 (br, 1H, NH), 7.58 (dd, *J* = 8.52, 1H), 7.27-7.29 (d, 1H), ¹³C NMR (100 MHz, DMSO-*d*₆): δ 166.6, 162.4, 148.3, 135.0, 132.5, 131.8, 131.3, 130.89, 130.8, 129.5, 126.4, 121.9. Mass: 337.5990, HRMS (ESI): calcd for [C₁₄H₁₀BrClN₂O + Na⁺] 358.9557, found 358.9568.

6-chloro-2-(4-chlorophenyl)-2,3-dihydroquinazolin-4(1H)-one (3o):⁵⁸ Colorless crystal (227 mg, 78%), m.p. 202-205 °C; ¹H NMR (400 MHz, DMSO-*d*₆): δ 8.49 (br, 1H, NH), 7.43-7.51(m, 5H), 7.34 (s, 1H), 7.26-7.28 (d, 1H), 6.75 (d, *J* = 8.76 Hz, 1H), 5.78 (br, 1H, NH), ¹³C NMR (100 MHz, DMSO-*d*₆): δ 162.8, 146.8, 140.7, 133.63, 133.6, 129.1, 128.8, 126.8, 121.4, 116.9, 116.4, 66.0. Mass: 293.1480, HRMS (ESI): calcd for [C₁₄H₁₀Cl₂N₂O + Na⁺] 315.0062, found 315.0084.

6-chloro-2-(3-nitrophenyl)-2,3-dihydroquinazolin-4(1H)-one (3p): Pale-yellow solid (242 mg, 80%), ¹H NMR (400 MHz, DMSO-*d*₆): δ 8.76 (s, 1H), 8.73 (s, 1H), 8.36-8.42 (m, 2H), 8.00 (br, 1H, NH), 7.85 (t, *J* = 7.76 Hz, 1H), 7.75 (d, 1H), 7.72 (br, 1H, NH), 7.59-7.63 (m, 1H), 7.30-7.32 (d, *J* = 8.52 Hz, 1H), ¹³C NMR (100 MHz, DMSO-*d*₆): δ 166.8, 161.5, 148.7, 147.8, 137.5, 135.3, 131.7, 131.6, 131.15, 131.12, 129.2, 126.7, 123.8, 121.9, Mass: 303.7005, HRMS (ESI): calcd for [C₁₄H₁₀ClN₃O₃ + Na⁺] 326.0303, found 316.0322.

6-chloro-2-(pyridin-2-yl)-2,3-dihydroquinazolin-4(1H)-one (3q): Colorless crystal (196 mg, 76%), ¹H NMR (400 MHz, CDCl₃): δ 11 (br, 1H, NH), 8.68 (d, 1H), 8.55 (d, 1H), 8.31 (d, 1H), 7.93 (t, *J* = 7.8 Hz, 1H), 7.71-7.78 (m, 2H), 7.41-7.52 (m, 1H), 7.26 (s, 1H), ¹³C NMR (100 MHz, CDCl₃): δ 160.3, 149.1, 148.8, 148.2, 148.1, 147.6, 137.6,

Chapter 3

135.0, 129.6, 126.4, 126.2, 123.5, 122.0, 77.2. Mass: 259.6910, HRMS (ESI): calcd for $[\text{C}_{13}\text{H}_{10}\text{ClN}_3\text{O} + \text{Na}^+]$ 282.0405, found 282.0420.

2-(furan-2-yl)-2,3-dihydroquinazolin-4(1H)-one (3r):³⁸ Light orange crystal (154 mg, 72%), m.p. 165-167 °C; ¹H NMR (400 MHz, CDCl_3): δ 7.90 (d, $J = 6.52$ Hz, 1H), 7.04 (d, 1H), 7.32 (t, $J = 8.76$ Hz, 1H), 6.88 (t, $J = 7.24$ Hz, 1H), 6.68 (d, $J = 8.00$ Hz, 1H), 6.43 (d, 1H), 6.34-6.35 (m, 1H), 6.32 (br, 1H, NH), 5.92 (t, 1H), 4.65 (br, 1H, NH), ¹³C NMR (100 MHz, CDCl_3): δ 164.4, 152.0, 146.1, 143.2, 134.0, 128.6, 119.9, 115.8, 115.0, 110.6, 108.3, 62.0. Mass: 214.2200, HRMS (ESI): calcd for $[\text{C}_{12}\text{H}_{10}\text{N}_2\text{O}_2 + \text{Na}^+]$ 237.0634, found 237.0651.

2-(thiophen-2-yl)-2,3-dihydroquinazolin-4(1H)-one (3s):⁴⁸ Light-brown solid (195 mg, 85%), m.p. 214-217 °C; ¹H NMR (400 MHz, $\text{DMSO}-d_6$): δ 8.42 (br, s, 1H, NH), 7.59 (d, $J = 7.76$ Hz, 1H), 7.43 (d, $J = 5.04$ Hz, 1H), 7.24 (t, $J = 8.04$ Hz, 1H), 7.23 (s, 1H), 7.10 (d, $J = 3.00$ Hz, 1H), 6.96 (t, $J = 4.04$ Hz, 1H), 6.73 (d, $J = 8.28$ Hz, 1H), 6.68 (t, $J = 7.52$ Hz, 1H), 6.0 (s, 1H, NH), ¹³C NMR (100 MHz, $\text{DMSO}-d_6$): δ 163.5, 147.7, 146.9, 133.8, 127.7, 126.9, 126.3, 126.1, 117.9, 115.5, 115.1, 63.0. Mass: 230.2856, HRMS (ESI): calcd for $[\text{C}_{12}\text{H}_{10}\text{N}_2\text{OS} + \text{Na}^+]$ 253.0406, found 253.0430.

2-(1-methyl-1H-indol-3-yl)-2,3-dihydroquinazolin-4(1H)-one (3t): Colorless crystal (180 mg, 65%), ¹H NMR (400 MHz, CDCl_3): δ 7.99 (d, $J = 9.04$ Hz, 1H), 7.88 (d, $J = 7.76$ Hz, 1H), 7.30-7.37 (m, 3H), 7.17 (t, $J = 8.0$ Hz, 1H), 6.91 (t, $J = 8.04$ Hz, 1H), 6.65 (d, $J = 8.04$ Hz, 1H), 6.19 (s, 1H), 5.88 (br, 1H, NH), 4.47 (br, 1H, NH), 3.81 (s, 3H), 3.48 (s, 1H), ¹³C NMR (100 MHz, CDCl_3): δ 147.9, 137.4, 133.8, 128.8, 128.4, 122.7, 120.17, 120.12, 119.5, 116.0, 114.6, 111.9, 109.7, 62.8, 33.0. Mass: 274.2753, HRMS (ESI): calcd for $[\text{C}_{17}\text{H}_{15}\text{N}_3\text{O} + \text{Na}^+]$ 300.1107, found 300.1121.

2-phenethyl-2,3-dihydroquinazolin-4(1H)-one (3u):³⁵ Pale-yellow crystal (191 mg, 76%), m.p. 170-173 °C; ¹H NMR (400 MHz, $\text{DMSO}-d_6$): δ 8.01 (br, s, 1H, NH), 7.57 (d, $J = 7.56$ Hz, 1H), 7.21-7.29 (m, 5H), 7.16 (t, $J = 7.0$ Hz, 1H), 6.72 (d, $J = 8.04$ Hz, 1H), 6.66 (t, $J = 7.28$ Hz, 2H), 4.72 (t, $J = 5.04$ Hz, 1H), 2.72-2.76 (q, $J = 8.04$ Hz, 2H), 1.88-1.94 (m, 2H), ¹³C NMR (100 MHz, CDCl_3): δ 164.5, 149.0, 142.1, 133.6, 128.8, 128.7, 127.9, 126.2, 117.5, 115.5, 114.9, 64.4, 37.1, 31.1. Mass: 252.3110, HRMS (ESI): calcd for $[\text{C}_{16}\text{H}_{16}\text{N}_2\text{O} + \text{Na}^+]$ 275.1155, found 275.1172.

2-isopropyl-2,3-dihydroquinazolin-4(1H)-one (3v):⁴⁹ Colorless crystal (138 mg, 73%), m.p. 158-161 °C; ¹H NMR (400 MHz, CDCl_3): δ 7.85 (d, $J = 9.32$ Hz, 1H), 7.28 (t, $J = 8.28$ Hz, 1H), 6.82 (t, $J = 7.04$ Hz, 1H), 6.63 (d, $J = 8.04$ Hz, 1H), 6.0 (br, 1H, NH), 4.68 (d, $J = 4.76$ Hz, 1H), 4.17 (br, 1H, NH), 1.91-1.99 (m, 1H), 1.02-1.05 (m, 6H). ¹³C NMR

(100 MHz, CDCl₃): δ 165.2, 147.4, 133.8, 128.5, 119.1, 115.5, 114.5, 70.2, 32.8, 17.0, 16.8. Mass: 190.2417, HRMS (ESI): calcd for [C₁₁H₁₄N₂O + Na⁺] 213.0998, found 213.1013.

2-(2-hydroxynaphthalene-1-yl)-2,3-dihydroquinazolin-4(1H)-one (3w):⁵⁹ Orange solid (240 mg, 83%), ¹H NMR (400 MHz, CD₃OD): δ 9.35 (s, 1H), 8.18 (d, J = 8.56 Hz, 1H), 7.75 (d, J = 9.28 Hz, 1H), 7.66 (d, J = 8.28 Hz, 1H), 7.61 (d, J = 7.76 Hz, 2H), 7.56 (t, J = 8.04 Hz, 1H), 7.45 (t, J = 8.28 Hz, 1H), 7.22-7.30 (m, 2H), 6.82 (d, J = 9.28 Hz, 1H), ¹³C NMR (100 MHz, DMSO-*d*₆): δ 172.6, 169.6, 154.2, 142.4, 137.8, 134.0, 131.6, 129.5, 129.4, 128.8, 128.6, 127.0, 126.0, 123.9, 123.5, 120.7, 119.5, 109.2. Mass: 274.2753, HRMS (ESI): calcd for [C₁₈H₁₄N₂O₂ + Na⁺] 313.0947, found 313.0961.

1'H-spiro[cyclohexane-1,2'-quinazolin]-4'(3'H)-one (5):⁴⁰ Colorless crystal (205 mg, 95%), m.p. 222-224 °C; ¹H NMR (400 MHz, CDCl₃): δ 7.85 (d, J = 7.8 Hz, 1H), 7.29 (t, J = 7.04 Hz, 1H), 6.81 (t, J = 7.8 Hz, 1H), 6.62 (d, J = 8.04 Hz, 1H), 5.93 (br, 1H, NH), 4.29 (br, 1H, NH), 1.83 (br, 4H), 1.43-1.61 (m, 6H), ¹³C NMR (100 MHz, CDCl₃ + DMSO-*d*₆): δ 168.9, 151.3, 138.2, 132.4, 122.2, 119.6, 73.0, 42.3, 29.5, 26.3. Mass: 216.2789, HRMS (ESI): calcd for [C₁₃H₁₆N₂O + Na⁺] 239.1155, found 239.1166.

1,3-dimethyl-1H, 1'H-spiro[pyrimidine-4,2'-quinazoline]-2,4',6(3H,3'H,5H)-trione (7): Light orange solid (213 mg, 78%), ¹H NMR (400 MHz, DMSO-*d*₆): δ 7.68 (br, 1H, NH), 7.49 (d, J = 8.04 Hz, 1H), 7.10 (t, J = 8.04 Hz, 1H), 7.01 (br, 1H, NH), 6.64 (d, J = 8.28 Hz, 1H), 6.45 (t, J = 7.28 Hz, 1H), 3.68 (s, 2H), 3.09 (s, 6H), ¹³C NMR (100 MHz, DMSO-*d*₆): δ 207.0, 171.7, 166.4, 152.8, 150.6, 132.3, 129.2, 116.8, 114.8, 114.1, 31.1, 28.2. Mass: 274.2753, HRMS (ESI): calcd for [C₁₃H₁₄N₄O₃ + Na⁺] 297.0958, found 297.0980.

2,2-dimethyl-1'H-spiro[[1,3]dioxane-4,2'-quinazoline]-4',6(3'H)-dione (9): Orange crystal (195 mg, 79%), ¹H NMR (400 MHz, CDCl₃): δ 7.84 (d, J = 7.76 Hz, 1H), 7.29 (t, J = 8.8 Hz, 1H), 6.81 (t, J = 8.0 Hz, 1H), 6.66 (br, 1H, NH), 6.59 (d, J = 8.04 Hz, 1H), 3.44-3.52 (m, 1H), 2.15 (s, 1H), 1.54 (s, 6H), ¹³C NMR (100 MHz, CDCl₃): δ 171.1, 164.8, 145.9, 134.1, 128.4, 118.9, 114.7, 114.3, 67.6, 30.9, 29.6. Mass: 248.1916, HRMS (ESI): calcd for [C₁₁H₈N₂O₅ + Na⁺] 271.0325, found 271.0348.

4-Formylphenyl 2,3,4,6-tetra-O-acetyl- β -D-galactopyranoside (10):⁴⁷ Orange liquid (293 mg, 65%), m.p. 143-145 °C; ¹H NMR (400 MHz, CDCl₃): δ 9.92 (s, 1H), 7.83 (d, J = 8.52 Hz, 2H), 7.09 (d, J = 8.76 Hz, 2H), 5.46-5.53 (m, 2H), 5.10-5.16 (m, 2H), 4.10-4.22 (m, 3H), 2.18 (s, 3H), 2.15 (s, 6H), 2.01 (s, 3H), ¹³C NMR (100 MHz, CDCl₃): δ 190.7, 170.3, 170.1, 170.0, 169.3, 161.3, 131.8, 116.7, 98.6, 71.3, 70.6, 68.4, 66.7, 61.3,

Chapter 3

20.7, 20.66, 20.64, 20.57. Mass: 452.4087, HRMS (ESI): calcd for [C₂₁H₂₄O₁₁ + Na⁺] 475.1211, found 475.1222.

2-(acetoxymethyl)-6-(4-(4-oxo-1,2,3,4-tetrahydroquinazolin-2-yl)phenoxy)tetrahydro-2H-pyran-3,4,5-triyl triacetate (11):²⁸ Colorless solid (376 mg, 66%), ¹H NMR (400 MHz, CDCl₃): δ 7.91 (d, *J* = 7.52 Hz, 1H), 7.51 (d, *J* = 8.76 Hz, 2H), 7.32 (t, *J* = 7.0 Hz, 1H), 7.03 (d, *J* = 8.76 Hz, 2H), 6.89 (t, *J* = 7.52 Hz, 1H), 6.64 (d, *J* = 8.04 Hz, 1H), 5.86 (s, 1H), 5.72 (br, 1H, NH), 5.45-5.51 (m, 2H), 5.10 (dd, *J* = 7.04 Hz, 1H), 5.06 (d, *J* = 7.76 Hz, 1H), 4.32 (br, 1H, NH), 4.13-4.24 (m, 2H), 4.07 (t, *J* = 6.52 Hz, 1H), 2.17 (s, 3H), 2.01-2.06 (m, 9H), ¹³C NMR (100 MHz, CDCl₃): δ 170.3, 170.2, 170.1, 169.3, 164.7, 158.08, 158.06, 147.1, 134.1, 133.47, 133.46, 128.9, 128.7, 119.8, 117.3, 115.6, 114.6, 99.38, 99.36, 71.2, 70.7, 68.56, 68.55, 66.8, 61.3, 20.75, 20.71, 20.67, 20.6. Mass: 570.5446, HRMS (ESI): calcd for [C₂₈H₃₀N₂O₁₁ + Na⁺] 593.1791, found 593.1810.

3-(benzylamino)propanenitrile (6a):³⁴ Yellow liquid (147 mg, 92%), ¹H NMR (400 MHz, CDCl₃): δ 7.19-7.29 (m, 5H), 3.76 (s, 2H), 2.86 (t, *J* = 6.52 Hz, 2H), 2.45 (t, *J* = 6.76 Hz, 2H), 2.18 (br, 1H, NH), ¹³C NMR (100 MHz, CDCl₃): δ 139.35, 128.64, 128.55, 128.06, 127.47, 127.26, 118.67, 53.14, 44.29, 18.72.

Ethyl 3-(benzylamino)propanoate (6b):⁵² Yellow liquid (186 mg, 90%), ¹H NMR (400 MHz, CDCl₃): δ 7.26-7.35 (m, 5H), 4.10-4.18(q, 2H), 3.83 (s, 2H), 2.92(t, *J* = 6.52 Hz, 2H), 2.56 (t, *J* = 6.52 Hz, 2H), 1.99 (br, 1H, NH), 1.27 (t, *J* = 7.0 Hz, 3H), ¹³C NMR (100 MHz, CDCl₃): δ 172.81, 139.98, 128.71, 128.45, 128.23, 128.14, 127.03, 60.49, 53.76, 44.47, 34.72, 14.25.

3-((4-methylbenzyl)amino)propanenitrile (6c):⁵⁶ Yellow liquid (163 mg, 94%), ¹H NMR (400 MHz, CDCl₃): δ 7.18-7.20 (d, *J* = 8 Hz, 2H), 7.12-7.14 (d, *J* = 8 Hz, 2H), 3.78 (s, 2H), 2.91 (t, *J* = 6.52 Hz, 2H), 2.50 (t, *J* = 6.52 Hz, 2H), 2.33 (s, 3H), 1.84 (br, 1H, NH), ¹³C NMR (100 MHz, CDCl₃): δ 136.98, 136.39, 129.28, 128.08, 118.67, 52.86, 44.34, 21.08, 18.77.

tert-butyl 3-((4-methylbenzyl)amino)propanoate (6d): Yellow liquid (219 mg, 88%), ¹H NMR (400 MHz, CDCl₃): δ 7.19-7.21 (d, *J* = 8 Hz, 2H), 7.11 (d, *J* = 8 Hz, 2H), 3.75 (s, 2H), 2.84 (t, *J* = 6.52 Hz, 2H), 2.45 (t, *J* = 6.52 Hz, 2H), 2.31 (s, 3H), 2.0 (br, 1H, NH), 1.42 (s, 9H), ¹³C NMR (100 MHz, CDCl₃): δ 172.12, 136.80, 129.14, 128.19, 80.58, 53.47, 44.63, 44.58, 35.76, 28.17, 21.11. Mass: 249.3486, HRMS (ESI): calcd for [C₁₅H₂₃NO₂ + Na⁺] 272.1621, found 272.1649.

Chapter 3

3-((2-methylbenzyl)amino)propanenitrile (6e): Yellow liquid (156 mg, 90%), ^1H NMR (400 MHz, CDCl_3): δ 7.10-7.19 (m, 4H), 3.74 (s, 2H), 2.90 (t, $J = 6.52$ Hz, 2H), 2.46 (t, $J = 6.52$ Hz, 2H), 2.29 (s, 3H), 1.56 (br, 1H, NH), ^{13}C NMR (100 MHz, CDCl_3): δ 137.37, 136.52, 130.49, 128.49, 127.37, 126.01, 118.77, 51.08, 44.77, 18.98, 18.83. Mass: 174.2423, HRMS (ESI): calcd for $[\text{C}_{11}\text{H}_{14}\text{N}_2 + \text{Na}^+]$ 197.1049, found 197.1065.

tert-butyl 3-((2-methylbenzyl)amino)propanoate (6f): Yellow liquid (211 mg, 85%), ^1H NMR (400 MHz, CDCl_3): δ 7.28 (m, 1H), 7.15-7.18 (m, 3H), 3.76 (s, 2H), 2.89 (t, $J = 6.28$ Hz, 2H), 2.46 (t, $J = 6.24$ Hz, 2H), 2.34 (s, 3H), 1.80 (br, 1H, NH), 1.44 (s, 9H), ^{13}C NMR (100 MHz, CDCl_3): δ 172.07, 137.82, 136.37, 130.28, 128.52, 127.07, 125.93, 80.51, 51.41, 45.11, 35.84, 28.14, 18.93. Mass: 249.3486, HRMS (ESI): calcd for $[\text{C}_{15}\text{H}_{23}\text{NO}_2 + \text{Na}^+]$ 272.1621, found 272.1641.

3-((4-chlorobenzyl)amino)propanenitrile (6g):⁵⁶ Yellow liquid (161 mg, 83%), ^1H NMR (400 MHz, CDCl_3): δ 7.27-7.33 (m, 4H), 3.82 (s, 2H), 2.94 (t, $J = 6.52$ Hz, 2H), 2.52 (t, $J = 6.52$ Hz, 2H), 1.63 (br, 1H, NH), ^{13}C NMR (100 MHz, CDCl_3): δ 138.02, 132.96, 129.41, 128.67, 118.69, 52.43, 44.30, 18.84.

3-((2-chlorobenzyl)amino)propanenitrile (6h): Yellow liquid (165 mg, 85%), ^1H NMR (400 MHz, CDCl_3): δ 7.38-7.43 (m, 2H), 7.24-7.30 (m, 2H), 3.96 (s, 2H), 2.96 (t, $J = 6.52$ Hz, 2H), 2.56 (t, $J = 6.76$ Hz, 2H), 2.23 (br, 1H, NH), ^{13}C NMR (100 MHz, CDCl_3): δ 136.80, 133.74, 130.10, 129.67, 128.69, 127.0, 118.60, 50.57, 44.36, 18.82. Mass: 194.6607, HRMS (ESI): calcd for $[\text{C}_{10}\text{H}_{11}\text{ClN}_2 + \text{Na}^+]$ 217.0503, found 217.0520.

tert-butyl 3-((2-chlorobenzyl)amino)propanoate (6i): Yellow liquid (220 mg, 82%), ^1H NMR (400 MHz, CDCl_3): δ 7.36-7.45 (m, 2H), 7.20-7.28 (m, 2H), 3.93 (s, 2H), 2.91 (t, $J = 6.52$ Hz, 2H), 2.50 (t, $J = 6.52$ Hz, 2H), 2.30 (br, 1H, NH), 1.46 (s, 9H), ^{13}C NMR (100 MHz, CDCl_3): δ 172.00, 137.17, 133.76, 130.15, 129.50, 128.41, 126.87, 80.64, 51.05, 44.65, 35.79, 28.13. Mass: 269.7671, HRMS (ESI): calcd for $[\text{C}_{11}\text{H}_8\text{N}_2\text{O}_5 + \text{Na}^+]$ 292.1075, found 292.1102.

tert-butyl 3-((3-methylbenzyl)amino)propanoate (6j): Yellow liquid (204 mg, 82%), ^1H NMR (400 MHz, CDCl_3): δ 7.19 (t, $J = 7.52$ Hz, 1H), 7.12 (s, 1H), 7.09-7.11 (d, $J = 7.52$ Hz, 1H), 7.03-7.05 (d, $J = 8.04$ Hz, 1H), 3.74 (s, 2H), 2.84 (t, $J = 6.52$ Hz, 2H), 2.44 (t, $J = 6.52$ Hz, 2H), 2.32 (s, 3H), 1.88 (br, 1H, NH), 1.43 (s, 9H), ^{13}C NMR (100 MHz, CDCl_3): δ 172.21, 140.04, 138.05, 128.96, 128.33, 127.73, 125.21, 80.56, 53.86, 44.80, 35.85, 28.16, 21.41. Mass: 249.3486, HRMS (ESI): calcd for $[\text{C}_{15}\text{H}_{23}\text{NO}_2 + \text{Na}^+]$ 272.1621, found 272.1639.

Chapter 3

3-((2-methoxybenzyl)amino)propanenitrile (6k): Yellow liquid (161 mg, 85%), ^1H NMR (400 MHz, CDCl_3): δ 7.23-7.31 (m, 2H), 6.90-6.97 (m, 2H), 3.87 (s, 3H), 3.85 (s, 2H), 2.91 (t, $J = 6.52$ Hz, 2H), 2.54 (t, $J = 6.76$ Hz, 2H), 1.93 (br, 1H, NH), ^{13}C NMR (100 MHz, CDCl_3): δ 157.65, 129.94, 128.72, 127.31, 120.54, 118.79, 110.39, 55.31, 48.75, 44.29, 18.66. Mass: 190.2417, HRMS (ESI): calcd for $[\text{C}_{11}\text{H}_{14}\text{N}_2\text{O} + \text{Na}^+]$ 213.0998, found 213.1019.

tert-butyl 3-((2-methoxybenzyl)amino)propanoate (6l): Yellow liquid (212 mg, 80%), ^1H NMR (400 MHz, CDCl_3): δ 7.20-7.24 (m, 2H), 6.83-6.91 (m, 2H), 3.82 (s, 3H), 3.78 (s, 2H), 2.82 (t, $J = 6.52$ Hz, 2H), 2.44 (t, $J = 6.76$ Hz, 2H), 1.95 (br, 1H, NH), 1.42 (s, 9H), ^{13}C NMR (100 MHz, CDCl_3): δ 172.15, 157.62, 129.81, 128.28, 128.05, 120.43, 110.25, 80.43, 55.26, 49.12, 44.73, 35.99, 28.14. Mass: 265.3480, HRMS (ESI): calcd for $[\text{C}_{15}\text{H}_{23}\text{NO}_3 + \text{Na}^+]$ 288.1570, found 288.1589.

3-(pyrrolidin-1-yl)propanamide (6m):¹³ Yellow liquid (126 mg, 89%), ^1H NMR (400 MHz, CDCl_3): δ 8.18 (br, 1H, NH), 5.73 (br, 1H, NH), 2.71 (t, $J = 5.76$ Hz, 2H), 2.52-2.55 (m, 4H), 2.38 (t, $J = 6.28$ Hz, 2H), 1.74-1.80 (m, 4H), ^{13}C NMR (100 MHz, CDCl_3): δ 175.49, 53.43, 51.63, 34.12, 23.52.

tert-butyl 3-(pyrrolidin-1-yl)propanoate (6n): Yellow liquid (173 mg, 87%), ^1H NMR (400 MHz, CDCl_3): δ 2.71 (t, $J = 7.52$ Hz, 2H), 2.49 (t, $J = 6.56$ Hz, 4H), 2.42 (t, $J = 7.76$ Hz, 2H), 1.75 (m, 4H), 1.41 (s, 9H), ^{13}C NMR (100 MHz, CDCl_3): δ 171.8, 80.3, 54.0, 51.4, 35.3, 28.1, 23.5. Mass: 199.2899, HRMS (ESI): calcd for $[\text{C}_{11}\text{H}_{21}\text{NO}_2 + \text{Na}^+]$ 222.1465, found 222.1483.

3-(piperidin-1-yl)propanenitrile (6o):³⁴ Yellow liquid (124 mg, 90%), ^1H NMR (400 MHz, CDCl_3): δ 2.67 (t, $J = 6.76$ Hz, 2H), 2.51 (t, $J = 7.24$ Hz, 2H), 2.43 (t, $J = 5.00$ Hz, 4H), 1.56-1.61 (m, 4H), 1.39-1.45 (m, 2H), ^{13}C NMR (100 MHz, CDCl_3): δ 118.97, 54.12, 54.01, 25.70, 24.0, 15.59.

tert-butyl 3-(piperidin-1-yl)propanoate (6p):⁵³ Yellow liquid (181 mg, 85%), ^1H NMR (400 MHz, CDCl_3): δ 2.64 (t, $J = 7.76$ Hz, 2H), 2.42-2.45 (m, 6H), 1.55-1.61 (m, 6H), 1.42 (s, 9H), ^{13}C NMR (100 MHz, CDCl_3): δ 171.99, 80.42, 54.31, 54.19, 33.27, 28.11, 25.73, 24.15.

3,3'-(ethane-1,2-diylbis(azanediy))dipropanenitrile (6q):⁵⁴ Yellow liquid (131 mg, 79%), ^1H NMR (400 MHz, CDCl_3): δ 2.90 (t, $J = 6.52$ Hz, 4H), 2.72 (s, 4H), 2.48 (t, $J = 6.52$ Hz, 4H), 1.67 (br, 2H, NH), ^{13}C NMR (100 MHz, CDCl_3): δ 118.81, 48.41, 44.98, 18.87.

Chapter 3

3-((furan-2-ylmethyl)amino)propanenitrile (6r):⁵⁵ Yellow liquid (117 mg, 78%), ¹H NMR (400 MHz, CDCl₃): δ 7.35-7.36 (m, 1H), 6.29-6.31 (m, 1H), 6.19 (m, 1H), 3.81 (s, 2H), 2.90 (t, *J* = 6.76 Hz, 2H), 2.49 (t, *J* = 6.76 Hz, 2H), 1.74 (br, 1H, NH), ¹³C NMR (100 MHz, CDCl₃): δ 152.91, 142.20, 118.60, 110.27, 107.48, 45.49, 44.12, 18.70.

tert-butyl 3-((furan-2-ylmethyl)amino)propanoate (6s): Yellow liquid (169 mg, 75%), ¹H NMR (400 MHz, CDCl₃): δ 7.33 (m, 1H), 6.28-6.29 (m, 1H), 6.16-6.17 (m, 1H), 3.77 (s, 2H), 2.82 (t, *J* = 6.52 Hz, 2H), 2.42 (t, *J* = 6.28 Hz, 2H), 1.91 (br, 1H, NH), 1.42 (s, 9H) ¹³C NMR (100 MHz, CDCl₃): δ 172.10, 153.62, 141.88, 110.13, 107.01, 80.66, 46.13, 44.47, 35.70, 28.13. Mass: 225.2842, HRMS (ESI): calcd for [C₁₂H₁₉NO₃ + Na⁺] 248.1257, found 248.1283.

3-((benzo[*d*][1,3]dioxol-5-ylmethyl)amino)propanenitrile (6t): Yellow liquid (147 mg, 72%), ¹H NMR (400 MHz, CDCl₃): δ 6.83 (s, 1H), 6.75 (s, 2H), 5.94 (s, 2H), 3.73 (s, 2H), 2.90 (t, *J* = 6.52 Hz, 2H), 2.51 (t, *J* = 6.52 Hz, 2H), 1.73 (br, 1H, NH), ¹³C NMR (100 MHz, CDCl₃): δ 147.87, 146.78, 133.37, 121.23, 118.75, 108.57, 108.19, 101.02, 52.98, 44.16, 18.81. Mass: 204.2252, HRMS (ESI): calcd for [C₁₁H₁₂N₂O₂ + Na⁺] 227.0791, found 227.0812.

3-(diethylamino)propanamide (6u):¹³ Yellow liquid (131 mg, 91%), ¹H NMR (400 MHz, CDCl₃): δ 8.32 (br, 1H, NH), 2.64 (t, *J* = 7.52 Hz, 2H), 2.49-2.52 (q, 4H), 2.32 (t, *J* = 7.84 Hz, 2H), 0.99 (t, 6H), ¹³C NMR (100 MHz, CDCl₃): δ 175.9, 48.7, 46.0, 32.5, 11.3.

tert-butyl 3-(diethylamino)propanoate (6v):⁵³ Yellow liquid (175 mg, 87%), ¹H NMR (400 MHz, CDCl₃): δ 2.77 (t, *J* = 7.76 Hz, 2H), 2.50-2.55 (q, 4H), 2.37 (t, *J* = 7.8 Hz, 2H), 1.42 (s, 9H), 1.03 (t, 6H).

tert-butyl 3-((benzo[*d*][1,3]dioxol-5-ylmethyl)amino)propanoate (6w): Yellow liquid (195 mg, 70%), ¹H NMR (400 MHz, CDCl₃): δ 6.83 (s, 1H), 6.75 (s, 2H), 5.92 (s, 2H), 3.69 (s, 2H), 2.82 (t, *J* = 6.56 Hz, 2H), 2.43 (t, *J* = 6.52 Hz, 2H), 1.97 (br, 1H, NH), 1.43 (s, 9H), ¹³C NMR (100 MHz, CDCl₃): δ 172.21, 147.71, 146.53, 134.03, 121.27, 108.72, 108.11, 100.90, 80.61, 53.61, 44.52, 35.77, 28.16. Mass: 279.3315, HRMS (ESI): calcd for [C₁₅H₂₁NO₄ + Na⁺] 302.1363, found 302.1384.

3.5 References

Chapter 3

1. Kitano M., Nakajima K., Kondo J. N., Hayashi S., Hara M. J. (2010), Protonated titanate nanotubes as solid acid catalyst, *J. Am. Chem. Soc.*, 132, 6622-6623 (DOI:10.1021/ja100435w)
2. Čorić, I., List B. (2012), Asymmetric spiroacetalization catalyzed by confined brønsted acids, *Nature*, 483, 315-319 (DOI: 10.1038/nature10932)
3. Clark J. H. (2002), Solid acids for green chemistry, *Acc. Chem. Res.*, 35, 791-797 (DOI:10.1021/ar010072a)
4. Juan A., Agulló M., Sevilla M., Diez M. A., Fuerters A. B. (2010), Synthesis of carbon-based solid acid microspheres and their application to the production of biodiesel, *ChemSusChem.*, 3, 1352-1354 (DOI: 10.1002/cssc.201000308)
5. Dreyer D. R., Bielawski C. W. (2011), Carbocatalysis: Heterogeneous carbons finding utility in synthetic chemistry, *Chem. Sci.*, 2, 1233-1240 (DOI:10.1039/c1sc00035g)
6. Machado B. F., Serp P. (2012), Graphene-based materials for catalysis, *Catal. Sci. Technol.*, 2, 54-75 (DOI:10.1039/c1cy00361e)
7. Yu H., Peng F., Tan J., Hu X., Wang H., Yang J., Zheng W. (2011), Selective catalysis of the aerobic oxidation of cyclohexane in the liquid phase by carbon nanotubes, *Angew. Chem. Int. Ed.*, 50, 3978-3982 (DOI:10.1002/anie.201007932)
8. Primo A., Neatu F., Florea M., Parvulescu V., Garcia H. (2014), Graphenes in the absence of metals as carbocatalysts for selective acetylene hydrogenation and alkene hydrogenation, *Nat. Commun.*, 5, 5291-5299 (DOI:10.1038/ncomms6291)
9. Su C., Acik M., Takai K., Lu J., Hao S. -J., Zheng Y., Wu P., Bao Q., Enoki T., Chabal Y. J., Loh K. P. (2012), Probing the catalytic activity of porous graphene oxide and the origin of this behaviour, *Nat. Commun.*, 3, 1298-1306 (DOI:10.1038/ncomms2315)

Chapter 3

10. Zhang J., Su D., Zhang A., Wang D., Schlögl R., Hébert C. (2007), Nanocarbon as robust catalyst: Mechanistic insight into carbon-mediated catalysis, *Angew. Chem. Int. Ed.*, 46, 7319-7323 (DOI: 10.1002/anie.200702466)
11. Wen G., Wu S., Li B., Dai C., Su D. S. (2015), Sulfated carbon quantum dots as efficient visible-light switchable acid catalysts for room-temperature ring-opening reactions, *Angew Chem. Int. Ed.*, 54, 4105-4109 (DOI:10.1002/anie.201501698)0
12. Dreyer D. R., Jia H. -P., Bielawski C. W. (2010), Graphene oxide: A convenient carbocatalyst for facilitating oxidation and hydration reactions, *Angew. Chem. Int. Ed.*, 49, 6813-6816 (DOI: 10.1002/anie.201002160)
13. Verma S., Mungse H. P., Kumar N., Choudhary S., Jain S. L., Sain B., Khatri O. P. (2011), Graphene oxide: An efficient and reusable carbocatalyst for aza-Michael addition of amines to activated alkenes, *Chem. Commun.*, 47, 12673-12675 (DOI:10.1039/c1cc15230k)
14. Dreyer D. R., Jarvis K. A., Ferreira P. J., Bielawski C. W. (2012), Graphite oxide as a carbocatalyst for the preparation of fullerene-reinforced polyester and polyamide nanocomposites, *Polym. Chem.*, 3, 757-766 (DOI: 10.1039/c2py00545j)
15. Dhakshinamoorthy A., Alvaro M., Concepción P., Fornés V., Garcia H. (2012), Graphene oxide as an acid catalyst for the room temperature ring opening of epoxides, *Chem. Commun.*, 48, 5443-5445 (DOI: 10.1039/c2cc31385e)
16. Kumar A. V., Rao K. R. (2011), Recyclable graphite oxide catalyzed Friedel–Crafts addition of indoles to α,β -unsaturated ketones, *Tetrahedron Lett.*, 52, 5188-5191 (DOI:10.1016/j.tetlet.2011.08.002)
17. Bhattacharya T., Majumdar B., Dey D., Sarma T. K. (2014), Ultrasound mediated synthesis of α -aminophosphonates and 3,4-dihydropyrimidin- 2-

Chapter 3

- ones using graphene oxide as a recyclable catalyst under solvent-free conditions, *RSC Adv.*, 4, 45831-45837 (DOI: 10.1039/c4ra08533g)
18. Wang, L.; Ambrosi, A.; Pumera, M. (2013), "Metal-Free" catalytic oxygen reduction reaction on heteroatom-doped graphene is caused by trace metal impurities, *Angew. Chem. Int. Ed.*, 52, 13818-13821 (DOI: 10.1002/anie.201309171)
19. Li H., Hi X., Kang Z., Huang H., Liu Y., Liu J., Lian S., Tsang C. H. A., Yang X., Lee S.-T. (2010), Water-soluble fluorescent carbon quantum dots and photocatalyst design, *Angew. Chem. Int. Ed.*, 49, 4430-4434 (DOI: 10.1002/anie.200906154)
20. Baker S. N., Baker G. A. (2010), Luminescent carbon nanodots: emergent nanolights, *Angew. Chem. Int. Ed.*, 49, 6726-6744 (DOI: 10.1002/anie.200906623)
21. Hu C., Yu C., Li M., Wang X., Dong Q., Wang G., Qiu J. (2015), Nitrogen-doped carbon dots decorated on graphene: a novel all-carbon hybrid electrocatalyst for enhanced oxygen reduction reaction, *Chem. Commun.*, 51, 3419-3422 (DOI: 10.1039/c4cc08735f)
22. Yu H., Shi R., Zhao Y., Waterhouse G. I. N., Wu L. -Z., Tung C. -H., Zhang T. (2016), Smart utilization of carbon dots in semiconductor photocatalysis, *Adv. Mater.*, 28, 9454-9477 (DOI: 10.1002/adma.201602581)
23. Yang K. D., Ha Y., Sim U., An J., Lee C. W., Jin K., Kim Y., Park J., Hong J. S., Lee J. H., Lee H. -E., Jeong H. -Y., Kim H., Nam K. T. (2016), Graphene quantum sheet catalyzed silicon photocathode for selective CO₂ conversion to CO, *Adv. Funct. Mater.*, 26, 233-242 (DOI: 10.1002/adfm.201502751)
24. Yu H., Zhao Y., Zhou C., Shang L., Peng Y., Cao Y., Wu L. -Z., Tung C. -H., Zhang T. (2014), Carbon quantum dots/TiO₂ composites for efficient photocatalytic hydrogen evolution, *J. Mater. Chem. A*, 2, 3344-3351 (DOI: 10.1039/c3ta14108j)

Chapter 3

25. Li H., Liu R., Kong W., Liu J., Liu Y., Zhou L., Zhang X., Lee S. -T., Kang Z. (2014), Carbon quantum dots with photo-generated proton property as efficient visible light controlled acid catalyst, *Nanoscale*, 6, 867-873 (DOI: 10.1039/c3nr03996j)
26. Dey D., Bhattacharya T., Majumdar B., Mandani S., Sharma B., Sarma T. K. (2013), Carbon dot reduced palladium nanoparticles as active catalysts for carbon-carbon bond formation, *Dalton Trans.*, 42, 13821-13825 (DOI: 10.1039/c3dt51234g)
27. Han Y., Huang H., Zhang H., Liu Y., Han X., Liu R., Li H., Kang Z. (2014), Carbon Quantum dots with photoenhanced hydrogen-bond catalytic activity in Aldol condensations, *ACS Catal.*, 4, 781-787 (DOI: 10.1021/cs401118x)
28. Sharma M., Pandey S., Chauhan K., Sharma D., Kumar B., Chauhan P. M. (2012), Cyanuric chloride catalyzed mild protocol for synthesis of biologically active dihydro/spiroquinazolinones and quinazolinone-glycoconjugates, *J. Org. Chem.*, 77, 929-937 (DOI: 10.1021/jo2020856)
29. Cohen E., Klarberg B., Vaughan J. R. (1959), Quinazolinone sulfonamides. A new class of diuretic agents, *J. Am. Chem. Soc.*, 82, 2731-2735 (DOI: 10.1021/ja01496a020)
30. Alagarsamy V., Solomon V. R., Murugan M. (2007), Synthesis and pharmacological investigation of novel 4-benzyl-1-substituted-4H-[1,2,4]triazolo[4,3-*a*]quinazolin-5-ones as new class of H₁-antihistaminic agents, *Bioorg. Med. Chem.*, 15, 4009-4015 (DOI: 10.1016/j.bmc.2007.04.001)
31. Kobayashi S., Ueno M., Suzuki R., Ishitani H. (1999), Catalytic asymmetric synthesis of febrifugine and isofebrifugine, *Tetrahedron Lett.*, 40, 2175-2178 (DOI:10.1016/S0040-4039(99)00142-2)
32. Hayashi Y., Rode J. J., Corey E. J. (1996), A novel chiral super-lewis acidic catalyst for enantioselective synthesis, *J. Am. Chem. Soc.*, 118, 5502-5503 (DOI:10.1021/ja960766)

Chapter 3

33. Xu L. W., Xia C. G., Hu X. X. (2003), An efficient and inexpensive catalyst system for the aza-Michael reactions of enones with carbamates, *Chem. Commun.*, 2570-2571 (DOI: 10.1039/b307733k)
34. Surendra K., Krishnaveni N. S., Sridhar R., Rao K. R. (2006), β -Cyclodextrin promoted aza-Michael addition of amines to conjugated alkenes in water, *Tetrahedron Lett.*, 47, 2125-2127 (DOI: 10.1016/j.tetlet.2006.01.124)
35. Ramesh K., Karnakar K., Satish G., Kumar B. S. P. A., Nageswar Y. V. D. (2012), A concise aqueous phase supramolecular synthesis of 2-phenyl-2,3-dihydroquinazolin-4(1H)-one derivatives, *Tetrahedron Lett.*, 53, 6936-6939 (DOI: 10.1016/j.tetlet.2012.10.029)
36. Kantam M. L., Neeraja V., Kavita B., Neelima B., Chaudhri M. K., Hussain S. (2005), Cu(acac)₂ Immobilized in ionic liquids: A recoverable and reusable catalytic system for aza-Michael reactions, *Adv. Synth. Catal.*, 347, 763-766 (DOI: 10.1002/adsc.200404361)
37. Xu L. -W., Li J. -W., Zhou S. -L., Xia C. -G. (2004), A green, ionic liquid and quaternary ammonium salt-catalyzed aza-Michael reaction of α , β -ethylenic compounds with amines in water, *New J. Chem.*, 28, 183-184 (DOI: 10.1039/b312047c)
38. Salehi P., Dabiri M., Zolfigol M. A., Baghbanzadeh M. (2005), A novel method for the one-pot three-component synthesis of 2,3-dihydroquinazolin-4(1H)-ones, *Synlett.*, 1155-1157 (DOI: 10.1055/s-2005-865200)
39. Salehi P., Dabiri M., Baghbanzadeh M., Bahramnejad M. (2006), One-pot, three-component synthesis of 2,3-dihydro-4(1H)-quinazolinones by montmorillonite K-10 as an efficient and reusable catalyst, *Synth. Commun.*, 36, 2287-2292 (DOI:10.1080/00397910600639752)
40. Wu J., Du X., Ma J., Zhang Y., Shi Q., Luo L., Song B., Yang S., Hu D. (2014), Preparation of 2,3-dihydroquinazolin-4 (1H)-one derivatives in

Chapter 3

- aqueous media with β -cyclodextrin-SO₃H as a recyclable catalyst, *Green chem.*, 16, 3210-3217 (DOI:10.1039/c3gc42400f)
41. Safari J., Ravandi S. G. J. (2013), Microwave-accelerated three components cyclocondensation in the synthesis of 2, 3-dihydroquinazolin-4(1H)-ones promoted by Cu-CNTs, *J. Mol. Catal. A: Chem.*, 371, 135-140 (DOI:10.1016/j.molcata.2013.01.031)
42. Lim S. Y., Shen W., Gao Z. (2015), Carbon quantum dots and their applications, *Chem. Soc. Rev.*, 44, 362-381 (DOI:10.1039/c4cs00269e)
43. Li H., Sun C., Ali M., Zhou F., Zhang X., MacFarlane D. R. (2015), Sulfated carbon quantum dots as efficient visible-light switchable acid catalysts for room-temperature ring-opening reactions, *Angew. Chem. Int. Ed.*, 54, 8420-8424 (DOI: 10.1002/anie.201501698)
44. Xu Y., Wu M., Feng X. -Z., Yin X. -B., He X. -W., Zhang Y. -K., (2013), Reduced carbon dots versus oxidized carbon dots: Photo and electro chemiluminescence investigations for selected applications, *Chem. Eur. J.*, 19, 6282-6288 (DOI:10.1002/chem.201204372)
45. Stankovich S., Dikin D. A., Piner R. D., Kohlhaas K. A., Kleinhammes A., Jia Y., Wu Y., Nguyen S. T., Ruoff R. S. (2007), Synthesis of graphene-based nanosheets via chemical reduction of exfoliated graphite oxide, *Carbon*, 45, 1558-1565 (DOI:10.1016/j.carbon.2007.02.034)
46. Goertzen S. L., Thériault K. D., Oickle A. M., Tarasuk A. C., Andreas H. A. (2010), Standardization of the Boehm titration. Part I. CO₂ expulsion and endpoint determination, *Carbon*, 48, 1252-1261 (DOI: 10.1016/j.carbon.2009.11.050)
47. Hussen R. S. D., Heidelberg T., Rodzi N. Z. M., Ng S. W., Tiekink E. R. T. (2011), 4-Formylphenyl 2,3,4,6-tetra-*O*-acetyl- β -d-glucopyranoside, *Acta Cryst.*, E67, o826 (DOI:10.1107/S1600536811008099)
48. Rahman M., Ling I., Abdullah N., Hashim R., Hajra A. (2015), Organocatalysis by *p*-sulfonic acid calix[4]arene: A convenient and

Chapter 3

- efficient route to 2,3-dihydroquinazolin-4(1*H*)-ones in water, RSC Adv., 5, 7755-7760 (DOI:10.1039/c4ra16374e)
49. Kausar N., Roy I., Chattopadhyay D., Das A. R., (2016), Synthesis of 2,3-dihydroquinazolinones and quinazolin-4(3*H*)-ones catalyzed by graphene oxide nanosheets in an aqueous medium: “on-water” synthesis accompanied by carbocatalysis and selective C–C bond cleavage, RSC Adv., 6, 22320-22330 (DOI:10.1039/c6ra00388e)
50. Rostami A., Tavakoli A. (2011), Sulfamic acid as a reusable and green catalyst for efficient and simple synthesis of 2-substituted-2,3-dihydroquinazolin-4(1*H*)-ones in water or methanol, Chin. Chem. Lett., 22, 1317-1320 (DOI:10.1016/j.cclet.2011.06.008)
51. Rajaka L., Penumati N. R., Nagaiah K., Poornachandra Y., Ganesh K. C. (2015), A Convenient and scalable synthesis of 2,3-dihydroquinazolin-4(1*H*)-one derivatives and their anticancer activity, Synth. Commun., 5, 1893-1901 (DOI:10.1080/00397911.2015.1046555)
52. Kalita P., Pegu C. D., Dutta P., Baruah P. K. (2014), Room temperature solvent free aza-Michael reactions over nano-cage mesoporous materials, J. Mol. Catal. A: Chem., 394, 145-150 (DOI: 10.1016/j.molcata.2014.06.031)
53. Dash C., Saikh M. M., Butcher R. J., Ghosh P. (2010), A comparison between nickel and palladium precatalysts of 1,2,4-triazole based N-heterocyclic carbenes in hydroamination of activated olefin, Dalton Trans., 39, 2515-2524 (DOI:10.1039/b917892a)
54. Polshettiwar V., Varma R. S. (2007), Tandem bis-aza-Michael addition reaction of amines in aqueous medium promoted by polystyrene sulfonic acid, Tetrahedron Lett., 48, 8735-8738 (DOI:10.1016/j.tetlet.2007.10.008)
55. Mukherjee C., Misra A. K. (2007), Aza-Michael addition of amines to activated alkenes catalyzed by silica supported perchloric acid under a solvent-free condition, Lett. Org. Chem., 4, 54-59 (DOI: 10.2174/157017807780037414)

Chapter 3

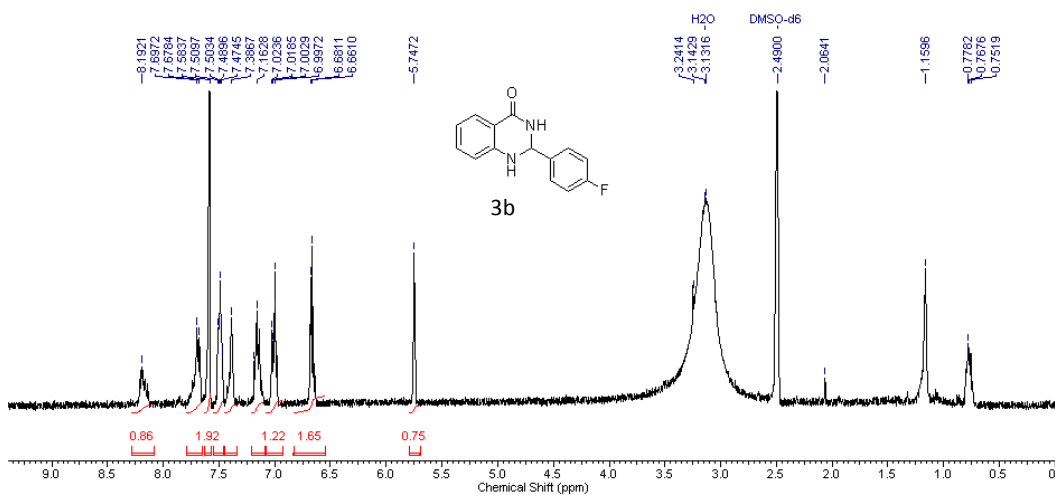
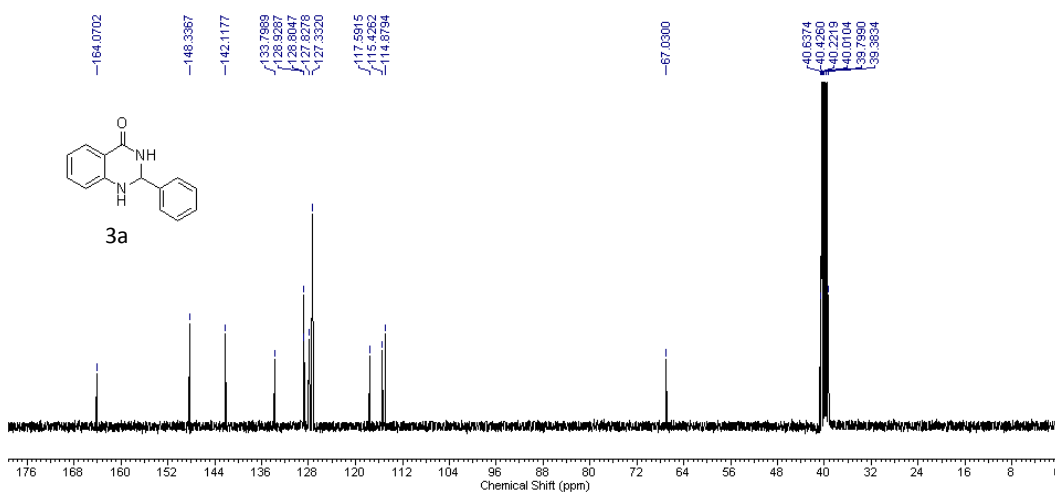
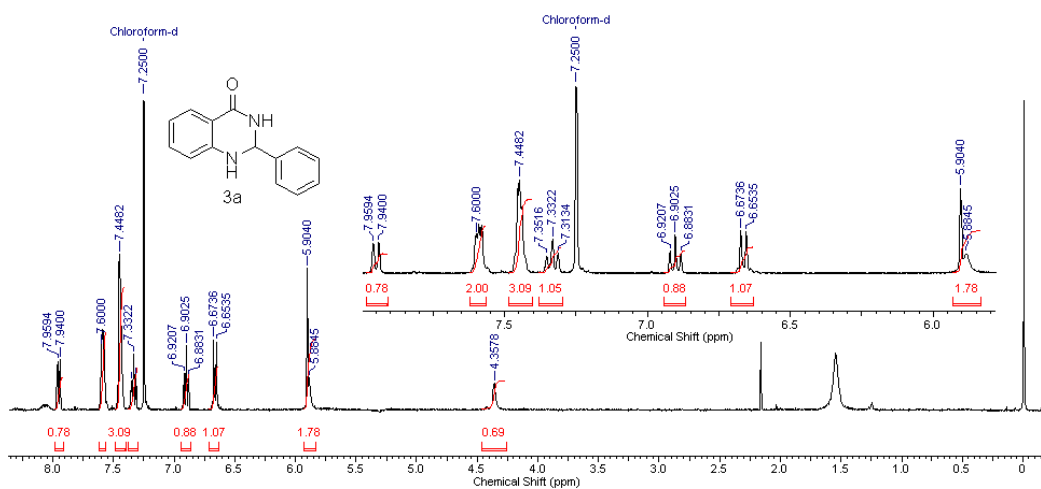
56. Surrey A. R., Leshner G. Y. J. (1956), New amebacides. IV. The preparation of some N-benzyl-N-(2-carbamylethyl)- and N-benzyl-N-(2-cyanoethyl)-haloacetamides, *J. Am. Chem. Soc.*, 78, 2573-2576 (DOI: 10.1021/ja01592a067)
57. Reddy K. S., Parthasarathy T., Kumar K. S., Satyender A. (2015), Green protocol for the synthesis of 2-aryl-2,3-dihydroquinazoline-4(1*H*)-ones using Indionina 225H resin, *Asian J. Chem.*, 27, 2222-2224 (DOI: 10.14233/ajchem.2015.18362)
58. Ding Q. -S., Zhang J. -L., Chen J. -X., Liu M. -C., Ding J. -C., Wu H. -Y. J. (2012), Tandem synthesis of 2,3-dihydroquinazolin-4(1*H*)-ones on grinding under solvent-free conditions, *Heterocyclic Chem.*, 49, 375-380 (DOI:10.1002/jhet.759)
59. Christie R. M., Moss S. J.(1985), Cyclisation of Schiff bases containing amide or hydroxamic acid groups to 1,2-dihydroquinazolin-4-ones; thermal decomposition reactions of the 1,2-dihydroquinazolin-4-ones, *J. Chem. Soc., Perkin Trans. 1*, 2779-2783 (DOI:10.1039/p19850002779)

Chapter 3

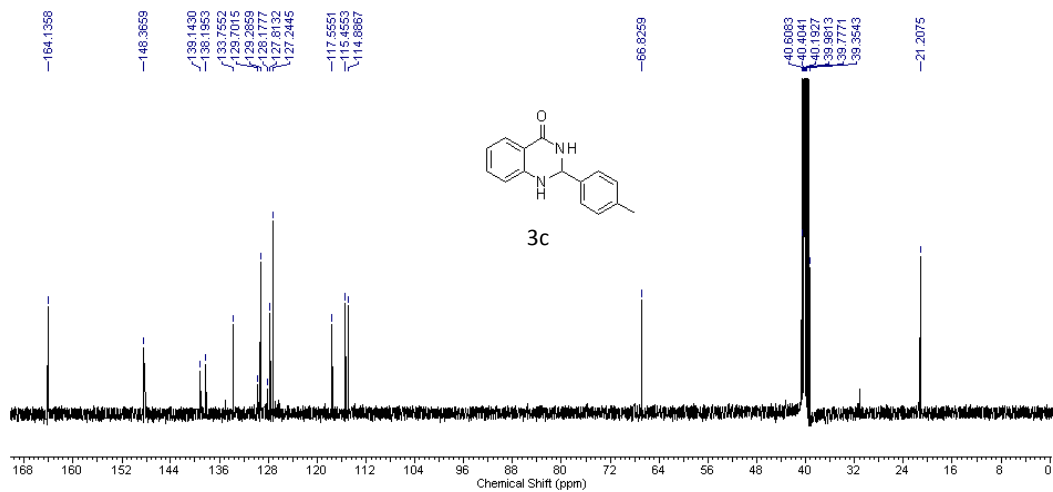
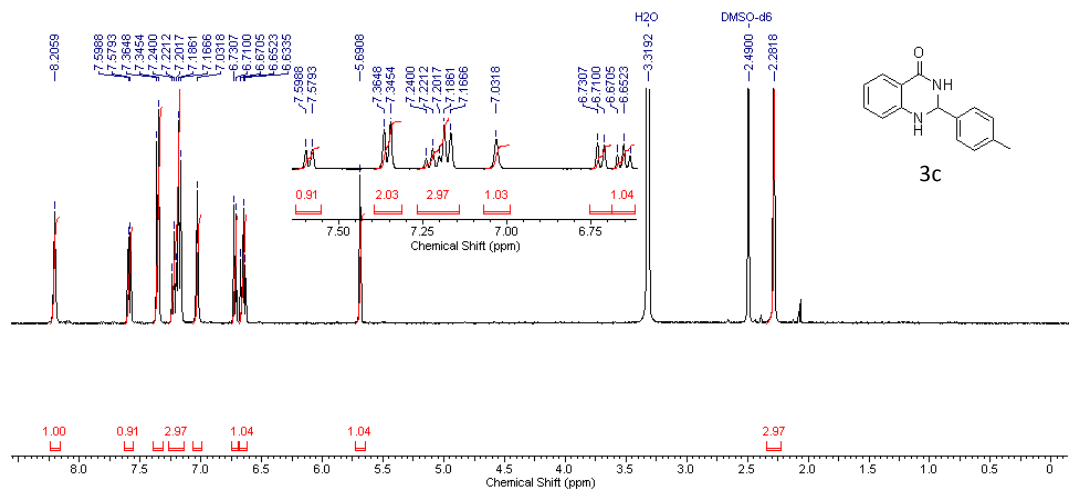
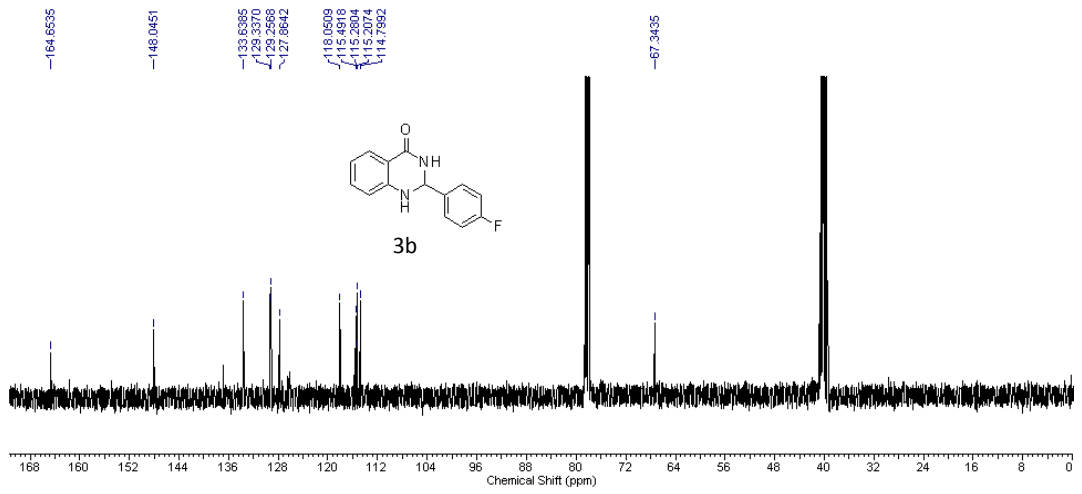
Appendix-Chapter 3

*¹H and ¹³C NMR Spectra of Dihydro/Spiro/Glyco
Quinazolinones and Aza-Michael Adducts*

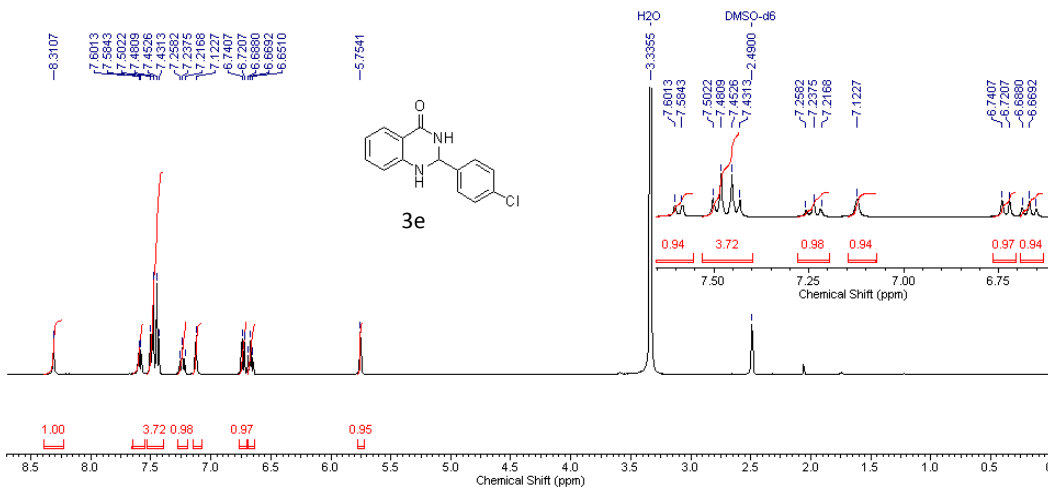
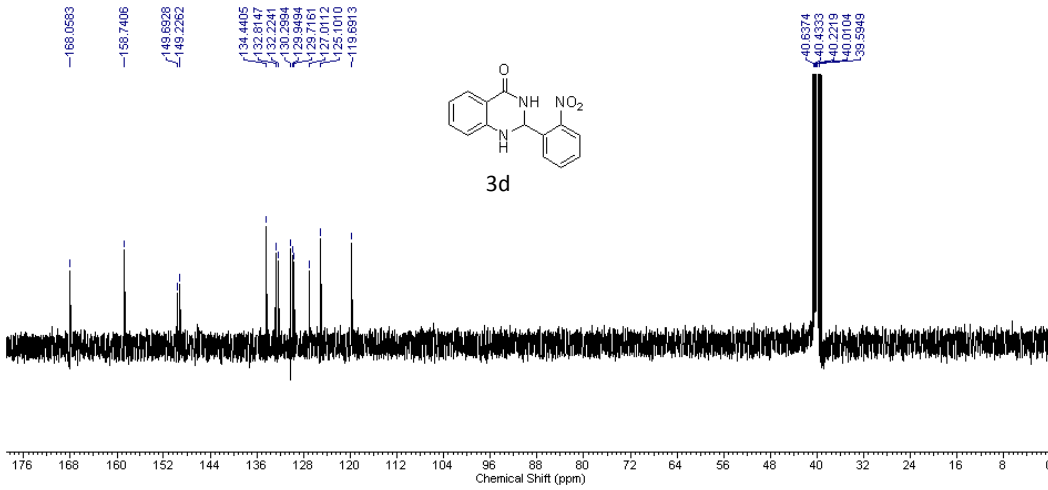
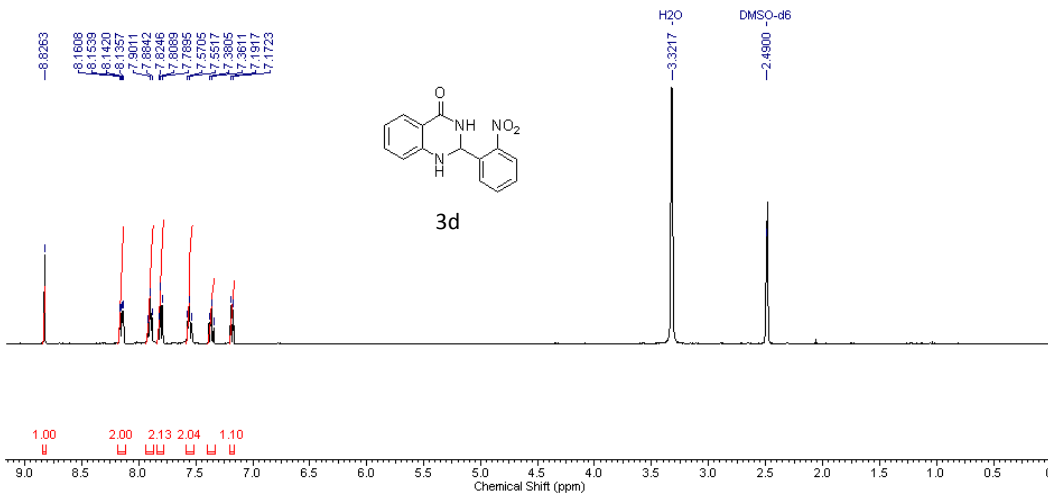
Chapter 3



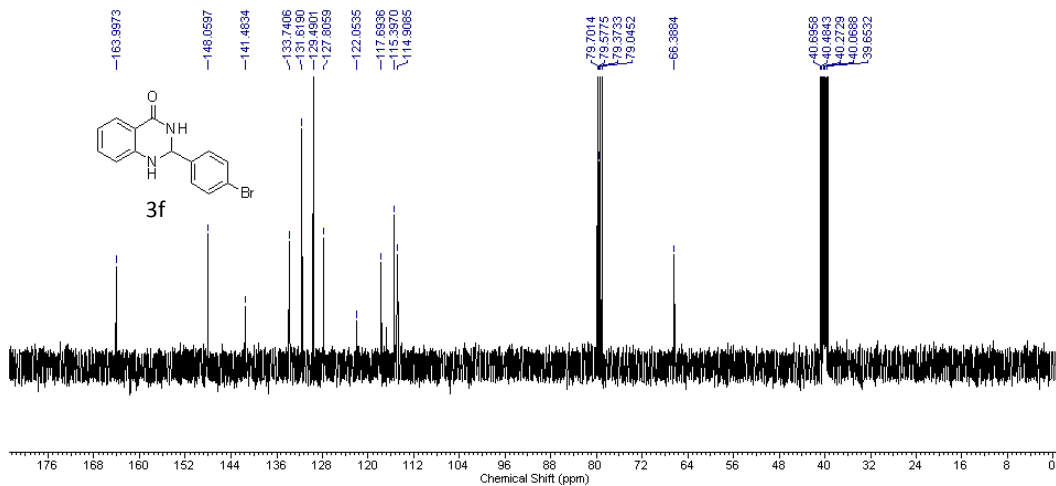
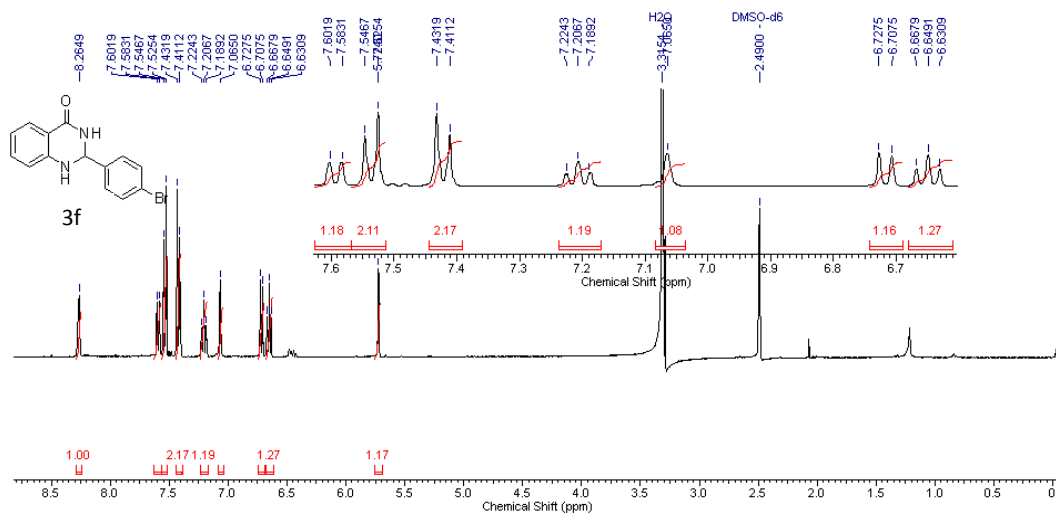
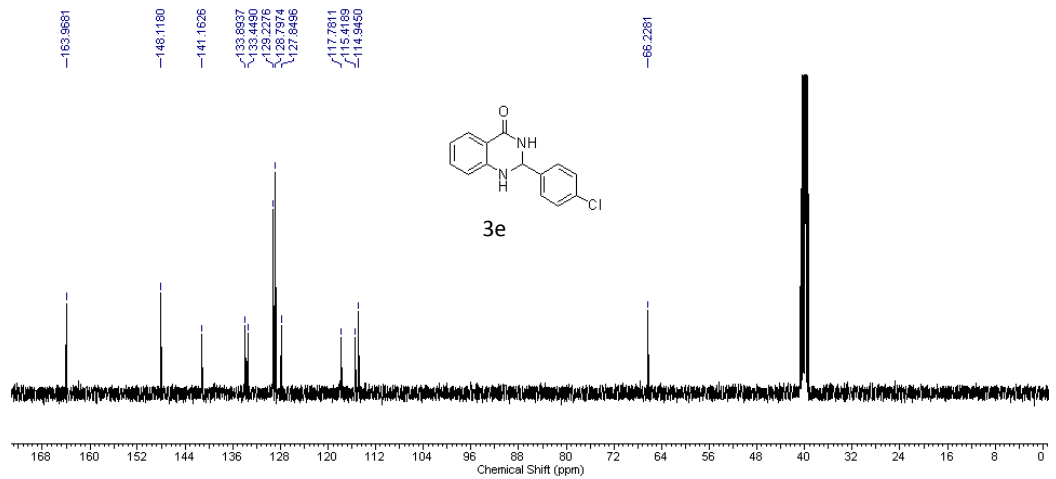
Chapter 3



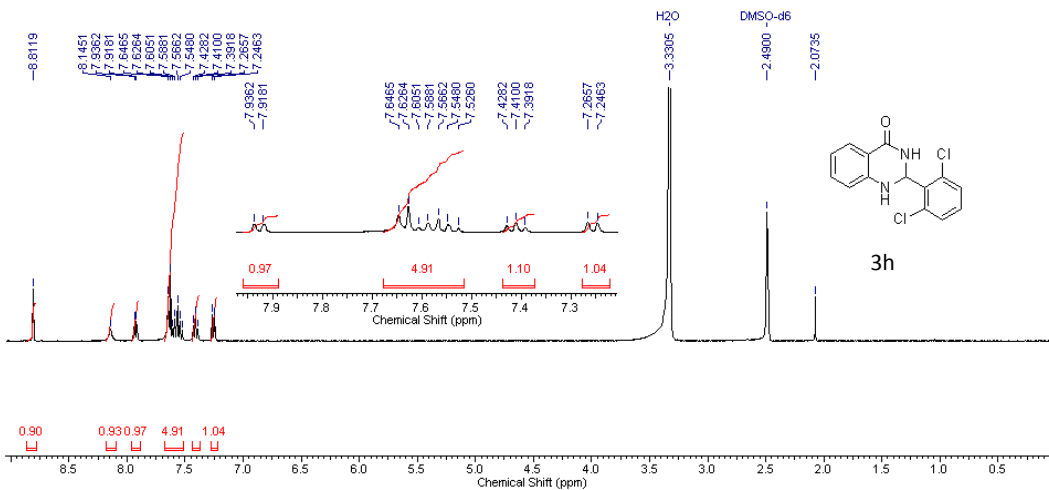
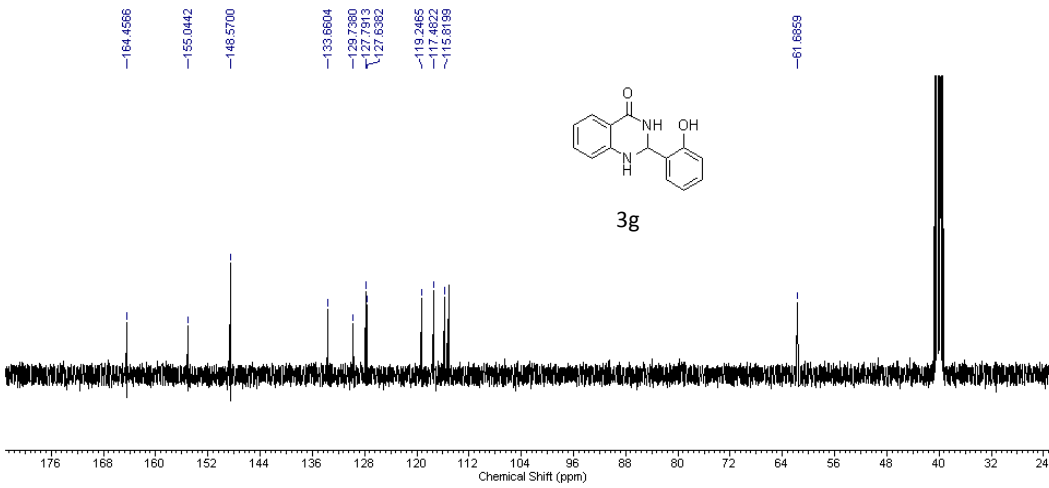
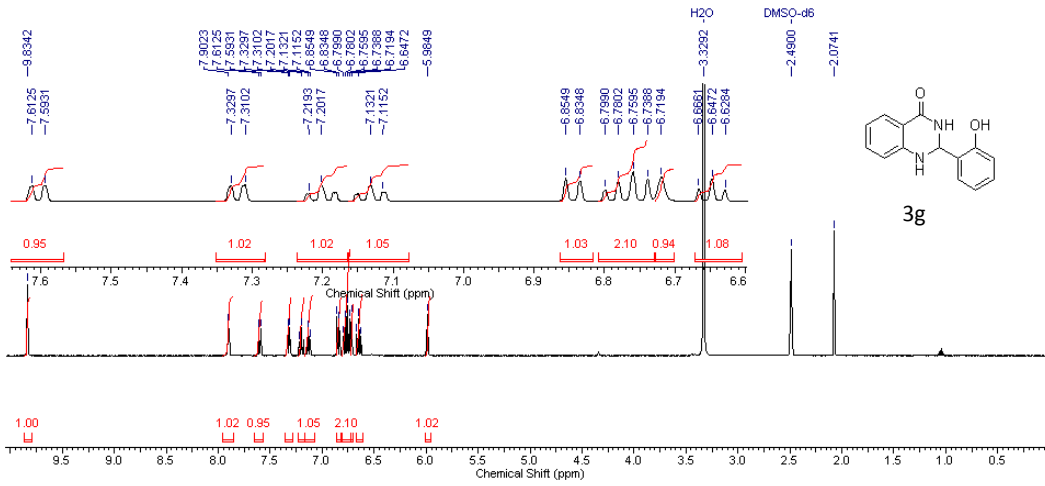
Chapter 3



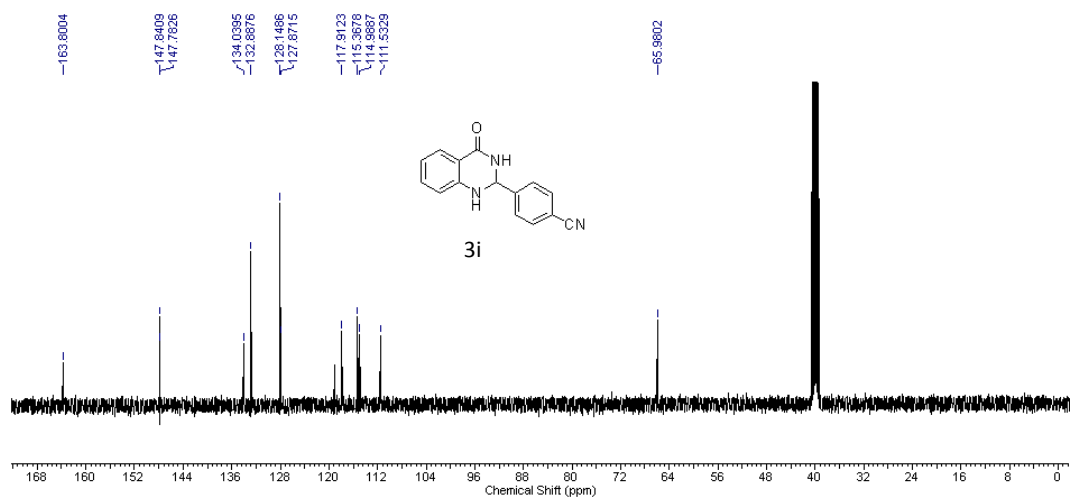
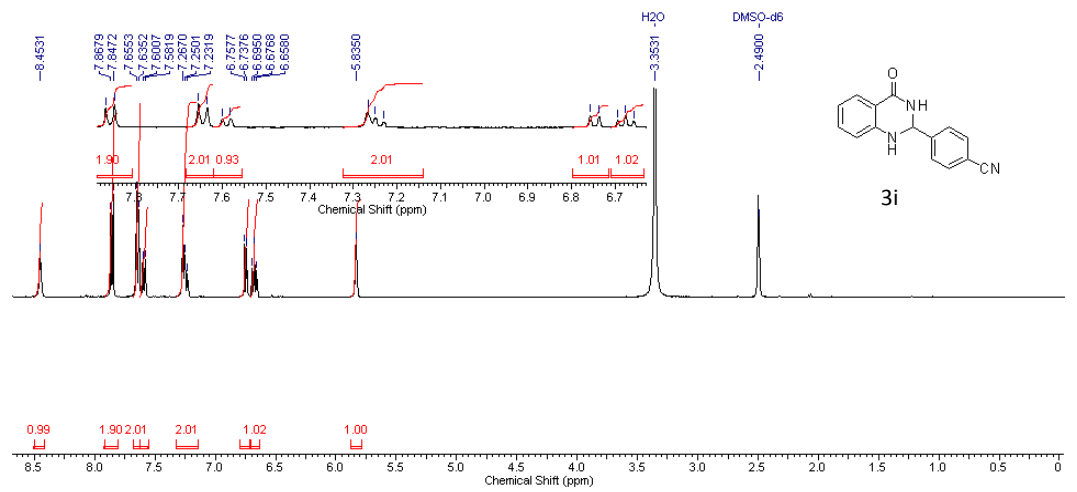
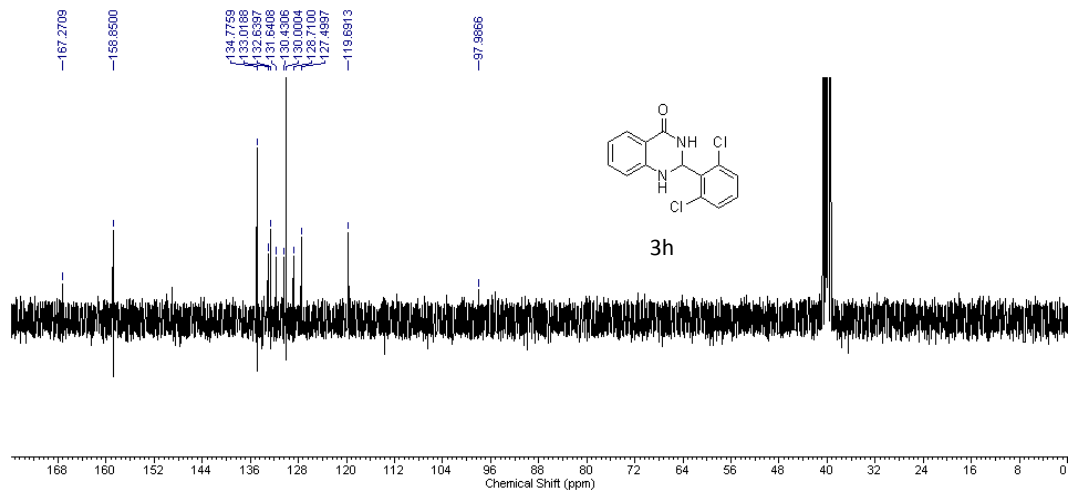
Chapter 3



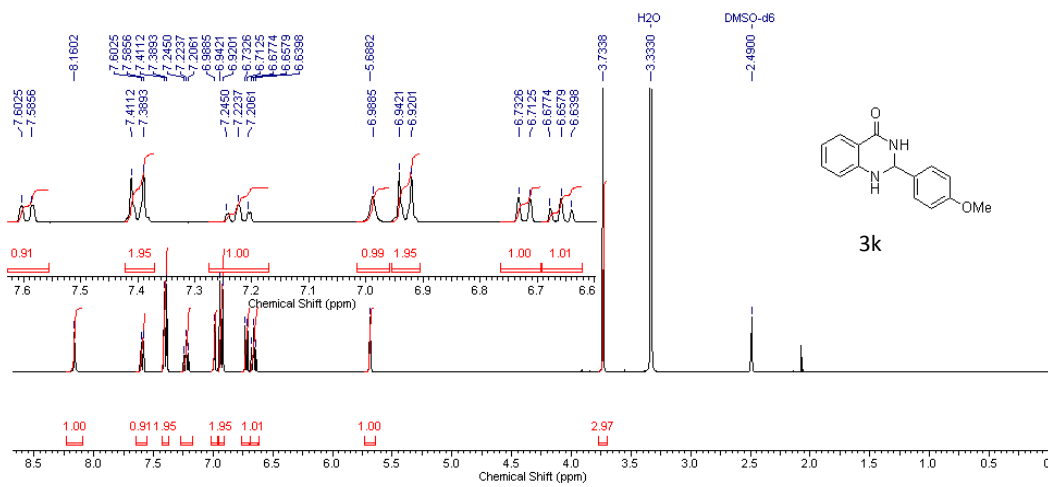
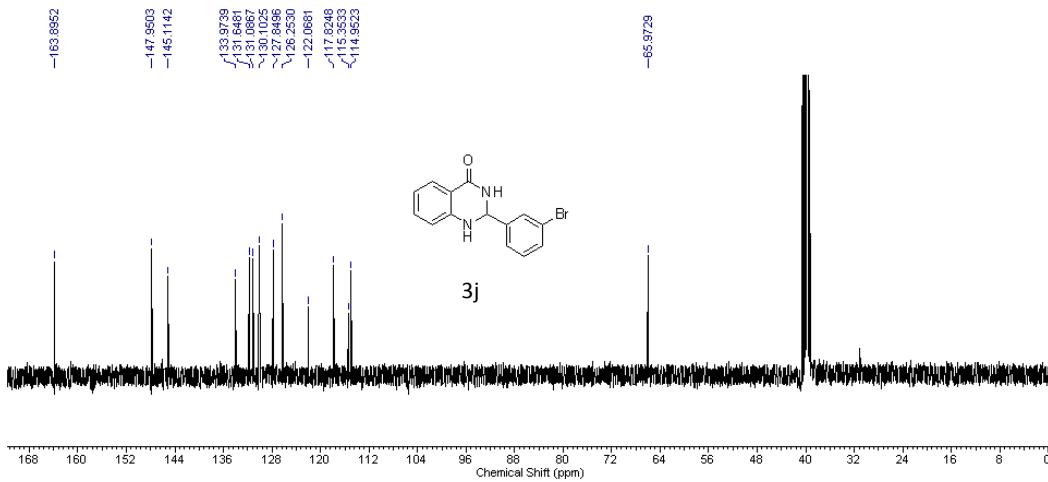
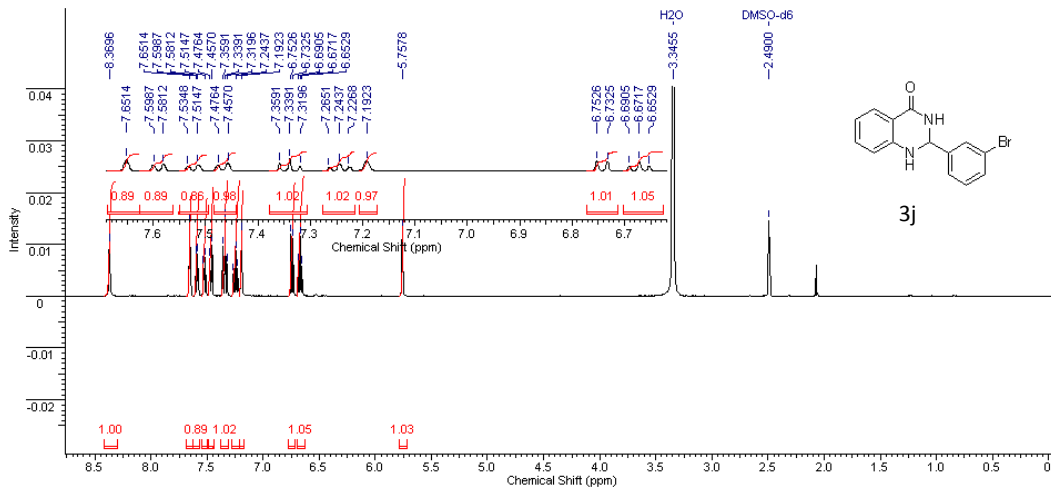
Chapter 3



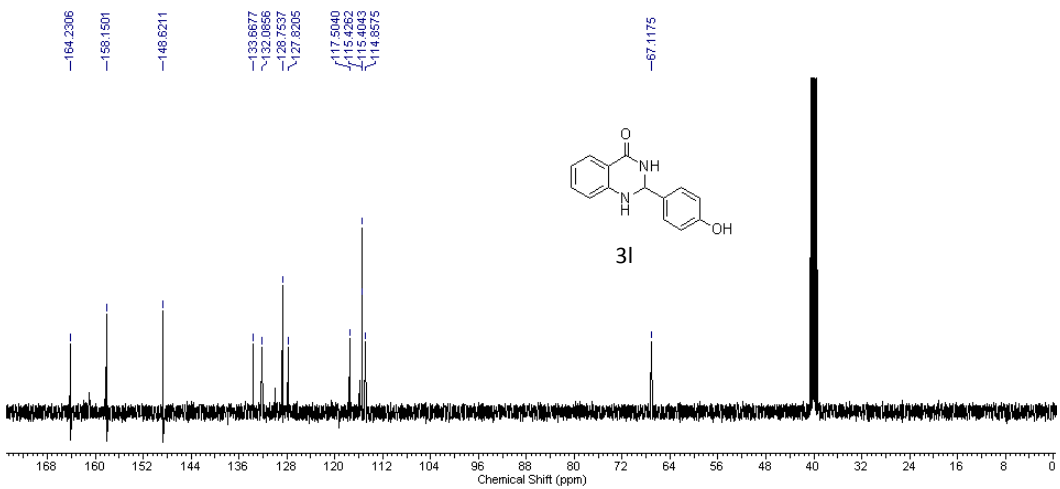
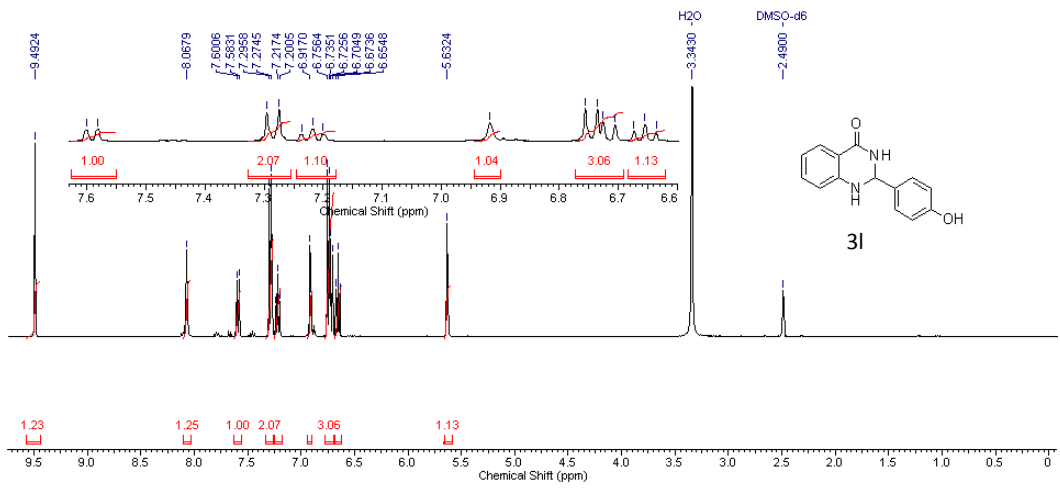
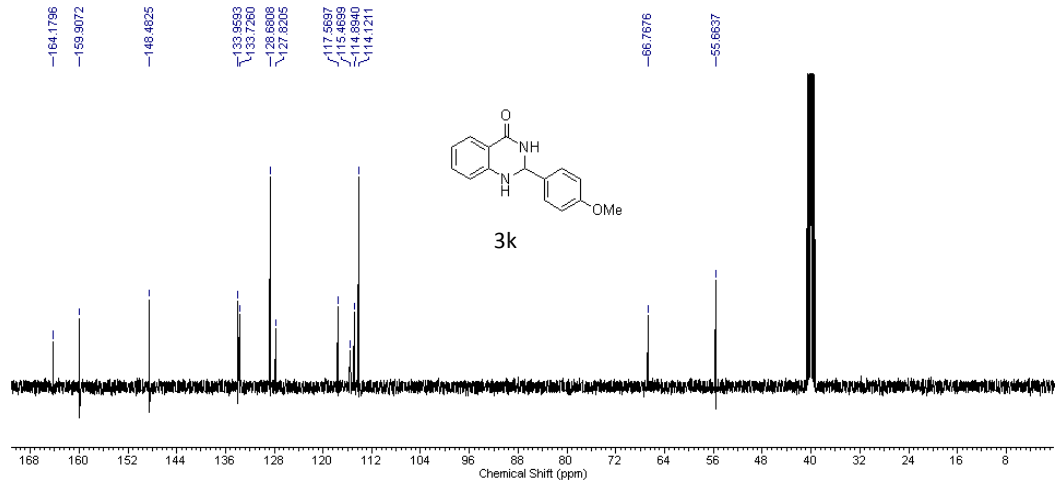
Chapter 3



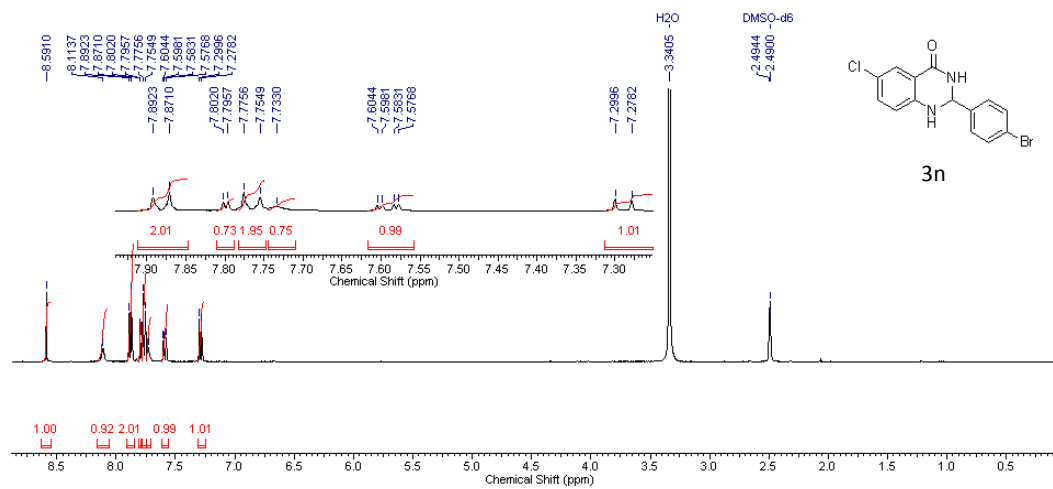
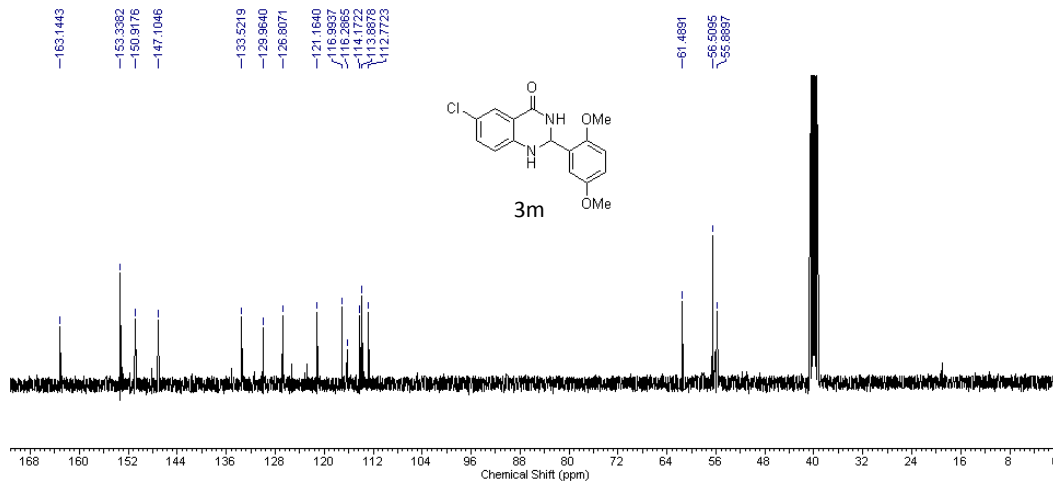
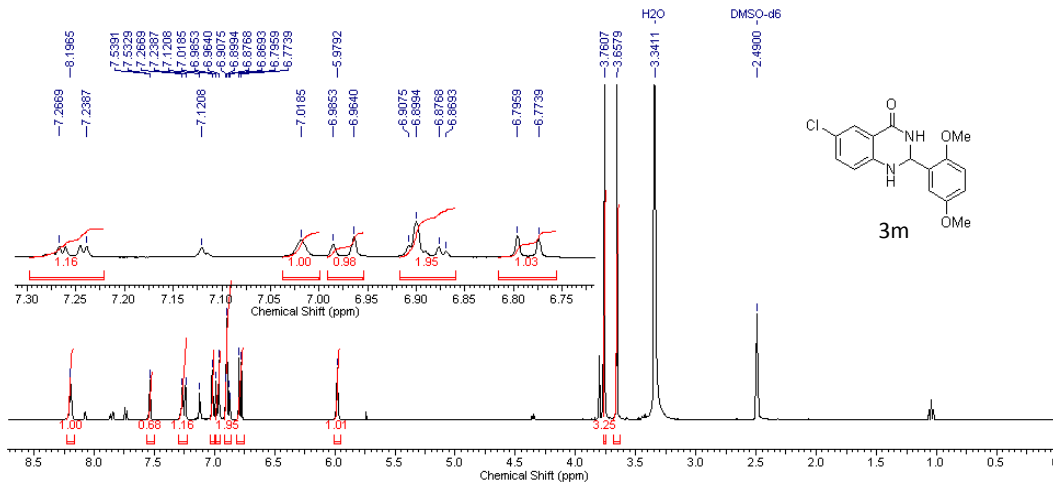
Chapter 3



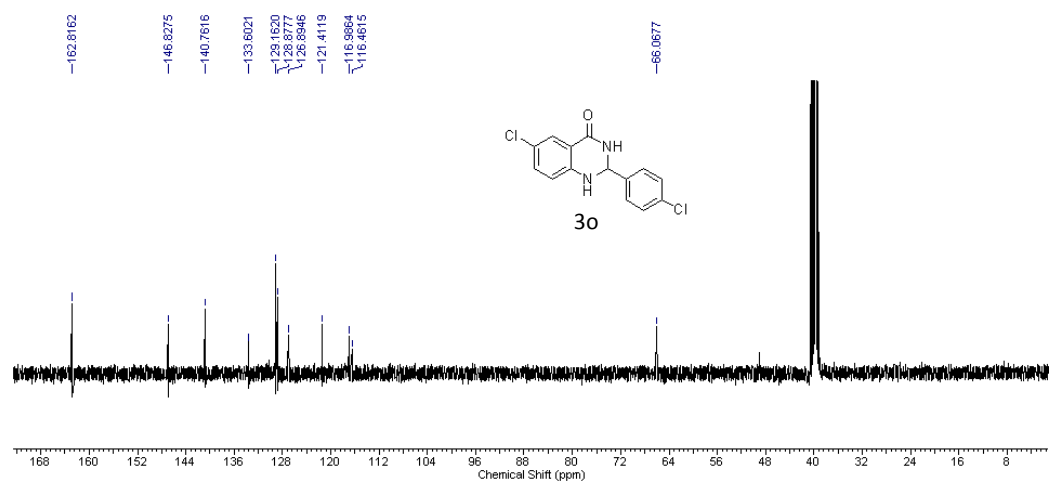
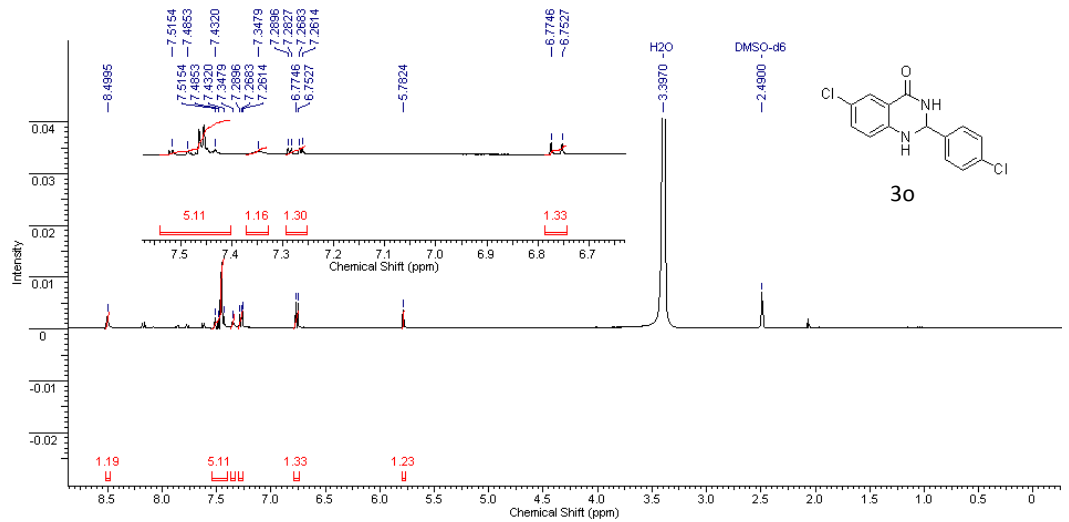
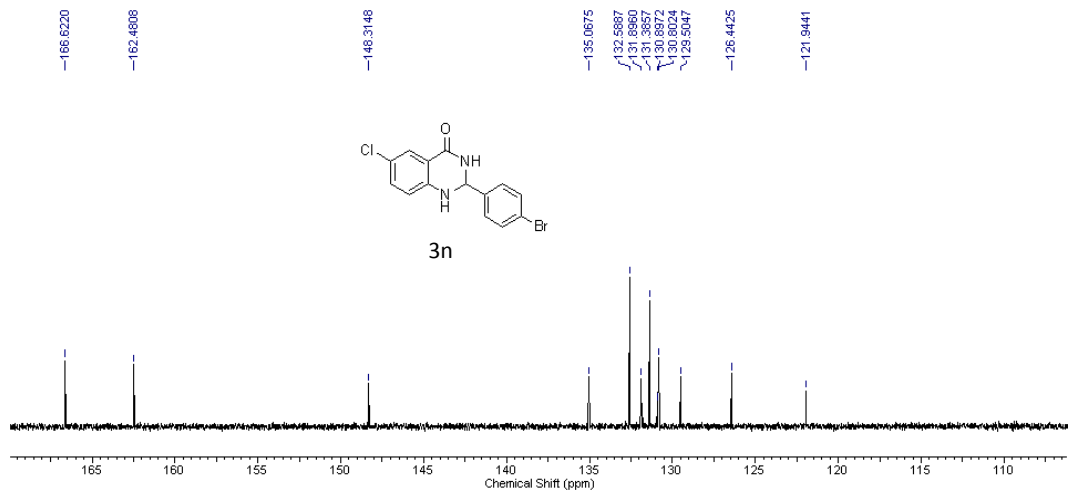
Chapter 3



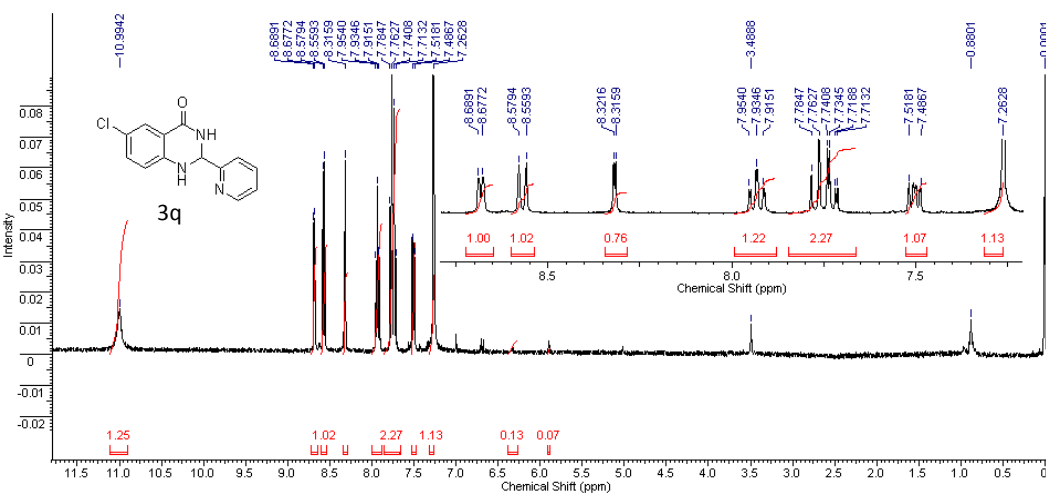
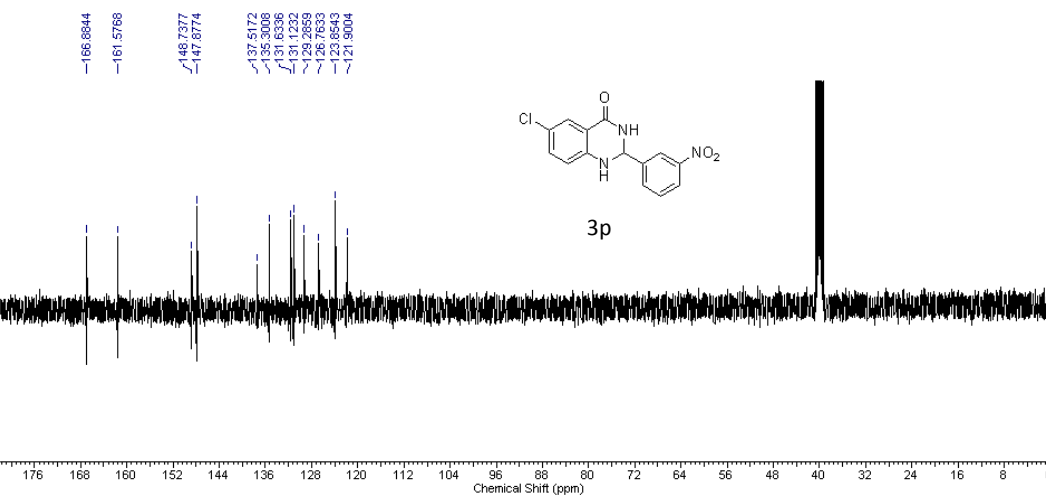
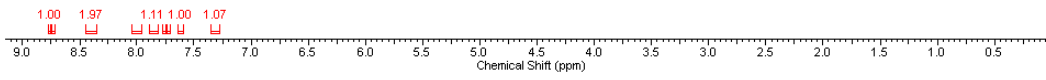
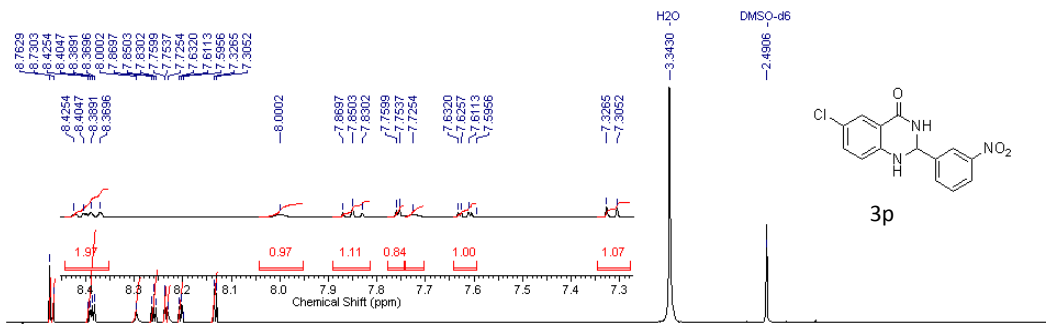
Chapter 3



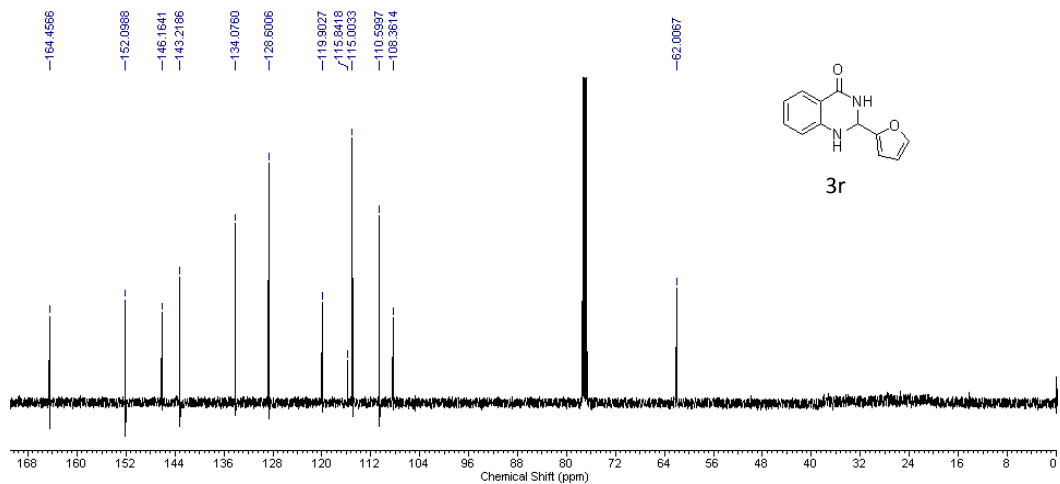
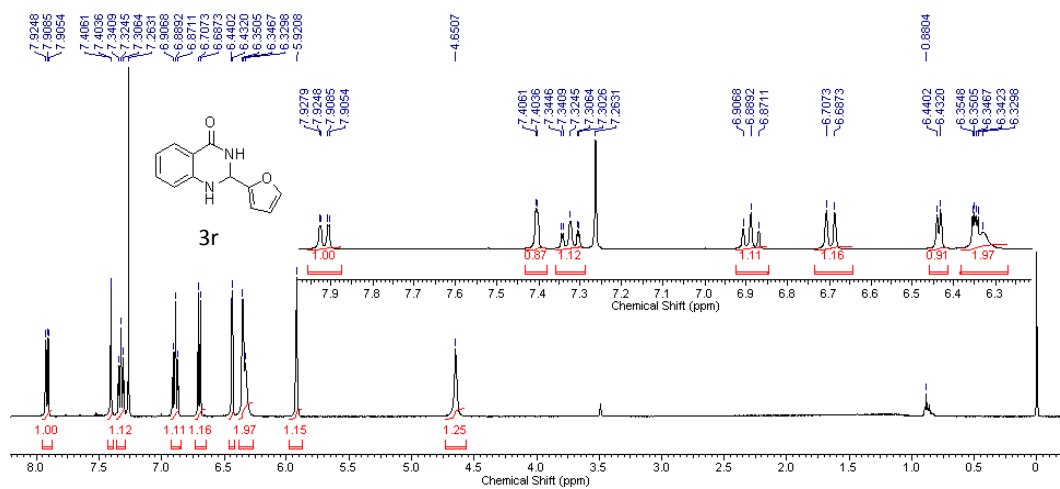
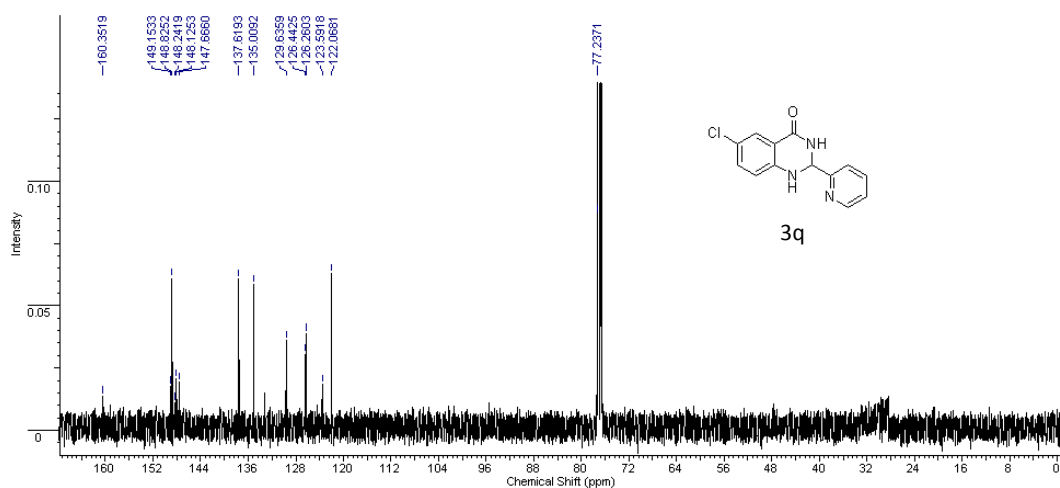
Chapter 3



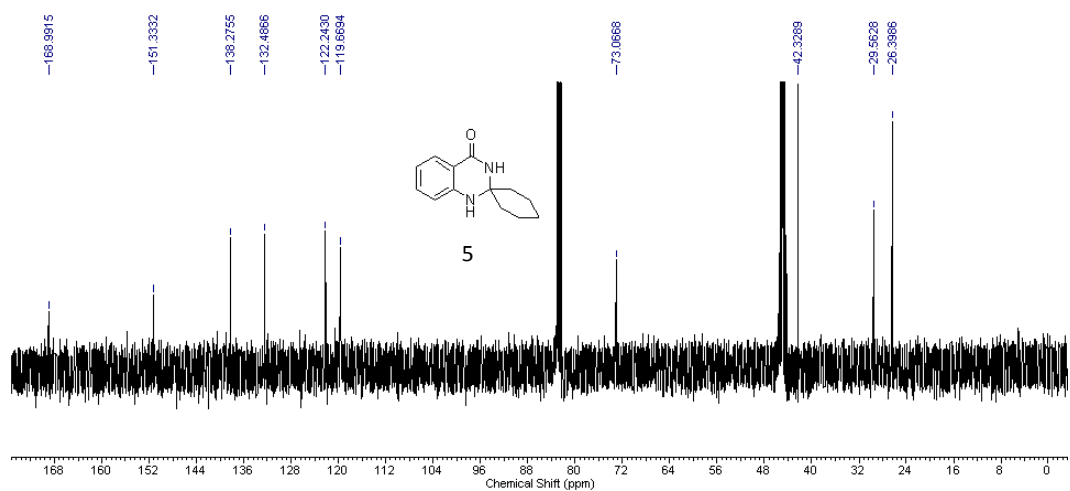
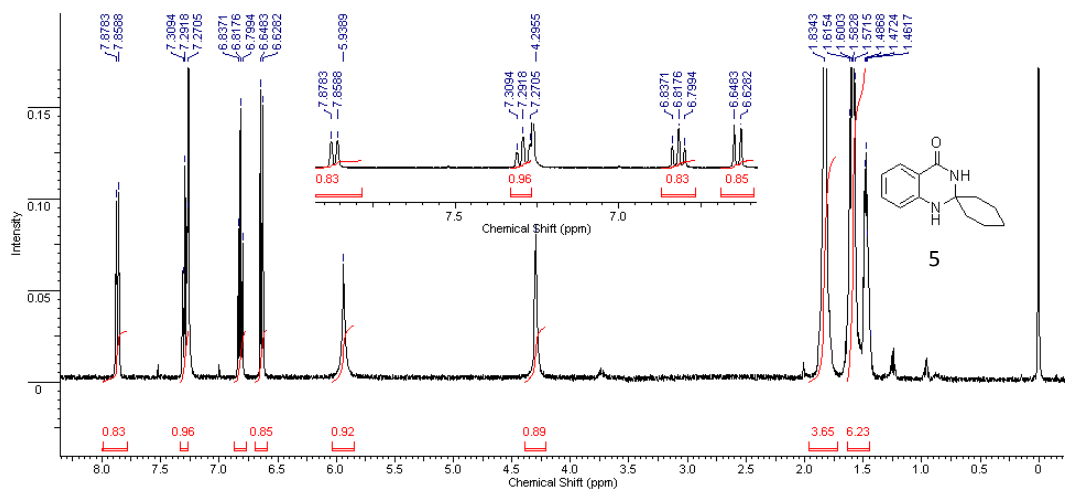
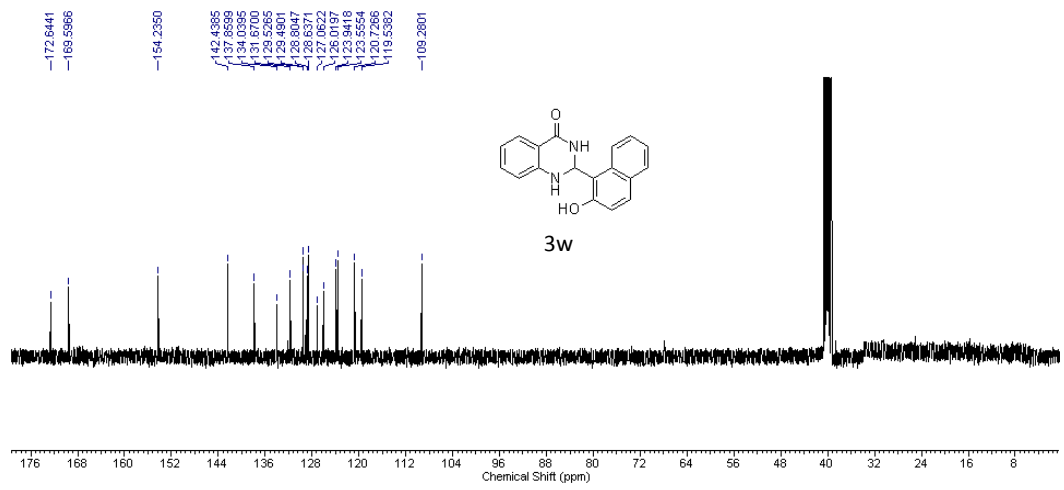
Chapter 3



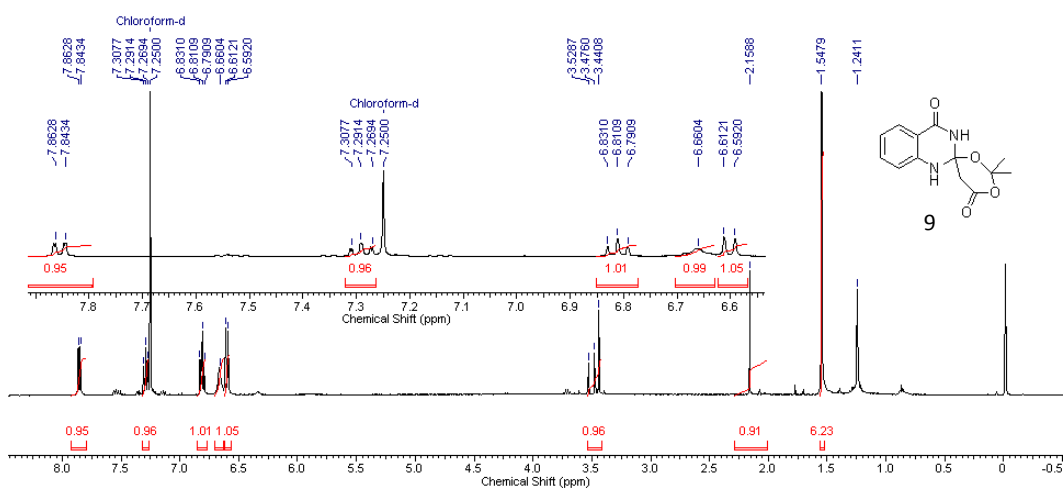
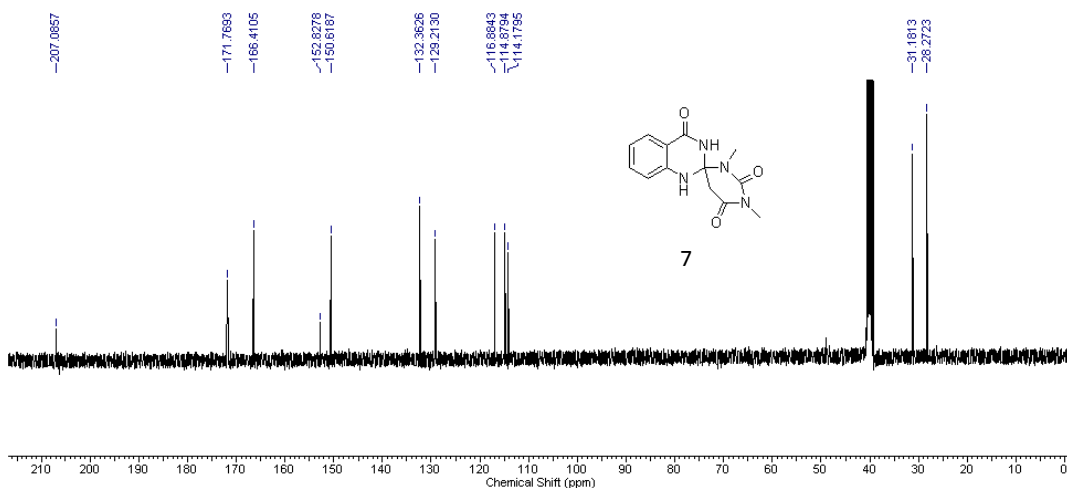
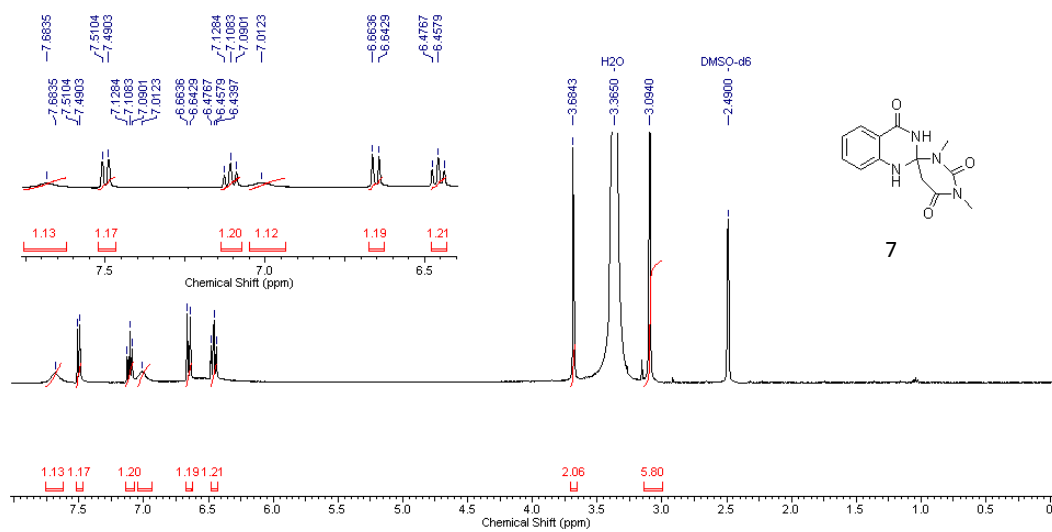
Chapter 3



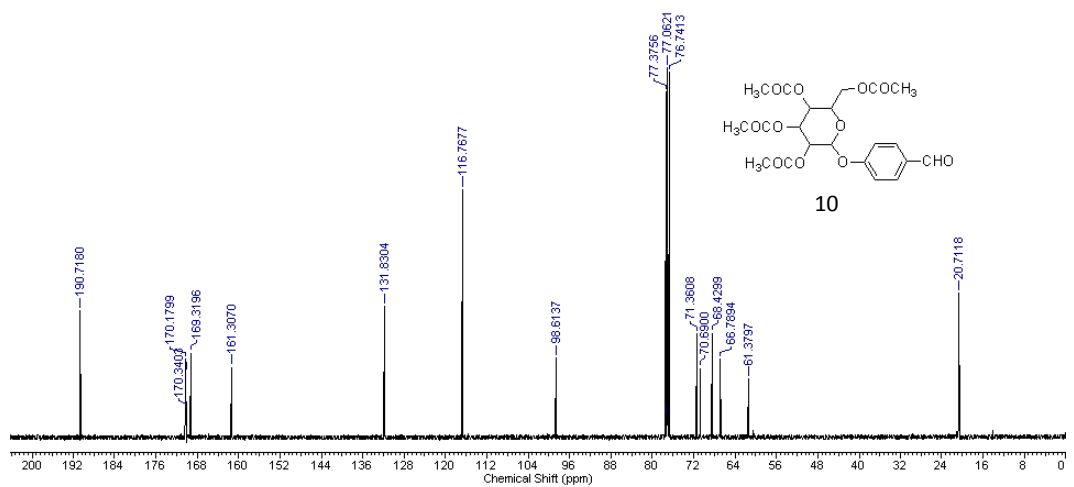
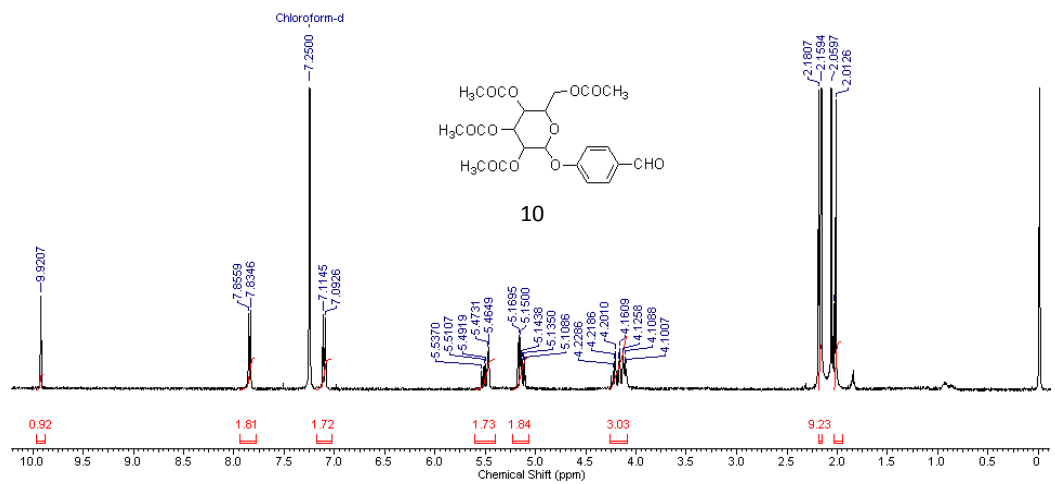
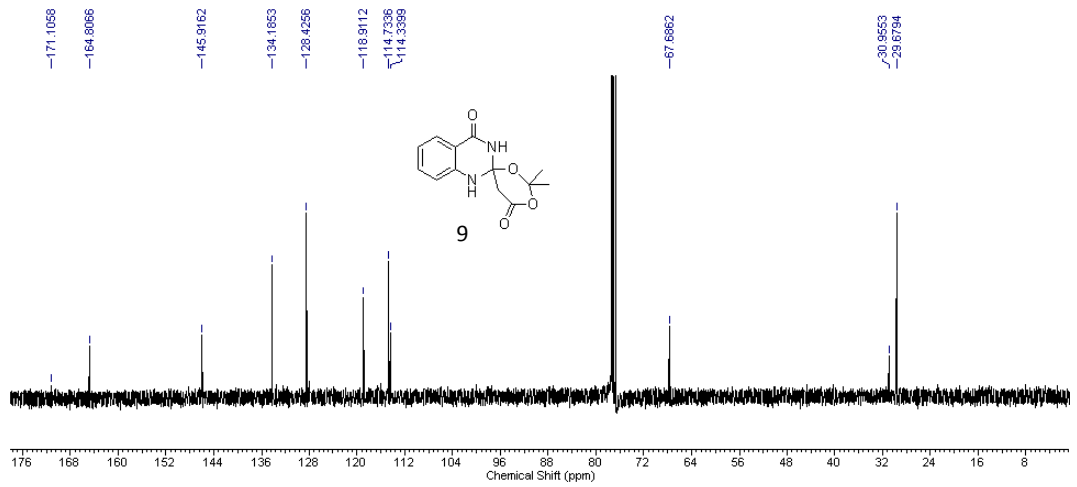
Chapter 3



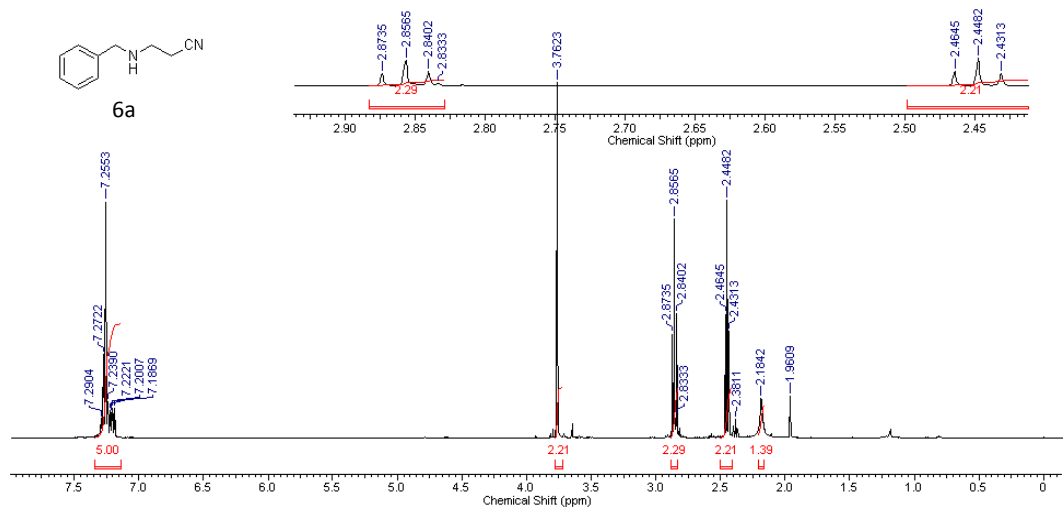
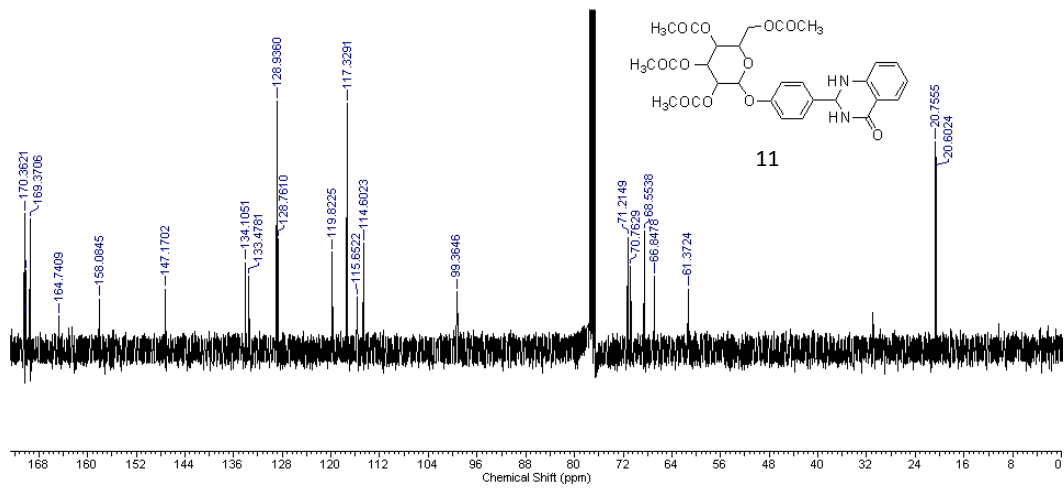
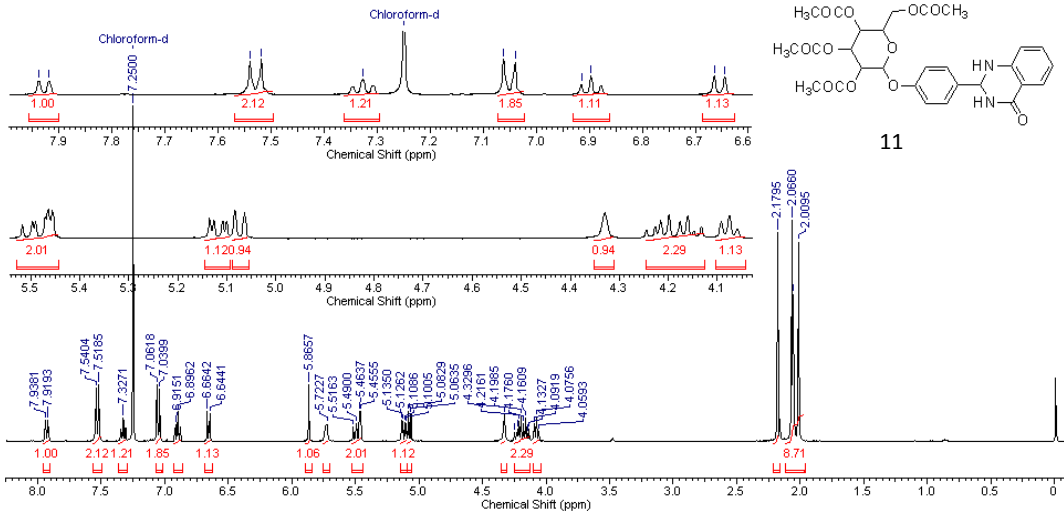
Chapter 3



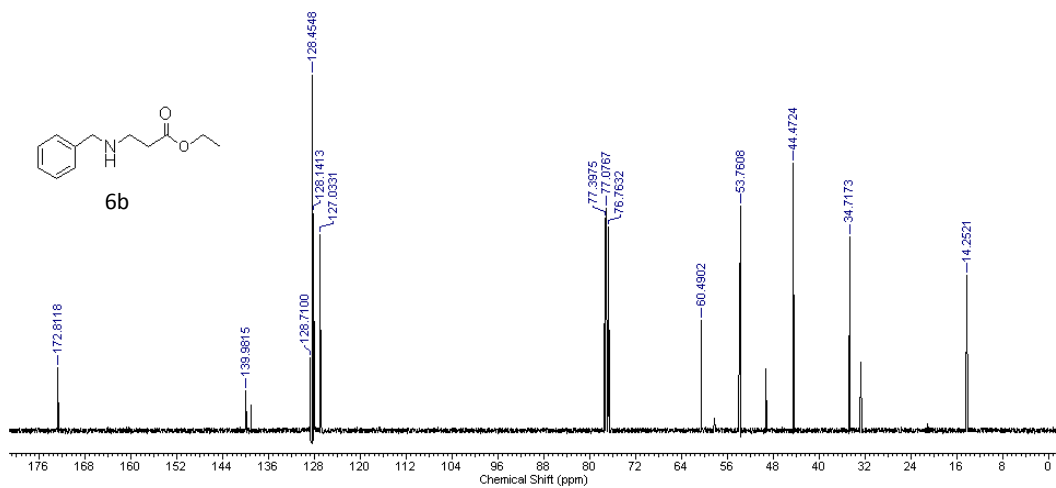
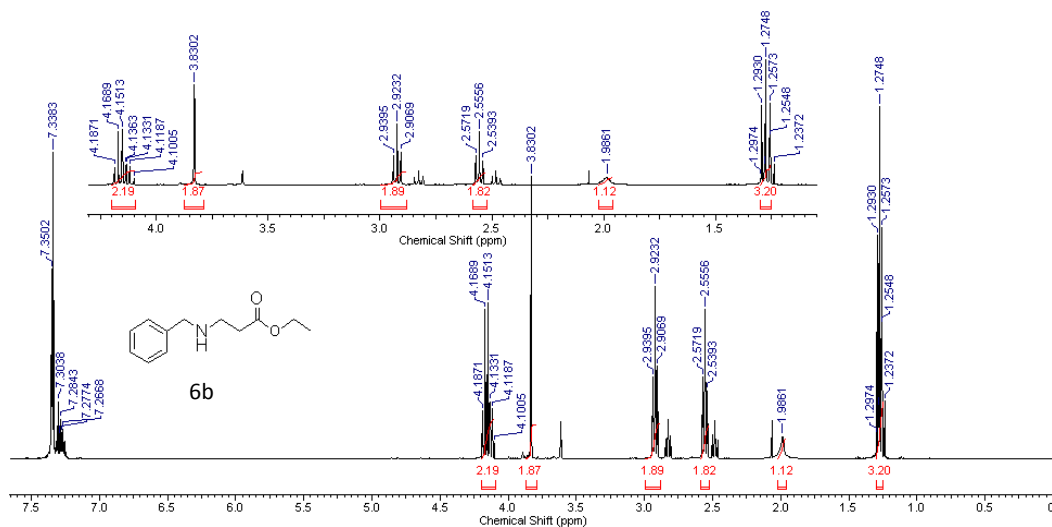
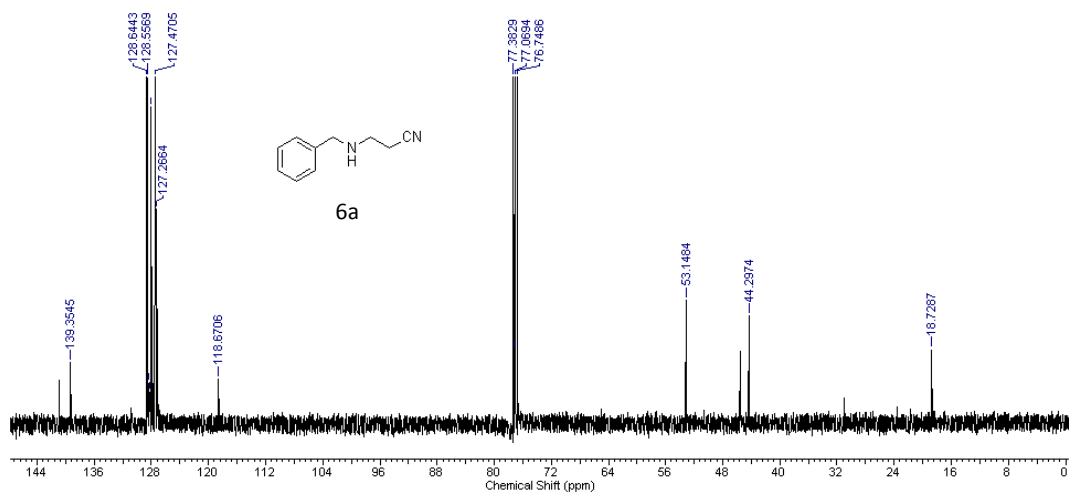
Chapter 3



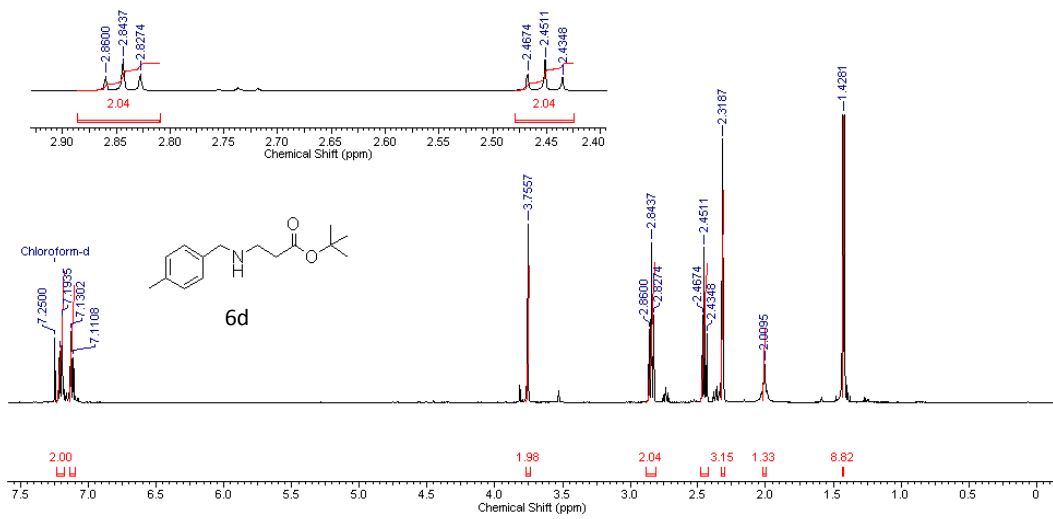
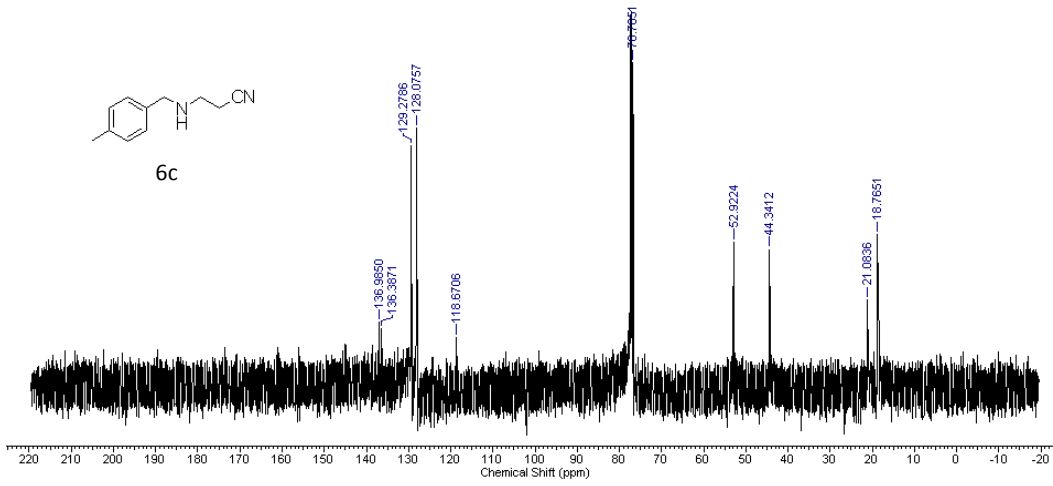
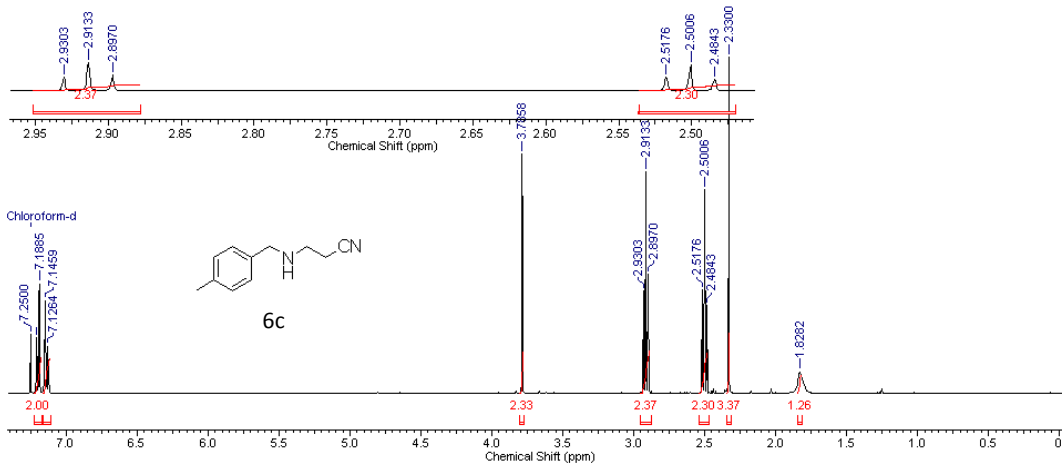
Chapter 3



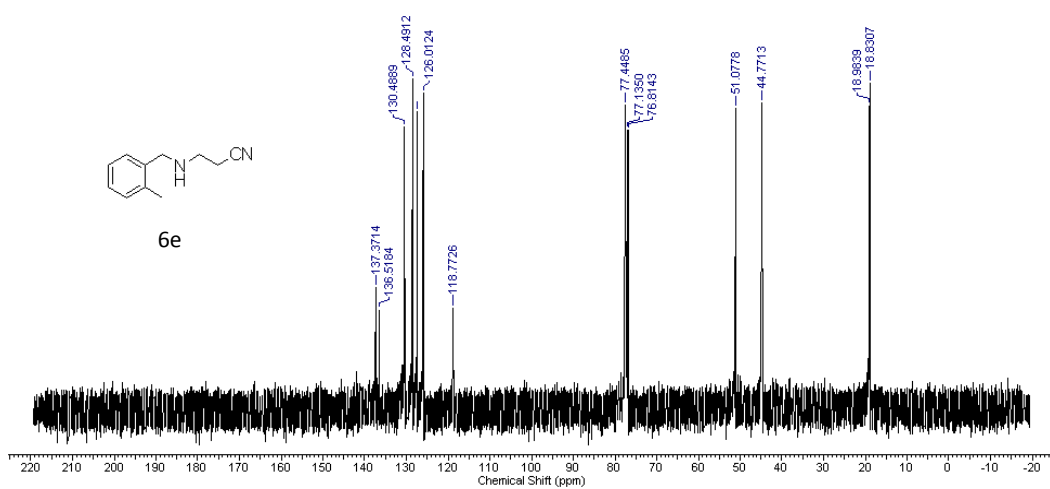
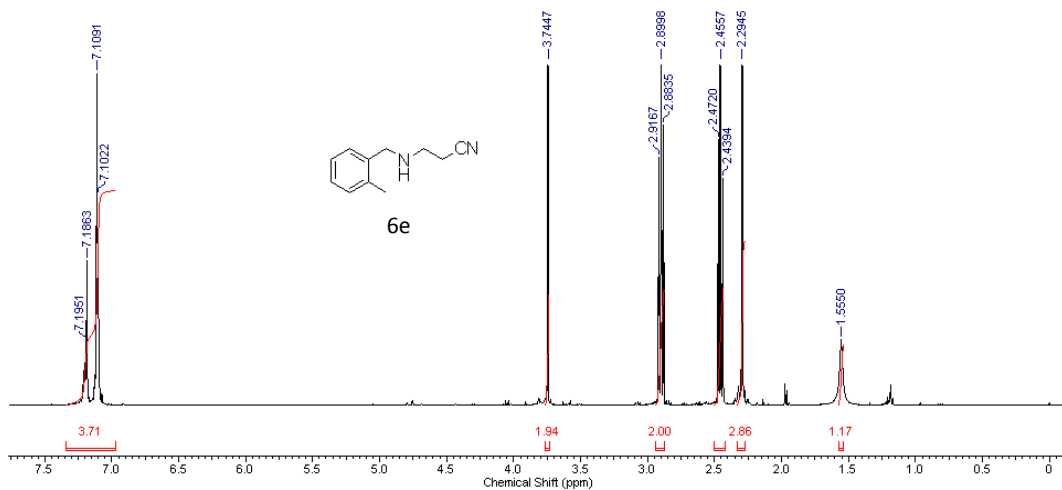
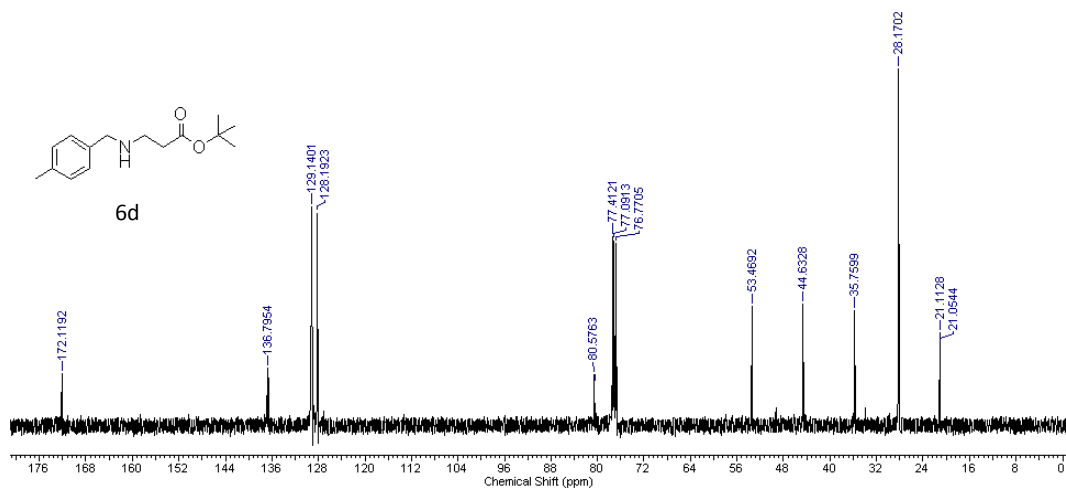
Chapter 3



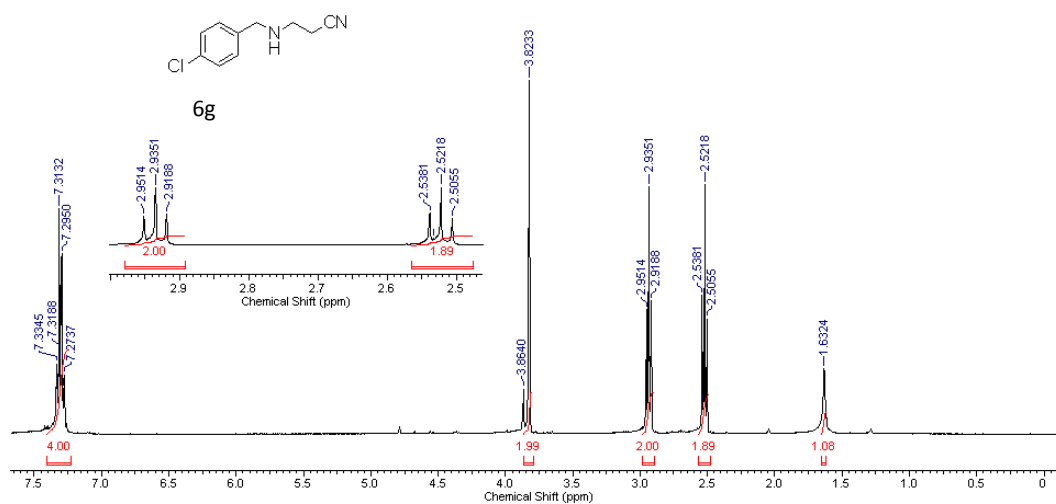
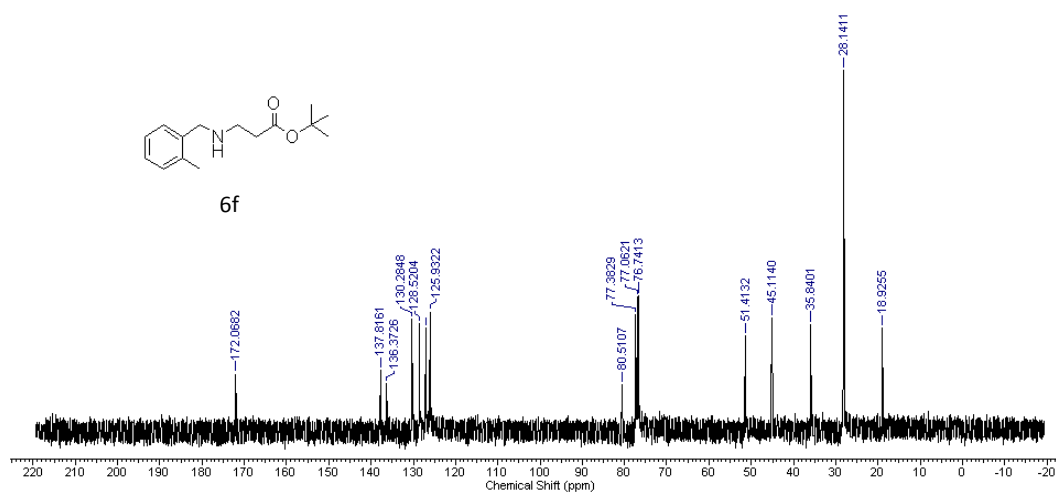
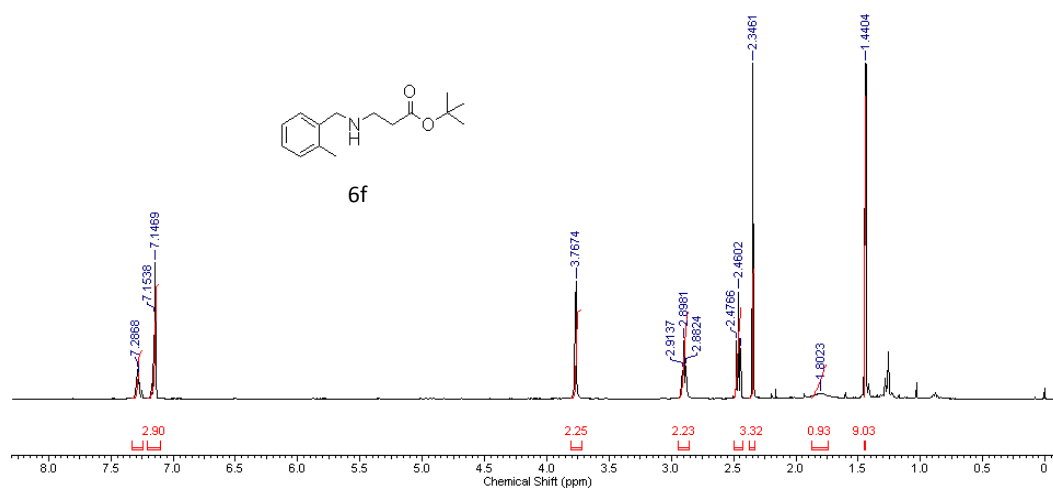
Chapter 3



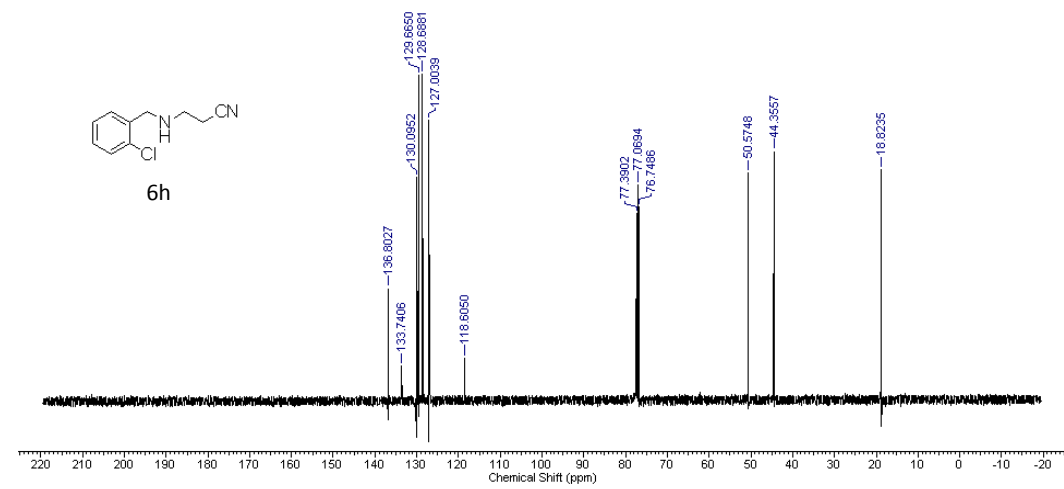
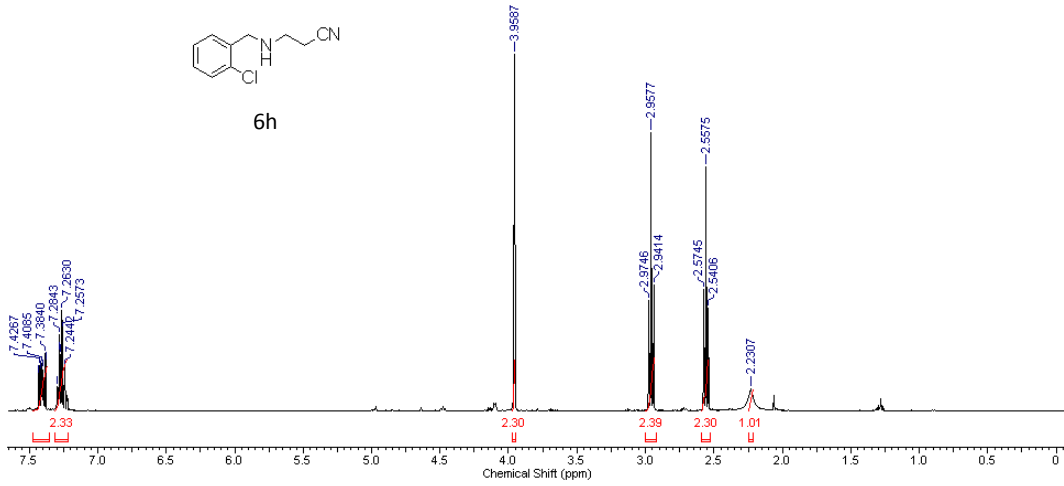
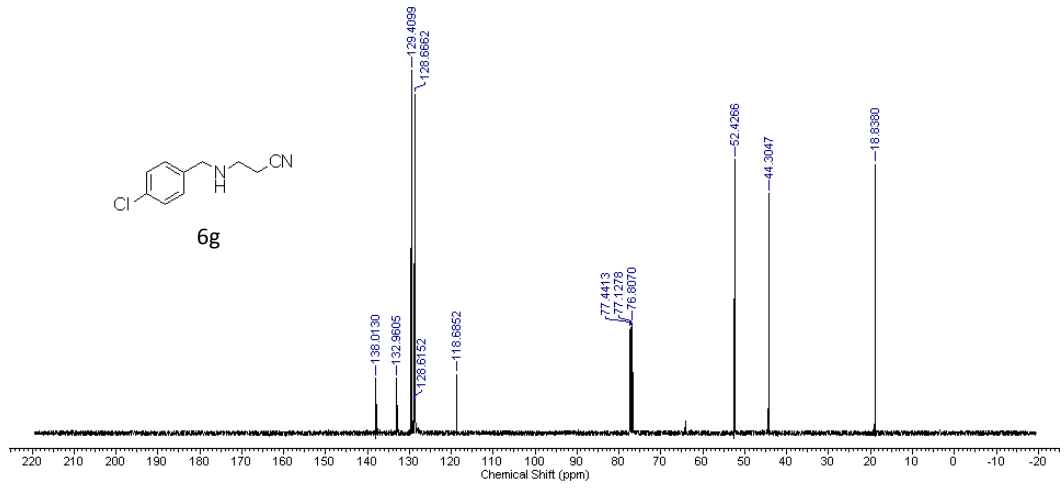
Chapter 3



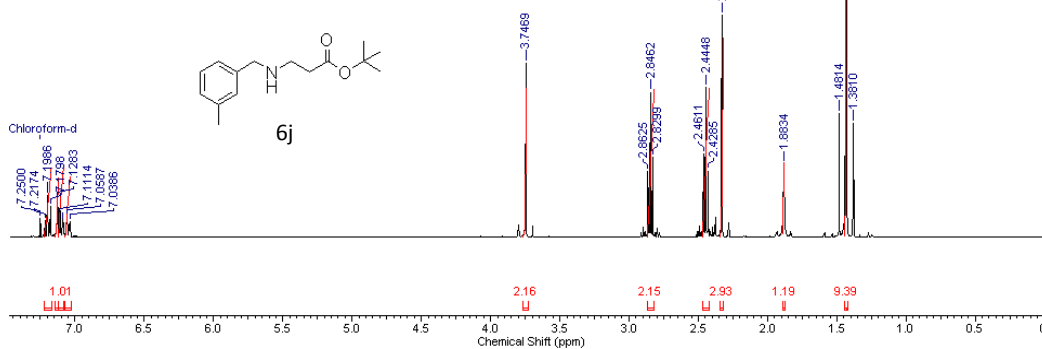
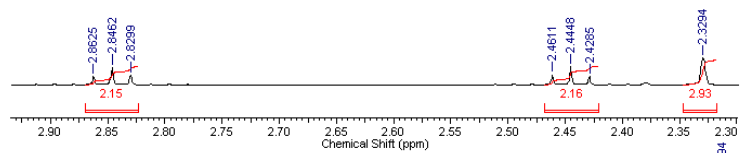
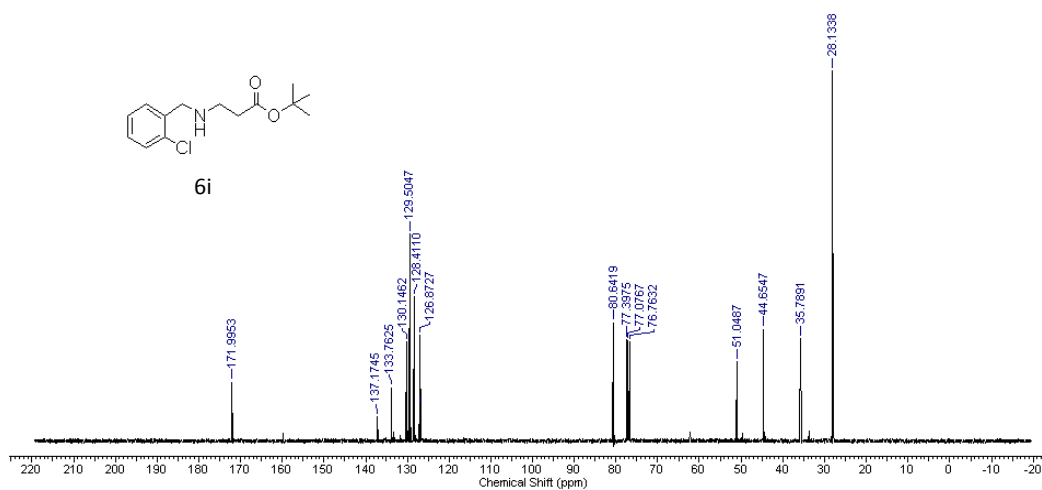
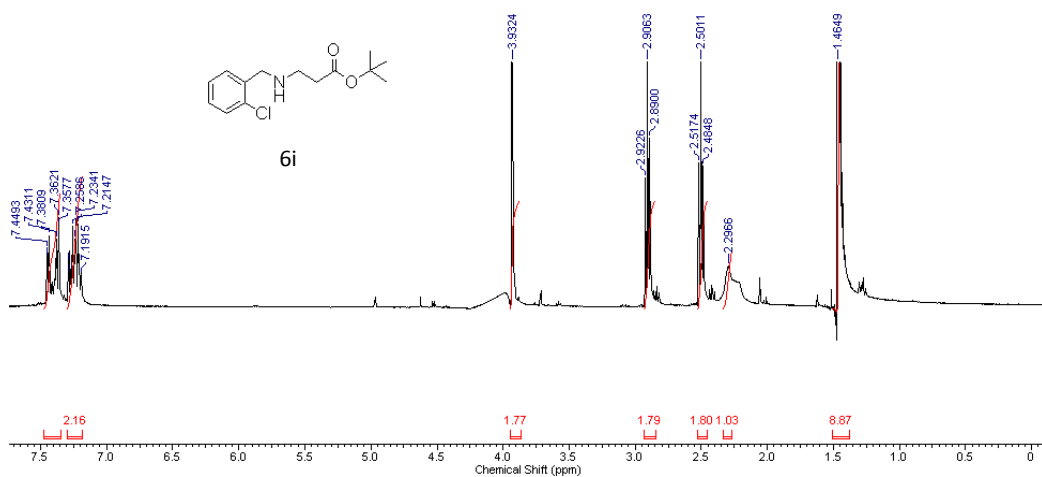
Chapter 3

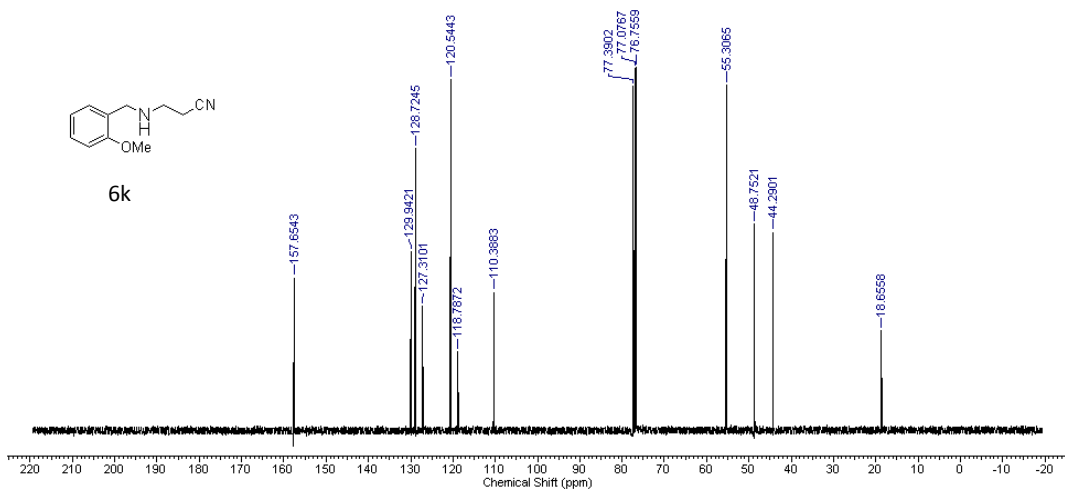
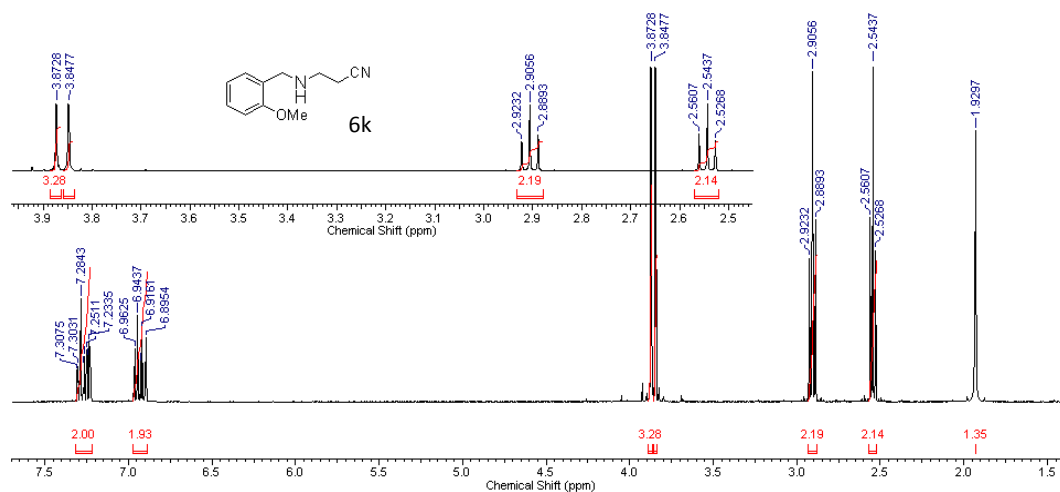
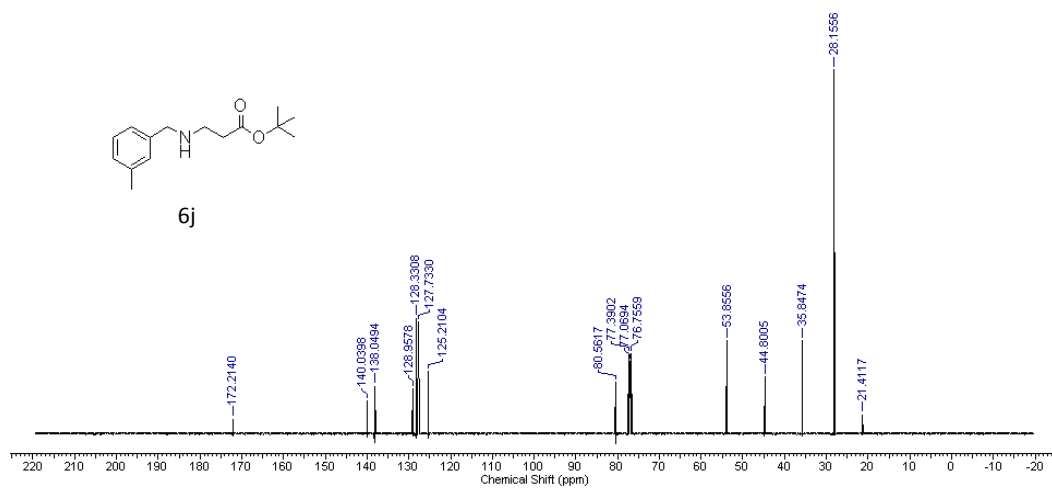


Chapter 3

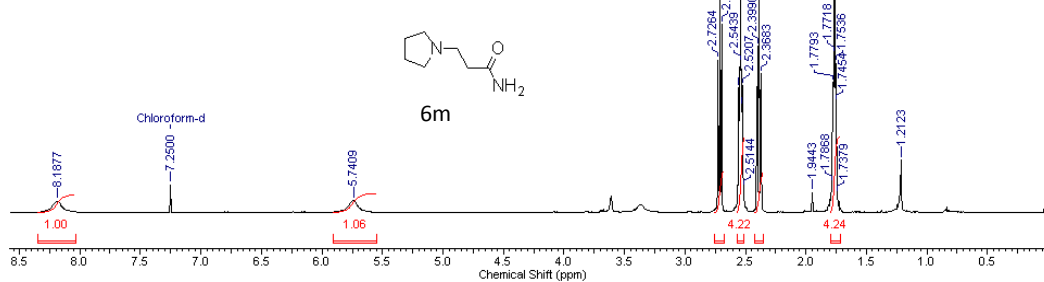
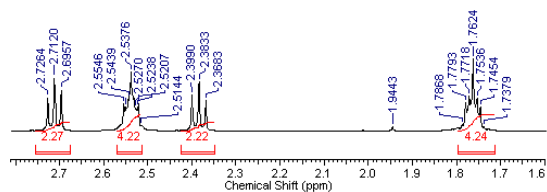
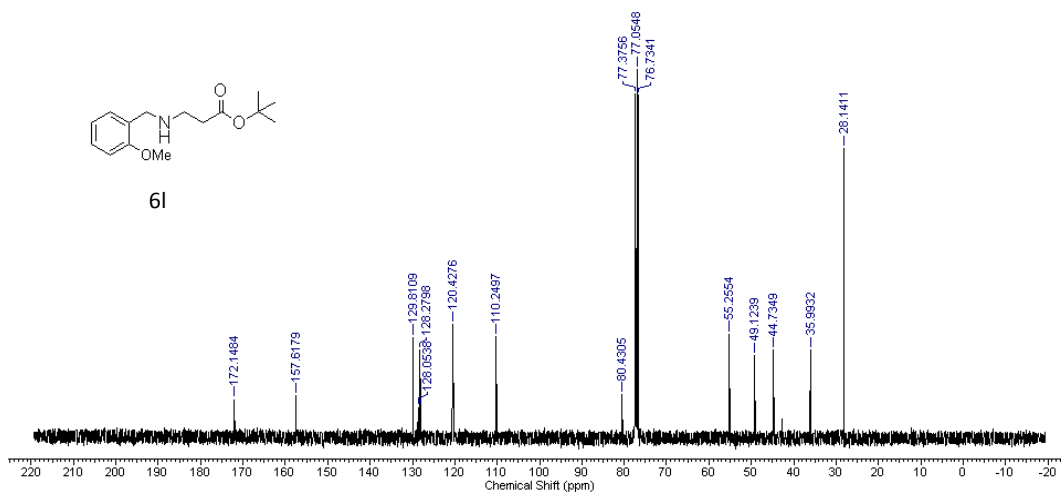
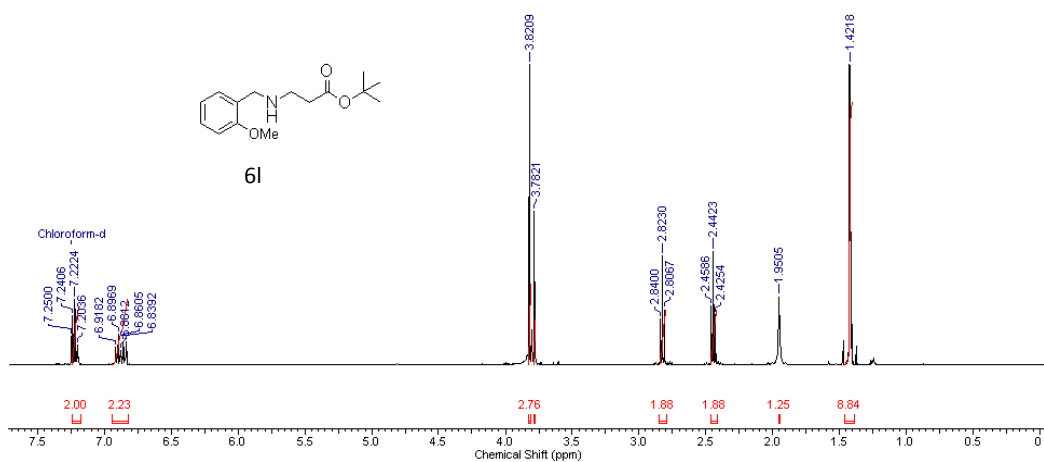


Chapter 3

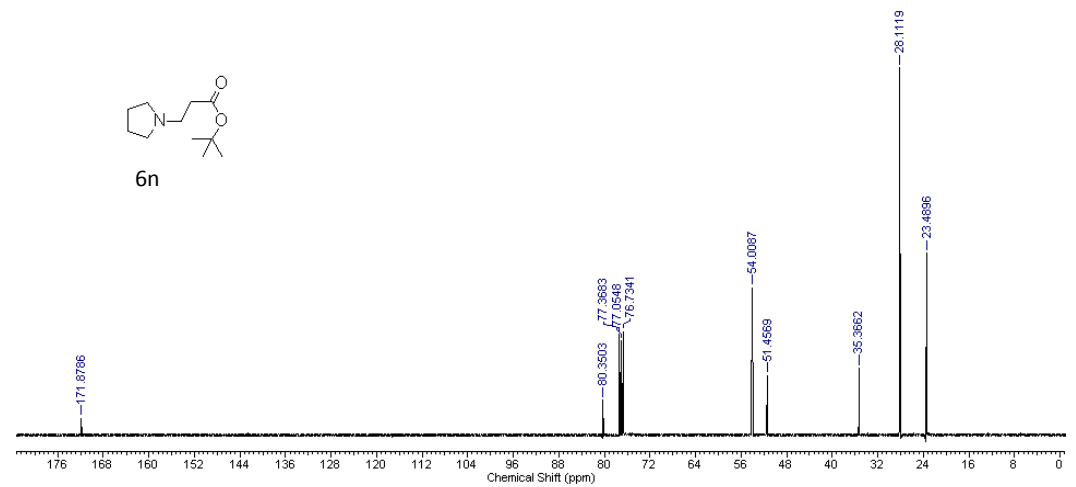
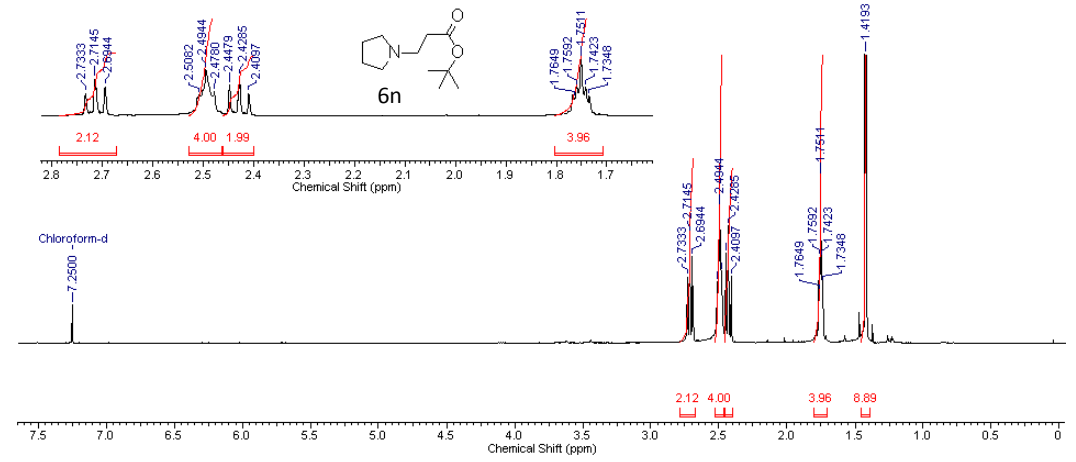
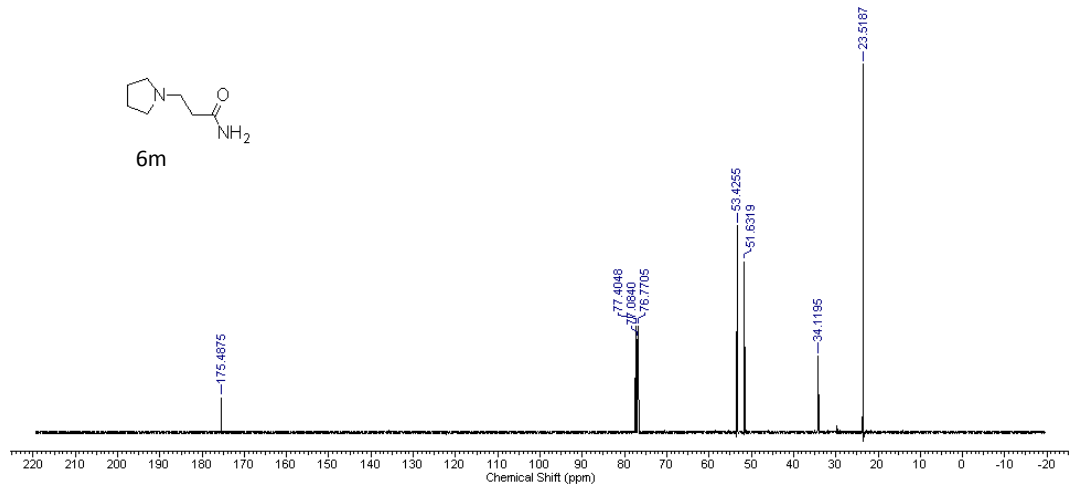




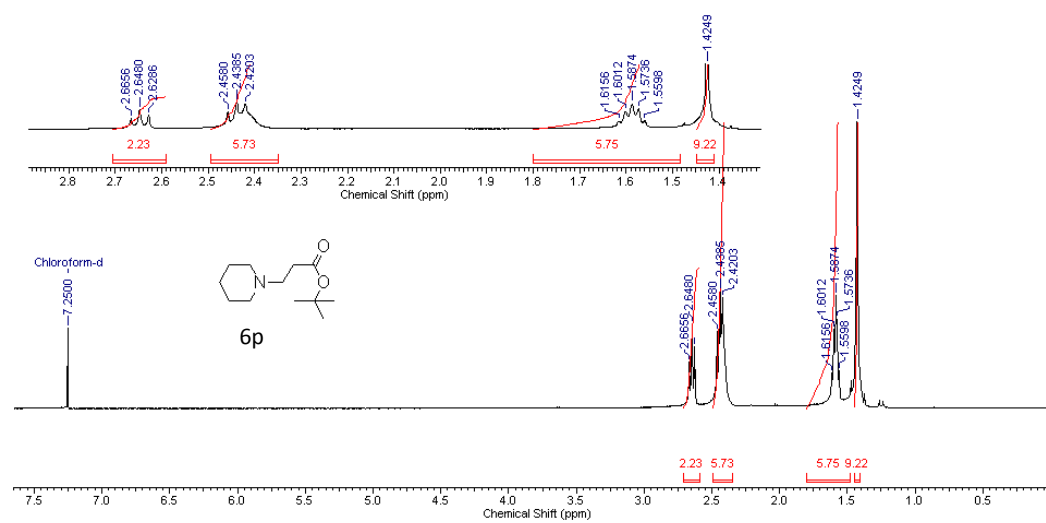
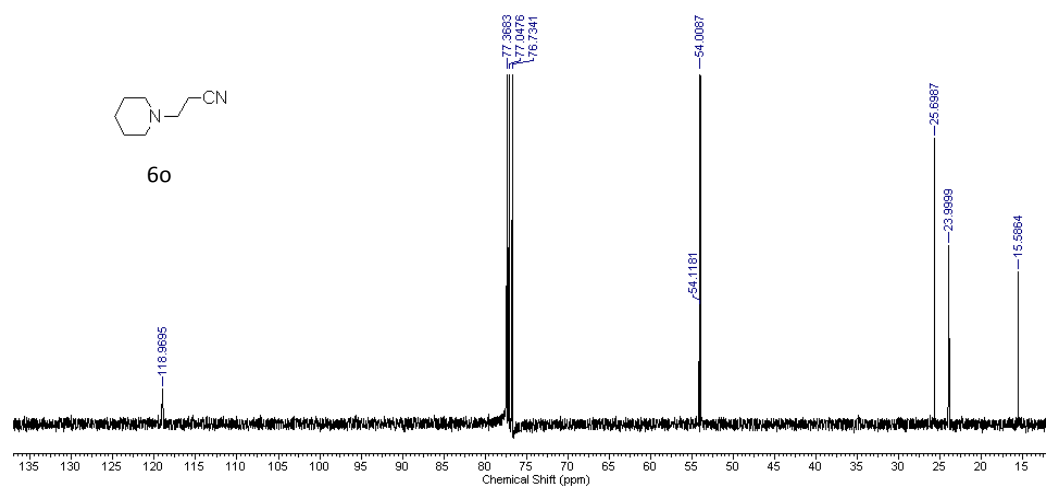
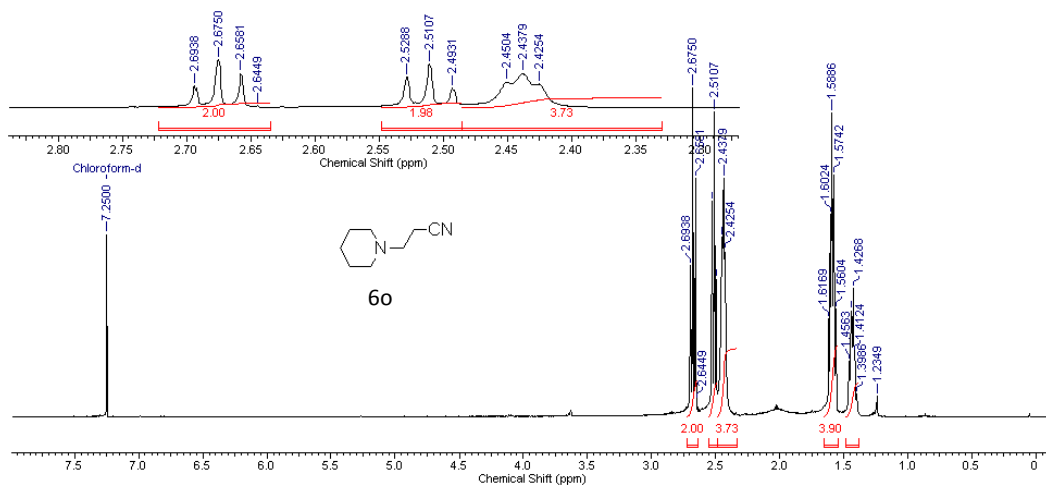
Chapter 3



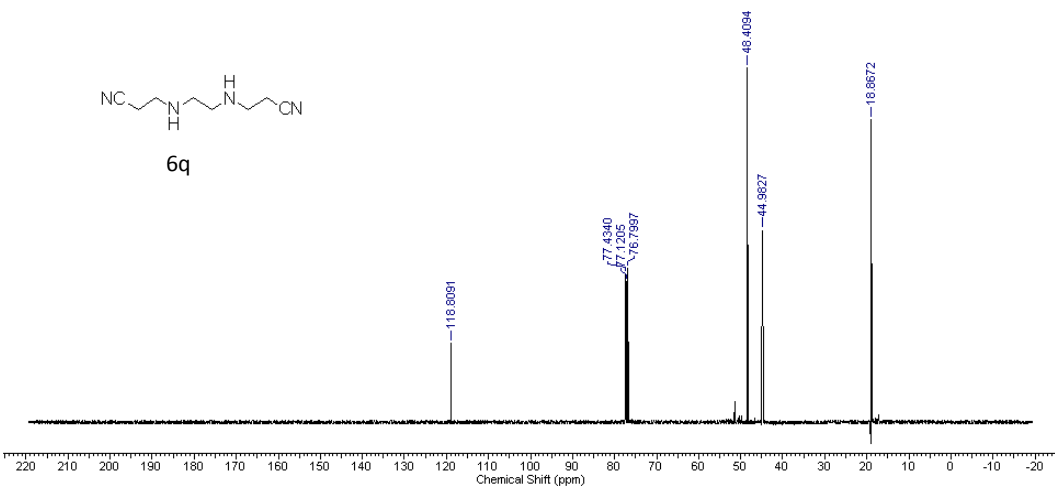
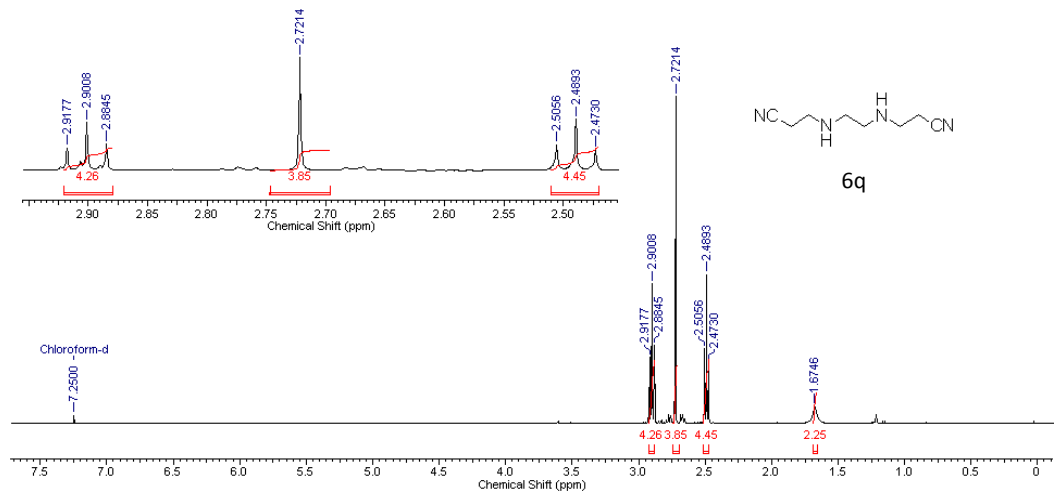
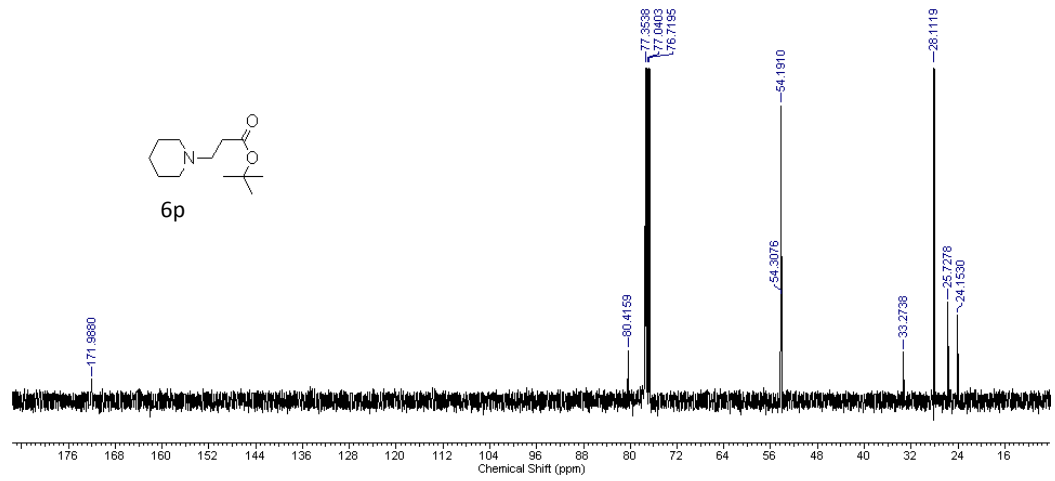
Chapter 3



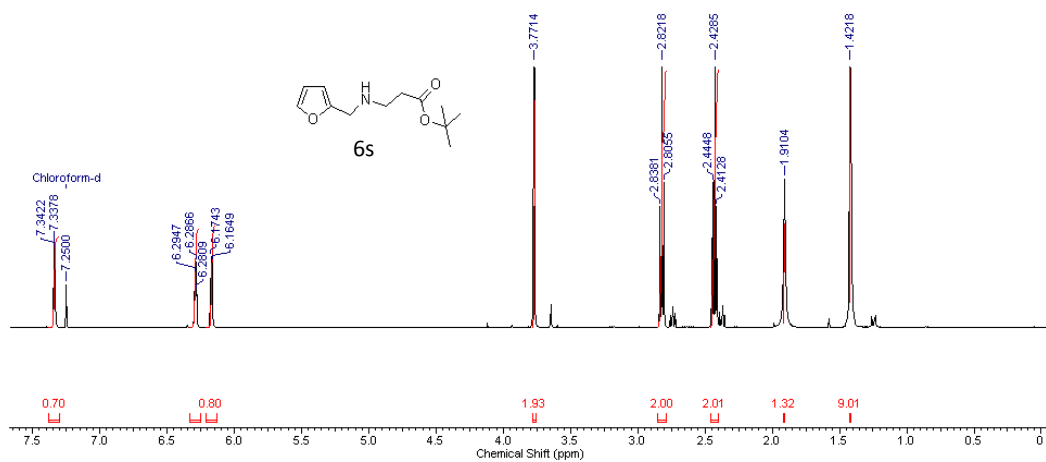
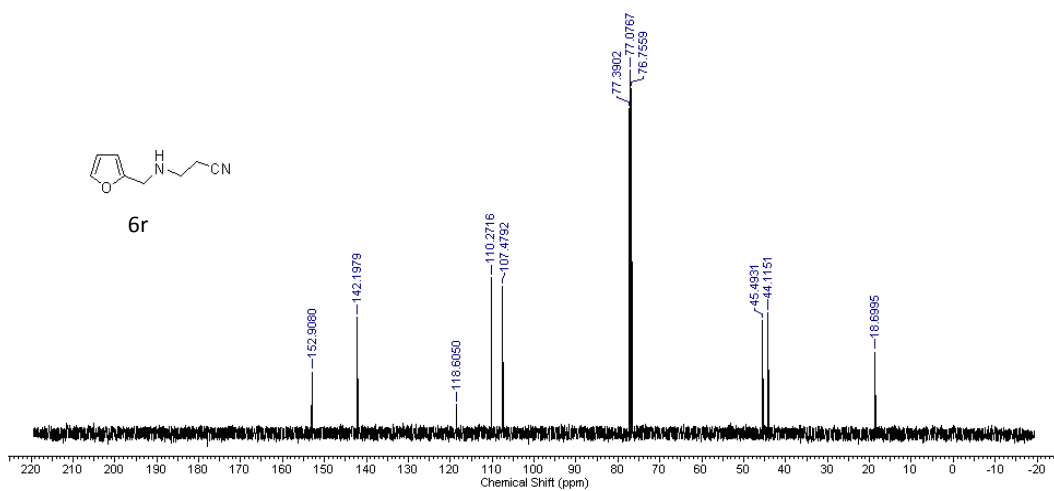
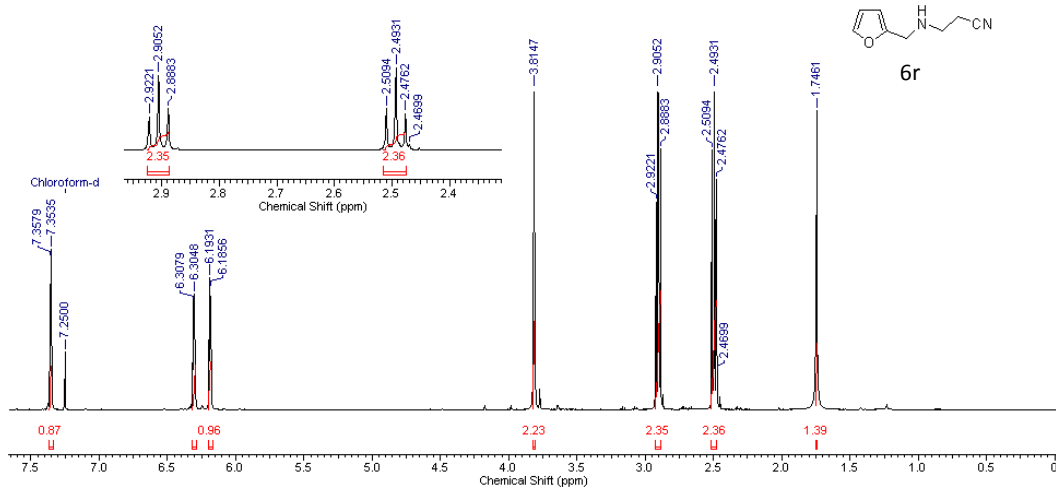
Chapter 3



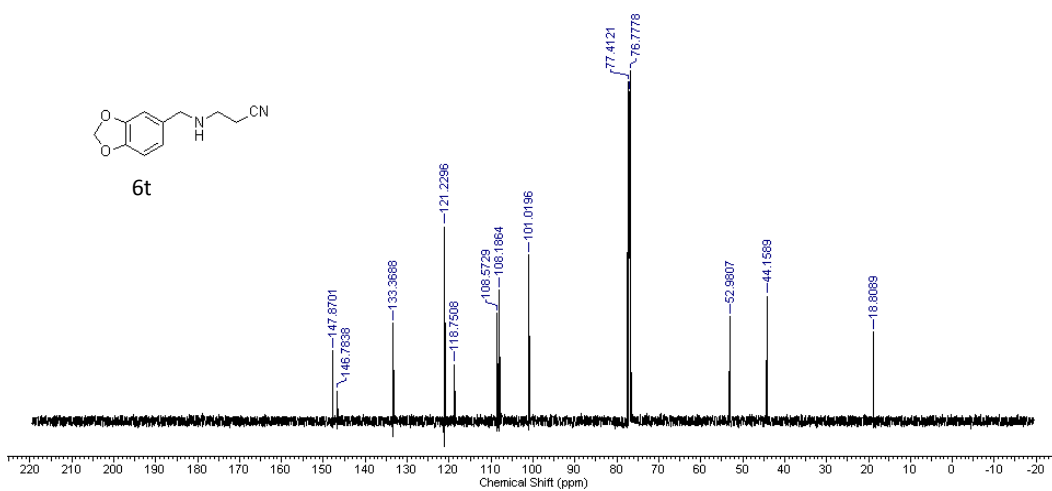
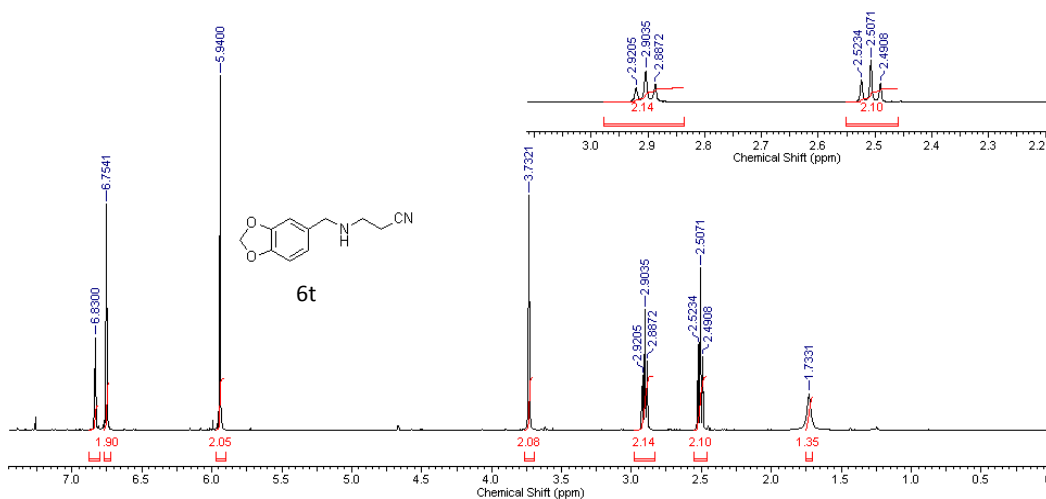
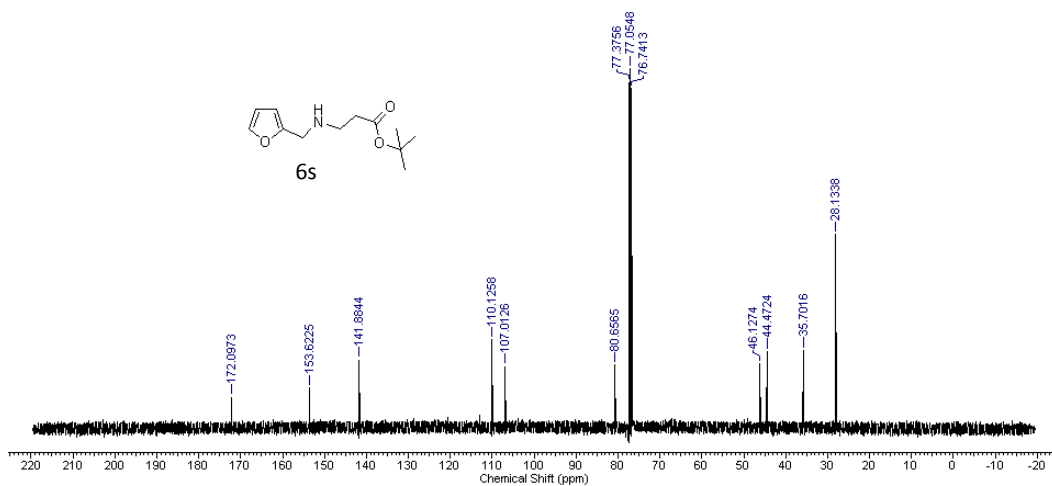
Chapter 3



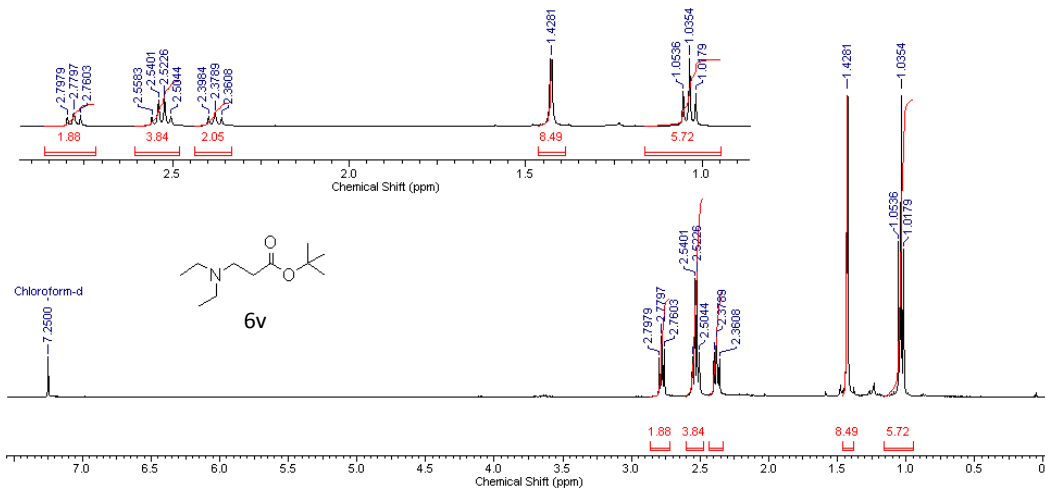
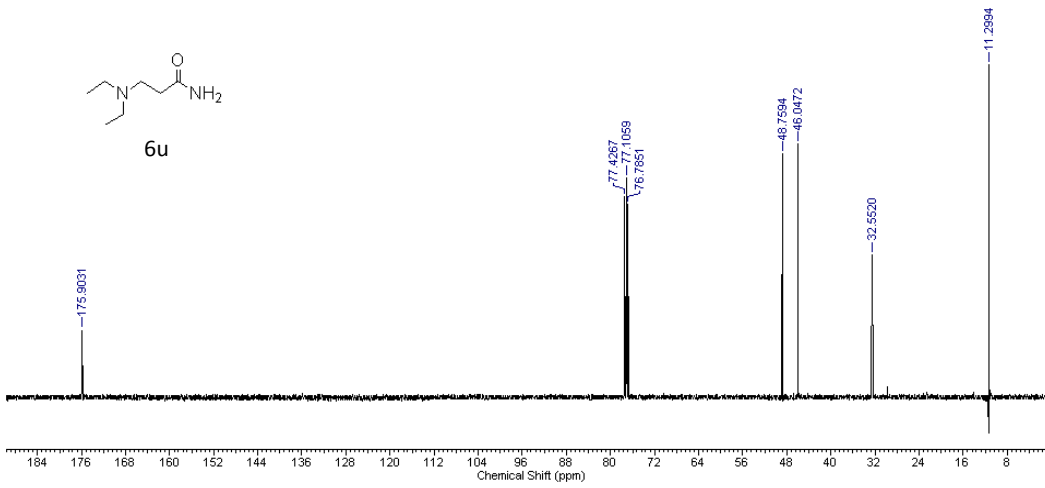
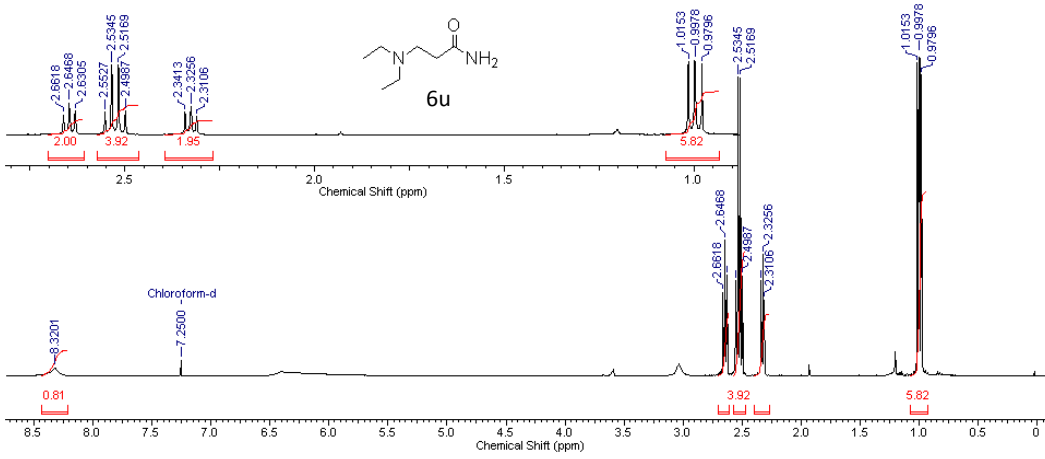
Chapter 3



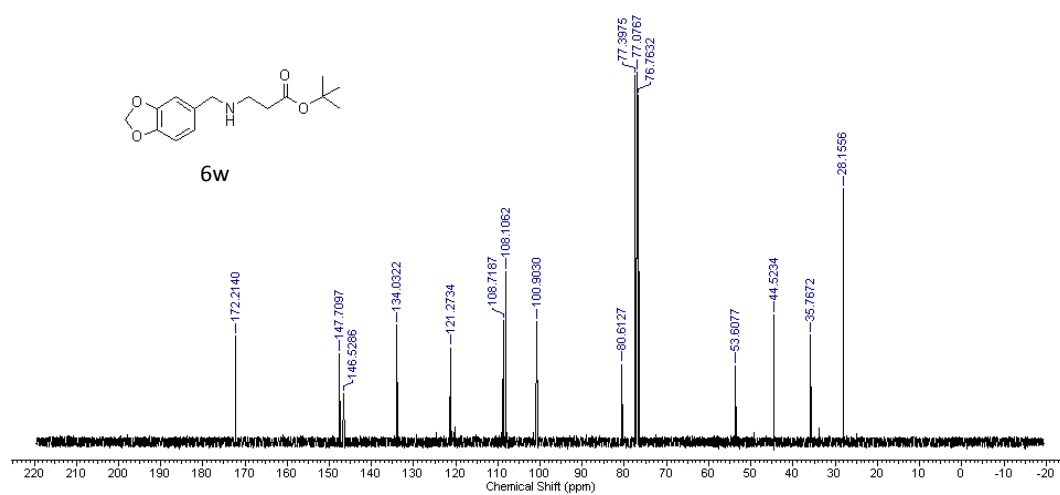
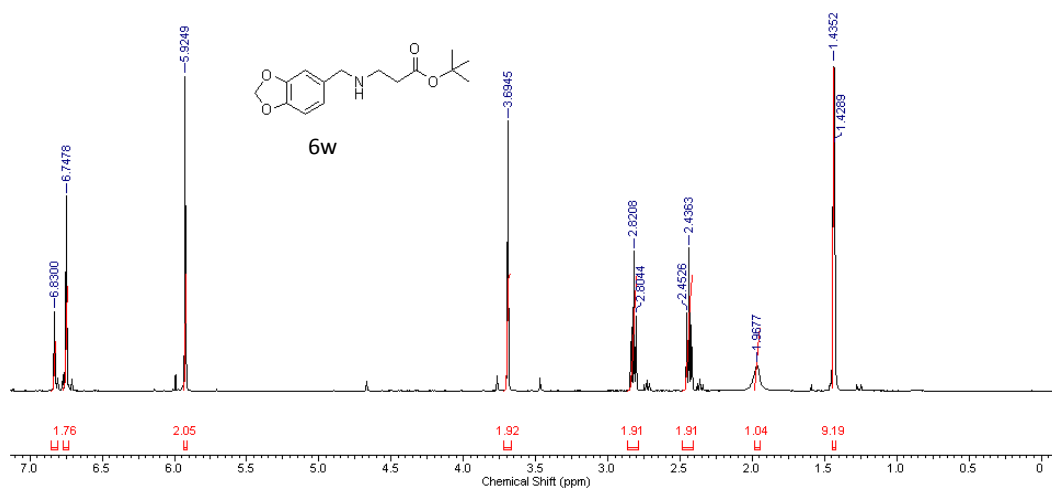
Chapter 3



Chapter 3



Chapter 3



Chapter 3

Chapter 4

Au Nanoparticle-Polydopamine-Reduced Graphene Oxide Ternary Nanocomposite as Efficient Catalyst for Selective Oxidation of Benzylic C(sp³)-H Bonds Under Mild Conditions

Chapter 4

4.1 Introduction

Heterogeneous catalysis is at the heart of green chemical pathways as it addresses most of the requirements of green protocols necessary in the manufacturing of diverse range of chemicals. Selective oxidation of primary sp^3 C–H bonds using molecular oxygen into useful functionalized chemicals is an important class of chemical transformations.^[1-9] This challenging transformation is significant not only in efficient and sustainable exploitation of organic feedstocks, but also in understanding the intrinsic features of the broadly existing C–H bonds in organic molecules in terms of their accessibility, activity and selectivity. Several protocols for highly efficient C–H transformation catalyzed by transition metal complexes such as those of Pd, Pt, Ru, Rh, Re, Fe, Au etc. have been developed.^[10-15] On the other hand, development of noble metal nanoparticle based heterogeneous catalytic systems for important organic transformations has taken centre stage due to several advantages such as availability of large surface area, the possibility of easy separation from the reaction mixture and further reusability.^[16-24] Following the seminal work of Hutchings's group on oxidation of C–H bonds in toluene leading to several oxygenates using alloyed AuPd nanoparticles supported on carbon or TiO_2 ,^[25] there has been a significant focus on the development of nanoparticle based heterogeneous thermocatalytic systems. However development of Au based heterogeneous catalysts for selective oxidation of C–H bonds under milder reaction conditions is crucial for effective applications.^[26-27] It has been demonstrated that in presence of an oxygen donor such as *tert*-butyl hydroperoxide (TBHP), AuPd nanoparticles facilitate the oxidation of hydrocarbons at relatively milder conditions (80 °C).^[28] The capability of nanoparticle surfaces in stabilizing free radicals that have longer half-life than the free radicals in solution induces oxygen activation leading to efficient oxidation of hydrocarbons at milder reaction conditions. Whereas, focus has been on the structural morphology of the bimetallic nanoparticles and their interaction with support materials, we envisioned that even monometallic Au NPs embedded on conducive supports could function effectively as catalysts for challenging organic transformation such as oxyfunctionalization of inert C–H bonds under mild conditions in presence of a free radical promoter. Qualitative explorations for the role of supports on catalysis have been carried out

Chapter 4

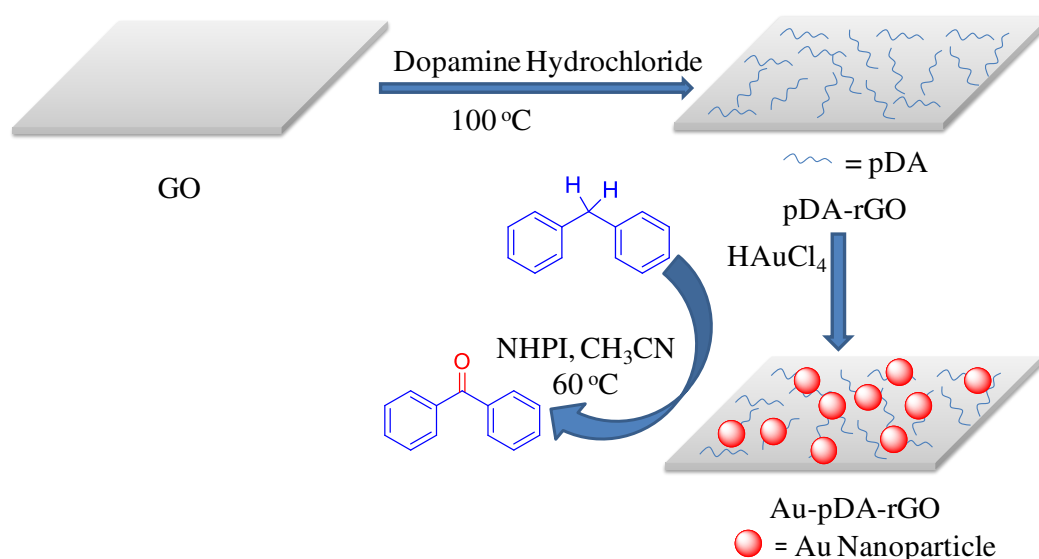
extensively; however applying these modifications in selective oxidation of hydrocarbons is still a challenge. Graphene oxide (GO), the two dimensional aromatic scaffold with both hydrophilic oxygenated functionalities and hydrophobic nanographene domain on the basal plane has been demonstrated as excellent support for metal^[29-32], metal oxide^[33-35] and bimolecules like hemin^[36] etc. for effective catalysis. The inherent catalytic properties of GO has been demonstrated for several organic transformations such as alcohol oxidation, hydration reaction, Aza-Michael additions, ring-opening polymerization and Friedel-Crafts reactions etc.^[37-40] However, for the oxidation of inert C-H bonds the activity of only GO was found to be sluggish. GO can function as an electron shuttle across its surface as well as transfer electrons to NPs embedded on it.^[41] This capability of GO has propelled GO or rGO to be used as an attractive platform for nanoparticle immobilization and catalytic studies.^[42] Among the free-radical promoters, *N*-hydroxyphthalimide (NHPI) has shown excellent activity towards C-H oxygenation of hydrocarbons when it is combined with a co-catalyst in presence of oxygen.^[43-47] It is believed that highly electrophilic phthalimide *N*-oxyl (PINO) radical, which is an *in situ* formed one electron oxidised form of NHPI initiates the radical propagation of autoxidation, thus efficiently promoting hydrocarbon oxyfunctionalization with reactive O₂ present. Ishii and co-workers showed that a combination of NHPI with transition metals notably cobalt (known as the Ishii system) or with polyoxometalates gives an excellent catalytic system for the autoxidation of broad range of organic substrates.^[48-53]

Even non-metallic compounds such as alkyl hydroperoxides,^[54-55] α,α' -azobisisobutyronitrile,^[56] aldehyde^[57-58] and NO₂^[59-60] have been used as mediators for NHPI based oxidation. The biomimetic catalytic system involving anthraquinone derivatives, zeolites and NHPI has also shown superior activity towards C-H oxygenation of hydrocarbons.^[61-62] However, use of expensive radical mediators and harsh reaction conditions like higher temperature, halogenated solvents etc. limits the industrial application of such systems. Moreover, one of the major issues associated with these catalytic systems is that the radical mediators are either consumed during the oxidation reaction or exhibit difficulties during the recovery process. So, development of catalytic system with

Chapter 4

extensive heterogeneous hallmark and environmentally benign reaction conditions is highly appealing for this NHPI based oxidation reaction.

Herein, we report the catalytic activity of Au NPs anchored on polydopamine (pDA) and rGO for benzylic C-H oxidation reactions. The catalytic system involves a simple and facile strategy for the generation of Au nanoparticles (NPs) on the surface of GO using dopamine hydrochloride (DA) as a reducing agent and nucleation site for the growth of nanocrystals (Scheme 4.1).



Scheme 4.1. Schematic of the ternary nanocomposite consisting of Au nanoparticles supported on polydopamine and reduced graphene oxide as catalysts for benzylic C-H bond oxidation

In combination with *N*-hydroxyphthalimide (NHPI) as radical initiator, the resulting Au-pDA-rGO nanocomposite exhibited excellent catalytic activity and selectivity towards the oxidation of benzylic sp^3 C-H bonds in hydrocarbons. High efficiency of the nanocatalytic system resulted in 80-90% conversion of the substrates under mild reaction conditions in a pathway that involved free radicals. Moreover, the recycling effectiveness of the nanocomposite was demonstrated without significant loss in catalytic activity over several cycles making the nanocatalytic system highly sustainable.

4.2 Results and Discussion

4.2.1 Synthesis and characterization of nanocomposite

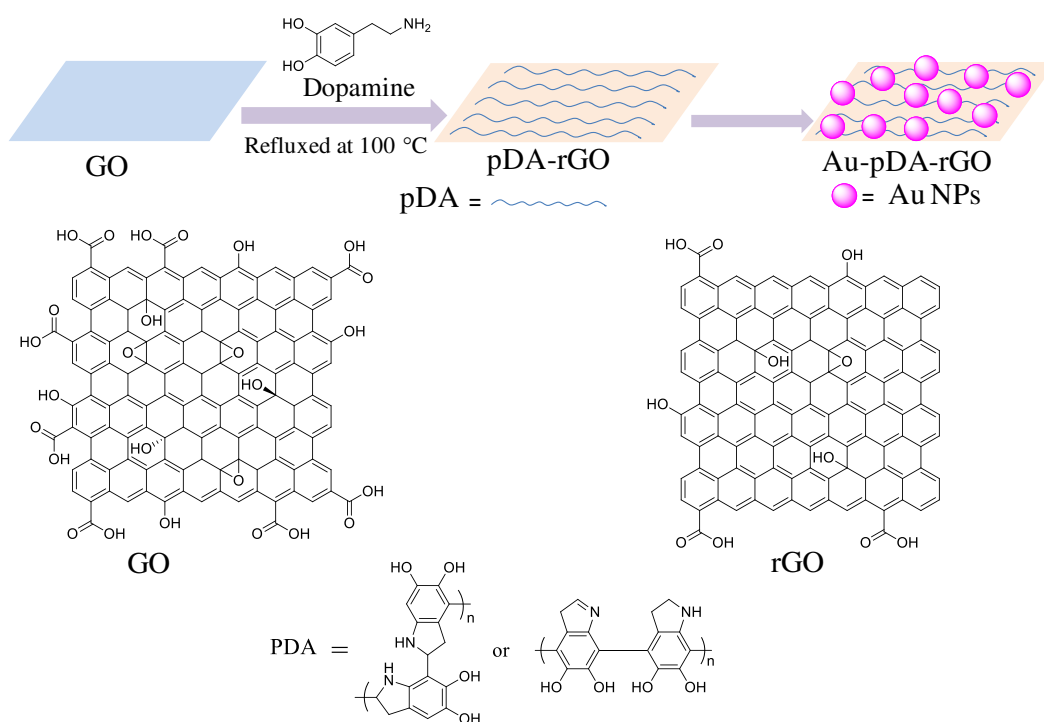


Figure 4.1. A pictorial depiction for the formation of Au NPs supported on pDA-rGO nanosheets

The mussel inspired synthetic method ^[63-64] for the growth of supported Au nanoparticle composite has been described in details in the ESI. Briefly, GO nanosheets synthesized by the modified Hummer's method were first functionalized with polydopamine (pDA) by polymerization of dopamine at elevated temperature (Fig. 4.1).^[65] During the process, GO was reduced by DA. The pDA layer (formed by polymerization of dopamine) on the surface of rGO was used as a nucleating site and reducing agent for the synthesis of uniform Au nanoparticles well dispersed on the rGO surface. Transmission electron microscopy (TEM) studies showed sheet like structure of GO (Fig. 4.2a) and successful formation of the uniform Au NPs decorated on these graphene sheets (Fig. 4.2b). The high resolution TEM image (HRTEM) showed a lattice separation of 0.23 nm corresponding to (111) plane of Au (Fig. 4.2c). The selected area electron diffraction pattern of the Au-pDA-rGO showed crystallinity (Fig. 4.2d). The formation of the Au NPs on the reduced graphene surface was further confirmed by atomic force microscopy (AFM) (Fig. 4.3). The UV-visible spectrum of the Au-pDA-rGO composite showed a broad plasmon resonance band at around 530 nm confirming the formation of Au NPs. Moreover, the peak at 230 nm in GO corresponding to the $\pi \rightarrow \pi^*$ transitions of

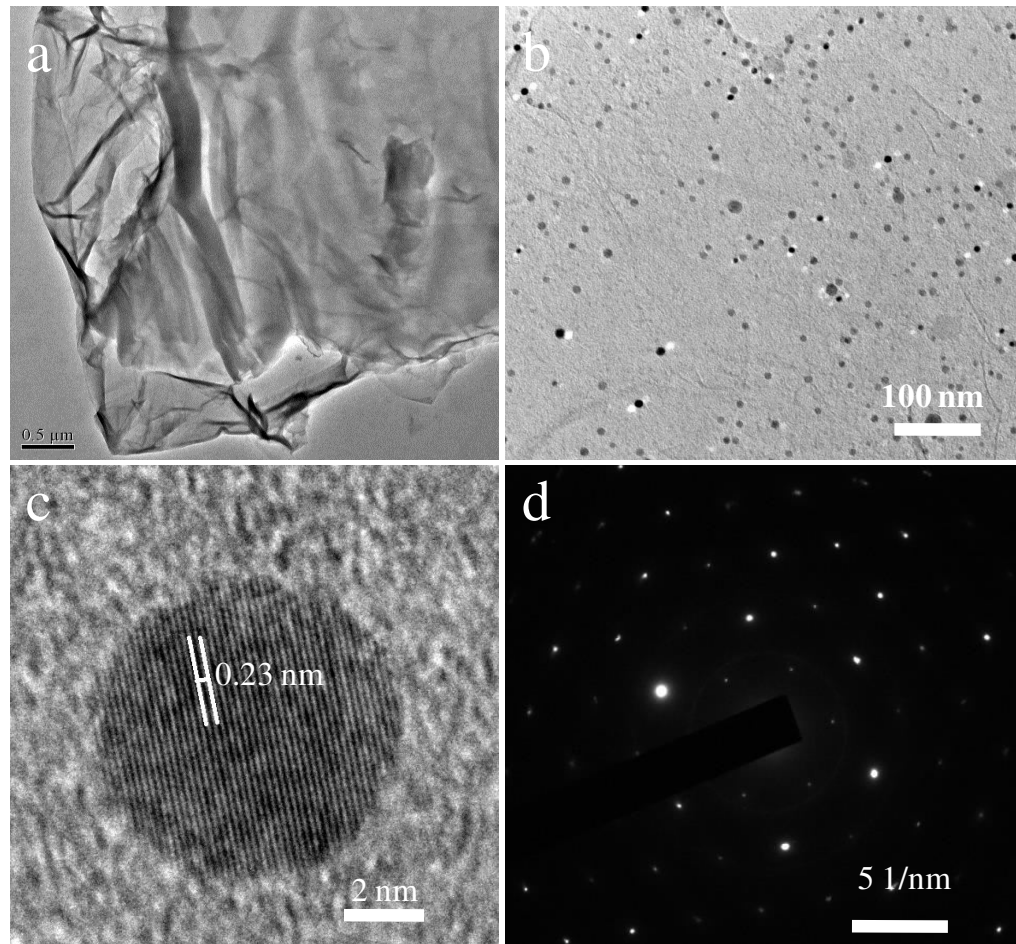


Figure 4.2. Transmission electron micrograph of a) graphene oxide; scale bar 500 nm, b) Au-pDA-rGO composite; scale bar 100 nm, c) High Resolution (HR-TEM)TEM image of Au-pDA-rGO composite, scale bar 2 nm and d) selected area electron diffraction (SAED) pattern of Au-pDA-rGO composite

aromatic C-C bonds was significantly red shifted (~ 15 nm) in case of Au-pDA-rGO composite, indicating the restoration of electronic conjugation within the graphene sheets (Fig. 4.4a).^[66-67] The powder XRD spectrum of Au-pDA-rGO composite consisted of peaks at 2θ values of 38.2, 44.4, 64.6 and 77.7 degrees, corresponding to the (111), (200), (220) and (311) facets of the fcc structure of Au respectively. In addition, a broad peak at 2θ value of 22.6° attributed to reduced graphene oxide (rGO)^[68] was also observed (Fig. 4.4b). The effects of the growth of Au NPs on the electronic structure of rGOs were also investigated

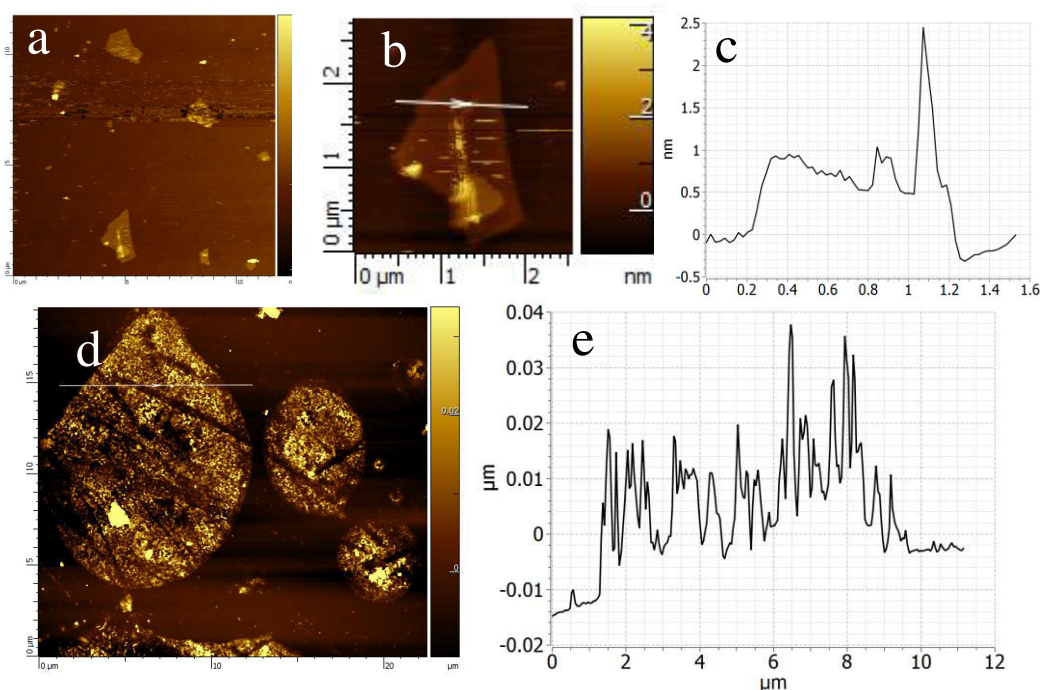


Figure 4.3. Atomic force microscopy studies of GO and Au-pDA-rGO; a) low resolution image of GO; (b, c) high resolution image and corresponding height profile of GO; d) AFM image of Au-pDA-rGO; (e) corresponding height profile

by Raman spectroscopy (Fig. 4.4c). As shown, the characteristic D and G bands at *ca.* 1328 and 1594 cm^{-1} respectively in case of GO were shifted to 1325 and 1572 cm^{-1} respectively in case of Au-pDA-rGO.^[69-70] Further, the ratio of intensities of D band to that of G band (I_D/I_G) decreased from approximately 1.14 for GO to about 0.92 for the Au-pDA-rGO composite. This signifies the formation of more extended networks of conjugated sp^2 carbons towards a more locally ordered graphene lattice. Further investigation of molecular structural changes associated with the formation of Au-pDA-rGO was carried out using FTIR spectroscopy (Fig. 4.4d). The characteristic vibration peak owing to C=O in GO at 1720 cm^{-1} decreased dramatically in Au-pDA-rGO composite signifying the conversion of GO to rGO. Further, the appearance of a new peak at 1570 cm^{-1} corresponding to N-H bending vibration confirmed the presence of polydopamine in the composite matrix.

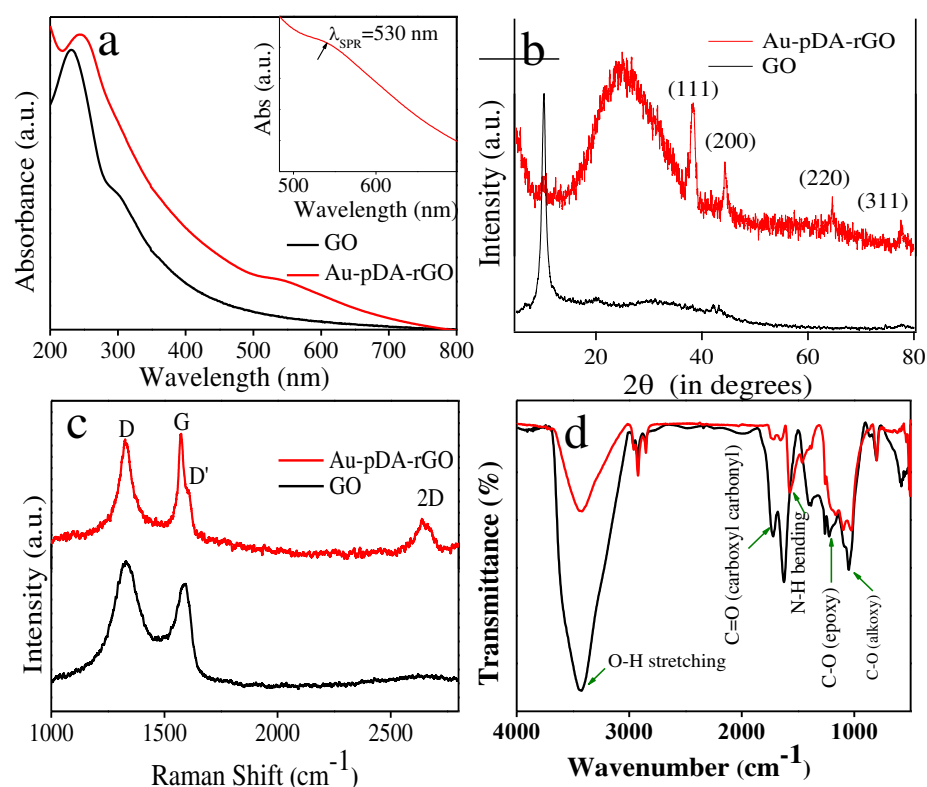


Figure 4.4. a) UV-Visible spectra (inset: enlarged view of Au surface Plasmon resonance band); b) powder X-ray diffraction pattern, c) Raman spectra and d) FTIR spectra of GO (black line) and Au-pDA-rGO (red line)

The reduction of GO to rGO and modification with pDA layer was further verified by X-ray photoelectron spectroscopy (XPS). Fig. 4.5 shows XPS analysis of GO, pDA-rGO and Au-pDA-rGO. The XPS survey spectra (Fig. 4.5a) shows the generation of N1s peak in the spectra of pDA-rGO and Au4f peak in Au-pDA-rGO respectively. The C1s core level spectrum of GO (Fig. 4.5b) was fitted into four components with binding energies (BEs) at about 284.5, 286.4, 287.6 and 288.9 eV which corresponds to C-C, C-O, C=O and O-C=O species respectively. The PDA-rGO C1s core-level spectrum (Fig. 4.5c) was fitted into five peak components with BEs at about 284.4, 285.5, 286.4, 287.8 and 288.9 eV attributed to the C-C, C-N, C-O, C=O, O-C=O species respectively. Compared to GO, a significant decrease of C-O peak component in pDA-rGO was observed which clearly indicated the reduction of GO by dopamine. The appearance of the C-N peak component at the BE of 285.5 eV in the C1s core-level spectrum of

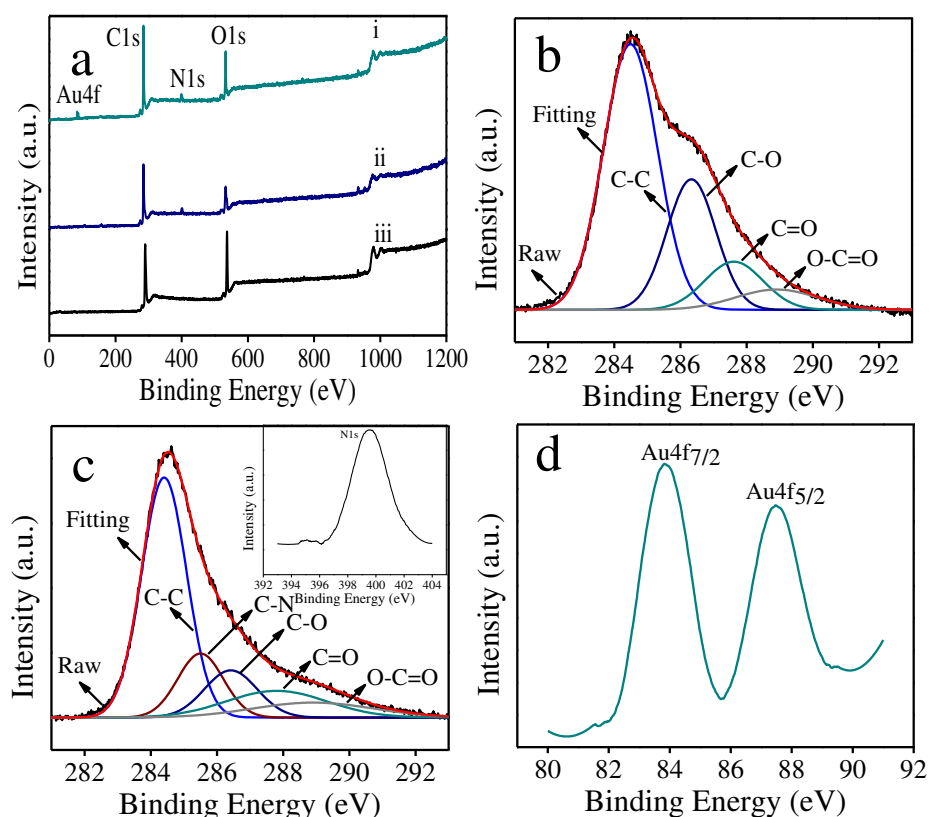


Figure 4.5. a) XPS survey spectra of (i) GO, (ii) pDA-rGO and (iii) Au-pDA-rGO. b) and c) XPS C1s core-level spectrum of GO and pDA-rGO respectively and d) Au4f core-level spectrum

level spectrum of pDA-rGO and an N1s core-level spectrum at the BE of ~400 eV (inset of Fig. 4.5c) are consistent with the presence of a surface modified pDA layer.^[71] Fig. 4.5d shows high-resolution Au4f core-level spectrum. The binding energies at 83.6 and 87.3 eV are ascribed to Au4f_{7/2} and Au4f_{5/2} of metallic Au respectively.

4.2.2 Catalytic Performance of Au-pDA-rGO composite at variable Au loading

We evaluated the catalytic efficiency of the heterogeneous Au-pDA-rGO nanocomposite for the oxidation of benzylic C-H bonds. Until now, development of Au based heterogeneous nanocatalysts for C-H oxidations were focused on bimetallic nanostructures, either in alloy or core-shell form, where the structure and synergy between metallic constituents played a critical role.^[25, 28, 72-73] To our surprise, even the monometallic Au NPs embedded on pDA-rGO layer could

Chapter 4

function as an effective catalyst in combination with NHPI and molecular oxygen under mild reaction conditions. For evaluating the optimization conditions, we selected diphenylmethane as a model substrate and evaluated its oxidation to diphenylketone under various optimized conditions such as catalytic loading, temperature, solvents, supports, oxidants, catalyst amount etc. First we evaluated the variation in catalytic activity with respect to Au loading on pDA-rGO surfaces. A series of nanocatalysts were prepared by varying the concentration of the metal precursor (HAuCl_4) keeping the concentration of pDA-rGO constant. The amount of Au in the composites was evaluated using inductively coupled plasma atomic emission spectroscopy (ICP-AES) (Table 4.1). While increasing the Au loading from 0.5wt% to 6wt%, we observed that average diameter of Au

Table 4.1. ICP-AES analysis and TON of Au catalysts with varying Au loading^a

Entry	%Au loading (Calculated)	%Au loading (Experimental)	Mean Diameter (nm)	TON
1	0.5	0.491	4.5 ± 0.5	108
2	1	1.010	5.9 ± 0.6	89
3	2	1.928	6.8 ± 0.7	78
4	4	3.792	7.9 ± 0.7	73
5	6	5.509	9.6 ± 1.0	63

^aReaction conditions: 1 mmol diphenylmethane, catalyst mass varied between 0.01 to 0.12g to give a substrate to metal molar ratio = 1000, $T = 60^\circ\text{C}$, stirring rate = 1000 rpm; O_2 pressure 10 bar, CH_3CN 5 mL, NHPI (10 mol%) TON = Moles of substrate transformed per mole of active catalyst. TONs were calculated on the basis of total loading of metals and 4 h of reaction

NPs increased congruently. From the TEM image and corresponding particle size distribution histogram (Fig. 4.6), the average diameter of Au NPs in 0.5wt%, 2wt%, 4wt% and 6wt% Au loaded nanocatalysts were calculated to be 4.5 ± 0.5 nm, 6.8 ± 0.7 nm, 7.9 ± 0.7 nm and 9.6 ± 1.0 nm respectively. With different

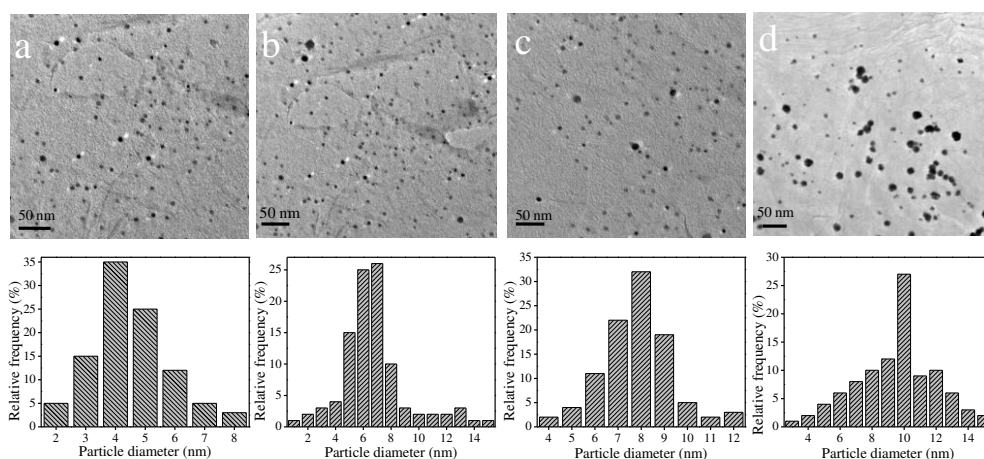


Figure 4.6. TEM images and corresponding particle size distribution histogram (below) of Au-pDA-rGO nanocomposite with different Au loading (a) 0.5 wt%, (b) 2 wt%, (c) 4 wt% and (d) 6 wt%

Au loaded Au-pDA-rGO composites, we performed the aerobic oxidation of diphenylmethane using acetonitrile as solvent in presence of NHPI (Table 4.2), under the best optimized conditions (as discussed in Table 4.4). For all the Au-pDA-rGO composites with variable Au loading, diphenylketone was formed as

Table 4.2. Effect of Au loading on the aerobic oxidation of diphenylmethane^a

Entry	Au loading (%)	Time (h)	Conv. (%)	Sel. (%)
1	0.5	14	44	98
2	1	13	62	96
3	2	12	92	97
4	4	12	93	95
5	6	11	90	92
6 ^b	2	8	91	87

^aReaction conditions: 1.0 mmol diphenylmethane, catalyst mass 0.02 g, reaction temperature 60 °C, stirring rate 1000 rpm; O₂ pressure 10 bar, CH₃CN 5 mL, NHPI (10 mol%),^breaction performed at 100 °C

the major product along with a small amount of diphenylmethanol as a side product. It was observed that Au-pDA-rGO nanocomposites with 0.5 wt% Au loading showed the highest Turn-over number (TON) (Table 4.1) when the

catalytic reactions were performed keeping the substrate to metal ratio constant. This was expected considering the smallest particle size of Au NPs formed in case of 0.5 wt% Au loading among all the NPs synthesized at various rGO-pDA: Au³⁺ ratio. Increasing the Au loading resulted in decrease in TON suggesting that the catalytic performance of the NPs was dependent on particle size of Au NPs. However, when we evaluated the catalytic conversion of our model reaction with respect to the weight of the catalytic mass of the composite, Au-pDA-rGO with 2 wt% Au loading offered the best catalytic conversion with high selectivity under standard reaction conditions (Table 4.2). The nanocomposite with 0.5 wt% Au loading afforded moderate catalytic conversion, on the other hand with decreasing rGO: Au ratio (upto 2 wt% Au loading) the conversion improved significantly. The results suggest that higher rGO: Au ratio might have a detrimental effect on the oxidation reaction. Further decrease in rGO: Au ratio (for 4 wt% and 6 wt% Au loading) did not result in any improvement. Although increasing temperature resulted in higher conversion at relatively lower time, selective formation of diphenylketone suffered (Table 4.2, entry 6). Based on these studies, we found that the nanocomposite with 2wt% Au loading offered the best catalytic conversion and high selectivity with respect to catalyst weight of the composite under the present reaction conditions. From these results, it can be concluded that rGO: Au ratio had a significant effect on the catalytic activity of the nanocomposite (Table 4.3).

Table 4.3. Effect of rGO: Au ratio in the catalytic conversion of diphenylmethane oxidation

Entry	Au loading (%)	rGO: Au ratio	Conv. (%)
1	0.5	100	44
2	2	25	92
3	4	12	93
4	6	8	90

Reaction conditions: 1.0 mmol diphenylmethane, catalyst mass 0.02 g, reaction temperature 60 °C, stirring rate 1000 rpm; O₂ pressure 10 bar, CH₃CN 5 mL, NHPI (10 mol%)

4.2.3 Optimization and scope of reaction

In order to optimize the reaction conditions for obtaining high conversion and selectivity for the C-H oxidations, we performed several controlled

Chapter 4

experiments using diphenylmethane as a model substrate (Table 4.4). The Au-pDA-rGO nanocomposite could not afford high conversion in presence of molecular oxygen as the single oxidant even at elevated temperature. Therefore, it was necessary to look for a secondary oxidant in order to facilitate higher conversion. Addition of commonly available oxidants such as H_2O_2 or *tert*-butylhydroperoxide (TBHP) to the reaction mixture afforded moderate yield of the desired product diphenylketone along with the formation of several by-products. However, in combination with NHPI, Au-pDA-rGO afforded high conversion and selectivity under mild reaction conditions (60 °C). 10 mol% of NHPI was found to be optimum for our catalytic reaction (Table 4.4, entry 8-10). Among the solvents, CH_3CN was found to be most suitable for the reaction, as other solvents like water, acetone and DMSO afforded low yield. Further, increasing the reaction temperature from 25 °C to 60 °C resulted in tremendous enhancement in conversion (Table 4.4, entry 8 and 11). Further increment in temperature, however, led to decrease in conversion and selectivity (Table 4.4, entry 12). In order to evaluate the role of individual constituents in the ternary composite, several controlled experiments were performed under the standard reaction conditions. Only NHPI, GO, pDA or combination of them was inefficient for the reaction and gave unfruitful results. Au NPs synthesized using only pDA as a reducing and stabilizing agent in absence of GO (Au-pDA) showed much lower catalytic activity compared to Au-pDA-rGO (Table 4.4, entry 20). TEM image of the Au-pDA composite showed the formation of agglomerated nanoparticles with average particle size of ~ 20 nm (Fig. 4.7a).

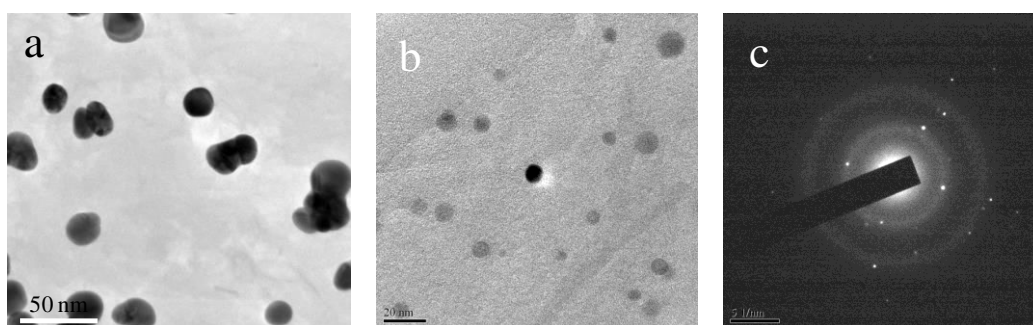


Figure 4.7. a) TEM image of Polydopamine stabilized Au nanoparticle (Au-pDA), b) TEM micrograph of Au-rGO^b composite synthesized by simultaneous reduction of Au^{3+} and GO using NaBH_4 ; scale bar 20 nm and c) corresponding SAED pattern. The particles showed an average size of 7.6 ± 1.6 nm

Chapter 4

Table 4.4. Optimization of reaction conditions[#]

Entry	Catalyst	Additive (mol%)	Reaction Conditions	Conv. (%)	Sel. (%)
1	Au-rGO ^b	NHPI (10)	CH ₃ CN, 60 °C, 12 h	38	96
2	Cat A	-	CH ₃ CN, 60 °C, 24 h	22	98
3	Cat A	K ₂ CO ₃ (10)	Water, 70 °C, 24 h	24	100
4	Cat A	H ₂ O ₂ (10)	CH ₃ CN, 60 °C, 12 h	38	82
5	Cat A	H ₂ O ₂ (15)	CH ₃ CN, 60 °C, 12 h	41	81
6	Cat A	TBHP (10)	CH ₃ CN, 60 °C, 12 h	61	79
7	Cat A	TBHP (5)	CH ₃ CN, 60 °C, 12 h	52	80
8	Cat A	NHPI (10)	CH ₃ CN, 25 °C, 12 h	49	98
9	Cat A	NHPI (5)	CH ₃ CN, 60 °C, 12 h	74	98
10	Cat A	NHPI (15)	CH ₃ CN, 60 °C, 12 h	92	97
11	Cat A	NHPI (10)	CH ₃ CN, 60 °C, 12 h	92, ^c 52, ^d 65, ^e 93	97
12	Cat A	NHPI (10)	CH ₃ CN, 80 °C, 12 h	90	89
13	Cat A	NHPI (10)	Water, 80 °C, 12 h	25	87
14	Cat A	NHPI (10)	Acetone, 60 °C, 12 h	45	96
15	Cat A	NHPI (10)	DMSO, 60 °C, 24 h	<1	99
16	Au-PVP	NHPI (10)	CH ₃ CN, 60 °C, 12 h	34	87
17	Au-C	NHPI (10)	CH ₃ CN, 60 °C, 12 h	22	100
18	Au-TiO ₂	NHPI (10)	CH ₃ CN, 60 °C, 15 h	48	97
19	Au-CeO ₂	NHPI (10)	CH ₃ CN, 60 °C, 14 h	43	95
20	Au-pDA	NHPI (10)	CH ₃ CN, 60 °C, 12 h	12	96

[#]Reaction conditions: Unless otherwise specified all the reactions were carried out with substrate diphenylmethane (1.0 mmol), catalyst 0.02 g (Au loading 2 wt%), additive (5-15 mol%) under magnetic stirring; Solvent 5 mL; O₂ pressure 10 bar; stirring rate 1000 rpm. Au-rGO^b:GO and Au³⁺ reduced by NaBH₄, Cat A: Au-pDA-rGO, ^{c,d,e}Au-pDA-rGO catalyst amount 0.01, 0.015 and 0.03 g respectively

Hence the deposition of pDA on GO was crucial in controlling the size of the Au NPs in the composite. On the other hand, Au-rGO^b composite without pDA

Chapter 4

(synthesized using NaBH_4 as reducing agent) afforded only 38% yield of the desired product under optimized reaction conditions. TEM image and corresponding SAED pattern showed formation of nanocrystalline Au particles of average diameter 7.6 ± 1.6 nm for Au-rGO^b composite synthesized by simultaneous reduction of GO and Au^{3+} by NaBH_4 . (Fig. 4.7b and 4.7c). It is well known that several other supports such as polyvinyl pyrrolidone (PVP), activated carbon and metal oxides such as TiO_2 and CeO_2 are used for anchoring nanoparticles. In order to have a better insight into the catalytic efficacy of Au-pDA-rGO nanocomposites, we performed the catalytic studies of Au-PVP, Au-C, Au- TiO_2 and Au- CeO_2 nanocomposites in presence of NHPI. Using Au-PVP as a catalyst under the standard reaction conditions, the conversion was moderate and the selectivity was poor as several other by-products such as diphenylmethanol and benzoic acid were observed. Further the nanoparticles were agglomerated even after one cycle of reaction. Au NPs stabilized with activated carbon (Au-C) could not afford higher yield of the oxidized product. In case of Au- TiO_2 or Au- CeO_2 as a catalyst in presence of NHPI, the oxidized products were obtained with moderate yield at 60 °C (Table 4.4, entry 18, 19), however, better conversion was observed at elevated temperature (Table 4.5). From these studies, it was apparent that Au-pDA-rGO

Table 4.5. Comparison of catalytic activity of different Au catalysts at elevated temperature

Catalysts	Temperature (°C)	Conversion (%)	Selectivity (%)
Au-PVP	80	48	85
Au-C	90	35	97
Au- TiO_2	90	75	92
Au- CeO_2	100	64	90

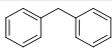
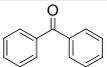
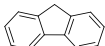
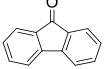
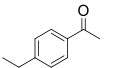
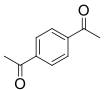
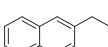
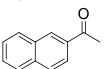
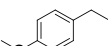
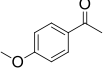
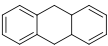
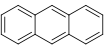
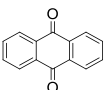
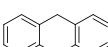
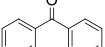
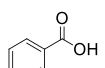
Reaction conditions: 1.0 mmol diphenylmethane, Au catalysts 20 mg (2 wt% Au loading), NHPI (10 mol%), CH_3CN 5ml, stirring rate 1000 rpm, O_2 pressure 10 bar

exhibited the best catalytic activity when coupled with NHPI resulting in successful oxidation of diphenylmethane with 92% conversion and 97% selectivity to diphenylketone in 12 h under mild conditions.

The scope of the oxidation reactions was surveyed using Au-pDA-rGO as a catalyst in presence of NHPI to catalyze oxygenations of various hydrocarbons

Chapter 4

Table 4.6. The Oxidation of benzylic hydrocarbons catalysed by Au-pDA-rGO nanocomposite ^a

Entry	Substrate	Product	Time (h)	Conv. (%)	Sel. (%)	TOF(h ⁻¹)
1			12	92.3	97.4	117
2			10	80.1	94.3	80
3			12	85.1	98.7	100
4			15	89.4	97.6	87
5			16	95.4	98.4	105
6			14	87.5	93.4	112
7			14	94.2	96.8	122
8			4	99.5	80	928
					20	232
9			10	90.5	98.8	137
10			24	60.1	99.6	30
11			24	4.8	99.3	17.8

^aReaction conditions: Substrate (1.0 mmol); Au-pDA-rGO catalyst 0.02 g (2 wt% Au loading); NHPI (10 mol%), CH₃CN (5 mL); Reaction temperature 60 °C; O₂ pressure 10 bar; Stirring rate = 1000 rpm. TOF (h⁻¹) was calculated after 4 h of reaction.^b TOF (h⁻¹) was calculated after 0.5 h of reaction

under the same conditions except for the reaction time (Table 4.6). In general, the C-H bond oxidation of benzylic compounds occurred smoothly under mild conditions to give ketone products. For example, Tetralin was oxygenated with high conversion and selectivity to tetralone with 85% yield. Indan, fluorene and xanthene were oxidized at good conversions (80-90%, Table 4.6 Entry 2, 4, 9). Exception was observed in case of 9, 10 dihydroanthracene, where the dehydrogenation product was favoured over the oxidation product (Table 4.6, entry 8). In case of toluene, the major oxidation product was benzoic acid, probably because aldehydes are known to be a radical-initiator for NHPI based

Chapter 4

oxygenation and is not stable in such radical reactions (Table 4.6, entry 10).^[61-62] The oxidation of cyclohexane was found to be sluggish, resulting in very low conversion under similar reaction conditions (Table 4.6, entry 11).

4.2.4 Conservation of mass and large scale synthesis

CO₂ formation is a frequently observed phenomenon in aerobic oxidation reactions either due to over-oxidation of the reaction mass caused by higher temperature or volatile nature of the oxidizable compounds.^[25, 74-78] Some of the compounds like toluene and cyclohexane due to their volatile nature, give rise to difficulties associated with quantification. In such cases determination of conservation of mass before and after the reaction is very important.^[76-77, 79] Therefore we evaluated mass balances for the oxidation reaction of toluene and cyclohexane. The mass balances were calculated from the weights of reaction mixture before and after the reaction based on their conversions and selectivity. The mass balances were found to be 100% and no CO₂ formation was observed in any of the reactions. In order to eliminate any doubt regarding any desiccation or mineralization of cyclohexane to CO₂ during the aerobic reaction, we performed a gram scale oxidation reaction of cyclohexane (Fig. 4.8). With



Figure 4.8. Gram scale oxidation reaction of cyclohexane

the rest of the compounds also (Table 4.6) we found 100% mass balances and no CO₂ formation was detected. Moreover, the stability of the pDA layer on the GO surface was evaluated by performing a blank reaction with the catalyst only. No evolution of CO₂ was detected during the reaction as 100% mass balance was found from the weight of the reaction before and after the reaction indicating high stability of the catalyst under the performed reaction conditions.

4.2.5 Initial activity studies

For any heterogeneous catalysts, the primary emphasis goes on to its stability under the set of conditions of a reaction. Even though we found no significant decrement in activity in the catalytic reaction from the yield at final stage, we performed the studies regarding the initial activity of the catalyst.^[80] A temporal profile comparing the extent of deactivation of Au-pDA-rGO and Au-pDA over four consecutive catalytic cycle is shown (Fig. 4.9). The Au-pDA-rGO catalyst was shown to be catalytically stable with minimal deactivation over the four catalytic cycles indicating that the catalyst was highly stable under reaction conditions whereas Au-pDA underwent severe deactivation upon consecutive reaction cycles. Further the possibility of recovering NHPI by column chromatography after cycles of reaction make the catalytic system highly effective.

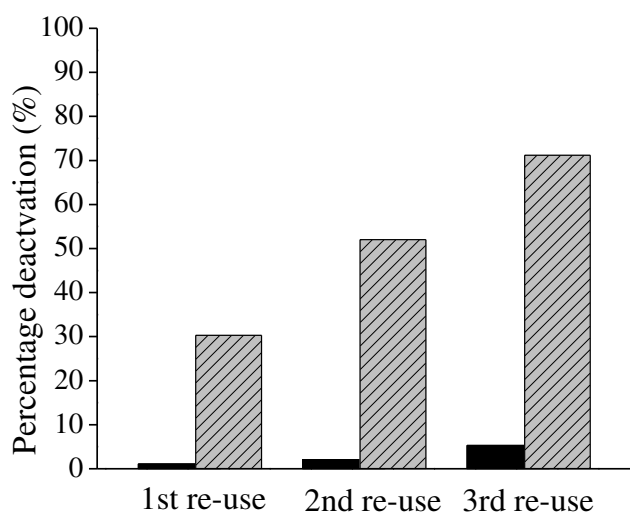


Figure 4.9. Percentage deactivation showing the initial activity of catalyst upon reuse; Au-pDA-rGO (black line) and Au-pDA (dashed line) over three diphenylmethane oxidation recycle test. Each reaction was performed under the standard conditions of diphenylmethane oxidation; substrate/metal molar ratio 1000; O₂ pressure 10 bar; stirring rate 1000 rpm; Reaction temperature 60 °C; NHPI 10 mol%; Reaction time 4 h

4.2.6 Recovery and reusability studies

The Au-pDA-rGO nanocomposite can be easily recovered by simple centrifugation followed by repeated washing and drying and then can be reused for several cycles without significant loss in activity or selectivity (Fig. 4.10).

Chapter 4

Without supplementing any fresh catalyst, the reused nanocatalyst afforded high conversion of the oxidation reaction with insignificant loss in activity. TEM studies of the nanocatalysts recovered after 3rd and 5th cycle of the catalytic

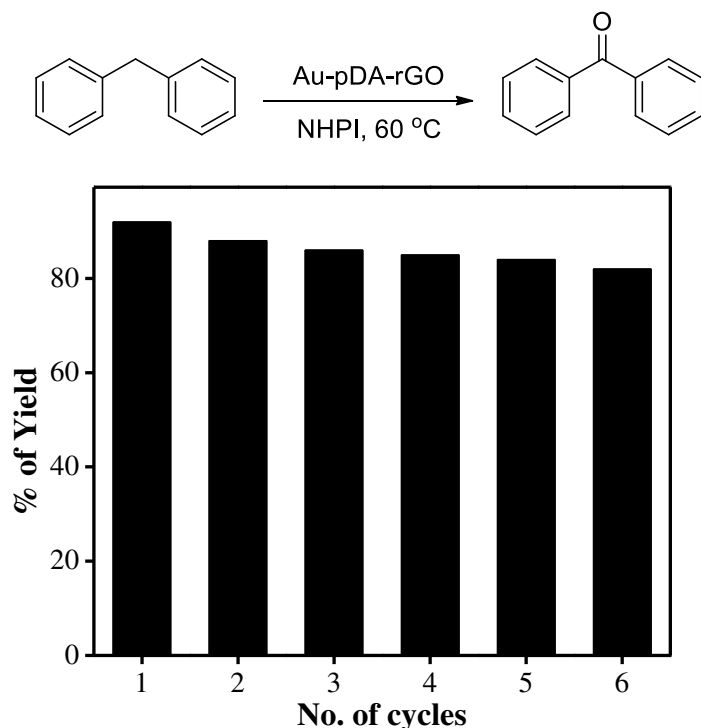


Figure 4.10. Reusability studies of Au-pDA-rGO nanocomposite on the oxidation of diphenylmethane

reaction showed minor changes in the average particle diameter as well as slight agglomeration of the Au NPs (Fig. 4.11). Wrinkling of the rGO was also observed on which Au NPs were embedded.

4.2.7 Leaching test

In order to have an insight into the nature of active species involved in the catalytic reaction, we performed leaching experiment to verify the heterogeneity of our catalytic system. No significant metal leaching was observed using Au-pDA-rGO nanocatalyst during the oxidation reaction of diphenylmethane under the optimized reaction conditions. The reaction was stopped after 4 h followed by removing the catalyst by centrifugation and then the reaction was continued with the supernatant. We observed no further reaction in absence of the catalyst which imply that no active metal species were leached during the course of the catalytic reaction (Fig. 4.12).^[25] To further determine any leaching metal particle during

the oxidation reaction, a fraction of the supernatant liquid was analysed by ICP-AES and the leaching metal was found to be 76 ppb (parts per billion) indicating that the leaching was negligible. In the regime of deactivation of the

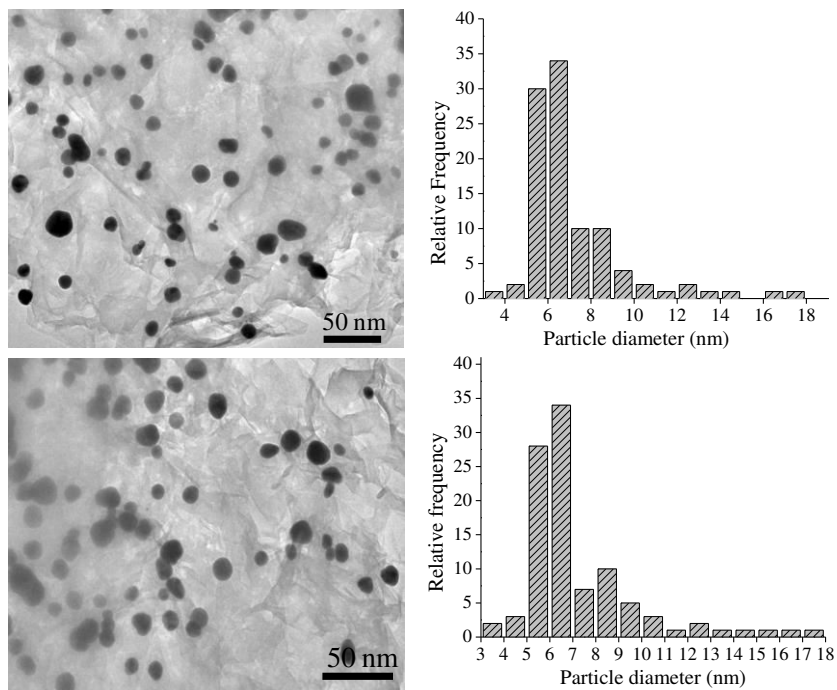


Figure 4.11. TEM image and corresponding particle size distribution of Au-pDA-rGO a) after 3rd cycle (scale bar 50 nm) and b) after 5th cycle (scale bar 50 nm)

nanocomposite upon reuse, possible adsorption of oxidised product on the surface of Au NPs blocking the active sites cannot be discounted.

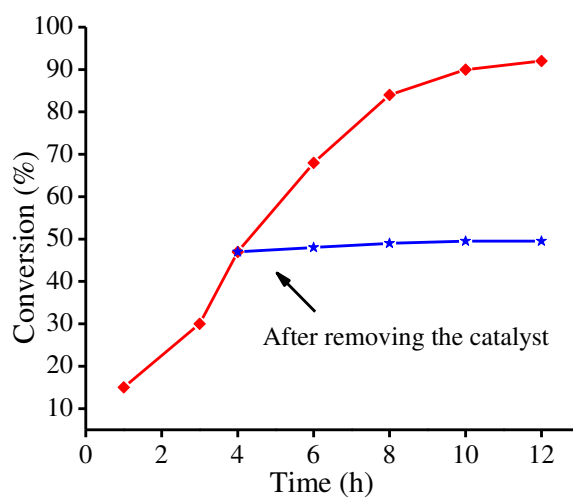


Figure 4.12. Formation of diphenylketone as a function of time under standard condition (red line) and removal of Au-pDA-rGO catalyst after 4 hour (blue line). Standard reaction conditions

of diphenylmethane oxidation (Substrate to metal molar ratio 1000; stirring rate 1000rpm, O_2 pressure 10 bar; 60 °C, NHPI 10 mol%) were employed in both the cases

4.2.8 Mechanistic Studies

The mechanistic insights into the activation of O_2 by Au NPs for oxidation reactions have been demonstrated by experimental as well as density functional calculations.^[81-86] O_2 activation takes place on the negatively charged Au NP surface through electron transfer from the anionic Au centre to the LUMO (π^*) of O_2 , generating a superoxide species ($\bullet O_2^-$).^[87] We believe that a similar mechanism takes place in the present catalytic reaction, where electron transfer from polydopamine anchored on rGO make Au NP surfaces more negatively charged, promoting the formation of superoxide species (Fig. 4.13).

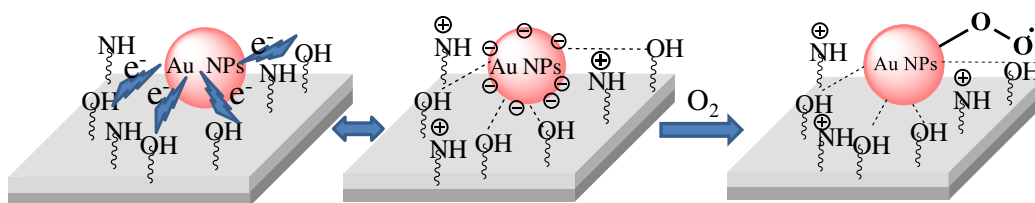


Figure 4.13. O_2 activation by pDA-rGO supported Au NPs forming the superoxo species

Although the superoxide is capable of reacting directly with the benzylic positions of the substrate, the conversion was very low in presence of O_2 as the single oxidant, possibly due to inertness of the C-H bond. It is well known that highly electrophilic radicals such as phthalimide N-oxyl radical (PINO) can easily abstract hydrogen atoms.^[61] When NHPI was added along with O_2 , the superoxide species abstracts the hydrogen atom from NHPI to form PINO radical. PINO then abstracts a hydrogen from the hydrocarbon initiating the oxygenation process. NHPI alone cannot afford C-H oxidation as the bond dissociation energy of the O-H bond in NHPI is quite high ($\sim 88 \text{ Kcalmol}^{-1}$).^[88] Thus, the initiation involves a two-step process in which oxygen activation first takes place on the surface of Au NPs resulting in superoxo-Au species and then subsequent hydrogen abstraction from NHPI resulting in the radical chain promoter PINO. Once PINO is formed the autoxidation can proceed further by the chain propagating steps (Fig. 4.14). In order to ascertain the role of polydopamine in the catalytic process, we performed the oxidation reaction under

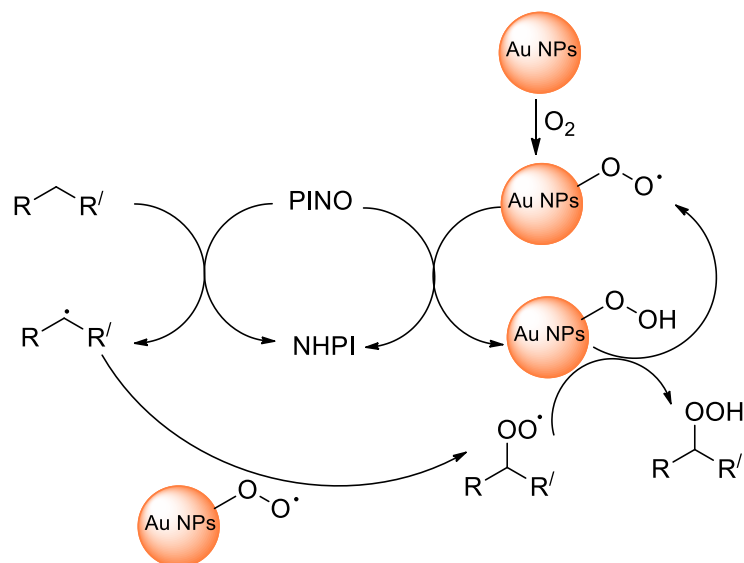


Figure 4.14. Plausible mechanistic cycle for oxidation of benzylic hydrocarbons by the Au-pDA-rGO/NHPI system

similar reaction conditions using another Au-rGO composite devoid of polydopamine (Au-rGO^b), which was formed by simultaneous reduction of HAuCl₄ and GO using NaBH₄ as reducing agent. We obtained substantially lesser conversion using the Au-rGO^b composite (Table 4.4, entry 1). Again, Au-pDA nanocomposite without rGO afforded much lesser conversion (Table 4.4, entry 20), showing that all the constituents in the nanocomposite, i.e. Au NPs, pDA and rGO induced cooperativity in enhancing the catalytic activity.

In contemplation of having a proper understanding of the electronic structure of the Au NPs in the composite, we performed X-ray photoelectron spectroscopy (XPS) measurements of Au-rGO^b, Au-pDA and Au-pDA-rGO nanocomposites. Fig. 4.15 shows XPS signature of the Au4f doublet (Au4f_{7/2} and Au4f_{5/2}) for the supported Au NP systems. For Au-rGO^b, Au peaks appeared at 83.9 eV and 87.5 eV, shifted to lower B.E.s compared to the corresponding peaks for metallic Au⁰ at 84.0 eV and 87.7 eV.^[89-94] In case of Au-pDA composites, the Au4f_{7/2} and Au4f_{5/2} peaks further shifted to lower B. E.s (83.6 and 87.3 eV respectively). Approximately similar binding energy for Au4f doublets were obtained for Au-pDA-rGO composite. The results suggest definite electron transfer from the support to Au NP, making the NP surface more negatively charged and favorable for oxygen activation. The higher catalytic activity of the

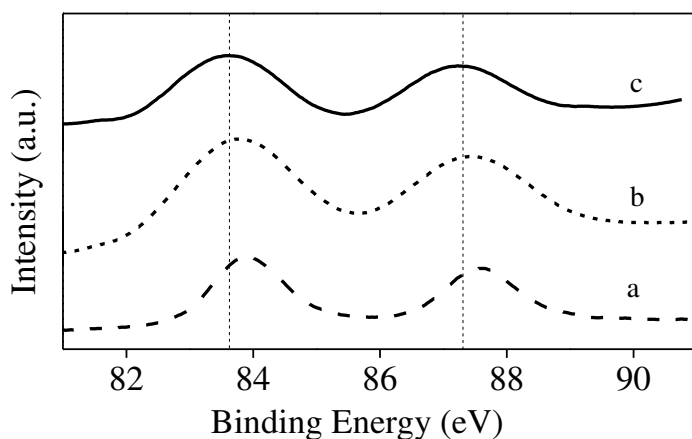


Figure 4.15. Comparative Au4f core-level XPS study of a) Au-rGO^b; b) Au-pDA and c) Au-pDA-rGO

Au-pDA-rGO composite compared to polymer coated Au NPs such as Au-PVP or Au-pDA could be due to the improved surface exposure of Au NPs embedded on 2-dimensional exfoliated rGO sheets. This ensures more accessibility of reactant molecules to the catalytically active site compared to 3-dimensional surface coating of Au NPs by polymer layers. Further high π -electron density on rGO surfaces might influence the approach of the reactant molecules to the active Au NP catalysts through hydrophobic interactions. Hence, a complex scenario involving different effects might contribute to the enhanced activity and selectivity of Au-pDA-rGO nanocomposites for C-H oxidation reactions.

Performing the oxidation reaction in dimethylsulphoxide (DMSO), a well-known free-radical scavenger, we found no intriguing oxidation proving the radical nature of the reaction pathway (Table 4.4, entry 15). Further evidences for free radicals were obtained by performing the reaction in presence of TEMPO (2,2,6,6-tetramethyl-1-piperidinyloxy) where no product formation was observed,^[95] rather the complex [Tempo-hydrocarbon] was detected by the mass spectrometry (Fig. 4.16). To further validate that the reaction mechanism involves free radicals, a control experiment was carried out with 2,2-diphenyl-1-picrylhydrazyl (DPPH). DPPH has strong absorption band centered at 520 nm for which it shows deep violet color in solution. DPPH is used as an indicator for the presence of free radicals as its violet color changes to pale yellow. In our case,

Chapter 4

an aliquot of the reaction in presence of Au-pDA-rGO was taken and decrement of absorbance of 2,2-diphenyl-1-picrylhydrazyl (DPPH) was measured. It was observed that the violet colour of DPPH completely disappeared suggesting the generation of free radicals during the reaction which formed an adduct with

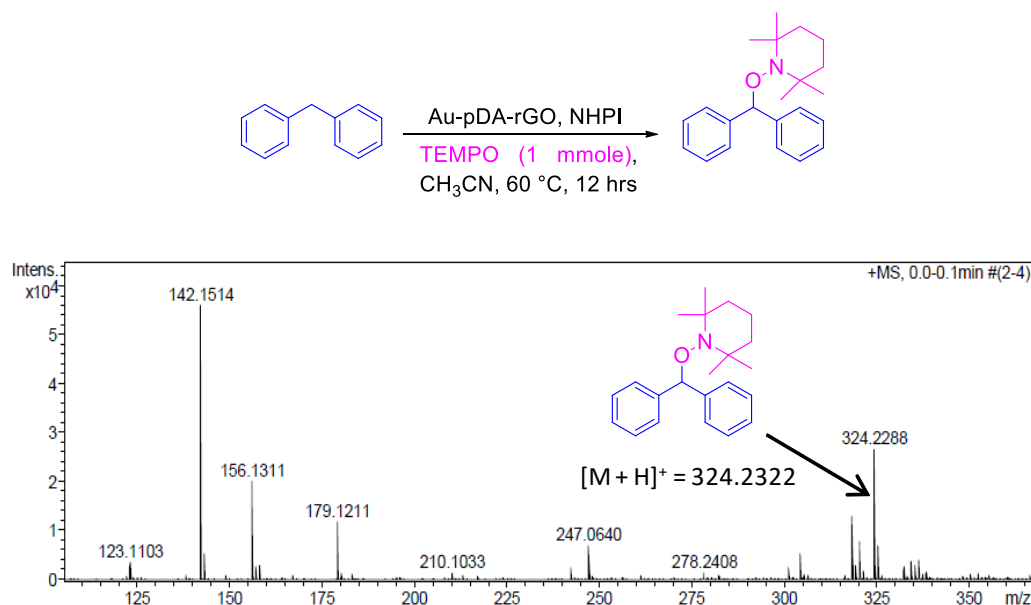


Figure 4.16. High resolution mass spectra of the Diphenylmethyl-TEMPO adduct

DPPH (Fig. 4.17).^[96-98] In a negative control experiment, no change in DPPH absorbance was observed when a small amount of reaction mixture without Au-pDA-rGO was added.

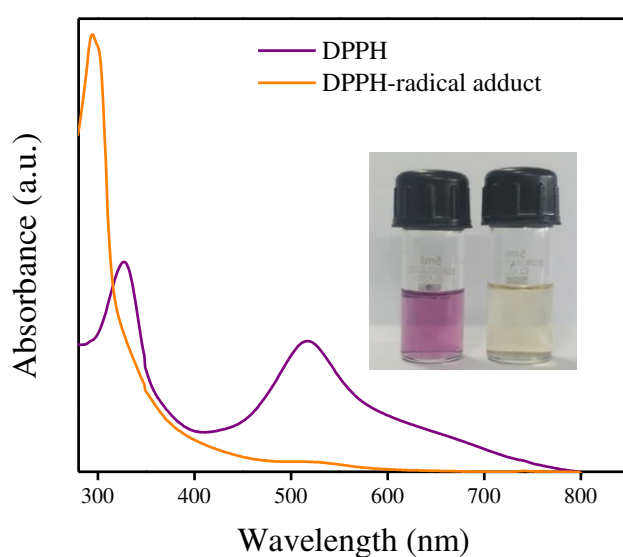


Figure 4.17. UV-Visible spectrum of DPPH and DPPH-radical adduct (inset digital images of the two solutions respectively)

Chapter 4

In order to confirm the involvement of free radicals in the mechanism, we employed a spin trapping electron paramagnetic resonance technique using 5,5-dimethyl-1-pyrroline N-oxide (DMPO) as the spin trapping probe to detect the superoxide ($\bullet\text{O}_2^-$) radical formed over Au surface during the reaction. We found that in presence of catalyst, EPR signal shows characteristic fingerprint of spin adducts due to superoxide radical ($\bullet\text{O}_2^-$). In a controlled study without any catalyst, spin signal due to oxygen radical showed very low intensity (Fig. 4.18).^[99-101]

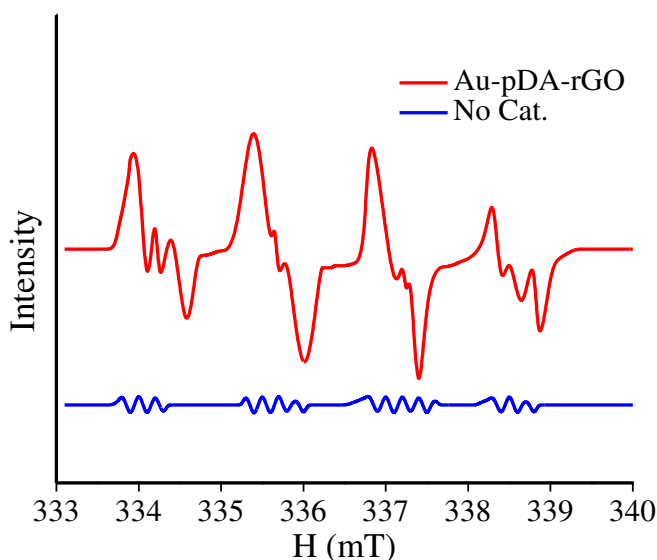


Figure 4.18. DMPO trapped EPR spectra with or without Au-pDA-rGO. DMPO binds with superoxide radicals ($\bullet\text{O}_2^-$) formed on Au NP surface

4.3 Conclusion

In conclusion, a smart nanocomposite comprising of Au nanoparticles anchored on polydopamine coated graphene oxide surface could function as a catalyst for the benzylic C-H oxidation with high efficiency and selectivity in presence of *N*-hydroxyphthalimide under mild reaction conditions. The monometallic Au nanocomposite along with NHPI could lead to the desired oxidation products under mild and neutral reaction conditions through a free radical mechanism involving diacylnitroxyl radicals such as PINO. Polydopamine and graphene surface not only played a crucial role in the generation and stabilization of active nanoparticle catalysts, but also was influential in activating the reaction by promoting generation of superoxo species on the nanoparticle surface. The high activity of the nanocomposites could be

attributed to the high access of reactants to the catalytically active nanoparticle surface decorated on the two-dimensional nanosheets. Furthermore, easy separation and excellent reusability without significant loss of activity over several iterations could propel Au-pDA-rGO composite as excellent heterogeneous catalyst for important organic transformations involving direct C-H functionalization.

4.4 Experimental Section

4.4.1 Materials

Graphite powder, dopamine hydrochloride, *N*-hydroxyphthalimide and hydrogen tetrachloroaurate (III) hydrate were purchased from Sigma Aldrich. NaNO₃, H₂O₂, KMnO₄ and concentrated H₂SO₄ were from Merck India. All other chemicals were purchased from Sigma Aldrich or Alfa Aesar and used without further purification. We used Millipore water (ultrapure level) throughout the experiments.

4.4.2 Instrumentation and characterization

The powder XRD measurements were carried out using a Bruker D8 Advance X-ray diffractometer with Cu K α source (wavelength of X-ray was 0.154 nm). TEM images were obtained using JEOL-JEM-2100 microscope operated at 200 kV. Atomic force microscopy was carried out using a AIST-NT instrument (model SMART SPM 10000, Tapping mode), the samples were prepared by drop casting a DMF suspension on mica. UV-visible measurements were performed using a Varian Cary 100 Bio Spectrophotometer. FTIR spectra were recorded in KBr pellet using a Bruker Tensor 27 instrument. Raman spectra were recorded on an Integrated Raman system from Jobin Yvon Horiba LABRAM-HR visible with a 632.8 nm He-Ne laser beam. XPS spectra were recorded using an ESCA instrument: VSW of UK make. EPR measurements were done using JEOL spectrometer (Model: JES-FA200). ¹H and ¹³C NMR spectra were recorded on a Bruker Advance (III) 400 MHz and 100 MHz spectrometer respectively. Data for ¹H NMR are reported as a chemical shift (δ ppm), multiplicity (s = singlet, d = doublet, t = triplet, m = multiplet), coupling constant *J* (Hz), integration, and assignment, data for ¹³C are reported as a

chemical shift. ICP-AES measurements were performed using a Spectro analytical simultaneous ICP spectrometer (model ARCOS).

4.4.3 Synthesis of graphene oxide

Graphite powder was converted into graphite oxide by the modified Hummer's procedure. In a typical synthesis, graphite powder (3.0 g) was added to 70 mL concentrated H_2SO_4 in presence of 1.5 g of NaNO_3 . The mixture was stirred for 1 h at ambient temperature. The container was cooled in an ice-bath and 9.0 g KMnO_4 was added slowly while stirring vigorously in a magnetic stirrer. The mixture was allowed to warm up naturally to ambient temperature. Double-distilled water (140 mL) was added slowly and carefully. This is a highly exothermic reaction and precautions are desirable. After the reaction temperature subsided to ambient conditions, another aliquot of 400 mL of distilled water was added to the mixture. Subsequently, 5.0 mL of 30% H_2O_2 was added and the color of the suspension changed from light yellow to brown, indicating oxidation of graphite to graphite oxide. The product was separated by centrifugation, washed with warm water and ethanol several times and vacuum dried. The graphite oxide was transferred into double-distilled water and sonicated for 3 h, during which graphite oxide was exfoliated to graphene oxide (GO).

4.4.4 Synthesis of Au-pDA-rGO nanocomposite

100 mg of graphene oxide was added to 320 mL of water and the suspension was dispersed by sonication for 1 h. The color of the mixture turns brown on sonication. 100 mg of dopamine hydrochloride was added to the mixture and stirred for another 2 h. Then, the mixture was refluxed vigorously at 100 °C for 12 h. The brown colored solution turns into black, signifying the formation of reduced graphene oxide. The mixture was centrifuged and washed with water for several times. Finally the precipitate was dispersed in water and dialyzed against water for 12 h to remove unreacted dopamine. Then the purified solution was transferred to a 500 mL round bottom flask and mixed with 1 mL of 0.023 M HAuCl_4 solution. The mixture was stirred at room temperature for 2 h. After reaction, the resulting Au NPs-deposited on polydopamine coated reduced

graphene oxide surfaces was separated from the suspension by centrifugation and washed with water for 3 times.

4.4.5 Synthesis of Au-rGO composite (Au-rGO^b)

Au-rGO composites were prepared by simultaneous reduction of HAuCl₄ and GO using NaBH₄. 0.077 g AuCl₃ was dissolved in 100 mL double-distilled water and 50 mg GO was added. The contents were sonicated for 15 min, and then 20 mL Na₂CO₃ solution (5 wt%) was added drop wise while stirring the contents. 0.6 g NaBH₄ was added to reduce both GO and Au³⁺ simultaneously while stirring the contents by a magnetic stirrer. The contents were kept at 80 °C and stirred for 1 h. The product of Au decorated RGO was separated by centrifugation, washed with double distilled water and ethanol, and dried at 60 °C for 12 h. Au loading in the composite was found to be 2.2wt% as measured by ICP-AES spectroscopy.

4.4.6 Synthesis of other Au catalysts

All the nanocatalysts Au-PVP, Au-CeO₂, Au-TiO₂ and Au-C were synthesized following reported procedures.^[102-103] Au loading in all these nanocatalysts were calculated by ICP-AES analysis.

4.4.6.1 Synthesis of Au-TiO₂ and Au-CeO₂

Au-TiO₂ and Au-CeO₂ were synthesized by a deposition-precipitation method. Typically, an aqueous solution of HAuCl₄.3H₂O (1.4 ml of 30 of mM solution) was adjusted to pH 10 with 1 M NaOH solution. Subsequently, 300 mg of the support (TiO₂ or CeO₂) was dispersed into the Au solution with rigorous stirring for 6h and the resulting powder was recovered by filtration, washed with water and dried at 40 °C under vacuum. Reduction of the Au ions was carried out by suspending the powder in 5 ml of ethanol followed by dropwise addition of 1 ml of 0.3 M NaBH₄ solution. The catalysts were then washed with water and ethanol and dried under vacuum. ICP-AES analysis of the catalysts showed 1.96 wt% and 1.82 wt% Au loading for Au-TiO₂ and Au-CeO₂ respectively.

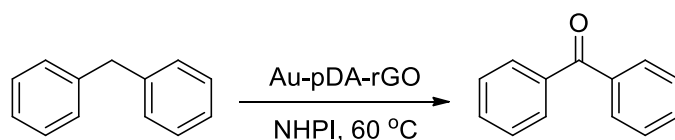
4.4.6.2 Synthesis of Au-C

Activated carbon(300 mg) was stirred in deionised water (300 ml) for 15 min. To it an aqueous solution of 1.4 ml of 30 mM HAuCl_4 was added slowly over a period of 30 min. The slurry was then refluxed for 30 min, cooled and reduced with formaldehyde over a period of 30 min. Again, the slurry was refluxed for 30 min. Then, the mixture was cooled and the catalyst was recovered by filtration and washed with water until the washings contained no chloride. The catalyst was dried for 16 h at 106 °C. (Au loading = 2.1 wt%).

4.4.6.3 Synthesis of Au-PVP

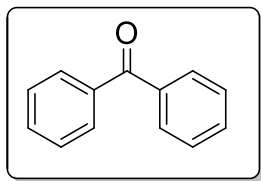
333 mg PVP was dissolved in 20 ml deionised water with stirring at room temperature. 1 ml 30 mM HAuCl_4 was added to the aqueous solution. Then a freshly prepared NaBH_4 solution (5ml, 100 mM) was added to get the PVP stabilized Au nanoparticles. The nanoparticles were then dialyzed for purification.

4.4.7 Aerobic sp^3 C-H bond oxidation

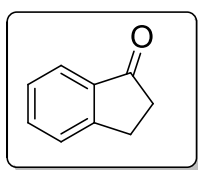


In a typical oxidation reaction, 1.0 mmol of substrate, 10mol% NHPI and Au-pDA-rGO nanocatalysts with 2 wt% Au loading were used in a round bottom flask containing 5ml acetonitrile. The reaction was performed at 60 °C in an oil bath under magnetic stirring in presence of oxygen atmosphere. The progress of the reaction was monitored by TLC. After completion of the reaction, the resulting mixture was extracted with ethyl acetate (3x 20 ml) and successively washed with water (1x 15 ml). The organic solution was dried over anhydrous sodium sulphate and evaporation of the solvent on a rotary evaporator gave a residue that was purified on silica gel column chromatography (100-200 mesh) using hexane and ethyl acetate as eluent.

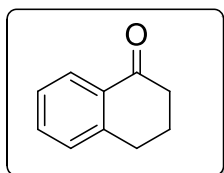
4.4.8 Characterization data



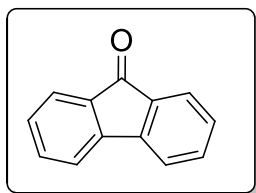
Benzophenone:¹⁰⁵ White solid; m.p. 47-50 °C; ¹H NMR (400 MHz, CDCl₃) δ 7.82(m, 4H), 7.59(m,2H), 7.49(m, 4H); ¹³C NMR (100 MHz, CDCl₃) δ 196.7, 137.6, 132.4, 130.0, 128.2.



Indan-1-one:⁶² Light Yellow Oil; m.p. 37-41 °C; ¹H NMR (400 MHz, CDCl₃) δ 7.77(d, *J* = 8 Hz, 1H), 7.59 (t, *J* = 2 Hz, 1H), 7.48 (d, *J* = 8 Hz, 1H), 7.37 (t, *J* = 8 Hz, 1H), 3.15(t, *J* = 6 Hz, 2H), 2.70 (t, *J* = 6 Hz, 2H); ¹³C NMR (100 MHz, CDCl₃) δ 207.14, 155.19, 137.12, 134.63, 127.32,126.73, 123.77, 36.26, 25.84.

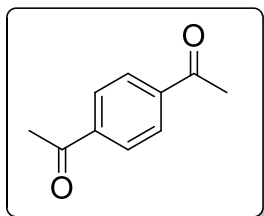


3,4-Dihydro-2H-naphthalen-1-one:⁶² Light yellow oil; ¹H NMR (400 MHz, CDCl₃) δ 8.03(dd, *J* = 7.9, 1.2 Hz, 1H), 7.46 (dt, *J* = 7.53, 1.49 Hz, 1H), 7.31-7.23 (m, 2H), 2.96 (t, *J* = 6 Hz, 2H), 2.65 (t, *J* = 6 Hz, 2H), 2.13 (quintet, *J* = 6 Hz, 2H); ¹³C NMR (100 MHz, CDCl₃) δ 198.4, 144.5, 133.4, 132.6, 128.7, 127.1, 126.6, 39.2, 29.7, 23.3.

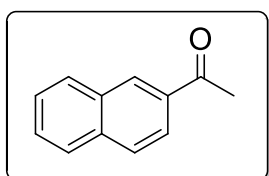


Chapter 4

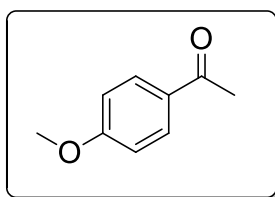
9H- fluoren-9-one:¹⁰⁴ white solid; m.p. 82-84 °C; ¹H NMR (400 MHz, CDCl₃) δ 7.66 (d, *J* = 7 Hz, 1H), 7.52 (d, *J* = 7 Hz, 1H), 7.47 (dt, *J* = 1.24 Hz, 1H) 7.29 (dt, *J* = 7, 1.5 Hz, 1H); ¹³C NMR (100 MHz, CDCl₃) δ 193.9, 144.4, 134.7, 134.1, 129.1, 124.3, 120.3.



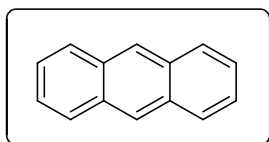
1,1'-(1,4-phenylene)diethanone:¹⁰⁵ White solid; m.p. 111-114 °C; ¹H NMR (400 MHz, CDCl₃) δ 8.03(s, 4H), 2.65 (s, 6H), ¹³C NMR (100 MHz, CDCl₃) δ 197.5, 140.1, 128.5, 26.9.



1-(naphthalene-2-yl)ethanone:¹⁰⁴ Yellow solid; m.p. 50-54 °C; ¹H NMR (400 MHz, CDCl₃) δ 8.47(s, 1H), 8.03 (dd, *J* = 8.6, 1.8 Hz, 1H), 7.97(d, *J* = 8 Hz, 1H), 7.87-7.91(m, 2H), 7.54-7.63(m, 2H); ¹³C NMR (100 MHz, CDCl₃) δ 198.1, 135.6, 134.5, 132.5, 130.2, 129.5, 128.5, 128.4, 126.8, 123.9, 26.7.

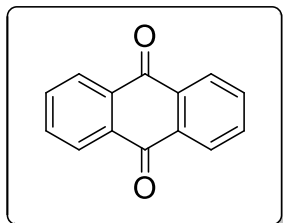


1-(4-methoxyphenyl)ethanone:¹⁰⁴ Pale yellow solid; m.p. 38-40 °C; ¹H NMR (400 MHz, CDCl₃) δ 7.94(d, *J* = 8 Hz, 2H), 6.93(d, *J* = 8 Hz, 2H), 3.87(s, 3H), 2.55(s, 3H); ¹³C NMR (100 MHz, CDCl₃) δ 196.8, 163.5, 130.6, 130.3, 113.7, 55.4, 26.3.

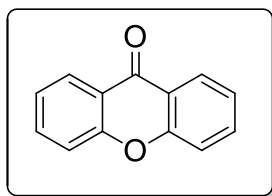


Chapter 4

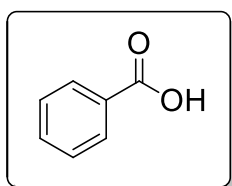
Anthracene:¹⁰⁴ White solid; m.p. 212-216 °C; ¹H NMR (400 MHz, CDCl₃) δ 8.44(s, 2H), 8.02(dd, *J* = 6.5, 3.5 Hz, 4H), 7.46(dd, *J* = 6.5, 3.5 Hz, 4H); ¹³C NMR (100 MHz, CDCl₃) δ 131.7, 128.1, 126.2, 125.3.



Anthracene-9,10-dione:¹⁰⁴ Yellow solid; m.p. 285-289 °C; ¹H NMR(400 MHz, CDCl₃) δ 8.32(dd, *J* = 5.8, 3.5 Hz, 4H), 7.8(dd, *J* = 5.8, 3.5 Hz, 4H); ¹³C NMR (100 MHz, CDCl₃) δ 183.1, 134.1, 133.5, 127.2.



9H-xanthen-9-one:¹⁰⁴ White solid; m.p. 172-176 °C; ¹H NMR (400 MHz, CDCl₃) δ 8.35(dd, *J* = 8, 1.6 Hz, 2H), 7.73(dt, *J* = 8.5, 1.8 Hz, 2H), 7.5(d, *J* = 8.5 Hz, 2H), 7.38(t, *J* = 8 Hz, 2H); ¹³C NMR (100 MHz, CDCl₃) δ 177.2, 156.2, 134.8, 126.7, 123.9, 121.9, 118.0.



Benzoic acid: White solid; m.p. 120-123 °C; ¹H NMR (400 MHz, CDCl₃) δ 8.13(m, 2H), 7.63(m, 1H), 7.49(m, 2H); ¹³C NMR(100 MHz, CDCl₃) δ 172.3, 134.1, 130.5, 129.6, 128.8.

4.5 References

1. Goldberg K. I., Goldman A. S. (2004), Eds. Activation and Functionalization of C-H bonds, ACS Symposium Series 885, American Chemical Society, Washington DC.
2. Bäckvall J. –E. (2004), Ed. Modern Oxidation Methods, WILEY-VCH Verlag GmbH & Co. KGaA, Weinheim.
3. Shi Z., Zhang C., Tang C., Jiao N. (2012), Recent advances in transition-metal catalyzed reactions using molecular oxygen as the oxidant, *Chem. Soc. Rev.*, 41, 3381-3430 (DOI: 10.1039/c2cs15224j)
4. Newhouse T., Baran, P. S. (2011), If C-H bonds could talk: Selective C-H bond oxidation, *Angew. Chem. Int. Ed.*, 50, 3362-3374 (DOI: 10.1002/anie.201006368)
5. Godula K., Sames D. (2006), C–H bond functionalization in complex organic synthesis, *Science*, 312, 67-72 (DOI: 10.1126/science.1114731)
6. Davies H. M. L., Manning J. R. (2008), Catalytic C–H functionalization by metal carbenoid and nitrenoid insertion, *Nature*, 451, 417-424 (DOI: 10.1038/nature06485)
7. Punniyamurthy T., Velusamy S., Iqbal, J. (2005), Recent advances in transition metal catalyzed oxidation of organic substrates with molecular oxygen, *Chem. Rev.*, 105, 2329-2363 (DOI: 10.1021/cr050523v)
8. Genovino J., Lutz S., Sames D., Toure B. B. (2013), Complementation of biotransformations with chemical C–H oxidation: Copper-catalyzed oxidation of tertiary amines in complex pharmaceuticals, *J. Am. Chem. Soc.*, 135, 12346-12352 (DOI: 10.1021/ja405471h)
9. Labinger J. A., Bercaw J. E. (2002), Understanding and exploiting C–H bond activation, *Nature*, 417, 507-514 (DOI: 10.1038/417507a)
10. Lyons T. W., Sanford M. S. (2010), Palladium-catalyzed ligand-directed C-H functionalization reactions, *Chem. Rev.*, 110, 1147-1169 (DOI: 10.1021/cr900184e)
11. Conejero S., Paneque M., Poveda M. L., Santos L. L., Carmona E. (2010), C-H bond activation reactions of ethers that generate iridium carbenes, *Acc. Chem. Res.*, 43, 572-580 (DOI: 10.1021/ar9002625)

Chapter 4

12. Colby D. A., Bergman R. G., Ellman J. A. (2010), Rhodium-catalyzed C-C bond formation via heteroatom-directed C-H bond activation *Chem. Rev.*, 110, 624-655 (DOI: 10.1021/cr900005n)
13. Yang S., Li Z., Jian X., He C. (2009), Platinum (II)-catalyzed intramolecular cyclization of o-substituted aryl alkynes through sp³ C-H activation, *Angew. Chem. Int. Ed.*, 48, 3999-4001 (DOI: 10.1002/anie.200900368)
14. Sun C. -L., Li B. -J., Shi Z. -J. (2011), Direct C-H transformation via iron catalysis, *Chem. Rev.*, 111, 1293-1314 (DOI: 10.1021/cr100198w)
15. Peng H., Lin A., Zhang Y., Jiang H., Zhou J., Cheng Y., Zhu C., Hu H. (2012), Oxidation and amination of benzylic sp³ C-H bond catalyzed by rhenium(V) complexes, *ACS Catal.*, 2, 163-167 (DOI: 10.1021/cs2003577)
16. Hashmi A. S. K., Hutchings G. J. (2006), Gold catalysis, *Angew. Chem. Int. Ed.*, 45, 7896-7936 (DOI: 10.1002/anie.200602454)
17. Corma A., Garcia H. (2008), Supported gold nanoparticles as catalysts for organic reactions, *Chem. Soc. Rev.*, 37, 2096-2126 (DOI: 10.1039/b707314n)
18. Astruc D. (2008), Ed. *Nanoparticles and Catalysis*, WILEY-VCH Verlag GmbH & Co. KGaA, Weinheim.
19. Astruc D., Lu F., Aranzaes J. R. (2005), Nanoparticles as recyclable catalysts: The frontier between homogeneous and heterogeneous catalysis, *Angew. Chem. Int. Ed.* 44, 7852-7872 (DOI: 10.1002/anie.200500766)
20. Ishida T., Haruta M. (2007), Gold catalysts: Towards sustainable chemistry, *Angew. Chem. Int. Ed.*, 46, 7154-7156 (DOI: 10.1002/anie.200701622)
21. Prati L., Villa A. (2014), Gold colloids: From quasi-homogeneous to heterogeneous catalytic systems, *Acc. Chem. Res.*, 47, 855-863 (DOI: 10.1021/ar400170j)
22. Porta F., Prati L. (2004), Selective oxidation of glycerol to sodium glycerate with gold-on-carbon catalyst: an insight into reaction selectivity, *J. Catal.*, 224, 397-403 (DOI: 10.1016/j.jcat.2004.03.009)

Chapter 4

23. Biella S., Prati L., Rossi M. (2002), Selective oxidation of D-glucose on gold catalyst, *J. Catal.*, 206, 242-247 (DOI: 10.1006/jcat.2001.3497)
24. Layek K., Maheswaran H., Kantam M. L. (2013), Ullmann coupling of aryl iodides catalyzed by gold nanoparticles stabilized on nanocrystalline magnesium oxide, *Catal. Sci. Technol.*, 3, 1147-1150 (DOI: 10.1039/C3CY20826E)
25. Kesavan L., Tiruvalam R., Ab Rahim M. H., bin Saiman M. I., Enache D. I., Jenkins R. L., Dimitratos N., Lopez-Sanchez J. A., Taylor S. H., Knight D. W., Kiely C. J., Hutchings G. J. (2011), Solvent-free oxidation of primary carbon-hydrogen bonds in toluene using Au-Pd alloy nanoparticles, *Science*, 331, 195-199 (DOI: 10.1126/science.1198458)
26. Donoeva B. G., Ovoshchnikov D. S., Golovko V. B. (2013), Establishing a Au nanoparticle size effect in the oxidation of cyclohexene using gradually changing Au catalysts, *ACS Catal.*, 3, 2986-2991 (DOI: 10.1021/cs400701j)
27. Liu Y., Tsunoyama H., Akita T., Xie S., Tsukuda T. (2011), Aerobic oxidation of cyclohexane catalyzed by size-controlled Au clusters on hydroxyapatite: Size effect in the sub-2 nm regime, *ACS Catal.*, 1, 2-6 (DOI: 10.1021/cs100043j)
28. Bin Saiman M. I., Brett G. L., Tiruvalam R., Forde M. M., Sharples K., Thetford A., Jenkins R. L., Dimitratos N., Lopez-Sanchez J. A., Murphy D. M., Bethell D., Willock D. J., Taylor S. H., Knight D. W., Kiely C. J., Hutchings G. J. (2012), Involvement of surface-bound radicals in the oxidation of toluene using supported Au-Pd nanoparticles, *Angew. Chem. Int. Ed.*, 51, 5981-5985 (DOI: 10.1002/anie.201201059)
29. Chen X., Wu G., Chen J., Chen X., Xie Z., Wang X. (2011), Synthesis of "clean" and well-dispersive Pd nanoparticles with excellent electrocatalytic property on graphene oxide, *J. Am. Chem. Soc.*, 133, 3693-3695 (DOI: 10.1021/ja110313d)
30. Muszynski R., Seger B., Kamat P. V. (2008), Decorating graphene sheets with gold nanoparticles, *J. Phys. Chem. C.*, 112, 5263-5266 (DOI: 10.1021/jp800977b)

31. Kundu P., Nethravathi C., Deshpande P. A., Rajamathi M., Madras G., Ravishankar N. (2011), Ultrafast microwave-assisted route to surfactant-free ultrafine Pt nanoparticles on graphene: Synergistic co-reduction mechanism and high catalytic activity, *Chem. Mater.*, 23, 2772-2780 (DOI: 10.1021/cm200329a)
32. Liu S., Tian J., Wang L., Li H., Zhang Y., Sun X. (2010), Stable aqueous dispersion of graphene nanosheets: Noncovalent functionalization by a polymeric reducing agent and their subsequent decoration with Ag nanoparticles for enzymeless hydrogen peroxide detection, *Macromolecules*, 43, 10078-10083 (DOI: 10.1021/ma102230m)
33. Chen C., Cai W., Long M., Zhou B., Wu Y., Wu D., Feng Y. (2010), Synthesis of visible-light responsive graphene oxide/TiO₂ composites with p/n heterojunction, *ACS Nano*, 4, 6425-6432 (DOI: 10.1021/nn102130m)
34. Zhang J., Liu X., Wang L., Yang T., Gou X., Wu S., Zhang S., Wang S. (2011), A simple one-pot strategy for the synthesis of ternary reduced graphite oxide/SnO₂/Au hybrid nanomaterials, *Carbon*, 49, 3538-3543 (DOI: 10.1016/j.carbon.2011.04.053)
35. Chen S., Zhu J., Wu X., Han Q., Wang X. (2010), Graphene oxide-MnO₂ nanocomposites for supercapacitors, *ACS Nano*, 4, 2822-2830 (DOI: 10.1021/nn901311t)
36. Xue T., Jiang S., Qu Y., Su Q., Cheng R., Dubin S., Chiu C.-Y., Kaner R., Huang Y., Duan X. (2012), Graphene-supported hemin as a highly active biomimetic oxidation catalyst, *Angew Chem. Int. Ed.*, 51, 3822-3825 (DOI: 10.1002/anie.201108400)
37. Dreyer D. R., Jia H. -P., Bielawski C. W. (2010), Graphene oxide: A convenient carbocatalyst for facilitating oxidation and hydration reactions, *Angew Chem. Int. Ed.*, 49, 6813-6816 (DOI: 10.1002/anie.201002160)
38. Verma S., Mungse H. P., Kumar N., Choudhary S., Jain S. L., Sain B., Khatri O. P. (2011), Graphene oxide: An efficient and reusable carbocatalyst for aza-Michael addition of amines to activated alkenes, *Chem. Commun.*, 12673-12675 (DOI: 10.1039/C1CC15230K)

Chapter 4

39. Dreyer D. R., Jarvis K. A., Ferreira P. J., Bielawski C. W. (2012), Graphite oxide as a carbocatalyst for the preparation of fullerene-reinforced polyester and polyamide nanocomposites, *Polym. Chem.*, 3, 757-766 (DOI: 10.1039/C2PY00545J)
40. Kumar A. V., Rao K. R. (2011), Recyclable graphite oxide catalyzed Friedel–Crafts addition of indoles to α , β -unsaturated ketones, *Tetrahedron Lett.*, 52, 5188-5199 (DOI: 10.1016/j.tetlet.2011.08.002)
41. Kamat P. V. (2011), Graphene-based nanoassemblies for energy conversion, *J. Phys. Chem. Lett.*, 2, 242–251 (DOI: 10.1021/jz101639v)
42. Wang J., Trindade F. J., de Aquino C. B., Pieretti J. C., Domingues S. H., Ando R. A., Camargo P. H. C. (2015), Probing the catalytic activity of reduced graphene oxide decorated with Au nanoparticles triggered by visible light, *Chem. Eur. J.*, 21, 9889–9894 (DOI: 10.1002/chem.201500677)
43. Saha B., Koshino N., Espenson J. H. (2004), N-hydroxyphthalimides and metal cocatalysts for the autoxidation of p-xylene to terephthalic acid, *J. Phys. Chem. A*, 108, 425-431 (DOI: 10.1021/jp035870s)
44. Baucherel X., Gonsalvi L., Arends I. W. C. E., Ellwood S., Sheldon R. A. (2004), Aerobic oxidation of cycloalkanes, alcohols and ethylbenzene catalyzed by the novel carbon radical chain promoter NHS (N-hydroxysaccharin), *Adv. Synth. Catal.*, 346, 286-296 (DOI: 10.1002/adsc.200303197)
45. Minisci F., Punta C., Recupero F., Fontana F., Pedulli G. F. (2002), Aerobic oxidation of N-alkylamides catalyzed by N-hydroxyphthalimide under mild conditions. Polar and enthalpic Effects, *J. Org. Chem.*, 67, 2671-2676 (DOI: 10.1021/jo016398e)
46. Koshino N., Cai Y., Espenson J. H. (2003), Kinetic study of the phthalimide N-Oxyl (PINO) radical in acetic acid. Hydrogen abstraction from C-H bonds and evaluation of O-H bond dissociation energy of N-hydroxyphthalimide, *J. Phys. Chem. A*, 107, 4262-4267 (DOI: 10.1021/jp0276193)
47. Arnaud R., Milet A., Adamo C., Einhorn C., Einhorn J. (2002), Hydrogen abstraction from ethylbenzene by imide-N-oxyl radicals with and without

Chapter 4

- O₂: a DFT theoretical study, *J. Chem. Soc. Perkin Trans. 2*, 1967-1972 (DOI: 10.1039/b205485j)
48. de Vondervoort L. S. V., Bouttemy S., Heu F., Weissenböck K., Alsters P. L. (2003), Low temperature, high Conversion, liquid-phase benzylic oxidation with dioxygen by metal/NHPI-catalyzed co-oxidation with benzaldehyde, *Eur. J. Org. Chem.*, 578-586 (DOI: 10.1002/ejoc.200390096)
49. Ishii Y., Iwahama T., Sakaguchi S., Nakayama K., Nishiyama Y. (1996), Alkane oxidation with molecular oxygen using a new efficient catalytic system: N-hydroxyphthalimide (NHPI) combined with Co(acac)_n (n = 2 or 3), *J. Org. Chem.*, 61, 4520-4526 (DOI: 10.1021/jo951970l)
50. Iwahama T., Syojyo K., Sakaguchi S., Ishii Y. (1998), Direct conversion of cyclohexane into adipic acid with molecular oxygen catalyzed by N-hydroxyphthalimide combined with Mn(acac)₂ and Co(OAc)₂, *Org. Proc. Res. Dev.*, 2, 255-260 (DOI: 10.1021/op980016y)
51. Sawatari N., Yokota T., Sakaguchi S., Ishii Y. (2001), Alkane oxidation with air catalyzed by lipophilic N-hydroxyphthalimides without any solvent, *J. Org. Chem.*, 66, 7889-7891 (DOI: 10.1021/jo0158276)
52. Ishii Y., Sakaguchi S., Iwahama T. (2001), Innovation of hydrocarbon oxidation with molecular oxygen and related reactions, *Adv. Synth. Cat.*, 343, 393-427 (DOI: 10.1002/1615-4169)
53. Yoshino Y., Hayashi Y., Iwahama T., Sakaguchi S., Ishii Y. (1997), Catalytic oxidation of alkylbenzenes with molecular oxygen under normal pressure and temperature by N-hydroxyphthalimide combined with Co(OAc)₂, *J. Org. Chem.*, 62, 6810-6813 (DOI: 10.1021/jo9708147)
54. Amorati R., Lucarini M., Mugnaini V., Pedulli G. F. (2003), Hydroxylamines as oxidation catalysts: Thermochemical and kinetic studies, *J. Org. Chem.*, 68, 1747-1754 (DOI: 10.1021/jo026660z)
55. Arends I. W. C. E., Sasidharan M., Kühnle A., Duda M., Jost C., Sheldon R. A. (2002), Selective catalytic oxidation of cyclohexylbenzene to cyclohexylbenzene-1-hydroperoxide: a coproduct-free route to phenol, *Tetrahedron*, 58, 9055-9061 (DOI: 10.1016/S0040-4020(02)01131-6)

Chapter 4

56. Aoki Y., Sakaguchi S., Ishii Y. (2004), Synthesis of naphthalenediols by aerobic oxidation of diisopropyl naphthalenes catalyzed by N-hydroxyphthalimide (NHPI)/ α , α' -azobisisobutyronitrile (AIBN), *Adv. Synth. Catal.*, 346, 199-202 (DOI: 10.1002/adsc.200303168)
57. Einhorn C., Einhorn J., Marcadal C., Pierre J. -L. (1997), Oxidation of organic substrates by molecular oxygen mediated by N-hydroxyphthalimide (NHPI) and acetaldehyde, *Chem. Commun.*, 447-448 (DOI: 10.1039/A607463D)
58. Tsujimoto S., Sakaguchi S., Ishii Y. (2003), Addition of aldehydes and their equivalents to electron-deficient alkenes using N-hydroxyphthalimide (NHPI) as a polarity-reversal catalyst, *Tetrahedron Lett.*, 44, 5601-5604 (DOI: 10.1016/S0040-4039(03)01375-3)
59. Eikawa M., Sakaguchi S., Ishii Y. (1999), A new approach for oxygenation using nitric oxide under the influence of N-hydroxyphthalimide, *J. Org. Chem.*, 64, 4676-4679 (DOI: 10.1021/jo982406o)
60. Nishiwaki Y., Sakaguchi S., Ishii Y. (2002), An efficient nitration of light alkanes and the alkyl side-chain of aromatic compounds with nitrogen dioxide and nitric acid catalyzed by N-hydroxyphthalimide, *J. Org. Chem.*, 67, 5663-5668 (DOI: 10.1021/jo025632d)
61. Yang G., Ma Y., Xu J. (2004), Biomimetic catalytic system driven by electron transfer for selective oxygenation of hydrocarbon, *J. Am. Chem. Soc.*, 126, 10542-10543 (DOI: 10.1021/ja047297b)
62. Yang G., Zhang Q., Miao H., Tong X., Xu J. (2005), Selective organocatalytic oxygenation of hydrocarbons by dioxygen using anthraquinones and N-hydroxyphthalimide, *Org. Lett.*, 7, 263-266 (DOI: 10.1021/ol047749p)
63. Jeon E. K., Seo E., Lee E., Lee W., Um M. -K., Kim B. -S. (2013), Mussel-inspired green synthesis of silver nanoparticles on graphene oxide nanosheets for enhanced catalytic applications, *Chem. Commun.*, 49, 3392-3394 (DOI: 10.1039/c3cc00115f)
64. Guo L., Liu Q., Li G., Shi J., Liu J., Wang T., Jiang G. (2012), A mussel-inspired polydopamine coating as a versatile platform for the in situ

- synthesis of graphene-based nanocomposites, *Nanoscale*, 4, 5864-5867 (DOI: 10.1039/c2nr31547e)
65. Zheng W., Fan H., Wang L., Jin Z. (2015), Oxidative self-polymerization of dopamine in an acidic environment, *Langmuir*, 31, 11671-11677 (DOI: 10.1021/acs.langmuir.5b02757)
66. Li D., Müller M. B., Gilje S., Kaner R. B., Wallace G. G. (2008), Processable aqueous dispersions of graphene nanosheets, *Nat. Nanotechnol.*, 3, 101-105 (DOI: 10.1038/nnano.2007.451)
67. Li J., Liu C. -Y., Liu Y. (2012), Au/graphene hydrogel: synthesis, characterization and its use for catalytic reduction of 4-nitrophenol, *J. Mater. Chem.*, 22, 8426-8430 (DOI: 10.1039/c2jm16386a)
68. Yu H., Xu P., Lee D. -W., Li X. (2013), Porous-layered stack of functionalized AuNP-rGO (gold nanoparticles-reduced graphene oxide) nanosheets as a sensing material for the micro-gravimetric detection of chemical vapor, *J. Mater. Chem. A*, 1, 4444-4450 (DOI: 10.1039/c3ta01401k)
69. Mohanty N., Nagaraja A., Armesto J., Berry V. (2010), High-throughput, ultrafast synthesis of solution-dispersed graphene via a facile hydride chemistry, *Small*, 6, 226-231 (DOI: 10.1002/sml.200901505)
70. Zhang H., Hines D., Akins D. L. (2014), Synthesis of a nanocomposite composed of reduced graphene oxide and gold nanoparticles, *Dalton Trans.*, 43, 2670-2675 (DOI: 10.1039/C3DT52573B)
71. Xu L. Q., Yang W. J., Neoh K. -G., Kang E. -T., Fu G. D. (2010), Dopamine-induced reduction and functionalization of graphene oxide nanosheets, *Macromolecules*, 43, 8336-8339 (DOI: 10.1021/ma101526k)
72. Hughes M. D., Xu Y. -J., Jenkins P., McMorn P., Landon P., Enache D. I., Carley A. F., Attard G. A., Hutchings G. J., King F., Stitt E. H., Johnston P., Griffin K., Kiely C. J. (2005), Tunable gold catalysts for selective hydrocarbon oxidation under mild conditions, *Nature*, 437, 1132-1135 (DOI: 10.1038/nature04190)
73. Long J., Liu H., Wu S., Liao S., Li Y. (2013), Selective oxidation of saturated hydrocarbons using Au-Pd alloy nanoparticles supported on

Chapter 4

- metal–organic frameworks, *ACS Catal.*, 3, 647-654 (DOI: 10.1021/cs300754k)
74. Goergen S., Yin C., Yang M., Lee B., Lee S., Wang C., Wu P., Boucher M. B., Kwon G., Seifert S., Winans R. E., Vajda S., Stephanopoulos M. F. (2013), Structure sensitivity of oxidative dehydrogenation of cyclohexane over FeOx and Au/Fe₃O₄ nanocrystals, *ACS Catal.*, 3, 529-539 (DOI: 10.1021/cs3007582)
75. Hattori H., Ide Y., Ogo S., Inumaru K., Sadakane M., Sano T. (2012), Efficient and selective photocatalytic cyclohexane oxidation on a layered titanate modified with iron oxide under sunlight and CO₂ atmosphere, *ACS Catal.*, 2, 1910-1915 (DOI: 10.1021/cs300339f)
76. Sa J., Ace M., Delgado J. J., Goguet A., Hardacre C., Morgan K. (2011), Activation of alkanes by gold-modified lanthanum oxide, *ChemCatChem.*, 3, 394–398 (DOI: 10.1002/cctc.201000285)
77. Dimitratos N., Lopez-Sanchez J. A., Meenakshisundaram S., Anthonykutti J. M., Brett G., Carley A. F., Taylor S. H., Knight D. W., Hutchings G. J. (2009), Selective formation of lactate by oxidation of 1,2-propanediol using gold palladium alloy supported nanocrystals, *Green Chem.*, 11, 1209-1216 (DOI: 10.1039/b823285g)
78. Pina C. D., Falletta E., Rossi M. (2012), Update on selective oxidation using gold, *Chem. Soc. Rev.*, 41, 350–369 (DOI: 10.1039/c1cs15089h)
79. Monjezi B. H., Yazdani M. E., Mokfi M., Ghiaci M. (2014), Liquid phase oxidation of diphenylmethane to benzophenone with molecular oxygen over nano-sized Co–Mn catalyst supported on calcined Cow bone, *J. Mol. Catal. A: Chem.*, 383–384, 58–63 (DOI: 10.1016/j.molcata.2013.11.019)
80. Wang J., Kondrat S. A., Wang Y., Brett G. L., Giles C., Bartley J. K., Lu L., Liu Q., Kiely C. J., Hutchings G. J. (2015), Au–Pd nanoparticles dispersed on composite titania/graphene oxide-supports as a highly active oxidation catalyst, *ACS Catal.*, 5, 3575-3587 (DOI: 10.1021/acscatal.5b00480)
81. Tsunoyama H., Ichikuni N., Sakurai H., Tsukuda T. (2009), Effect of electronic structures of Au clusters stabilized by poly(N-vinyl-2-

- pyrrolidone) on aerobic oxidation catalysis, *J. Am. Chem. Soc.*, 131, 7086–7093 (DOI: 10.1021/ja810045y)
82. Tsukuda T., Tsunoyama H., Sakurai H. (2011), Aerobic oxidations catalyzed by colloidal nanogold, *Chem. Asian J.*, 6, 736 – 748 (DOI: 10.1002/asia.201000611)
83. Boronat M., Corma A. (2010), Oxygen activation on gold nanoparticles: separating the influence of particle size, particle shape and support interaction, *Dalton Trans.*, 39, 8538–8546 (DOI: 10.1039/c002280b)
84. Okumura M., Kitagawa Y., Kawakami T., Haruta M. (2008), Theoretical investigation of the hetero-junction effect in PVP-stabilized Au₁₃ clusters. The role of PVP in their catalytic activities, *Chem. Phys. Lett.*, 459, 133–136 (DOI: 10.1016/j.cplett.2008.04.120)
85. Hernández N. C., Sanz J. F., Rodríguez J. A. (2006), Unravelling the origin of the high-catalytic activity of supported Au: A density-functional theory-based interpretation, *J. Am. Chem. Soc.*, 128, 15600-15601 (DOI: 10.1021/ja0670153)
86. Ionita P., Gilbert B. C., Chechik V. (2005), Radical mechanism of a place-exchange reaction of Au nanoparticles, *Angew. Chem. Int. Ed.*, 44, 3720-3722 (DOI: 10.1002/anie.200500518)
87. Kotobuki M., Leppelt R., Hansgen D. A., Widmann D., Behm R. J. (2009), Reactive oxygen on a Au/TiO₂ supported catalyst, *J. Catal.*, 264, 67-76 (DOI: 10.1016/j.jcat.2009.03.013)
88. Minisci F., Recupero F., Cecchetto A., Gambarotti C., Punta C., Faletti R., Paganelli R., Pedulli G. F. (2004), Mechanisms of the aerobic oxidation of alcohols to aldehydes and ketones, catalysed under mild conditions by persistent and non-persistent nitroxyl radicals and transition metal salts-polar, enthalpic, and captodative effects, *Eur. J. Org. Chem.*, 109-119 (DOI: 10.1002/ejoc.200300332)
89. Leppelt R., Schumacher B., Plzak V., Kinne M., Behm R. J. (2006), Kinetics and mechanism of the low-temperature water–gas shift reaction on Au/CeO₂ catalysts in an idealized reaction atmosphere, *J. Catal.*, 244, 137-152 (DOI: 10.1016/j.jcat.2006.08.020)

Chapter 4

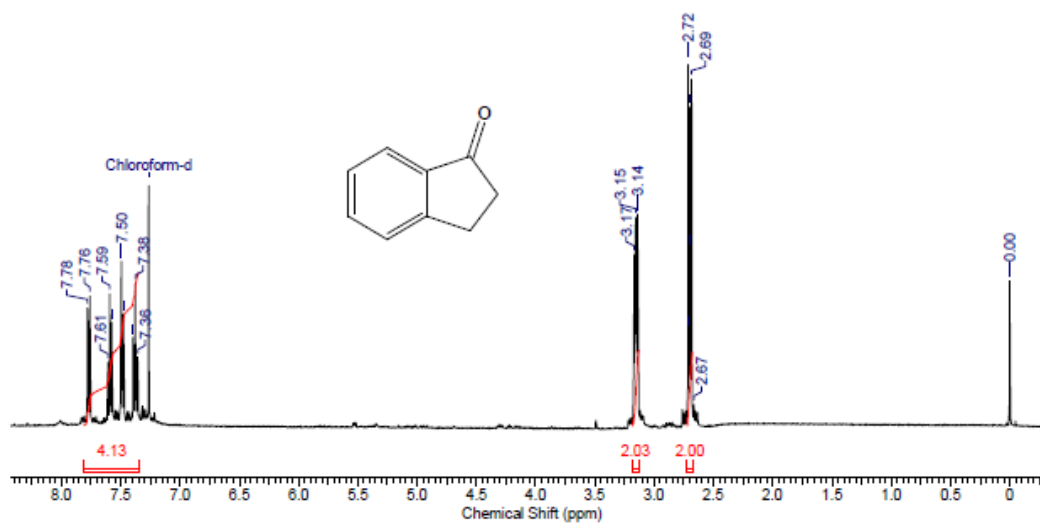
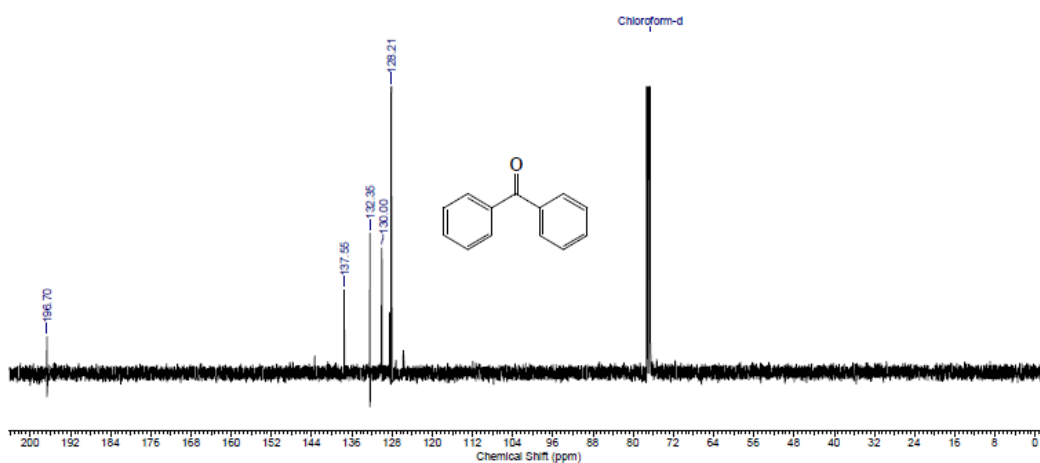
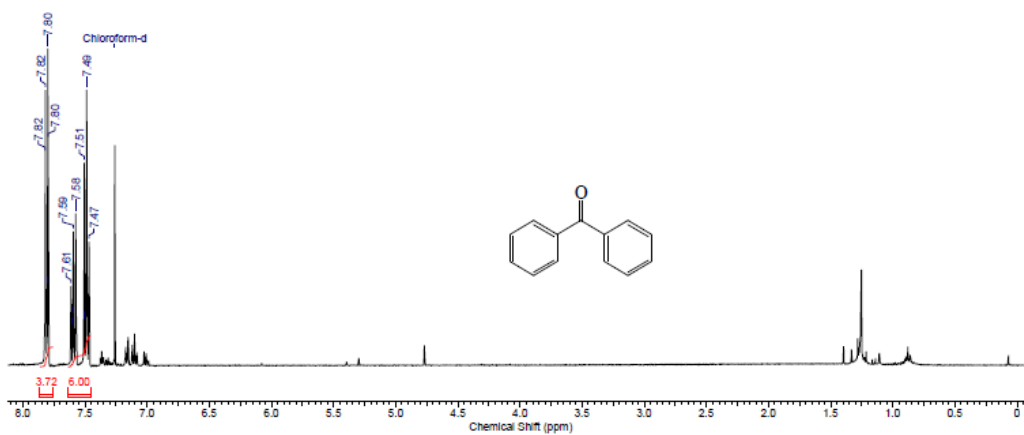
90. Boyen H. -G., Kästle G., Weigl F., Koslowski B., Dietrich C., Ziemann P., Spatz J. P., Riethmüller S., Hartmann C., Möller M., Schmid G., Garnier M. G., Oelhafen P. (2002), Oxidation-resistant gold-55 clusters, *Science*, 297, 1533-1536 (DOI: 10.1126/science.1076248)
91. Li J., Liu C.-Y., Liu Y. (2012), Au/graphene hydrogel: synthesis, characterization and its use for catalytic reduction of 4-nitrophenol, *J. Mater. Chem.*, 22, 8426– 8430 (DOI: 10.1039/c2jm16386a)
92. Xiong Z., Zhang L. L., Ma J., Zhao X. S. (2010), Photocatalytic degradation of dyes over graphene–gold nanocomposites under visible light irradiation, *Chem. Commun.*, 46, 6099-6101 (DOI: 10.1039/c0cc01259a)
93. Wu X., Zeng X. C. (2009), Periodic graphene nanobuds, *Nano Lett.*, 9, 250-256 (DOI: 10.1021/nl802832m)
94. Yeo Y. -C., King T. -J., Hu C. (2002), Metal-dielectric band alignment and its implications for metal gate complementary metal-oxide-semiconductor technology, *J. Appl. Phys.*, 92, 7266-7271 (DOI: 10.1063/1.1521517)
95. Ding S., Jiao N. (2012), N,N-dimethylformamide: A multipurpose building block, *Angew. Chem. Int. Ed.*, 51, 9226-9237 (DOI: 10.1002/anie.201200859)
96. Friaa O., Brault D. (2006), Kinetics of the reaction between the antioxidant Trolox® and the free radical DPPH· in semi-aqueous solution, *Org. Biomol. Chem.*, 4, 2417-2423 (DOI: 10.1039/B602147F)
97. Amorati R., Menichetti S., Viglianisi C., Foti M. C. (2012), Proton–electron transfer pathways in the reactions of peroxy and dpph· radicals with hydrogen-bonded phenols, *Chem. Commun.*, 48, 11904-11906 (DOI: 10.1039/c2cc36531f)
98. Ingold K. U., Pratt D. A. (2014), Advances in radical-trapping antioxidant chemistry in the 21st century: A kinetics and mechanisms perspective, *Chem. Rev.*, 114, 9022-9046 (DOI: 10.1021/cr500226n)
99. Conte M., Miyamura H., Kobayashi S., Chechik V. (2009), Spin trapping of Au-H intermediate in the alcohol oxidation by supported and

Chapter 4

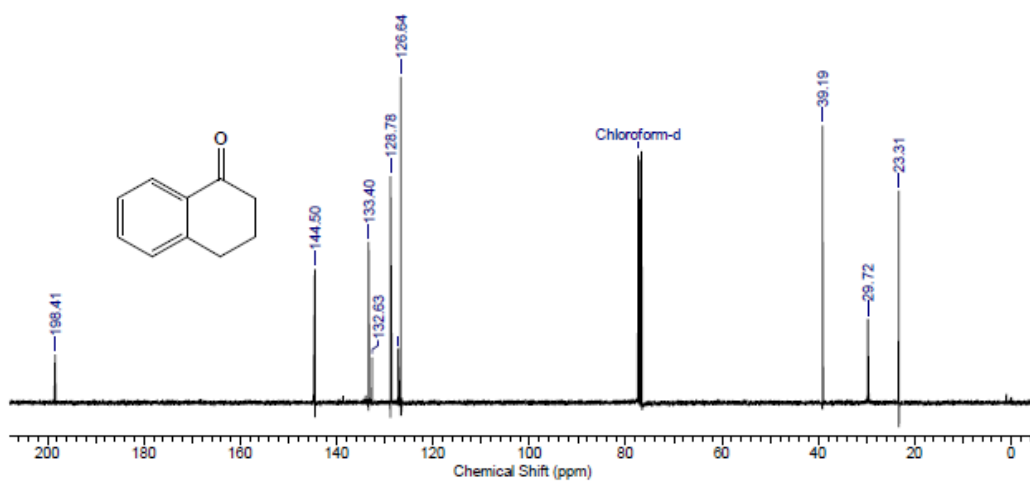
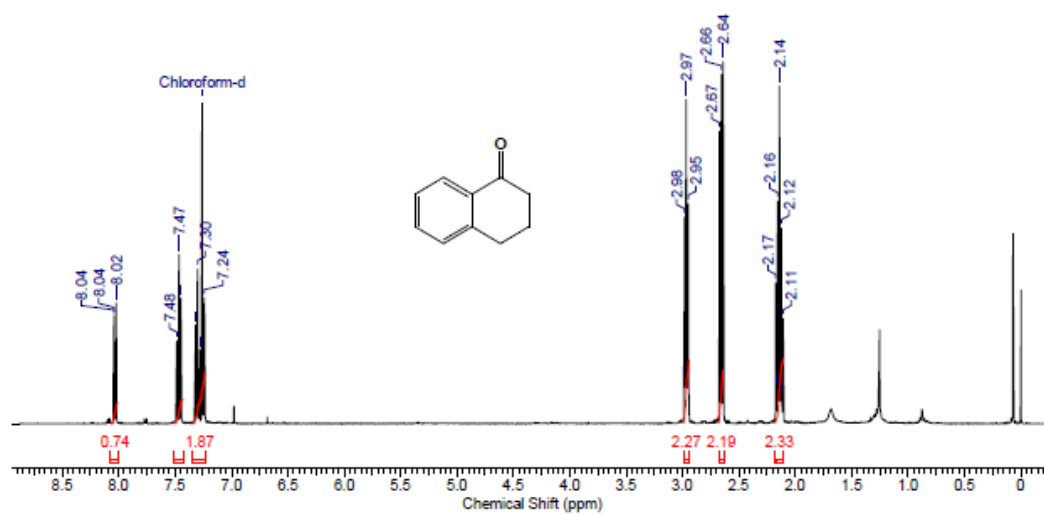
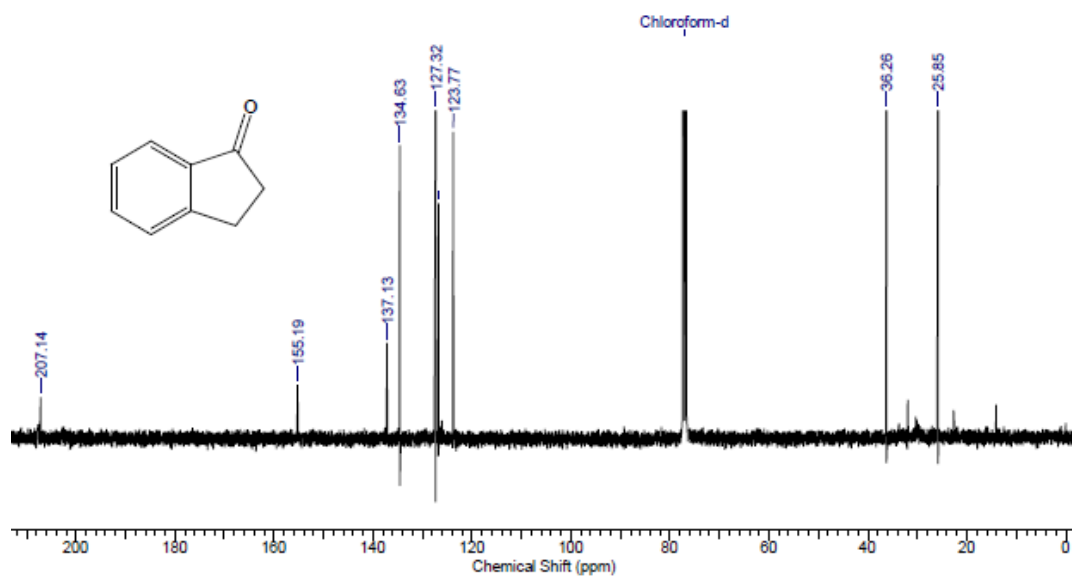
- unsupported gold catalysts, *J. Am. Chem. Soc.*, 131, 7189-7196 (DOI: 10.1021/ja809883c)
100. Su C., Acik M., Takai K., Lu J., Hao S. -J., Zheng Y., Wu P., Bao Q, Enoki T., Chabal Y. J., Loh K. P. (2012), Probing the catalytic activity of porous graphene oxide and the origin of this behaviour, *Nat. Comm.*, 3, 1298 (DOI: 10.1038/ncomms2315)
101. Amorelli A., Evans J. C., Rowlands C. C. (1988), An electron spin resonance study of the superoxide radical anion in polycrystalline magnesium oxide and titanium dioxide powders, *J. Chem. Soc. Faraday Trans. 1*, 84, 1723-1728 (DOI: 10.1039/F19888401723)
102. Tamiolakis I., Fountoulaki S., Vordos N., Lykakis I. N. Armatas G. S. (2013), Mesoporous Au–TiO₂ nanoparticle assemblies as efficient catalysts for the chemoselective reduction of nitro compounds, *J. Mater. Chem. A*, 1, 14311-14319 (DOI: 10.1039/C3TA13365F)
103. Carrettin S., McMorn P., Johnston P., Griffin K., Hutchings G. J. (2002), Selective oxidation of glycerol to glyceric acid using a gold catalyst in aqueous sodium hydroxide, *ChemCommun.*, 696-697 (DOI: 10.1039/b201112n)
104. Yi C. S., Kwon K. -H., Lee D. W. (2009), Aqueous phase C-H bond oxidation reaction of arylalkanes catalyzed by a water-soluble cationic Ru(III) complex [(pymox-Me₂)₂RuCl₂]⁺BF₄⁻, *Org. Lett.*, 11, 1567-1569 (DOI: 10.1021/ol900097y)
105. Shen D., Miao C., Wang S., Xia C., Sun W. (2014), Efficient benzylic and aliphatic C–H oxidation with selectivity for methylenic sites catalyzed by a bioinspired manganese complex, *Org. Lett.*, 16, 1108-1111 (DOI: 10.1021/ol4037083)

Appendix-Chapter 4
 ^1H and ^{13}C NMR Spectra of Oxidized
Products

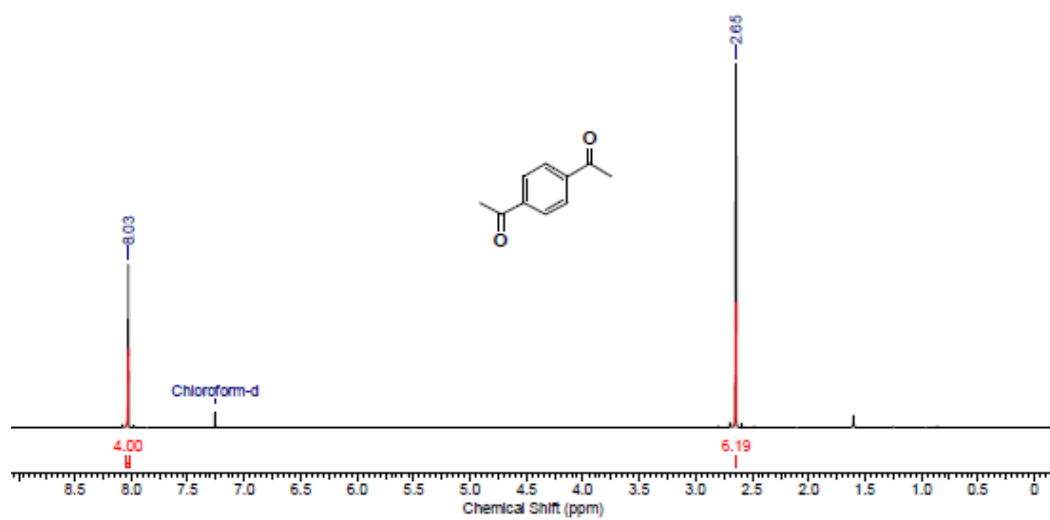
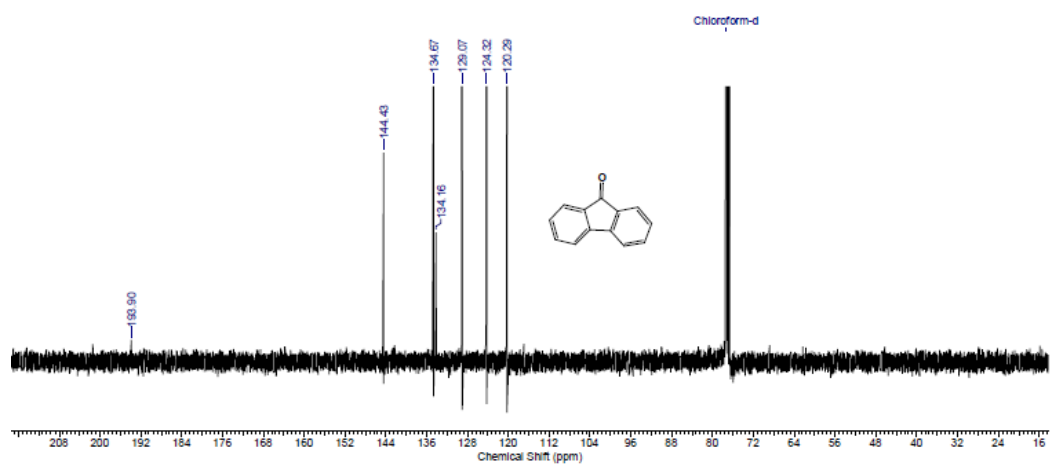
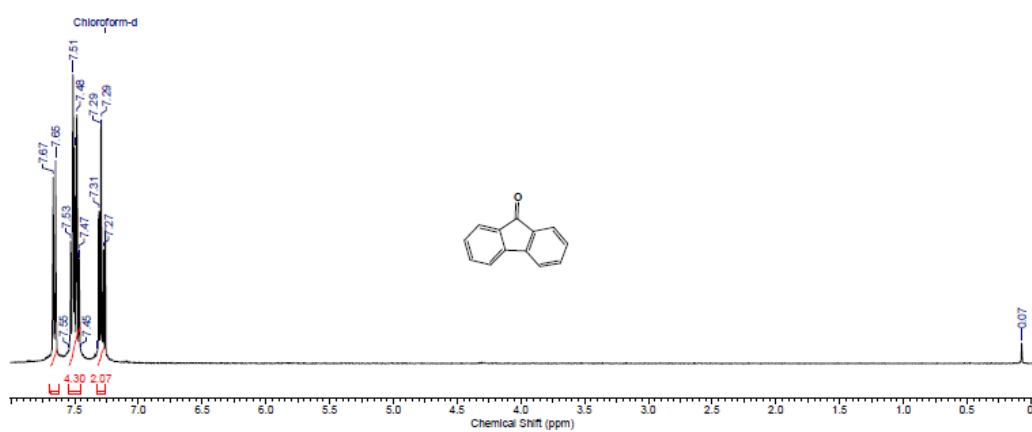
Chapter 4



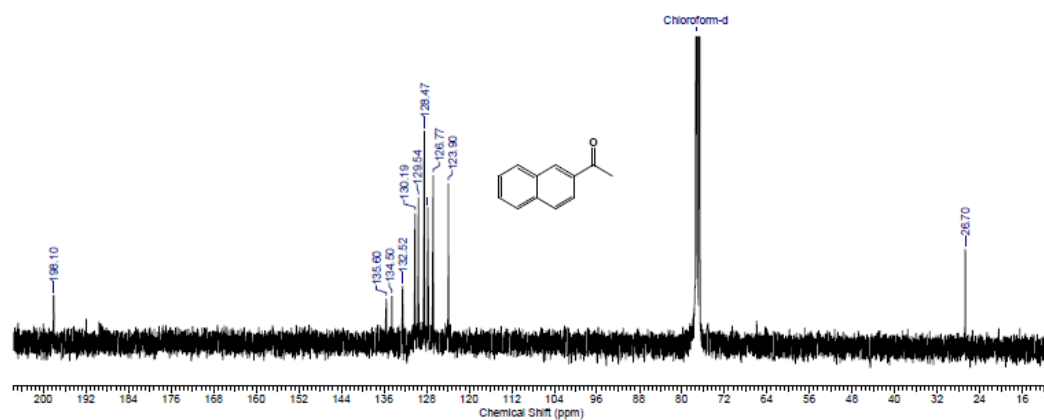
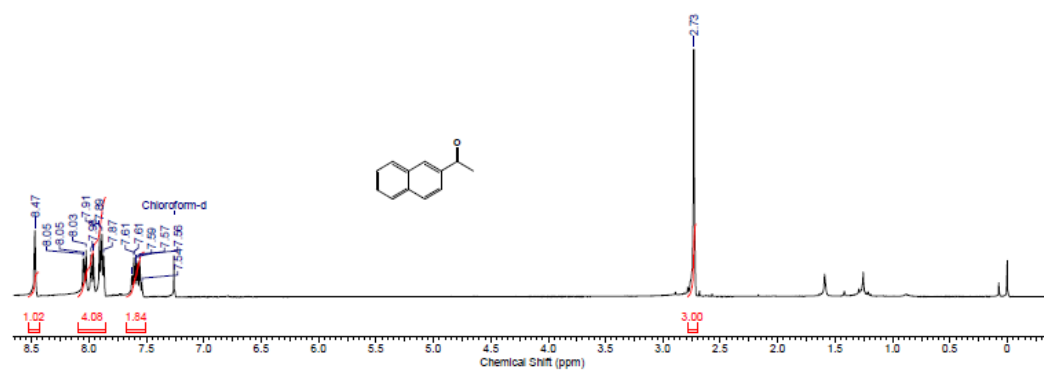
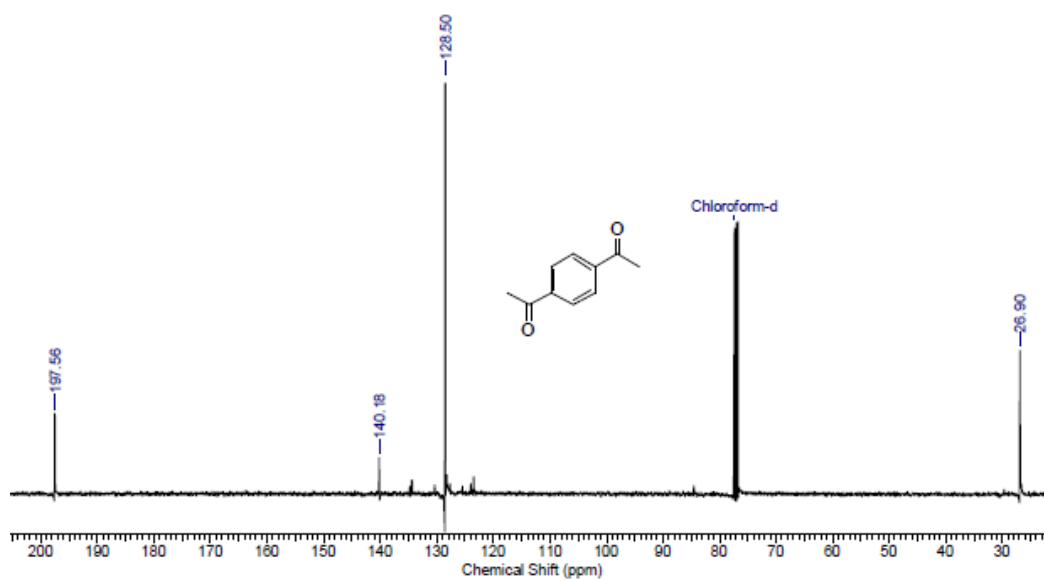
Chapter 4



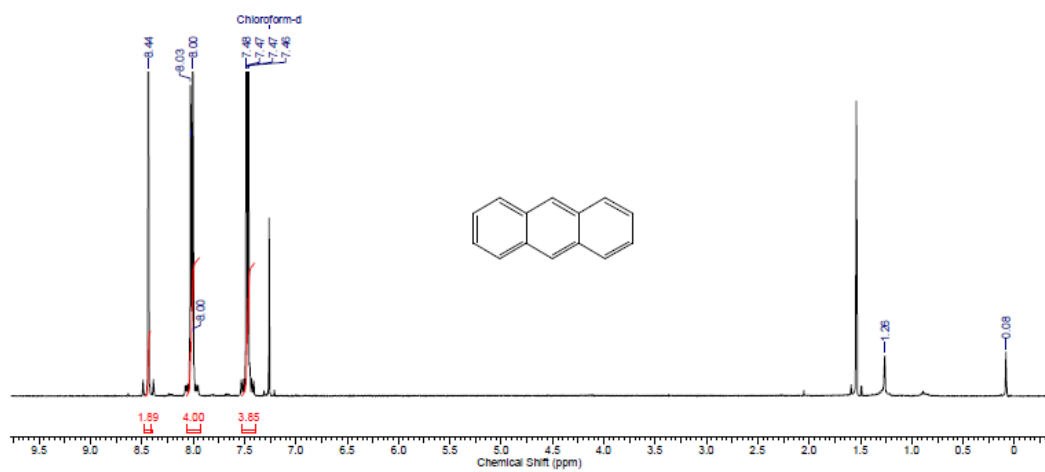
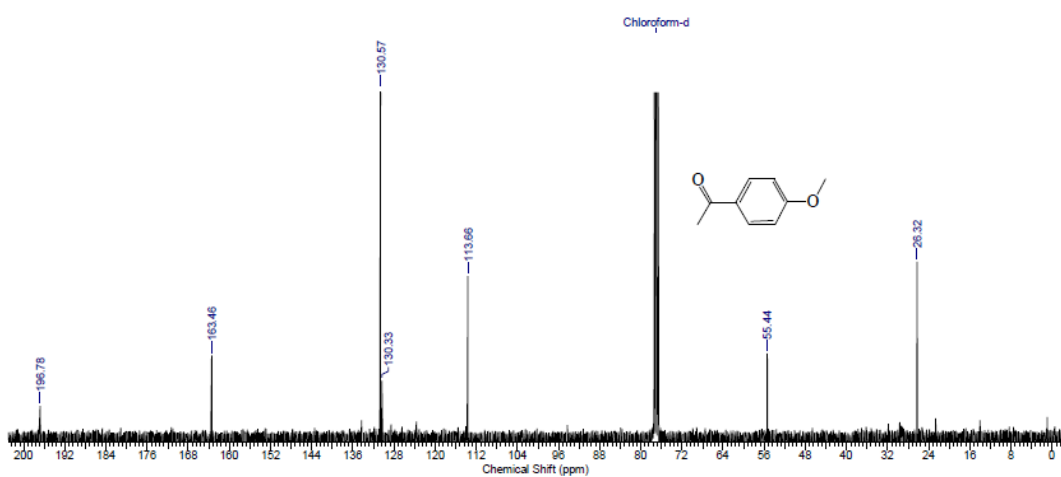
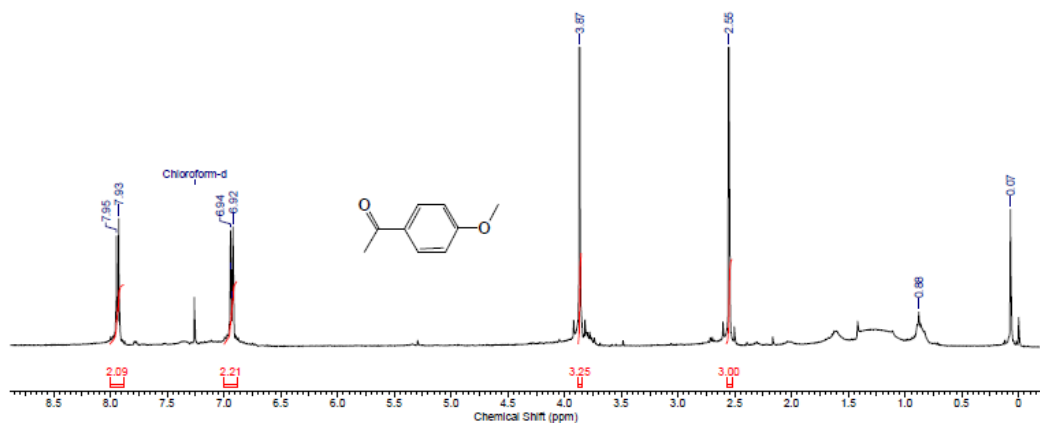
Chapter 4



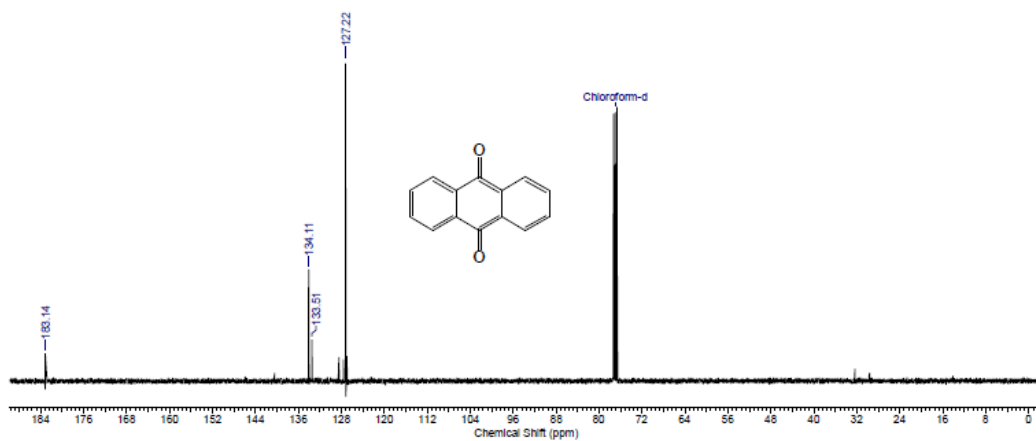
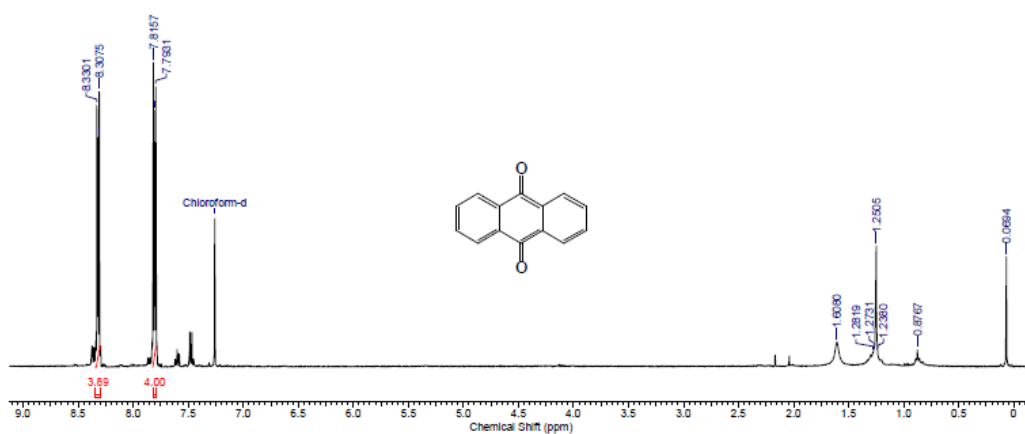
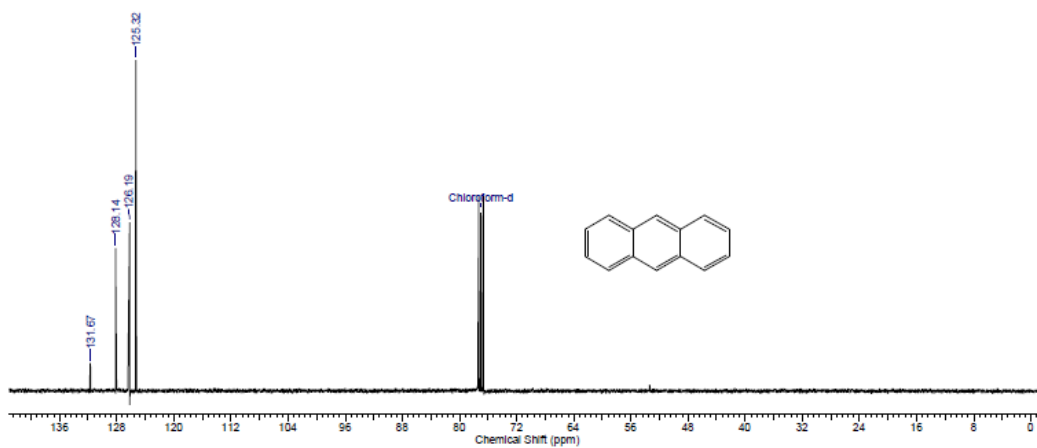
Chapter 4



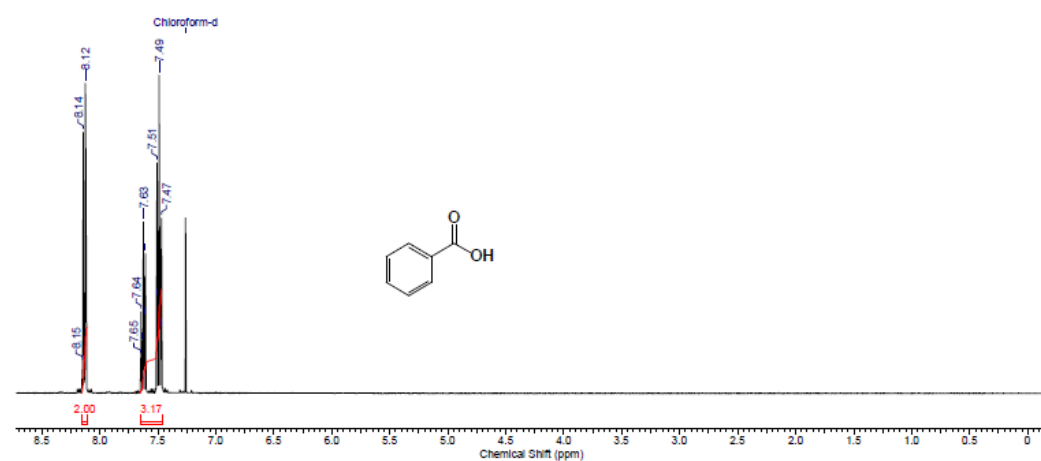
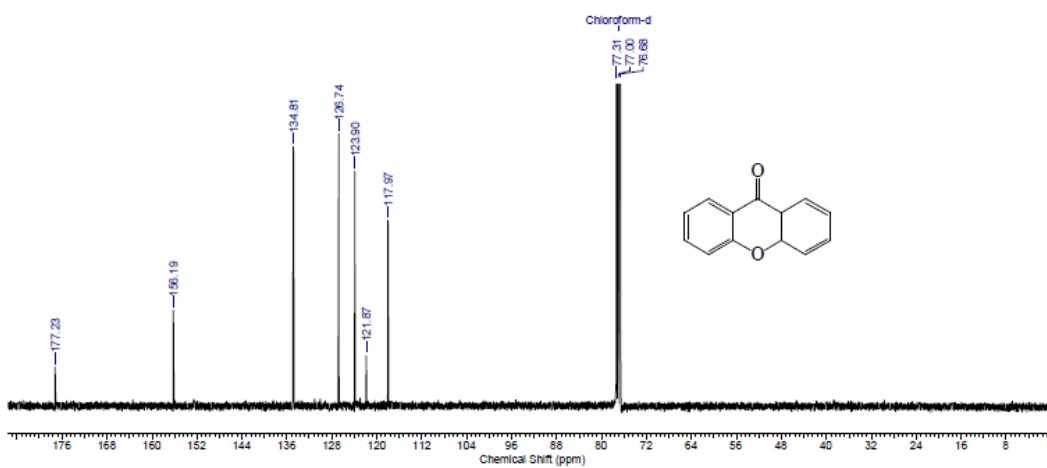
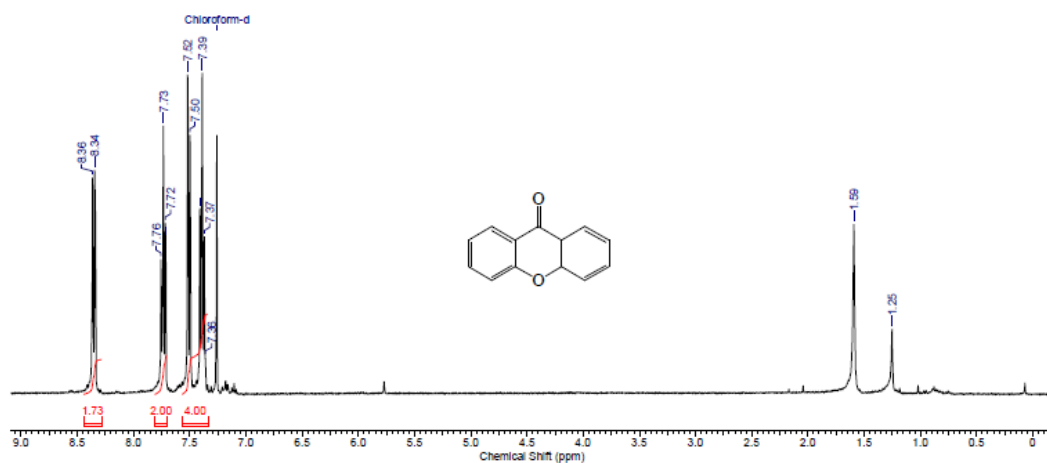
Chapter 4



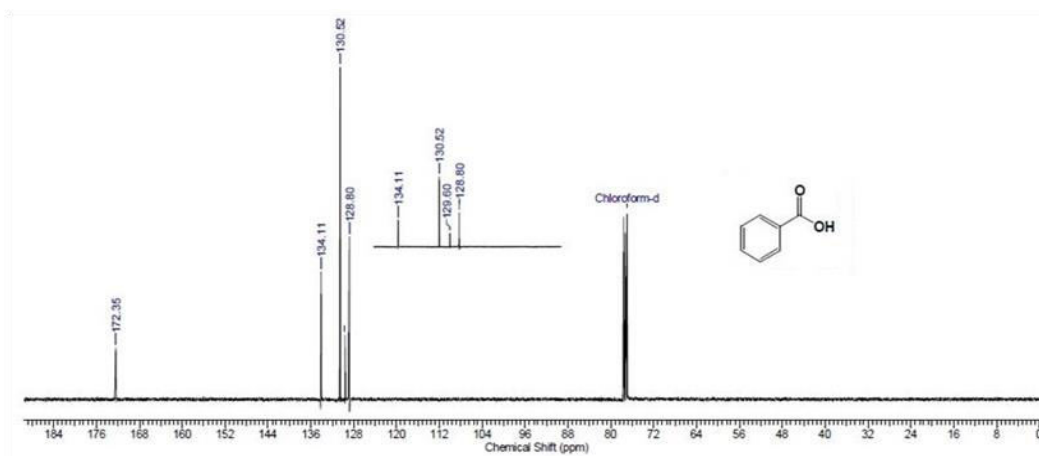
Chapter 4



Chapter 4



Chapter 4



Chapter 5

One-Pot Magnetic Iron Oxide Carbon Nanodots Composite Catalyzed Cyclooxidative Aqueous Tandem Synthesis of Quinazolinones in Presence of Tert-butyl hydroperoxide

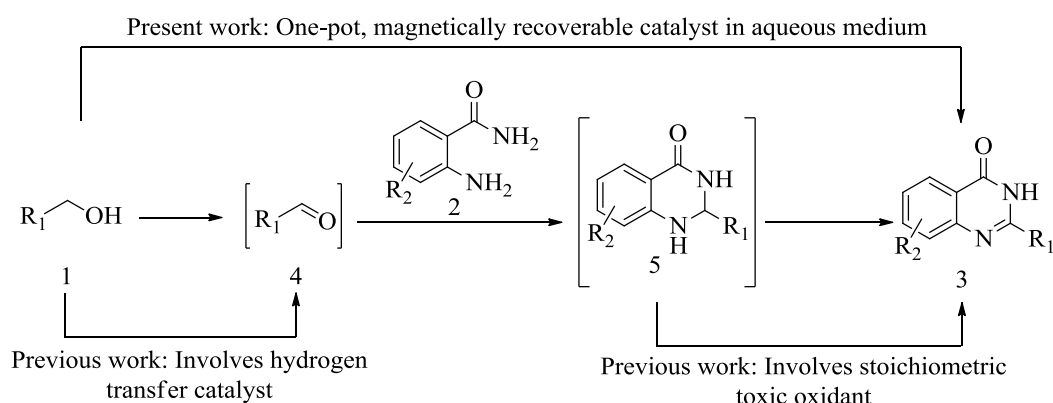
Chapter 5

5.1 Introduction

Homogeneous catalysts involving transition metals such as Au, Ru, Pd, Fe etc. have gained tremendous interest owing to their ability to trigger excellent activity and selectivity of catalytic reactions.^[1-7] However, most of the industrial processes prefer the use of heterogeneous catalysts due to their inbuilt simplicity of recovery and further reuse.^[8] Amidation of C(sp³)-H bonds is very important in organic synthesis since the N containing compounds, primarily N-heterocycles, have potential importance in natural products, advanced materials, crop protecting agents, and pharmaceuticals. Among the N-heterocycles, quinazolinones are key units in a wide range of relevant pharmacophores with a broad spectrum of activities such as anticancer, antiviral, anti-inflammatory, as well as anti-microbial activity.^[9-18] Due to its utmost prevalence, several synthetic methodologies have been developed towards quinazolinone derivatives making them more and more flippant. Some quinazolinones were synthesized by coupling halobenzoic acid with different ammonia sources including amides,^[13] amino acids,^[12] amidines,^[10] benzylamines^[11] etc. But the method suffered several disadvantages as it involved use of excessive amounts of bases and formation of salt wastes. The classical method of quinazolinones synthesis involves condensation of aldehydes and 2-aminobenzamides giving aminal intermediates followed by their oxidation to quinazolinones.^[14-18] However use of hazardous oxidants such as KMnO₄, CuCl, 2,3-dichloro-5,6-dicyano-1,4-benzoquinone (DDQ) and chemically unstable aldehydes limits the use of this method.^[14-18] Recent advancement in catalytic methods involve use of alcohol as the starting material which happens to be more benign and readily available than aldehydes.^[19] The reaction takes place through one pot two step oxidation pathway, where alcohols are first oxidised to aldehydes followed by coupling with 2-aminobenzamides forming the aminal derivatives and their oxidation to the final compound quinazolinone. Various heterogeneous and homogeneous systems including ZnI₂,^[20] homogeneous Ru and Pd catalysts,^[21-22] heterogeneous Pt nanoclusters,^[23] [Cp*IrCl₂]₂^[24] catalyst have been developed for successful synthesis of quinazolinones. However, to avoid use of high catalysts loading, excessive ligand based catalyst, toxic additives and formation of hazardous reaction byproducts, there remains a scope for the development of easy, reusable,

Chapter 5

low cost, environmental friendly catalytic system (Scheme 5.1) towards the formation of quinazolinones.



Scheme 5.1. One-pot synthesis of quinazolinones with alcohols and 2-aminobenzamides as the starting materials

In recent years, focus has been shifted towards nanoparticle (NP) based heterogeneous catalytic systems as effective catalysts for various organic transformations following green chemistry protocols.^[5-7, 25-28] Transition metal oxides have widely been used as catalysts for several important organic reactions.^[6, 29-35] However, their wider applications have been impeded by two important parameters viz. recovery issue and maintaining the particle dimension after repeated use. Recently, nanocrystalline manganese oxides has been used as excellent catalyst towards the synthesis of quinazolinone in presence of *tert*-butylhydroperoxide (TBHP).^[36] However, the reactions were carried out using chlorobenzene as a solvent. Therefore, exploration of metal oxide nanocatalytic systems for the synthesis of this important class of materials in aqueous medium is of great significance for industrial applications. Iron oxide nanoparticles have been used as catalyst for organic transformations as well as a support for anchoring other active metal catalysts.^[5-7, 25, 37-38] These quasi-homogeneous catalysts possess numerous benefits such as ease of isolation and separation from the desired reaction mixtures using an external magnet resulting in excellent recyclability and thus led to a dramatic expansion of their potential applications in environmentally-friendly and sustainable catalytic processes. Further, the stability of the nanocatalytic systems under the reaction conditions in an important parameter as agglomeration during the catalytic reactions might

significantly influence the catalytic activity due to decreased surface area. Further the cooperativity of the stabilizing ligands in enhancing the catalytic performance of the active catalytic sites for various organic transformations has been studied.

Carbon nanodots (CNDs) have emerged as an alternative to the semiconducting quantum dots due to their intrinsic emission properties that can be tuned by changing surface functionalities. Due to their natural abundance, nontoxicity, biocompatibility and photo stability, these tiny carbon nanomaterials have drawn immense attention in the area of biosensing, bio imaging and optoelectronic applications.^[39-47] The presence of surface functional groups such as carboxylic and hydroxyl groups not only confer CNDs excellent water solubility and biocompatibility, but also as a support for stabilizing metal and metal oxide nanoparticles through self-assembled monolayer principles.^[45, 48-51] CNDs can also function as reducing agents for the synthesis of metal nanoparticles such as Pd, that showed high efficiency for C-C coupling reactions.^[50] CNDs are known to demonstrate excellent peroxidase activities in presence of H₂O₂.^[52] Therefore, we envisioned that CND stabilized iron oxide NPs could efficiently catalyze the synthesis of quinazolinones from alcohols as starting materials in aqueous medium providing a green pathway for the development of these important class of materials. In our exploration using CND stabilized Fe₃O₄ nanoparticles (Fe₃O₄-CND) as catalyst and TBHP as oxidant, we observed that the catalyst can be used for the dehydrogenation of both C-H and N-H bond in a one-pot protocol, and thus realizing the direct oxidative cyclization of 2-aminobenzamides with alcohols. A wide range of quinazolinones are synthesized with 69-94% yields. Further, easy recovery and good activity over repeated cycles make the Fe₃O₄-CND composite as efficient catalysts for one-pot tandem reactions.

5.2 Results and Discussion

5.2.1 Synthesis of CND and CND stabilized (Fe₃O₄) NPs (Fe₃O₄-CNDs)

The CNDs were synthesized by microwave treatment of polyethylene glycol - 200(PEG-200) according to a previously reported protocol.^[53] 15 mL of PEG-200

Chapter 5

was treated with microwave irradiation in a domestic microwave oven that resulted in a brown dispersion of CNDs. The dialyzed CNDs free from PEG were used directly as stabilizers for iron oxide nanoparticles. Iron oxide NPs were synthesized by the co-precipitation method using FeCl_3 and FeSO_4 salts. In a typical synthesis, two iron salts ($\text{Fe}^{3+}:\text{Fe}^{2+}$) were added in 2:1 ratio in an aqueous solution containing CNDs in a 3-neck flask. The reaction mixture was vigorously stirred at 60 °C under inert atmosphere and 10 mL 2.5 M NaOH solution was added. The *in situ* synthesized Fe_3O_4 NPs were stabilized by the CNDs present in the solution. The catalyst was purified by centrifugation with repeated washing using water and ethanol to remove unbound CNDs followed by drying under vacuum. Bare and citrate stabilized Fe_3O_4 nanoparticles were synthesized by following the co-precipitation method in presence of no stabilizer and Na-citrate respectively. The synthesized Fe_3O_4 -CND nanocomposite was characterized by different spectroscopic and microscopic techniques.

5.2.2 Characterization of Fe_3O_4 -CND composite

The powder X-ray diffraction (PXRD) patterns of the synthesized CNDs and Fe_3O_4 -CNDs were measured (Fig. 5.1a). A broad peak at $2\theta = 23^\circ$, corresponding d spacing of 3.8 Å, signified the presence of CNDs in the nanocomposite. Further, peaks at $2\theta = 30.17, 35.46, 43.38, 53.69, 57.23$ and 62.77° correspond to (220), (311), (400), (422), (511) and (440) planes for Fe_3O_4 NPs.^[51]

To have a better understanding of the interaction between CNDs and Fe_3O_4 NPs, we studied photoluminescence (PL) properties of CNDs and Fe_3O_4 -CNDs. Similar to the CNDs synthesized from β -carotene as described in chapter 3, CNDs synthesized from PEG-200 also showed excitation dependent emission properties with maximum emission at 490 nm when excited at 375 nm. However, upon interaction with the Fe_3O_4 NPs, the emission owing to CNDs quenched significantly, suggesting that CNDs acted as effective stabilizers for Fe_3O_4 NPs. It is well known that CNDs show high fluorescence detection selectivity for Fe^{3+} ions, due to fast electron transfer between Fe^{3+} and CNDs surface passivated with oxygen rich groups. The high binding affinity of Fe^{3+} groups towards the electron rich $-\text{CO}_2\text{H}$ and $-\text{OH}$ groups results in transfer of excited electrons on CNDs to the unfilled orbital of Fe^{3+} . The resulting non-radiative electron/hole

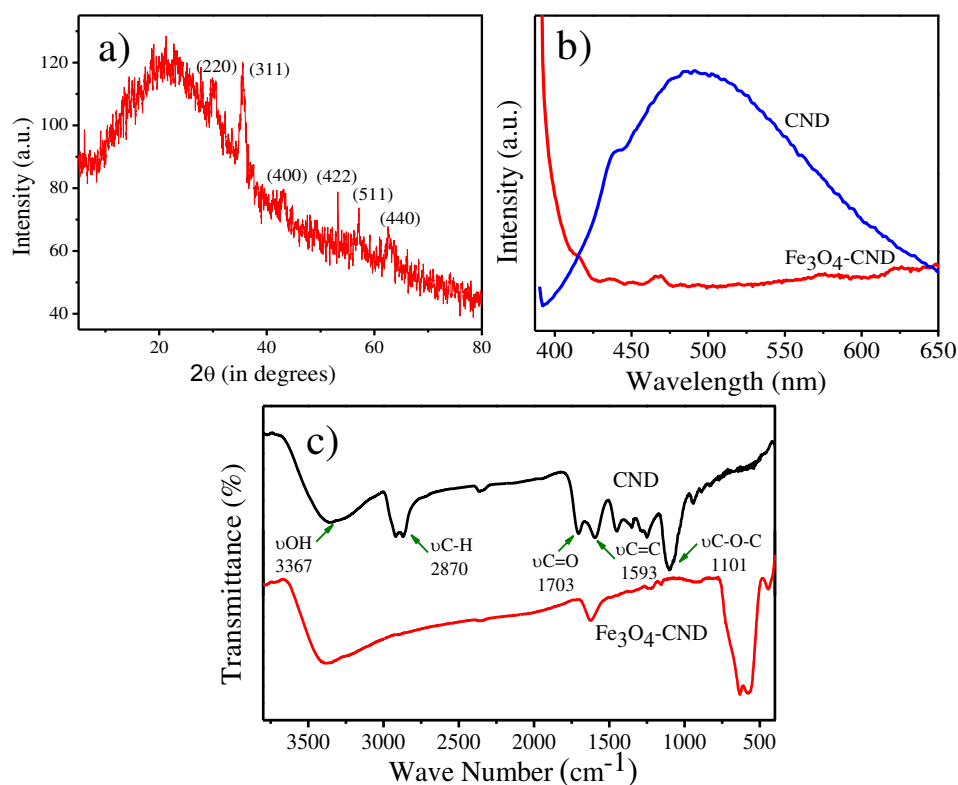


Figure 5.1. a) Powder X-ray diffraction pattern of Fe_3O_4 -CND composite, b) and c) Emission spectra and FTIR spectra for CNDs and Fe_3O_4 -CND respectively

recombination directly leads to fluorescence quenching of CNDs.^[54] In case of Fe_3O_4 -CND composite also, the electron transfer from the CNDs to the surface Fe^{3+} groups results in effective quenching of the CND emission (Fig. 5.1b). Further evidence for the CND binding to the iron oxide surface was obtained from FTIR studies. The peak intensity of the oxygenated functional groups of CNDs such as $-\text{C}=\text{O}$ and $\text{C}-\text{O}-\text{C}$ ($\sim 1703 \text{ cm}^{-1}$ and 1101 cm^{-1}) were decreased significantly in the Fe_3O_4 -CND composite indicating the involvement of these groups in Fe_3O_4 surface stabilization. In addition, a new peak at $\sim 594 \text{ cm}^{-1}$ corresponding to Fe-O stretching was also observed (Fig. 5.1c).^[55]

We further performed X-ray photoelectron spectroscopy (XPS) measurements of the synthesized nanocomposite. The wide scan XPS spectrum of Fe_3O_4 -CND composite shows that the photoelectron lines at binding energies (BEs) of about 284.6, 530.7 and 710.7-724.6 eV are attributed to C 1s, O 1s, and Fe 2p, respectively (Fig. 5.2a). XPS signals appeared at BEs 710.7 and 724.6 eV corresponding to $\text{Fe}2p_{3/2}$ and $\text{Fe}2p_{1/2}$ levels are characteristic peaks for Fe_3O_4

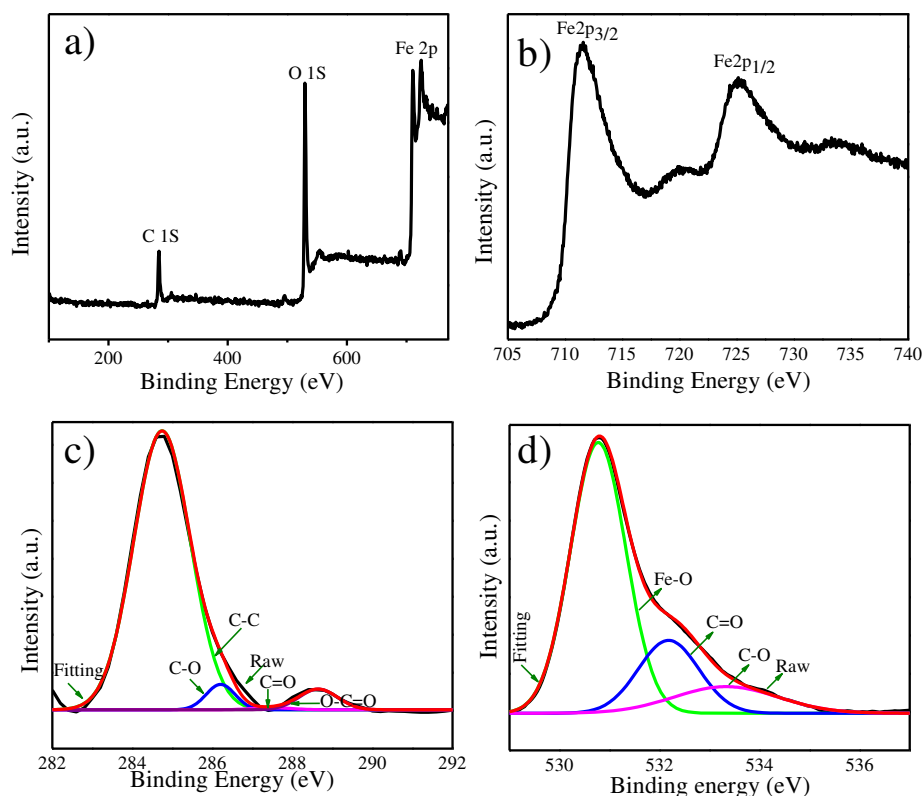


Figure 5.2. a) Wide scan XPS spectrum of $\text{Fe}_3\text{O}_4\text{-CND}$, b) $\text{Fe}2p$, c) $\text{C}1s$ and d) $\text{O}1s$ core level XPS spectrum of $\text{Fe}_3\text{O}_4\text{-CND}$

nanoparticles (Fig. 5.2b). The $\text{C}1s$ core level spectrum of $\text{Fe}_3\text{O}_4\text{-CND}$ composite was fitted into four components with BEs at about 284.8, 286.2, 287.9 and 289.0 eV which correspond to non-oxygenated carbon in C-C, epoxy carbon in C-O, carbonyl carbon in C=O and carboxyl carbon in O-C=O respectively (Fig. 5.2c).^[56-57] $\text{O}1s$ core level spectrum of $\text{Fe}_3\text{O}_4\text{-CND}$ composite was fitted into three components with BEs at about 530.7, 532.2 and 533.2 which correspond to anionic oxygen in Fe_3O_4 , carbonyl oxygen in C=O and alkoxy oxygen in C-O (Fig. 5.2d).^[58]

Transmission electron microscope (TEM) image confirmed the formation of uniform spherical Fe_3O_4 NPs with average diameter of 7 nm (Fig. 5.3a). High resolution transmission electron microscope (HRTEM) image clearly showed the formation of a low-contrast CND layer ca. 2.5 nm surrounding Fe_3O_4 NP. The formation of a continuous layer of CNDs on the Fe_3O_4 NP surface showed the highly dense monolayer formation of CNDs. Selected area electron diffraction

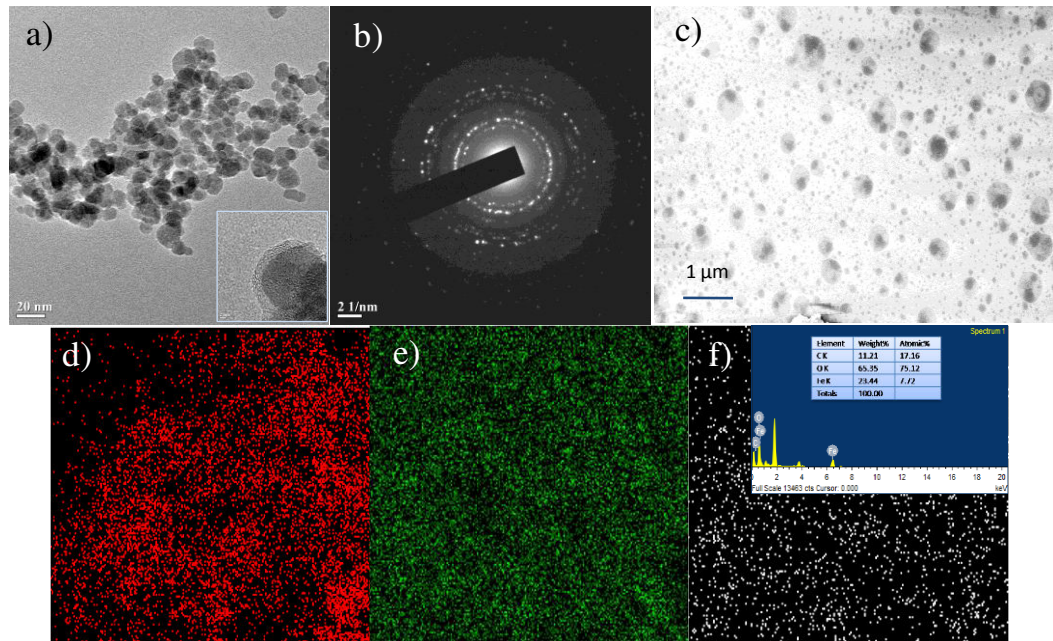


Figure 5.3. a) TEM image of $\text{Fe}_3\text{O}_4\text{-CND}$ with scale bar 20 nm (inset a: high resolution TEM image), b) SAED pattern, c) SEM image and d), e), f) elemental mapping of $\text{Fe}_3\text{O}_4\text{-CND}$ representing Fe, O and C respectively (inset f: EDS spectrum)

pattern showed high crystallinity of the composite (Fig. 5.3b). Scanning electron microscope (SEM) image of the $\text{Fe}_3\text{O}_4\text{-CND}$ composite revealed the formation of spherical Fe_3O_4 NPs surrounded by CND layer on their surface (Fig. 5.3c). The energy-dispersive spectrum (EDS) obtained from SEM confirmed the presence of Fe, C and O species in the composite material (Fig. 5.3d, e, f).

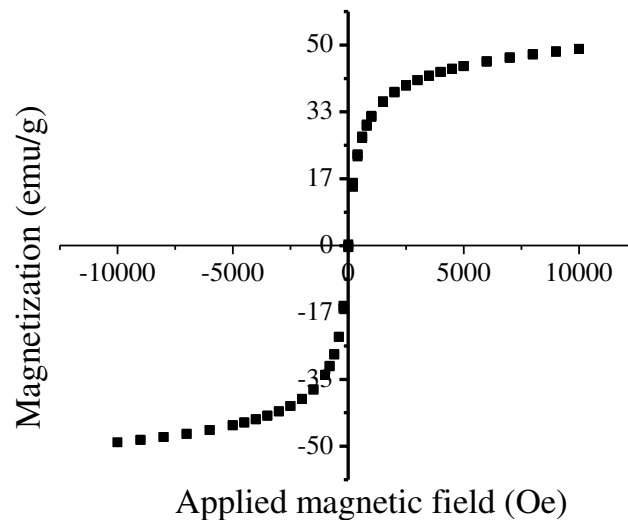


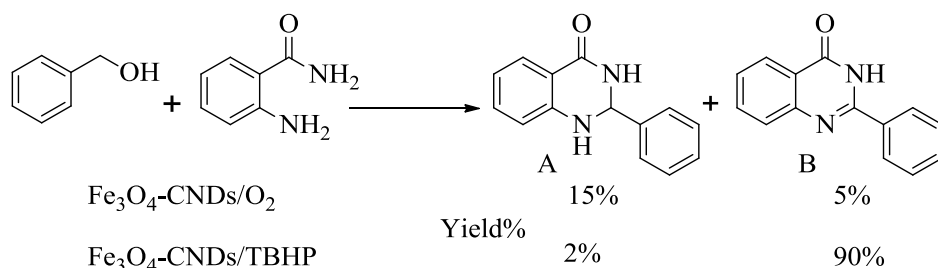
Figure 5.4. Magnetization curve for CND stabilized iron oxide nanoparticles

Chapter 5

We further studied magnetic susceptibility measurement of Fe_3O_4 -CND composite (Fig. 5.4). Interestingly we observed decrease in the magnetization value (48.6 emu/g) of Fe_3O_4 NPs in Fe_3O_4 -CND composite compared to that of earlier reported bare Fe_3O_4 NPs (64 emu/g).^[51] This indicated that the Fe_3O_4 NPs surface has been modified with CND layer. Moreover, zero coercivity remanence on the magnetization loop, and the absence of a hysteresis loop suggested the superparamagnetic behaviour of Fe_3O_4 -CND composite.

5.2.3 Catalytic activity of Fe_3O_4 -CND composite towards the formation of quinazolinones

The initial studies were carried out by performing the reaction of benzyl alcohol (1a) and 2-aminobenzamide (2a) in presence of Fe_3O_4 -CND using molecular oxygen as the terminal oxidant in aqueous medium (Scheme 5.2) for 12 hours. We observed poor conversion of the reaction with dihydroquinazolinone as the major product. On the other hand, when we replaced molecular oxygen with an external oxidant TBHP, we observed quinazolinone as the major product with high conversion. Using only TBHP (in absence of catalyst) again resulted in quinazolinone as the major product, however, with lower conversion (25% yield).

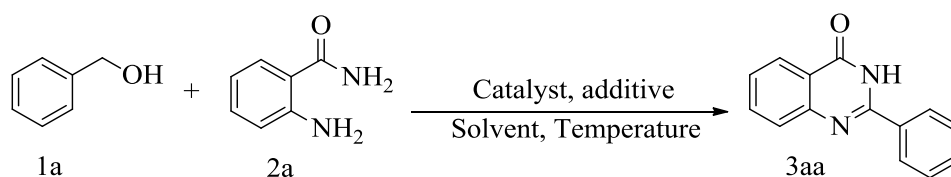


Scheme 5.2. C-H amidation leading to dihydroquinazolinone and quinazolinone

These results prompted us to further explore the activity of Fe_3O_4 -CND at varying reaction parameters toward one-pot synthesis of quinazolinone using alcohol as the starting material. Benzyl alcohol (1a) with 2-aminobenzamide (2a) was selected as the model substrate to test the tandem reaction (Table 5.1). In a controlled reaction, with only nanocatalyst at room temperature in aqueous medium, the reaction resulted only with the starting materials with no product formation (Table 5.1, entry 1). However, increasing the reaction temperature to 90 °C using molecular oxygen as the terminal oxidant resulted in the

Chapter 5

Table 5.1. Oxidative coupling of (1a) and (2a) under various conditions^a



entry	catalyst (wt%)	solvent	additive (eq.)	temp. (°C)	yield ^b (%)
1	Fe ₃ O ₄ -CND (10)	H ₂ O	-	r.t	nr
2	Fe ₃ O ₄ -CND (10)	H ₂ O	-	50	trace
3	Fe ₃ O ₄ -CND (10)	H ₂ O	-	90	5
4	Fe ₃ O ₄ -CND (10)	H ₂ O	TBHP (1)	90	62
5	Fe ₃ O ₄ -CND (10)	H ₂ O	TBHP (2)	90	94
6	Fe ₃ O ₄ -CND (10)	CH ₃ CN	H ₂ O ₂ (2)	90	trace
7	Fe ₃ O ₄ -CND (5)	H ₂ O	TBHP (2)	90	65
8	Fe ₃ O ₄ -CND (15)	H ₂ O	TBHP (2)	90	91
9	-	H ₂ O	TBHP (2)	90	25
10	Fe ₃ O ₄ -CND (10)	CH ₃ CN	TBHP (2)	90	46
11	Fe ₃ O ₄ -CND (10)	Toluene	TBHP (2)	90	95
12	Fe ₃ O ₄ -CND (10)	Ethanol	TBHP (2)	90	65
13	Fe ₃ O ₄ -CND (10)	H ₂ O	TBHP (4)	90	64
14	Fe ₃ O ₄ (10)	H ₂ O	TBHP (4)	90	57
15	Fe ₃ O ₄ -Citrate (10)	H ₂ O	TBHP (2)	90	68
16	Fe ₃ O ₄ -CND (10)	H ₂ O	K ₂ CO ₃ (2)	90	trace

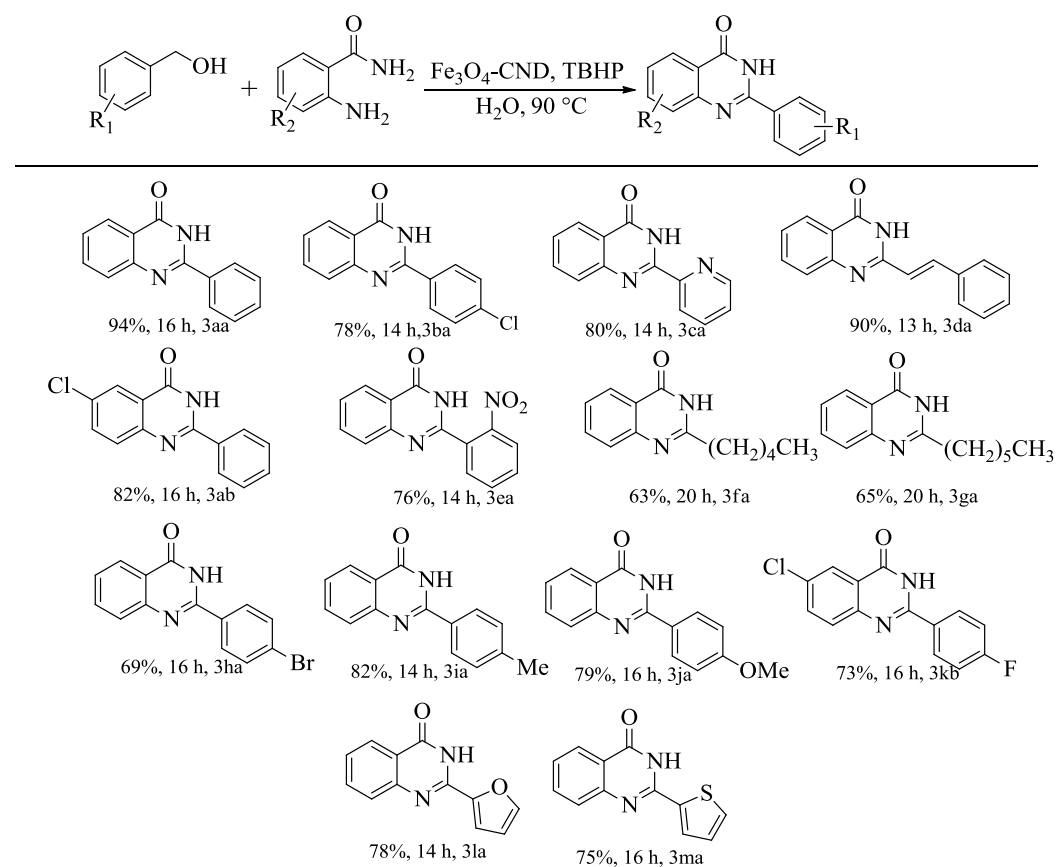
^aReaction conditions: 1a (1.5 mmol), 2a (0.5 mmol), catalyst 5-15 wt%, additives 1-4 equiv. and solvent 2mL, 16 hr, ^b yields of isolated product

quinazolinone product with 5% yield. Use of H₂O₂ as the oxidant resulted in trace amount of quinazolinone formation. On the other hand, using TBHP (2 equiv.) as the oxidant instead of molecular oxygen or H₂O₂ resulted in significant enhancement in the reaction rate and resulted in 94% of quinazolinone (Table 5.1, entry 5). Reactions with variable catalyst loading showed that 10 wt% of Fe₃O₄-CND nanocatalyst to be optimal for the reaction. When the reaction was performed in absence of the catalyst using TBHP as the oxidant, 25% of the product was obtained indicating importance of both Fe₃O₄-CND and TBHP in the catalytic reaction (Table 5.1, entry 9). Among the solvents screened, using

Chapter 5

toluene gave excellent yield of the desired product. However, we preferred water as the solvent for all our studies as it also resulted in 94% of the product. Increase in the amount of TBHP to 4 equivalents had detrimental effect on the reaction as lower yield of the product was obtained (Table 5.1, entry 13). Further use of bare Fe₃O₄ NPs as the catalyst resulted only in 54% yield of the product (Table 5.1, entry 14). This can be attributed to the stability of the NPs as they are expected to agglomerate without any stabilizing agents under thermal reaction conditions. Further, citrate stabilized Fe₃O₄ NPs resulted in 68% yield of quinazolinone under similar reaction conditions (Table 5.1, entry 15). Since inorganic bases play an important role in alcohol oxidation reactions, we also tested the reaction with inorganic base such as K₂CO₃. However, K₂CO₃ was found to be ineffective for the reaction and resulted only in trace formation of the product (Table 5.1, entry 16). After all these studies, the optimal reaction condition was found to be when the reaction was carried out using 10 wt% Fe₃O₄-CND catalyst in presence of TBHP as the oxidant at 90 °C for 16 hours in aqueous medium.

Having the optimized reaction conditions in hand, we evaluated the substrate scope for the reaction. Various primary alcohols were used as substrates to react with 2-aminobenzamide (2a), and the results are summarized in table 5.2. A wide range of quinazolinones could be synthesized with good to excellent yields under the present reaction condition. Both electronically activating and deactivating substituents (-CH₃, -OCH₃ and -NO₂) in the phenyl ring were found to have minor effect in the reaction and could be coupled easily with 2-aminobenzamide to give the corresponding quinazolinones in 76-82% yields (entry 3ea, 3ia and 3ja, table 2). Halo-substituted benzyl alcohols were also found to be stable under the reaction conditions and could be introduced in the quinazolinone skeleton with excellent yields (entry 3ba, 3ha and 3kb, table 2). In case of cinnamyl alcohol, the olefinic C=C bond survived well under the reaction conditions and resulted corresponding quinazolinone with 90% yield (entry 3da, table 2). 5-chloro-2-aminobenzamide was also found to be compatible under the present reaction conditions and yielded the desired products with excellent yields (entry 3ab and 3kb, table 2). Heteroatoms are known to poison the metal oxide surface by strongly coordinating to the active catalytic site. However, in the present case, heterocyclic alcohols such as 2-pyridine carboxaldehyde, furfural, 2-

Table 5.2. Synthesis of quinazolinones catalyzed by Fe_3O_4 -CND composite

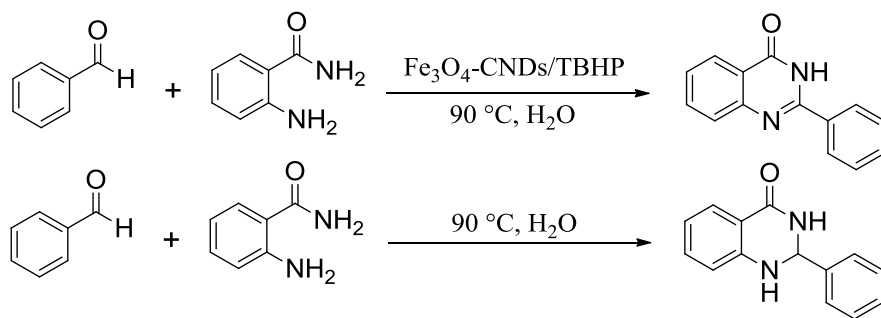
Reaction conditions: Alcohol (1.5 mmol), 2-aminobenzamide (0.5 mmol), Fe_3O_4 -CND 10 wt%, TBHP 2.0 equiv. and H_2O 2 mL, 900 rpm, 13-20 hr at $90\text{ }^\circ\text{C}$

thiophenecarboxaldehyde could be efficiently transformed into the desired products with high yields (entry 3ca, 3la and 3ma, table 2). Furthermore, inactive aliphatic alcohols could also be coupled to give the desired product with reasonably good yields (entry 3fa and 3ga, table 2).

5.2.4 Investigation of reaction mechanism

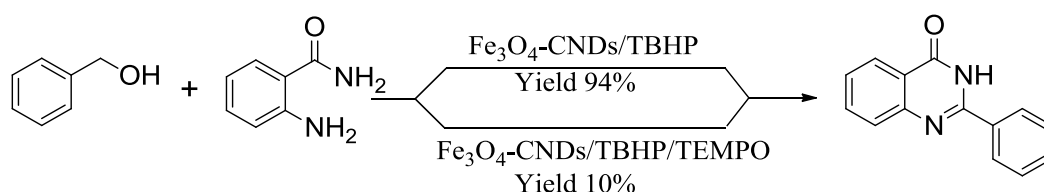
To further investigate the mechanism of the reaction, we performed a few controlled experiments (Scheme 5.3). We choose benzaldehyde and 2-aminobenzamide as the starting materials and allowed them to react to get the corresponding coupled products. We observed that in presence of the catalyst Fe_3O_4 -CND and TBHP under the optimized conditions, the reaction of benzaldehyde and 2-aminobenzamide yielded quinazolinone as the exclusive product. On the other hand, when the reaction was performed in absence of the catalyst and TBHP keeping the other conditions constant, we obtained the

Chapter 5



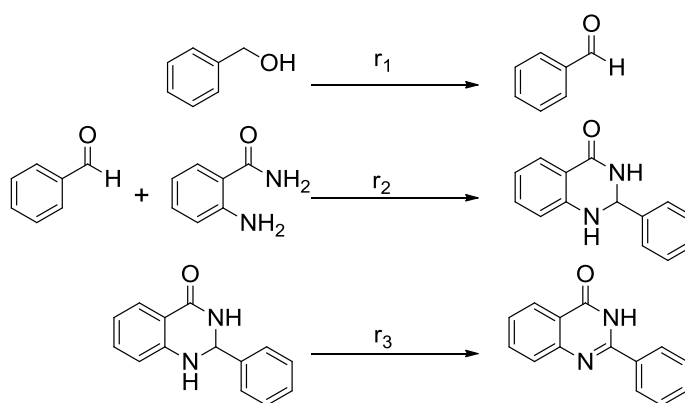
Scheme 5.3. Control experiments with benzaldehyde and 2-aminobenzamide as the starting materials

dihydroquinazolinone product in the major amount.^[59-60] These results indicate that benzaldehyde and dihydroquinazolinone should be the intermediates in our model coupling reaction of benzyl alcohol and 2-aminobenzamide. Further, the reaction was significantly inhibited when radical inhibitors such as (2, 2, 6, 6-tetramethylpiperidin-1-yl) oxy (TEMPO) and butylated hydroxytoluene (BHT) was added to the reaction (Scheme 5.4 and Scheme 5.5). This result indicates that the reaction should follow a free radical pathway.^[61-65]



Scheme 5.4. Presence of radical inhibitor indicating free radical process

Based on these results, we proposed a reaction sequence for the cyclooxidative tandem reaction of benzyl alcohol and 2-aminobenzamide (Scheme 5.5). In step 1, benzyl alcohol oxidizes to give benzaldehyde. In step 2, benzaldehyde reacts with 2-aminobenzamide to generate dihydroquinazolinone and in step 3, dihydroquinazolinone oxidizes to give the final product quinazolinone. Among these 3 steps, step 1 i.e. oxidation of benzyl alcohol to benzaldehyde is the rate determining step as this step has the lowest reaction rate. Further this step also involves free radical process as presence of free radical scavengers such as BHT greatly reduced the reaction rate. On the other hand, step 3, i. e. oxidation of dihydroquinazolinone does not involve any radical process as the corresponding reaction rate was not affected by the presence of BHT. It is well reported that the



Rate (10^{-5} mol/s)	No BHT	BHT
r_1	2.7	0.6
r_2	8.3	8.3
r_3	11.1	11.1

Scheme 5.5. All the reactions were carried out using 0.5 mmol substrate, 1.0 mmol TBHP, 0.5 mmol BHT, 10 mg catalyst and 2 mL H_2O at 90 °C

solution based reactive oxygen species (ROS) derived from TBHP or other peroxides are short lived in solution and do not survive long enough to catalyze oxidation reactions. In most cases stoichiometric amount of TBHP is used to maintain the generated ROS concentration in solution for a long period.^[66] However, on nanoparticle surfaces, these ROS can be stabilized and their life time can be extended to facilitate the oxidation reactions.^[67] In our case the unprecedented catalytic activity of the Fe_3O_4 -CND and TBHP system may be attributed to the rapid decomposition of TBHP to its radicals catalyzed by Fe_3O_4 -CND and their enhanced stability on the nanoparticle surface. Further, the enhanced activity of Fe_3O_4 -CND nanocomposite compared to bare or citrate stabilized Fe_3O_4 NPs towards the formation of quinazolinones could be attributed to the cooperativity between CND and Fe_3O_4 NPs, as CNDs are known to have intrinsic peroxidase activities.

5.2.5 Recovery and reusability

The superparamagnetic nature of Fe_3O_4 -CND permits easy recovery of the catalyst from the reaction mixture with the help of a simple magnet without loss of catalyst mass followed by washing and drying (Fig. 5.5a). Further the catalyst

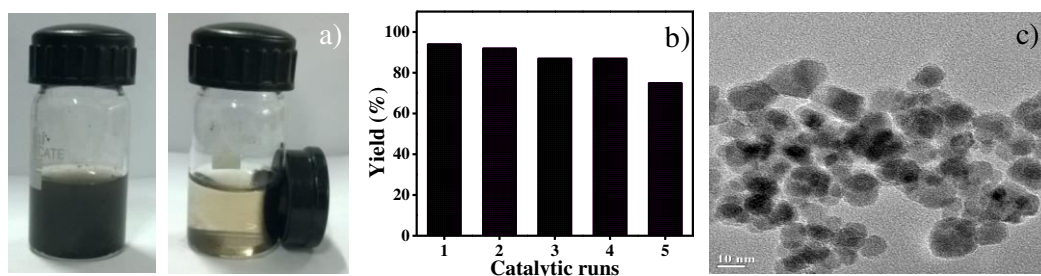


Figure 5.5. a) Digital image showing dispersion of Fe_3O_4 -CND nanoparticles in presence and absence of external magnet, b) reusability study of Fe_3O_4 -CND for the model reaction and c) TEM image of Fe_3O_4 -CND recovered after 3rd cycles of reaction

could be used for at least up to 4th cycle maintaining more than 90% of its original activity (Fig. 5.5b). However, modest decrease in catalytic activity was observed after 4th cycle of reaction. Morphological studies of Fe_3O_4 -CND recovered after 3rd cycle of reaction showed no significant changes in the particle size or agglomeration (Fig. 5.5c). On the other hand, significant decrease in catalytic activity was observed for recovered bare Fe_3O_4 NPs (34%) or Fe_3O_4 -Citrate (43%), due to loss structural integrity only after 1st cycle.

5.3 Conclusion

In conclusion, a cost-effective, stable and heterogenic carbon dot stabilized magnetic iron oxide nanoparticle composite is demonstrated as an effective catalytic system for one-pot synthesis of quinazolinones from alcohols and 2-aminobenzamides in a cyclooxidative pathway in presence of TBHP. The rapid decomposition of TBHP into its radicals (ROS) and their stability over the iron oxide surface accounts the driving force of the exceptional catalytic activity of the system. Further, inherent magnetic nature of the catalytic system renders easy recovery of the catalyst from the reaction mixture without contamination of the product as well as excellent reusability manifesting efficient catalytic activity of the system.

5.4 Experimental section

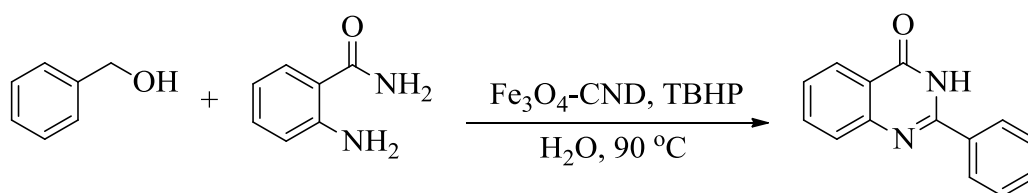
5.4.1 Generation Information

The powder XRD measurements were carried out by using a Bruker D8 Advance X-ray diffractometer with CuK α source (wavelength= 0.154 nm). TEM images were obtained by using a JEOL JEM- 2100 microscope operated at 200 kV. UV/Visible measurements were performed by using a Varian Cary 100 Bio Spectrophotometer. FTIR spectra were recorded with KBr pellets by using a Bruker Tensor 27 instrument. Emission spectra were recorded using a fluoromax-4p fluorometer from Horiba (Model: FM-100). XPS spectra were recorded by using an ESCA instrument, VSW of UK make. Magnetic susceptibility measurement was done using EverCool 7 Tesla SQUID Magnetometer. ^1H and ^{13}C NMR spectra were recorded with Bruker Advance (III) 400 MHz or 100 MHz spectrometers, respectively. Data for ^1H NMR spectra are reported as chemical shift (δ ppm), multiplicity (s=singlet, d = doublet, t = triplet, m = multiplet), coupling constant (J Hz) and integration and assignment data for ^{13}C NMR spectra are reported as a chemical shift. High resolutions mass spectral analyses (HRMS) were carried out using ESI- TOF-MS.

5.4.2 Materials and methods

Polyethylene glycol (PEG-200) we used a the carbon source to synthesize carbon nanodots was purchased from Alfa Aesar. Iron sulphate, iron chloride and sodium hydroxide were purchased from merck India and rankem respectively. *Tert*-butylhydroperoxide, hydrogen peroxide and all other chemical were purchased from Sigma aldrich and Merck India and used without further purification. We used Millipore water (ultrapure level) throughout the experiments.

5.4.3 Cyclooxidative synthesis of quinazolinones



Chapter 5

In a Teflon sealed glass tube, 1.5 mmol alcohol, 0.5 mmol 2-aminobenzamide, 193 μL TBHP, 25 mg $\text{Fe}_3\text{O}_4\text{-CND}$ and 2 mL H_2O were taken and the mixture was heated at 90 $^\circ\text{C}$ in an oil bath under magnetic stirring for 13-20 hours. The progress of the reaction was monitored by TLC. After completion of the reaction, the reaction was cooled to room temperature and the catalyst was removed by using a magnet. The resulting mixture was extracted with ethyl acetate (3x 20 ml) and successively washed with water (1x 15 ml). The organic solution was dried over anhydrous sodium sulphate and the solvent was evaporated using a rotary evaporator to get the crude reaction mixture. Further, the pure product was obtained by purifying the mixture on silica gel column chromatography (100-200 mesh) using hexane and ethyl acetate as the eluents.

5.4.4 Characterization data of quinazolinones

2-phenylquinazolin-4(3H)-one (3aa):²² Colourless solid, m.p. 231-233 $^\circ\text{C}$; ^1H NMR (CDCl_3 , 400 MHz): δ = 11.28 (br, s, 1H), 8.33-8.31 (m, 1H), 8.23-8.20 (m, 2H), 7.84-7.78 (m, 2H), 7.60-7.56 (m, 3H), 7.52-7.48 (m, 1H); ^{13}C NMR (CDCl_3 , 100 MHz): δ = 163.6, 151.6, 149.4, 134.8, 132.8, 131.6, 129.0, 128.0, 127.2, 126.8, 126.3, 120.8; HRMS (ESI): calcd for $[\text{C}_{14}\text{H}_{10}\text{N}_2\text{O}^+ + \text{Na}^+]$ 245.0685, found 245.0691.

2-(4-chlorophenyl)quinazolin-4(3H)-one (3ba):⁶⁸ m.p. >300 $^\circ\text{C}$; ^1H NMR (DMSO-d^6 , 400 MHz): δ = 12.59 (br, s, 1H), 8.20-8.18 (d, $J=8.56$ Hz, 2H), 8.15-8.14 (d, $J=7.56$ Hz, 1H), 7.84 (t, $J=7.0$ Hz, 1H), 7.74-7.72 (d, $J=8.0$ Hz, 1H), 7.63-7.60 (d, $J=8.8$ Hz, 2H), 7.52 (t, $J=7.0$ Hz, 1H); ^{13}C NMR (DMSO-d^6 , 100 MHz): δ = 181.0, 151.4, 148.2, 136.4, 134.7, 129.6, 128.7, 127.6, 126.9, 125.9, 121.0; HRMS (ESI): calcd for $[\text{C}_{14}\text{H}_9\text{ClN}_2\text{O}^+ + \text{Na}^+]$ 279.0296, found 279.0303.

2-(pyridin-2-yl)quinazolin-4(3H)-one (3ca):²³ Yellow solid, ^1H NMR (DMSO-d^6 , 400 MHz): δ = 11.79 (br, s, 1H), 8.75-8.72 (m, 1H), 8.46-8.41 (m, 1H), 8.19-8.15 (m, 1H), 8.09-8.02 (m, 1H), 7.89-7.76 (m, 2H), 7.66-7.61 (m, 1H), 7.58-7.52 (m, 1H); ^{13}C NMR (DMSO-d^6 , 100 MHz): δ = 160.7, 149.8, 148.9, 148.6, 148.4, 137.9, 134.7, 127.7, 127.3, 126.5, 126.1, 122.1, 121.9; HRMS (ESI): calcd for $[\text{C}_{13}\text{H}_9\text{N}_3\text{O}^+ + \text{Na}^+]$ 223.0746, found 223.0752.

(E)-2-styrylquinazolin-4(3H)-one (3da):⁶⁸ m.p. 224-227 °C; ¹H NMR (DMSO-d⁶, 400 MHz): δ = 12.31 (br, s, 1H), 8.11-8.09 (d, *J* = 7.8 Hz, 1H), 7.96-7.92 (d, *J* = 16.3 Hz, 1H), 7.81-7.77 (t, *J* = 7.04 Hz, 1H), 7.70-7.64 (m, 3H), 7.51-7.36 (m, 4H), 7.01-6.98 (d, *J* = 15.2 Hz, 1H); ¹³C NMR (DMSO-d⁶, 100 MHz): δ = 161.8, 159.9, 151.4, 149.0, 138.3, 135.0, 129.8, 129.1, 127.7, 126.3, 125.9, 121.1; HRMS (ESI): calcd for [C₁₆H₁₂N₂O⁺ + Na⁺] 271.0842, found 271.0853.

6-chloro-2-phenylquinazolin-4(3H)-one (3ab):²⁴ m.p. 294-296 °C; ¹H NMR (DMSO-d⁶, 400 MHz): δ = 12.69 (br, s, 1H), 8.17-8.15 (m, 2H), 8.08 (s, 1H), 7.87-7.85 (m, 1H), 7.78-7.76 (m, 1H), 7.64-7.51 (m, 3H); HRMS (ESI): calcd for [C₁₄H₉ClN₂O⁺ + Na⁺] 279.0296, found 279.0302.

2-(2-nitrophenyl)quinazolin-4(3H)-one (3ea): ¹H NMR (DMSO-d⁶, 400 MHz): δ = 12.81 (br, s, 1H), 8.21-8.19 (d, *J* = 8.28 Hz, 1H), 8.18-8.16 (d, *J* = 7.28 Hz, 1H), 7.92-7.80 (m, 4H), 7.65-7.63 (d, *J* = 8.04 Hz, 1H), 7.58-7.55 (t, *J* = 7.2 Hz, 1H); ¹³C NMR (DMSO-d⁶, 100 MHz): δ = 161.5, 151.6, 148.5, 147.4, 134.7, 133.9, 131.5, 129.1, 127.4, 127.1, 125.9, 124.5, 121.2; HRMS (ESI): calcd for [C₁₄H₉N₃O₃⁺ + Na⁺] 290.0536, found 290.0540.

2-pentylquinazolin-4(3H)-one (3fa):⁶⁸ m.p. 152-154 °C; ¹H NMR (CDCl₃, 400 MHz): δ = 12.28 (br, s, 1H), 8.27 (d, *J* = 6.86 Hz, 1H), 7.77-7.75 (m, 1H), 7.68 (d, *J* = 7.45 Hz, 1H), 7.45 (t, *J* = 7.62 Hz, 1H), 2.80 (t, *J* = 7.76 Hz, 2H), 1.92-1.87 (m, 2H), 1.46-1.39 (m, 4H), 0.92 (t, *J* = 7.76 Hz, 3H); ¹³C NMR (CDCl₃, 100 MHz): δ = 165.5, 158.2, 150.6, 135.2, 128.3, 127.8, 127.2, 121.1, 36.6, 31.9, 28.1, 22.8, 14.2; HRMS (ESI): calcd for [C₁₃H₁₆N₂O⁺ + Na⁺] 239.1155, found 239.1167.

2-hexylquinazolin-4(3H)-one (3ga):²⁰ ¹H NMR (CDCl₃, 400 MHz): δ 12.47 (br, s, 1H), 8.32 (d, *J* = 8.27 Hz, 1H), 7.78-7.75 (m, 1H), 7.75 (d, *J* = 8.32 Hz, 1H), 7.46-7.47 (m, 1H), 2.80 (t, *J* = 7.62 Hz, 2H), 1.90-1.87 (m, 2H), 1.47-1.45 (m, 2H), 1.37-1.30 (m, 4H), 0.88 (t, *J* = 6.90 Hz, 3H); ¹³C NMR (CDCl₃, 100 MHz): δ 165.3, 156.1, 149.3, 134.5, 127.4, 126.2, 126.7, 120.1, 35.8, 31.4, 28.6, 27.4, 22.4, 14.0; HRMS (ESI): calcd for [C₁₄H₁₈N₂O⁺ + Na⁺] 253.1311, found 253.1319.

Chapter 5

2-(4-bromophenyl)quinazolin-4(3H)-one (3ha):⁶⁸ m.p. 290-292 °C; ¹H NMR (DMSO-d⁶, 400 MHz): δ = 12.59 (br, s, 1H), 8.15-8.10 (m, 3H), 7.85-7.82 (t, *J* = 7.04 Hz, 1H), 7.76-7.72 (m, 3H), 7.54-7.51 (t, *J* = 7.04 Hz, 1H); ¹³C NMR (DMSO-d⁶, 100 MHz): δ = 159.7, 151.4, 148.2, 134.6, 131.6, 129.7, 127.5, 126.7, 125.8, 125.2, 121.0; HRMS (ESI): calcd for [C₁₄H₉BrN₂O⁺ + Na⁺] 322.9790, found 322.9798.

2-(*p*-tolyl)quinazolin-4(3H)-one (3ia):²² m.p. 230-232 °C; ¹H NMR (CDCl₃, 400 MHz): δ = 11.40 (br, s, 1H), 8.32-8.30 (d, *J* = 7.52 Hz, 1H), 8.12-8.10 (d, *J* = 8.28 Hz, 2H), 7.82-7.76 (m, 2H), 7.50-7.46 (t, *J* = 7.76 Hz, 1H), 7.37-7.35 (d, *J* = 8.0 Hz, 2H); ¹³C NMR (CDCl₃, 100 MHz): δ = 164.1, 151.7, 149.6, 142.1, 134.8, 130.1, 129.9, 129.7, 129.0, 127.8, 127.3, 126.5, 126.3, 120.6, 21.5; HRMS (ESI): calcd for [C₁₅H₁₂N₂O⁺ + Na⁺] 259.0842, found 259.0848.

2-(4-methoxyphenyl)quinazolin-4(3H)-one (3ja):²² m.p. 230-233 °C; ¹H NMR (CDCl₃, 400 MHz): δ = 10.80 (br, s, 1H), 8.30-8.28 (d, *J* = 7.52 Hz, 1H), 8.14-8.12 (d, *J* = 8.0 Hz, 2H), 7.78 (m, 2H), 7.46 (m, 1H), 7.07-7.05 (d, *J* = 8.04 Hz, 2H), 3.90 (s, 3H); HRMS (ESI): calcd for [C₁₅H₁₂N₂O₂⁺ + Na⁺] 275.0791, found 275.0798.

2-(furan-2-yl)quinazolin-4(3H)-one (3la):⁶⁸ m.p. 272-275 °C; ¹H NMR (DMSO-d⁶, 400 MHz): δ = 12.48 (br, s, 1H), 8.12-8.10 (d, *J* = 8.04 Hz, 1H), 7.99 (m, 1H), 7.82-7.78 (t, *J* = 8.52 Hz, 1H), 7.68-7.66 (d, *J* = 8.0 Hz, 1H), 7.62-7.61 (d, *J* = 3.52 Hz, 1H), 7.50-7.46 (t, *J* = 7.04 Hz, 1H), 6.74-6.73 (m, 1H); ¹³C NMR (DMSO-d⁶, 100 MHz): δ = 161.5, 148.6, 146.5, 146.0, 144.0, 134.6, 127.2, 126.4, 125.9, 121.1, 114.5, 112.5; HRMS (ESI): calcd for [C₁₂H₈N₂O₂⁺ + Na⁺] 235.0478, found 235.0479.

2-(thiophen-2-yl)quinazolin-4(3H)-one (3ma):⁶⁸ m.p. 220-222 °C; ¹H NMR (DMSO-d⁶, 400 MHz): δ = 12.63 (br, s, 1H), 8.22-8.21 (d, *J* = 4.76 Hz, 1H), 8.12-8.10 (d, *J* = 7.8 Hz, 1H), 7.86-7.85 (d, *J* = 5.76 Hz, 1H), 7.81-7.77 (t, *J* = 8.52 Hz, 1H), 7.65-7.63 (d, *J* = 8.0 Hz, 1H), 7.49-7.45 (t, *J* = 8.04 Hz, 1H), 7.23-7.21 (m, 1H); ¹³C NMR (DMSO-d⁶, 100 MHz): δ = 161.8, 148.6, 147.8, 137.3, 134.7, 132.1, 129.4, 128.5, 126.9, 126.3, 125.9, 120.8; HRMS (ESI): calcd for [C₁₂H₈N₂OS⁺ + Na⁺] 251.0250, found 251.0252.

2-phenyl-2,3-dihydroquinazolin-4(1H)-one (A): Colorless crystal (217 mg, 97%), ^1H NMR (400 MHz, CDCl_3): δ 7.94 (d, $J = 7.76$ Hz, 1H), 7.60 (m, 2H), 7.44 (m, 3H), 7.33 (t, $J = 7.52$ Hz, 1H), 6.90 (t, $J = 7.76$ Hz, 1H), 6.67 (d, $J = 8.04$ Hz, 1H), 5.90 (s, 1H), 5.88 (br, 1H, NH), 4.35 (br, 1H, NH), ^{13}C NMR (100 MHz, $\text{DMSO}-d_6$): δ 164.0, 148.3, 142.1, 133.8, 128.9, 128.8, 127.8, 127.3, 117.6, 115.4, 114.8, 67.0; HRMS (ESI): calcd for $[\text{C}_{14}\text{H}_{12}\text{N}_2\text{O} + \text{Na}^+]$ 247.0842, found 247.0864.

5.5 References

1. Sui-Seng C., Freutel F., Lough A. J., Morris R. H. (2008), Highly efficient catalyst systems using iron complexes with a tetradentate PNNP ligand for the asymmetric hydrogenation of polar bonds, *Angew. Chem. Int. Ed.*, 47, 940-943 (DOI: 10.1002/anie.200705115)
2. Rao H., Li C. -J. (2011), Rearrangement of 2-Aryloxybenzaldehydes to 2-Hydroxybenzophenones by Rhodium-Catalyzed Cleavage of Aryloxy C-O Bonds, *Angew. Chem. Int. Ed.*, 50, 8936 –8939 (DOI: 10.1002/anie.201103599)
3. Chase P. A., Jurca T., Stephan D. W. (2008), Lewis acid-catalyzed hydrogenation: $\text{B}(\text{C}_6\text{F}_5)_3$ -mediated reduction of imines and nitriles with H_2 , *Chem. Commun.*, 1701–1703 (DOI: 10.1039/b718598g)
4. Campeau L.-C., Schipper D. J., Fagnou K. (2008), Site-selective sp^2 and benzylic sp^3 palladium-catalyzed direct arylation, *J. Am. Chem. Soc.*, 130, 3266–3267 (DOI: 10.1021/ja710451s)
5. Gawande M. B., Branco P. S., Varma R. S. (2013), Nano-magnetite (Fe_3O_4) as a support for recyclable catalysts in the development of sustainable methodologies, *Chem. Soc. Rev.*, 42, 3371–3393 (DOI: 10.1039/c3cs35480f)
6. Baig R. B. N., Varma R. S. (2013), Magnetically retrievable catalysts for organic synthesis, *Chem. Commun.*, 49, 752–770 (DOI: 10.1039/c2cc35663e)

Chapter 5

- Baig R. B. N., Varma R. S. (2013), Organic synthesis via magnetic attraction: Benign and sustainable protocols using magnetic nanoferrites, *Green Chem.*, 15, 398–417 (DOI: 10.1039/c2gc36455g)
- Cole-Hamilton D. J., Tooze R. P., (2006) Catalyst separation, recovery and recycling: Chemistry and process design, Springer.
- Horton D. A., Bourne G. T., Smythe M. L. (2003), The combinatorial synthesis of bicyclic privileged structures or privileged substructures, *Chem. Rev.*, 103, 893-930 (DOI: 10.1021/cr020033s)
- Huang C., Fu Y., Fu H., Jiang Y., Zhao Y. (2008), Highly efficient copper-catalyzed cascade synthesis of quinazoline and quinazolinone derivatives, *Chem. Commun.*, 6333-6335 (DOI: 10.1039/b814011a)
- Xu W., Jin Y., Liu H., Jiang Y., Fu H. (2011), Copper-catalyzed domino synthesis of quinazolinones via Ullmann-type coupling and aerobic oxidative C-H amidation, *Org. Lett.*, 13, 1274-1277 (DOI: 10.1021/ol1030266)
- Xu W., Fu H. (2011), Amino acids as the nitrogen-containing motifs in copper-catalyzed domino synthesis of N-heterocycles, *J. Org. Chem.*, 76, 3846-3852 (DOI: 10.1021/jo2002227)
- Xu, L. Jiang Y., Ma D. (2012), Synthesis of 3-substituted and 2,3-disubstituted quinazolinones via Cu-catalyzed aryl amidation, *Org. Lett.*, 14, 1150-1153 (DOI: 10.1021/ol300084v)
- Hisano T., Ichikawa M., Nakagawa A., Tsuji M. (1975), Studies on organosulfur compounds. xii. syntheses and pharmacological activities of 2-heterocyclic substituted 4(3H)-quinazolinones, *Chem. Pharm. Bull.*, 23, 1910-1916 (DOI: 10.1248/cpb.23.1910)
- Abdel-Jalil R. J., Aldoqum H. M., Ayoub M. T., Voelter W. (2005), Synthesis and antitumor activity of 2-aryl-7-fluoro-6-(4-methyl-1-piperazinyl)-4(3H)-quinazolinones, *Heterocycles*, 65, 2061-2070 (DOI: 10.3987/COM-05-10387)

Chapter 5

16. Mitobe Y., Ito S., Mizutani T., Nagase T., Sato N., Tokita S. (2009), Development of a selective and potent radioactive ligand for histamine H₃ receptors: A compound potentially useful for receptor occupancy studies, *Bioorg. Med. Chem. Lett.*, 19, 4075-4078 (DOI: 10.1016/j.bmcl.2009.06.025)
17. Bakavoli M., Shiri A., Ebrahimpour Z., Rahimizadeh M. (2008), Clean heterocyclic synthesis in water: I₂/KI catalyzed one-pot synthesis of quinazolin-4(3H)-ones, *Chin. Chem. Lett.*, 19, 1403-1406 (DOI: 10.1016/j.ccllet.2008.07.016)
18. Balakumar C., Lamba P., Kishore D. P., Narayana B. L., Rao K. V., Rajwinder K., Rao A. R., Shireesha B., Narsaiah B. (2010), Synthesis, anti-inflammatory evaluation and docking studies of some new fluorinated fused quinazolines, *Eur. J. Med. Chem.*, 45, 4904-4913 (DOI: 10.1016/j.ejmech.2010.07.063)
19. Ge W., Zhu X., Wei Y. (2013), Iodine-catalyzed oxidative system for cyclization of primary alcohols with o-aminobenzamides to quinazolinones using DMSO as the oxidant in dimethyl carbonate, *RSC Adv.*, 3, 10817-10822 (DOI: 10.1039/C3RA40872H)
20. Sharif M., Opalach J., Langer P., Beller M., Wu X.-F. (2014), Oxidative synthesis of quinazolinones and benzothiadiazine 1,1-dioxides from 2-aminobenzamide and 2-aminobenzenesulfonamide with benzyl alcohols and aldehydes, *RSC Adv.*, 4, 8-17 (DOI: 10.1039/c3ra45765f)
21. Watson A. J. A., Maxwell A. C., Williams J. M. (2012), Ruthenium-catalysed oxidative synthesis of heterocycles from alcohols, *Org. Biomol. Chem.*, 10, 240-243 (DOI: 10.1039/c1ob06516e)
22. Hikawa H., Ino Y., Suzuki H., Yokoyama Y. (2012), Pd-Catalyzed benzylic C–H amidation with benzyl alcohols in water: A strategy To construct quinazolinones, *J. Org. Chem.*, 77, 7046-7051 (DOI: 10.1021/jo301282n)

Chapter 5

23. Siddiki S. M. A. H., Kon K., Touchy A. S., Shimizu K. (2014), Direct synthesis of quinazolinones by acceptorless dehydrogenative coupling of o-aminobenzamide and alcohols by heterogeneous Pt catalysts, *Catal. Sci. Technol.*, 4, 1716–1719 (DOI: 10.1039/c4cy00092g)
24. Zhou J., Fang J. (2011), One-pot synthesis of quinazolinones via iridium-catalyzed hydrogen transfers, *J. Org. Chem.*, 76, 7730-7736 (DOI: 10.1021/jo201054k)
25. Polshettiwar V., Varma R. S. (2010), Green chemistry by nanocatalysis, *Green Chem.*, 12, 743-754 (DOI: 10.1039/b921171c)
26. Molenbroek A. M., Helveg S., Topsøe H., Clausen B. S. (2009), Nanoparticles in heterogeneous catalysis, *Top. Catal.*, 52, 1303-1311 (DOI: 10.1007/s11244-009-9314-1)
27. Astruc D., Lu F., Aranzaes J. R. (2005), Nanoparticles as recyclable catalysts: The frontier between homogeneous and heterogeneous catalysis, *Angew. Chem., Int. Ed.*, 44, 7852–7872 (DOI: 10.1002/anie.200500766)
28. Varma R. S. (2013), Greener routes to organics and nanomaterials: Sustainable applications of nanocatalysts, *Pure Appl. Chem.*, 85, 1703–1710 (DOI:10.1351/PAC-CON-13-01-15)
29. Jin X., Yamaguchi K., Mizuno N. (2014), Gold-catalyzed heterogeneous aerobic dehydrogenative amination of α,β -unsaturated aldehydes to enaminals, *Angew. Chem., Int. Ed.*, 53, 455–458 (DOI: 10.1002/anie.201308260)
30. Zhang Q., Deng W., Wang Y. (2011), Effect of size of catalytically active phases in the dehydrogenation of alcohols and the challenging selective oxidation of hydrocarbons, *Chem. Commun.*, 47, 9275–9292 (DOI: 10.1039/c1cc11723h)
31. Zhao G., Wu X.-P., Chai R., Zhang Q., Gong X.-Q., Huang J., Lu Y. (2015), Tailoring nano-catalysts: Turning gold nanoparticles on bulk

- metal oxides to inverse nano-metal oxides on large gold particles, *Chem. Commun.*, 51, 5975–5978 (DOI: 10.1039/c5cc00016e)
32. Wang Y., Wang F., Zhang C., Zhang J., Li M., Xu J. (2014), Transformylating amine with DMF to formamide over CeO₂ catalyst, *Chem. Commun.*, 50, 2438–2441 (DOI: 10.1039/c3cc48400a)
33. Wang Y., Wang F., Song Q., Xin Q., Xu S., Xu J. (2013), Heterogeneous ceria catalyst with water-tolerant lewis acidic sites for one-pot synthesis of 1,3-diols via Prins condensation and hydrolysis reactions, *J. Am. Chem. Soc.*, 135, 1506–1515 (DOI: 10.1021/ja310498c)
34. Guo Z., Liu B., Zhang Q., Deng W., Wang Y., Yang Y. (2014), Recent advances in heterogeneous selective oxidation catalysis for sustainable chemistry, *Chem. Soc. Rev.*, 43, 3480–3524 (DOI: 10.1039/c3cs60282f)
35. Venkanna A., Swapna K., Rao P. V. (2014), Recyclable nano copper oxide catalyzed synthesis of quinoline-2,3-dicarboxylates under ligand free conditions, *RSC Adv.*, 4, 15154–15160 (DOI: 10.1039/c3ra47212d)
36. Zhang Z., Wang M., Zhang C., Zhang Z., Lu J., Wang F. (2015), The cascade synthesis of quinazolinones and quinazolines using an α -MnO₂ catalyst and *tert*-butyl hydroperoxide (TBHP) as an oxidant, *Chem. Commun.*, 51, 9205–9207 (DOI: 10.1039/c5cc02785c)
37. Polshettiwar V., Luque R., Fihri A., Zhu H., Bouhrara M., Bassett, J.-M. (2011), Magnetically recoverable nanocatalysts, *Chem. Rev.*, 111, 3036–3075 (DOI: 10.1021/cr100230z)
38. Lu A. H., Salabas E. L., Schüth F. (2007), Magnetic nanoparticles: Synthesis, protection, functionalization, and application, *Angew. Chem., Int. Ed.*, 46, 1222–1244 (DOI: 10.1002/anie.200602866)
39. Lim S. Y., Shen W., Gao Z. (2015), Carbon quantum dots and their applications, *Chem. Soc. Rev.*, 44, 362–381 (DOI:10.1039/C4CS00269E)

Chapter 5

40. Yang S. -T., Cao L., Luo P. G., Lu F., Wang X., Wang H. *et al.*(2009), Carbon dots for optical imaging in vivo, *J. Am. Chem. Soc.*, 131, 11308-11309 (DOI: 10.1021/ja904843x)
41. Cao L., Wang X., Mezziani M. J., Lu F., Wang H., Luo P. G. *et al.* (2007), Carbon dots for multiphoton bioimaging, *J. Am. Chem. Soc.*, 129, 11318-11319 (DOI: 10.1021/ja073527l)
42. Dong Y., Wang R., Li G., Chen C., Chi Y., Chen G. (2012), Polyamine-functionalized carbon quantum dots as fluorescent probes for selective and sensitive detection of copper ions, *Anal. Chem.*, 84, 6220-6224 (DOI: 10.1021/ac3012126)
43. Zhu S., Meng Q., Wang L., Zhang J., Song Y., Jin H. *et al.*(2013), Highly photoluminescent carbon dots for multicolor patterning, sensors, and bioimaging, *Angew. Chem. Int. Ed.*, 52, 3953-3957 (DOI: 10.1002/anie.201300519)
44. Li H., He X., Kang Z., Huang H., Liu Y., Liu J. *et al.* (2010), Water soluble fluorescent carbon quantum dots and photocatalyst design, *Angew. Chem. Int. Ed.*, 49, 4430-4434 (DOI: 10.1002/anie.200906154)
45. Liu J., Liu Y., Liu N., Han Y., Zhang X., Huang H. *et al.* (2015), Metal-free efficient photocatalyst for stable visible water splitting via a two-electron pathway, *Science*, 347, 970-974 (DOI: 10.1126/science.aaa3145)
46. Li X., Rui M., Song J., Shen Z., Zeng H. (2015), Carbon and graphene quantum dots for optoelectronic and energy devices: a review, *Adv. Funct. Mater.*, 25, 4929-4947 (DOI: 10.1002/adfm.201501250)
47. Choi H., Ko S. -J., Choi Y., Joo P., Kim T., Lee B. R. *et al.* (2013), Versatile surface plasmon resonance of carbon-dot-supported silver nanoparticles in polymer optoelectronic devices, *Nat. Photon.*, 7, 732-738 (DOI: 10.1038/nphoton.2013.181)
48. Luo P., Li C., Shi G. (2012), Synthesis of gold@ carbon dots composite nanoparticles for surface enhanced Raman scattering, *Phys. Chem. Chem. Phys.*, 14, 7360-7366 (DOI:10.1039/C2CP40767A)

49. Qin X., Lu W., Asiri A. M., Al-Youbi A. O., Sun X., Green X. (2013), Low-cost synthesis of photoluminescent carbon dots by hydrothermal treatment of willow bark and their application as an effective photocatalyst for fabricating Au nanoparticles–reduced graphene oxide nanocomposites for glucose detection, *Catal. Sci. Technol.*, 3, 1027-1035 (DOI:10.1039/C2CY20635H)
50. Dey D., Bhattacharya T., Majumdar B., Mandani S., Sharma B., Sarma T. K. (2013), Carbon dot reduced palladium nanoparticles as active catalysts for carbon–carbon bond formation, *Dalton Trans.*, 42, 13821-13825 (DOI:10.1039/C3DT51234G)
51. Gholinejad M., Seyedhamzeh M., Razeghi M., Najera C., Zareh M. K. (2016), Iron oxide nanoparticles modified with carbon quantum nanodots for the stabilization of palladium nanoparticles: An efficient catalyst for the suzuki reaction in aqueous media under mild conditions, *ChemCatChem*, 8, 441-447 (DOI: 10.1002/cctc.201500925)
52. Shi W., Wang Q., Long Y., Cheng Z., Chen S., Zheng H., Huang Y. (2011), Carbon nanodots as peroxidase mimetics and their applications to glucose detection, *Chem Comm.*, 47, 6695-6697 (DOI: 10.1039/c1cc11943e)
53. Zhao Y., Zuo S., Miao M. (2017), The effect of oxygen on the microwave-assisted synthesis of carbon quantum dots from polyethylene glycol, *RSC Adv.*, 7, 16637-16643 (DOI: 10.1039/C7RA01804E)
54. Yang G., Wan X., Su Y., Zeng X., Tang J. (2016), Acidophilic S-doped carbon quantum dots derived from cellulose fibers and their fluorescence sensing performance for metal ions in an extremely strong acid environment, *J. Mater. Chem. A*, 4, 12841-12849 (DOI: 10.1039/c6ta05943k)
55. Yang X., Chen C., Li J., Zhao G., Ren X., Wang X. (2012), Graphene oxide-iron oxide and reduced graphene oxide-iron oxide hybrid materials for the removal of organic and inorganic pollutants, *RSC Adv.*, 2, 8821-8826 (DOI: 10.1039/C2RA20885G)

Chapter 5

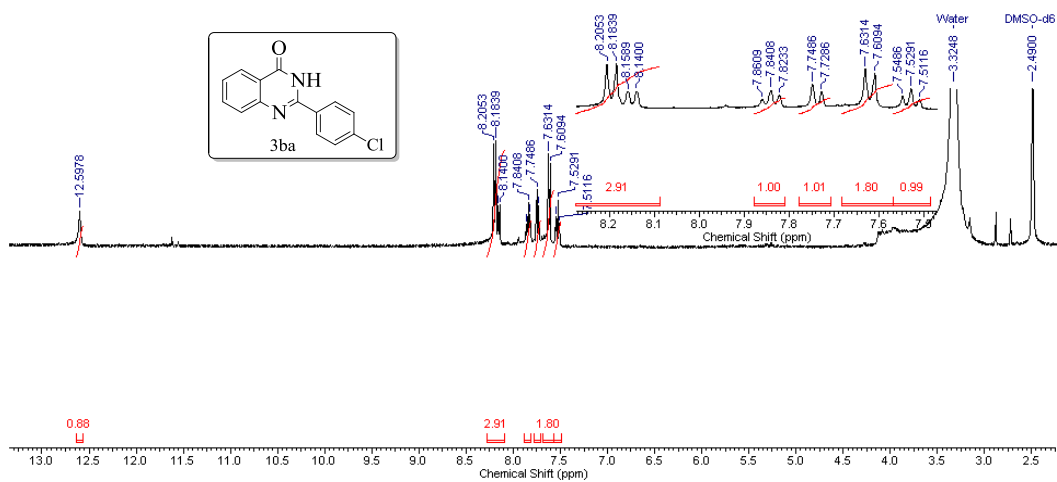
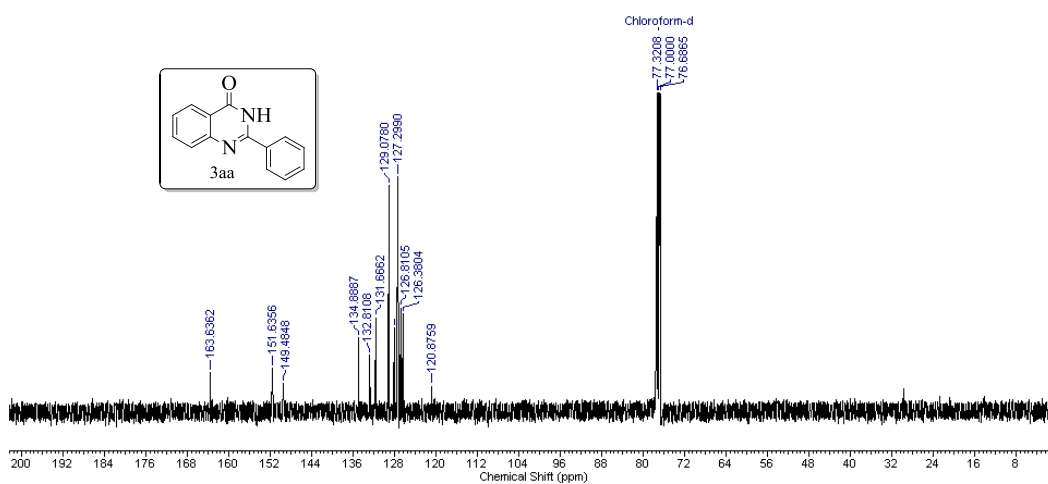
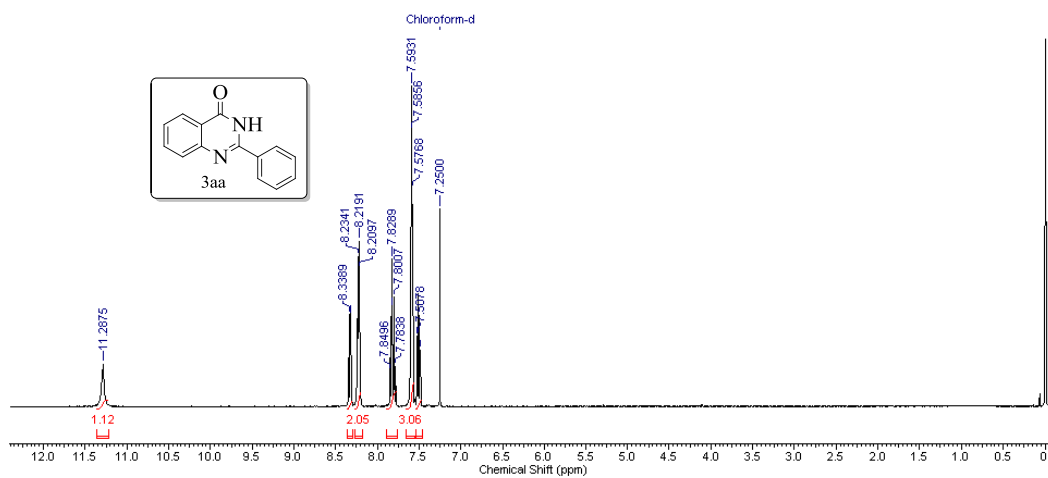
56. Wu X. L., Wang L., Chen C. L., Xu A. W., Wang X. K. (2011), Water-dispersible magnetite-graphene-LDH composites for efficient arsenate removal, *J. Mater. Chem.*, 21, 17353-17359 (DOI: 10.1039/C1JM12678D)
57. Chandra V., Park J., Chun Y., Lee J. W., Hwang I. C., Kim, K. S. (2010), Water-dispersible magnetite-reduced graphene oxide composites for arsenic removal, *ACS nano*, 4, 3979-3986 (DOI: 10.1021/nn1008897)
58. Geng Z., Lin Y., Yu X., Shen Q., Ma L., Li Z., Wang X. (2012), Highly efficient dye adsorption and removal: A functional hybrid of reduced graphene oxide-Fe₃O₄ nanoparticles as an easily regenerative adsorbent, *J. Mater. Chem.*, 22, 3527-3535 (DOI: 10.1039/C2JM15544C)
59. Huang D., Li X. J., Xu F. X., Li L. H., Lin X. F. (2013), Highly enantioselective synthesis of dihydroquinazolinones catalyzed by SPINOL-phosphoric acids, *ACS Catal.*, 3, 2244-2247 (DOI: 10.1021/cs400591u)
60. Honjo T., Phipps R. J., Rauniyar V., Toste F. D. (2012), A doubly axially chiral phosphoric acid catalyst for the asymmetric tandem oxyfluorination of enamides, *Angew. Chem., Int. Ed.*, 51, 9684-9688 (DOI: 10.1002/anie.201205383)
61. Wu X. F., Bheeter C. B., Neumann H., Dixneuf P. H., Beller M. (2012), Lewis acid-catalyzed oxidation of benzylamines to benzamides, *Chem. Commun.*, 48, 12237-12239 (DOI: 10.1039/c2cc37149a)
62. Wang L., Zhu H., Guo S. J., Cheng J., Yu J. T. (2014), TBHP-promoted sequential radical silylation and aromatisation of aryl isonitriles with silanes, *Chem. Commun.*, 50, 10864-10867 (DOI: 10.1039/c4cc04773g)
63. Tu H. Y., Liu Y. R., Chu J. J., Hu B. L., Zhang X. G. (2014), FeCl₃-promoted carboxamidation and cyclization of aryl isonitriles with formamides toward phenanthridine-6-carboxamides, *J. Org. Chem.*, 79, 9907-9912 (DOI: 10.1021/jo502022c)

64. Ratnikov M. O., Doyle M. P. (2013), Mechanistic investigation of oxidative Mannich reaction with tert-butyl hydroperoxide. The role of transition metal salt, *J. Am. Chem. Soc.*, 135, 1549–1557 (DOI: 10.1021/ja3113559)
65. Luo J. Y., Hua H. L., Chen Z. S., Zhou Z. Z., Yang Y. F., Zhou P. X., He Y. T., Liu X. Y., Liang Y. M. (2014), Metal-free cascade radical cyclization of 1,6-enynes with aldehydes, *Chem. Commun.*, 50, 1564–1566 (DOI: 10.1039/c3cc48339h)
66. Tan J., Zheng T., Yu Y., Xu K. (2017), TBHP-promoted direct oxidation reaction of benzylic Csp³–H bonds to ketones, *RSC Adv.*, 7, 15176–15180 (DOI: 10.1039/C7RA00352H)
67. Bin Saiman M. I., Brett G. L., Tiruvalam R., Forde M. M., Sharples K., Thetford A., Jenkins R. L., Dimitratos N., Lopez-Sanchez J. A., Murphy D. M., Bethell D., Willock D. J., Taylor S. H., Knight D. W., Kiely C. J., Hutchings G. J. (2012), Involvement of surface-bound radicals in the oxidation of toluene using supported Au-Pd nanoparticles, *Angew. Chem. Int. Ed.*, 51, 5981–5985 (DOI: 10.1002/anie.201201059)
68. Upadhyaya K., Thakur R. K., Shukla S. K., Tripathi R. P. (2016), One-pot copper(I)-catalyzed ligand/base-free tandem cyclooxidative synthesis of quinazolinones, *J. Org. Chem.*, 81, 5046–5055 (DOI: 10.1021/acs.joc.6b00599)

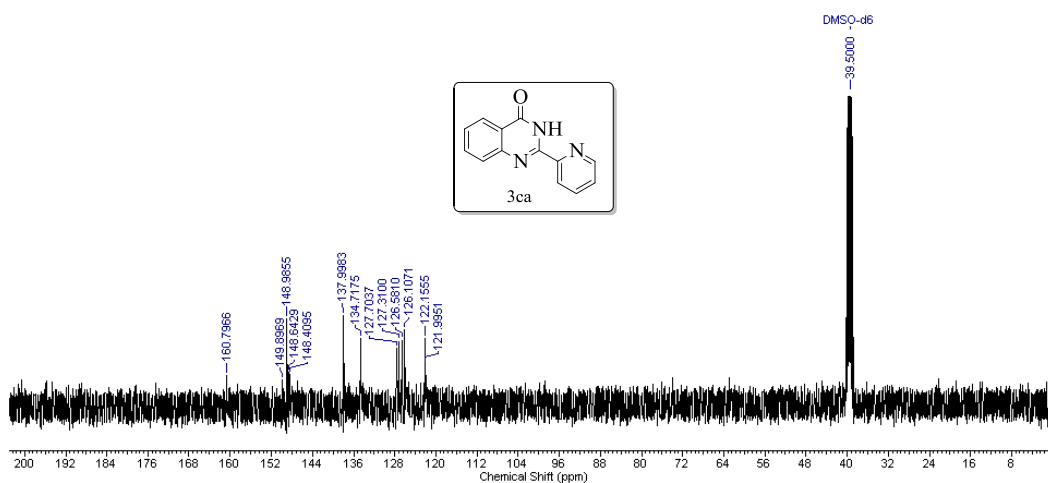
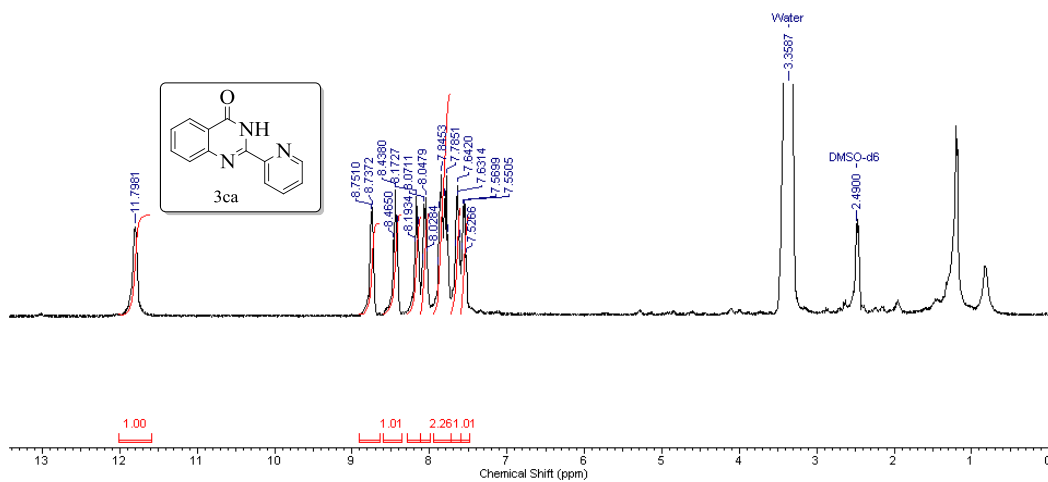
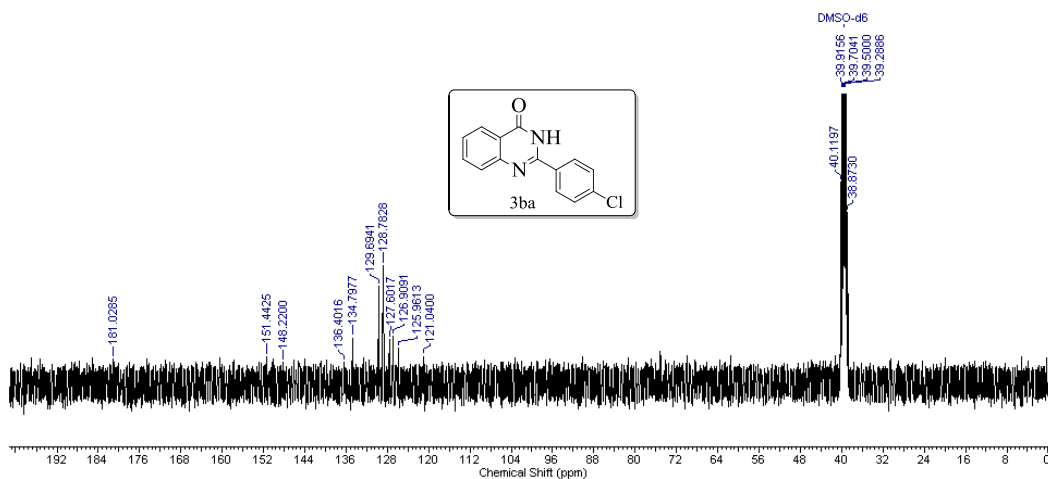
Appendix-Chapter 5

^1H and ^{13}C NMR Spectra of Quinazolinones

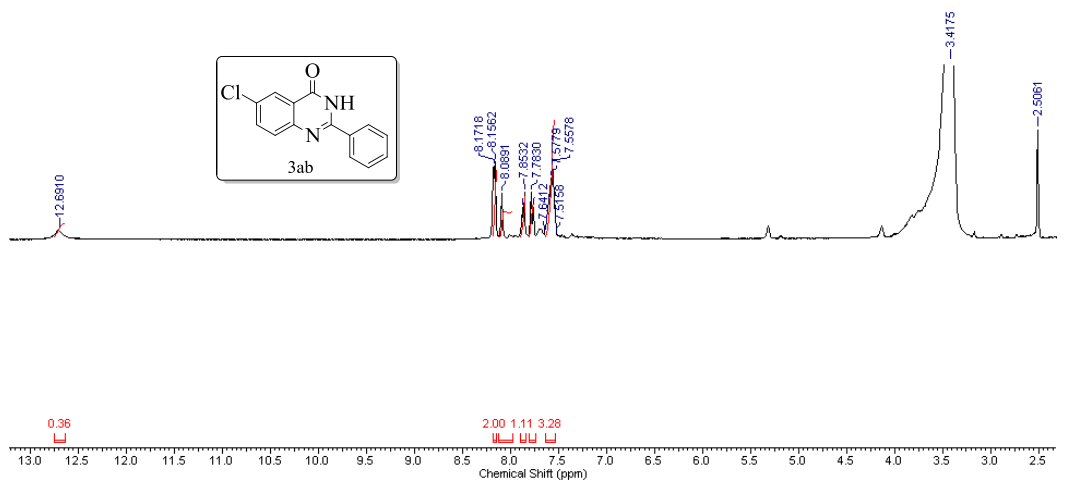
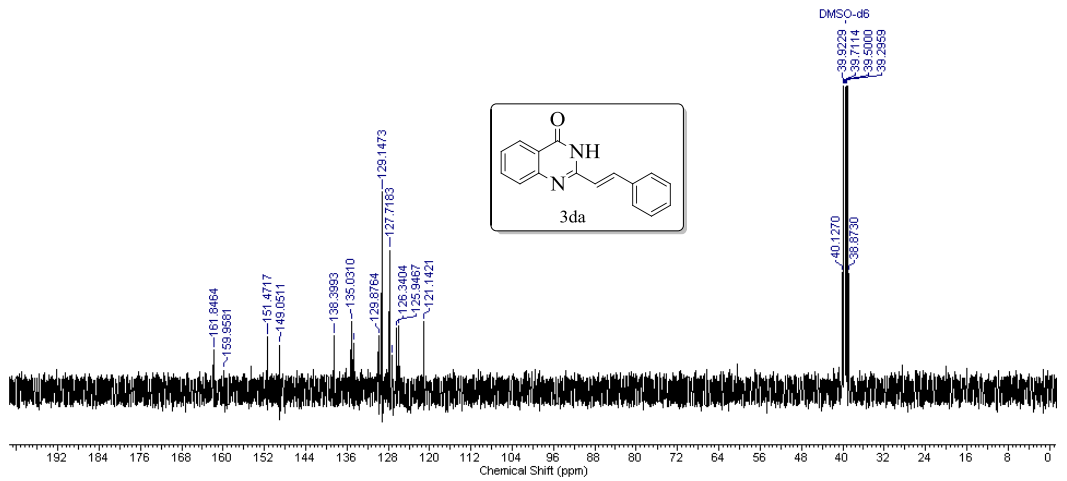
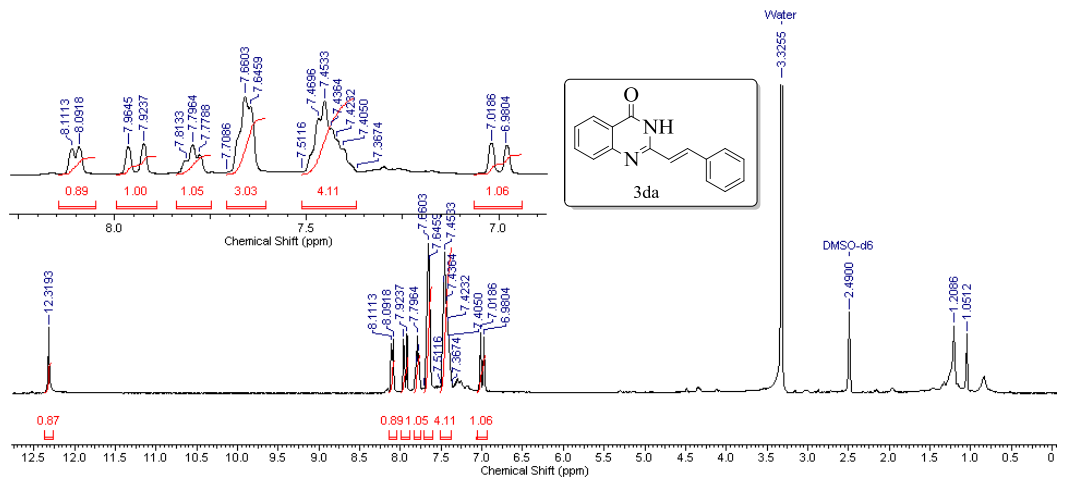
Chapter 5



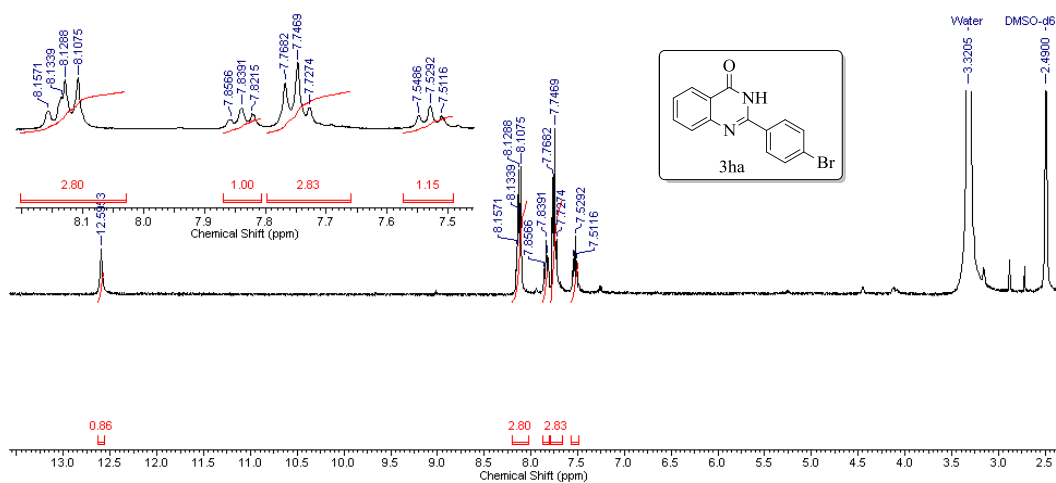
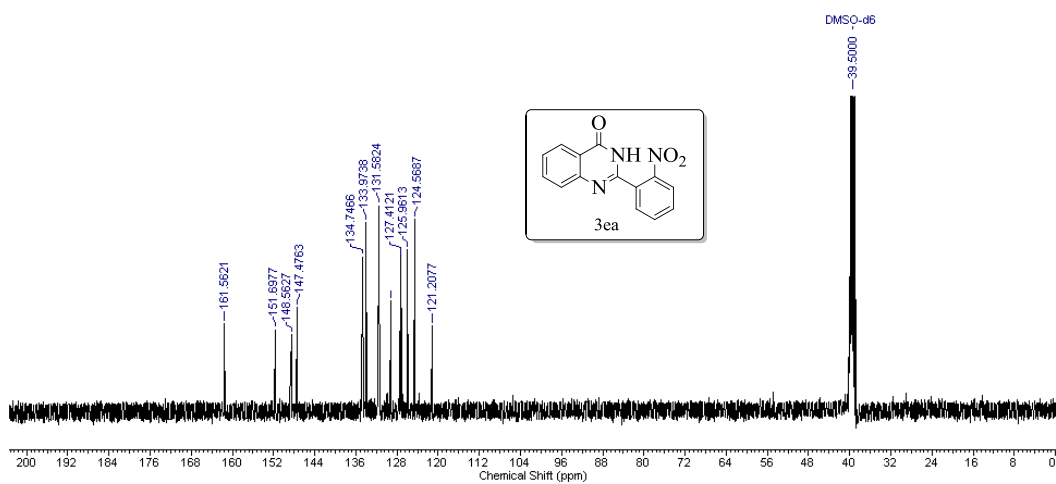
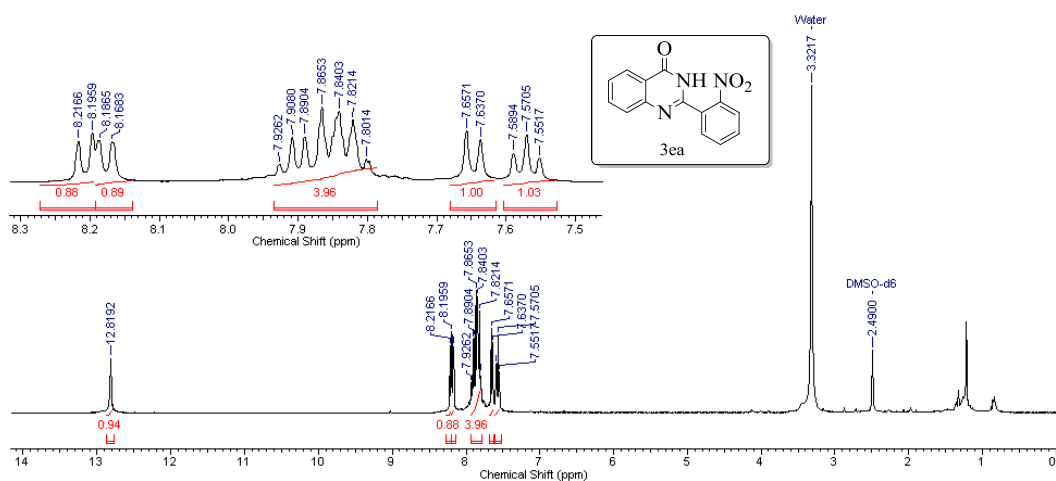
Chapter 5



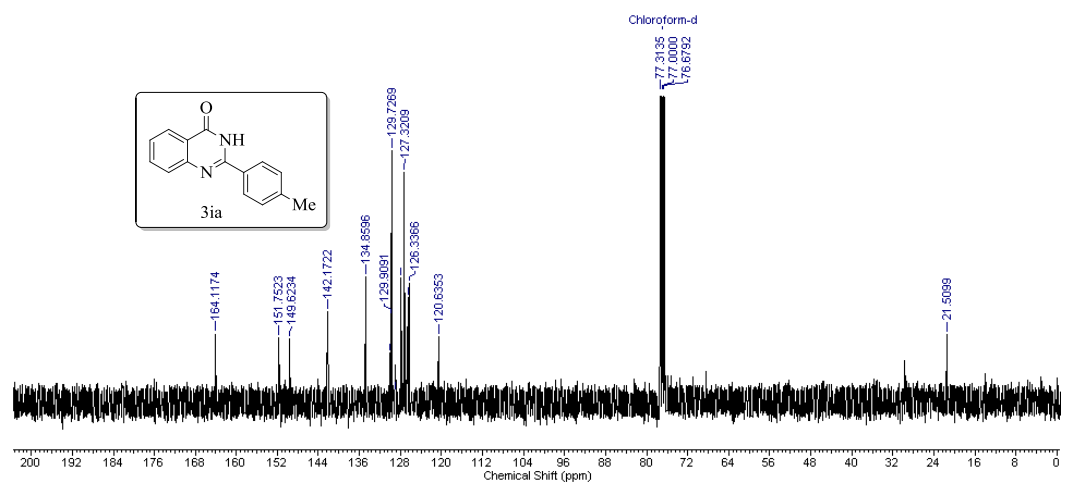
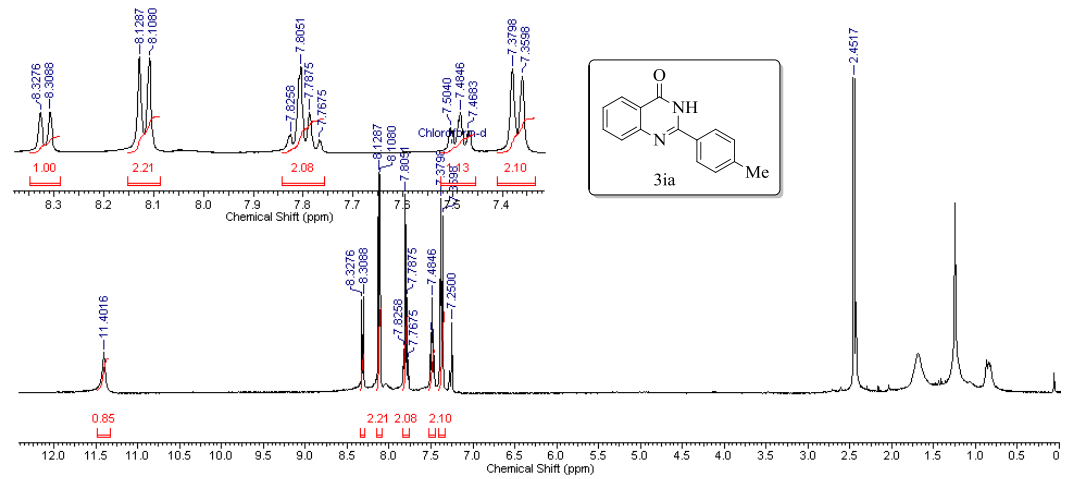
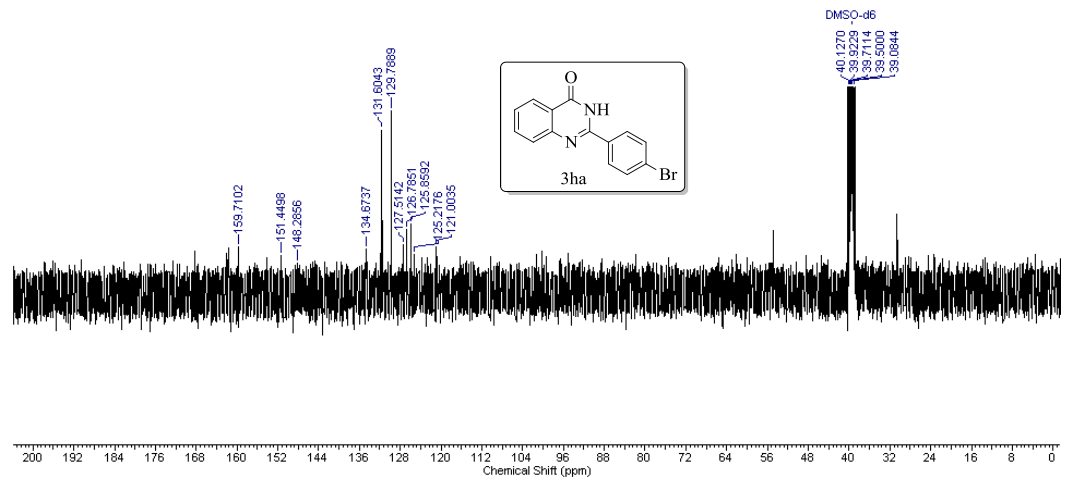
Chapter 5



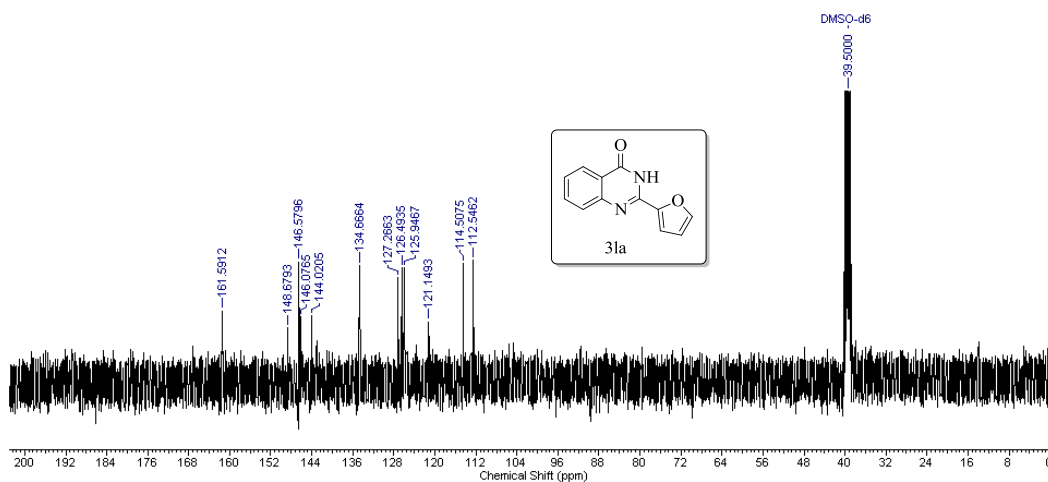
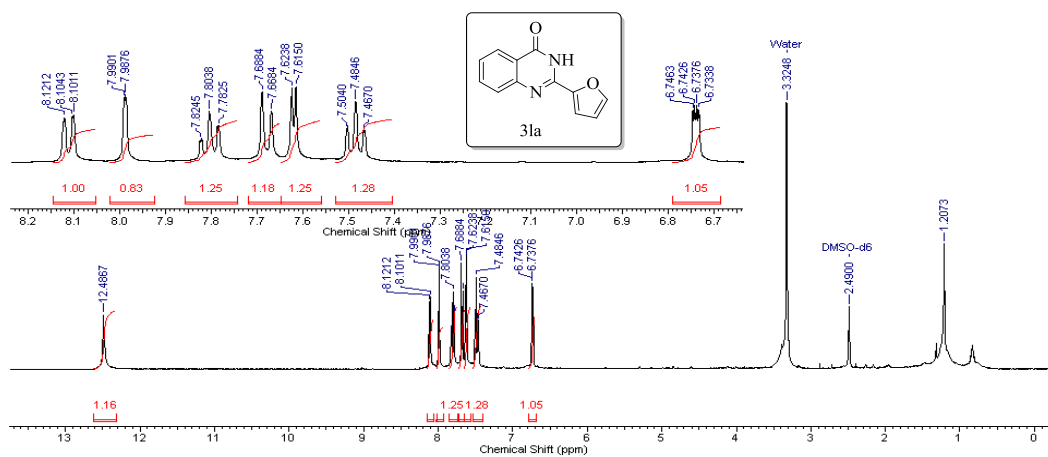
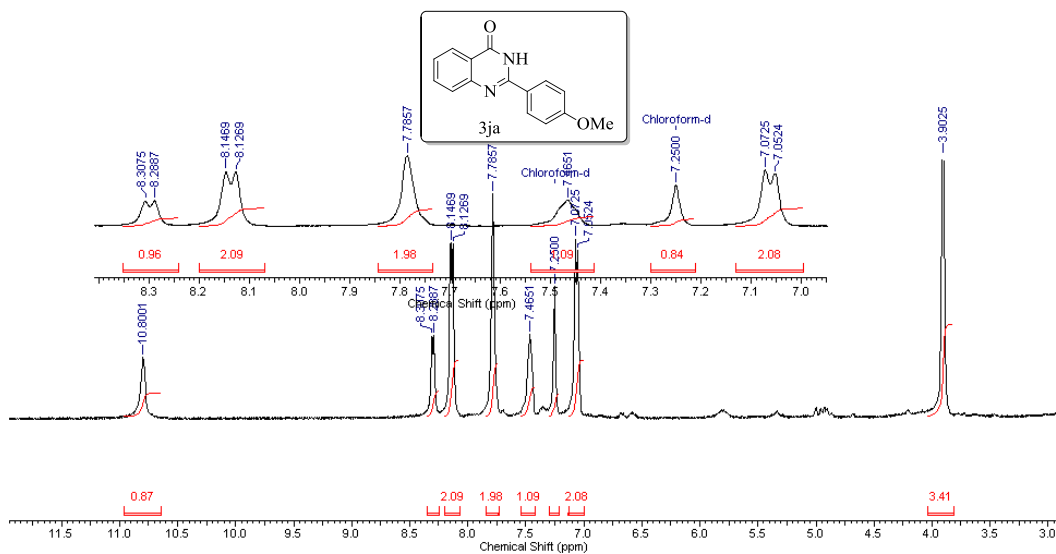
Chapter 5



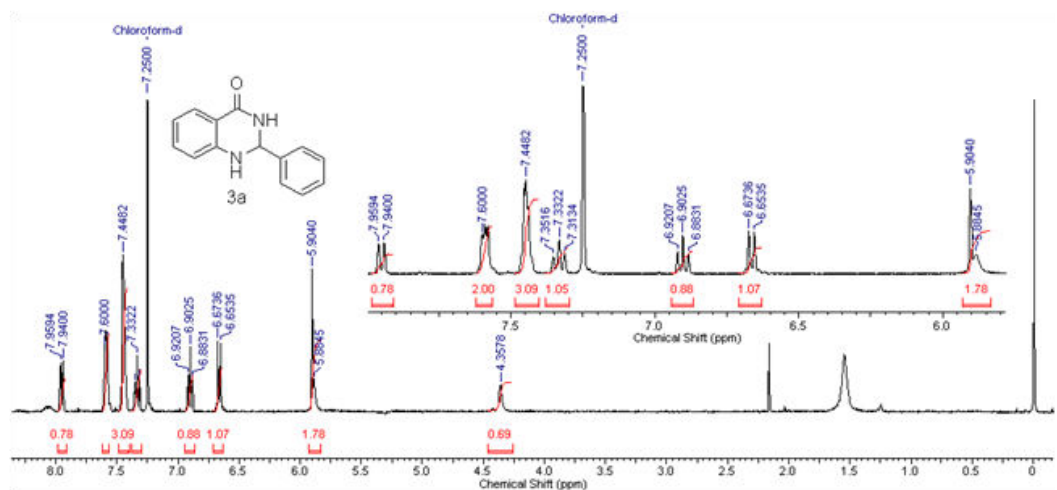
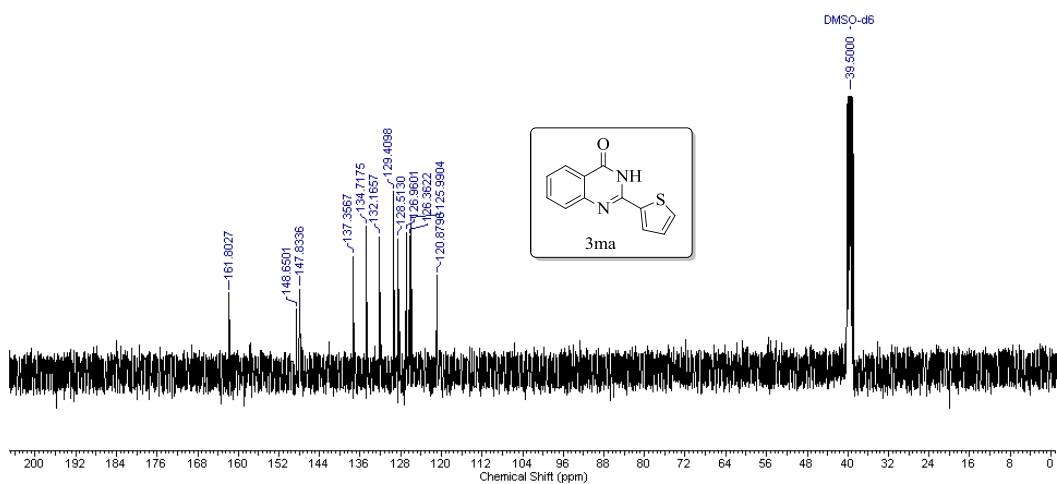
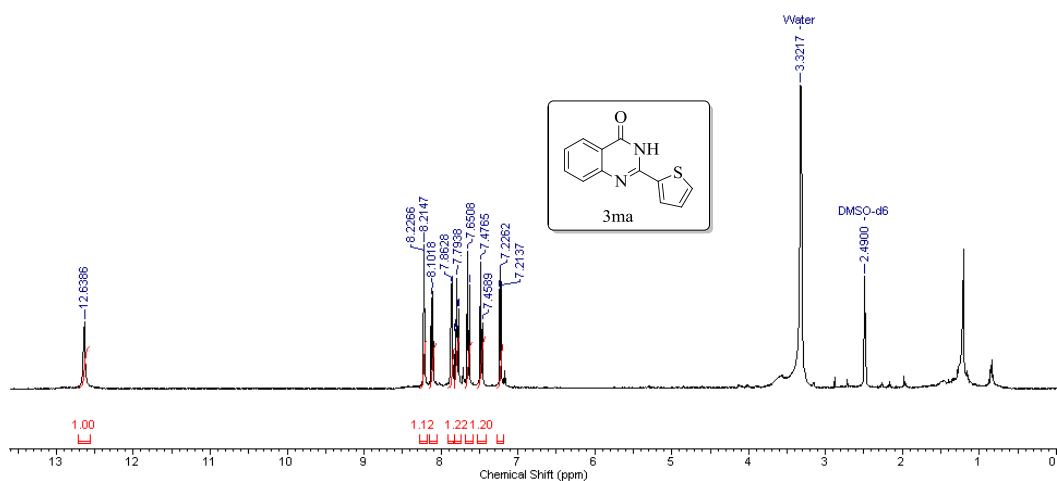
Chapter 5



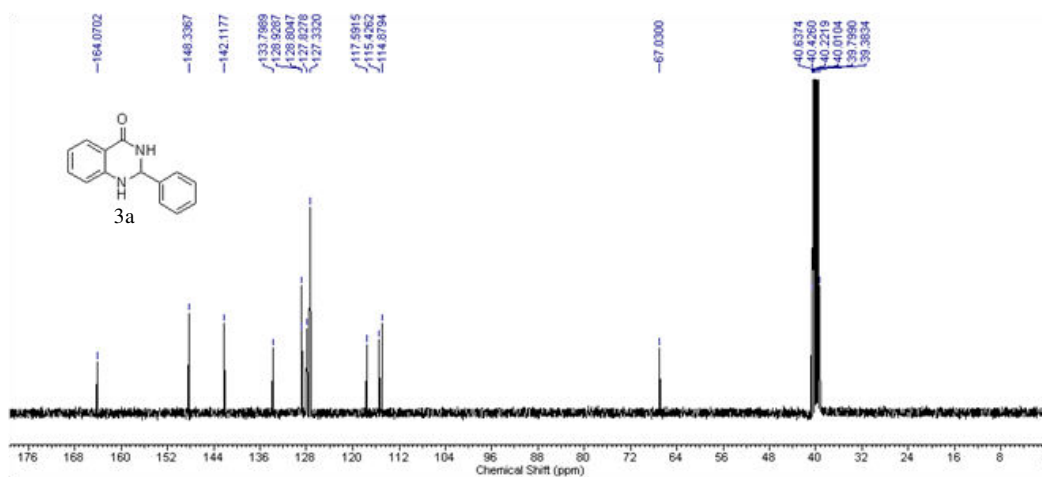
Chapter 5



Chapter 5



Chapter 5



Chapter 6

Conclusion and Future Outlook

Chapter 6

6.1 Conclusion

In this thesis, we have explored the inherent carbocatalytic activity of graphene oxide and carbon nanodots towards different organic transformations. The mild acidic behaviour rendered by carboxylic group present over the surface of carbon nanodots could catalyze the formation of quinazolinone derivatives with different structurally perplexing substituents. In case of graphene oxide, the π - π^* network as well as oxygenated functional groups both contributed towards the enhanced catalytic activity. The presence of π - π^* network on graphene surface helped the substrate molecules getting adsorbed over the catalyst surface and the oxygenated functional groups catalyzed the reaction. The carboxylic acid groups acted as the active site for the C-N coupling reaction leading to the α -ketoamide product where the function of both the acidic as well as oxidising character of carboxylic group was established. The presence of various functionalities on the surfaces of both carbon nanodots as well as graphene oxide could be used for anchoring other active catalysts such as metal and metal oxide nanoparticles. The reducing capability of these nanocarbons could also be envisaged for reduction of metal ions to nanoparticles. Herein, we demonstrated the efficiency of these nanocarbons in anchoring Au and Fe₃O₄ nanoparticles. The catalytic activity of the resulting nanocomposites was studied towards oxidation reactions such as selective C-H oxidation and cyclooxidative synthesis of quinazolinones. We showed that apart from acting as a support, a cooperativity effect between the active catalyst and the support were instrumental in enhancing the catalytic activity of the catalyst.

6.2 Future Outlook

The carbon based nanomaterials have already demonstrated their enormous potential either as catalysts or heterogeneous catalyst supports. Various forms of carbon including activated carbon, graphite, fullerenes, carbon nanotubes etc. showed superior surface characteristics that have been explored for the development of hybrid catalytic systems with high and selective activity in chemical-, electro- or photocatalysis. Graphene oxide and carbon nanodots with oxygenated functional groups on their surface could act as active sites for various acid catalyzed and oxidative catalytic reactions. Recent advancement of these

Chapter 6

graphene based materials shows that the modification of graphene surface by different methods leads to generation of holes which acts as traps for reactive oxygen species for many challenging organic reactions. Further doping with foreign atoms such as N, P, S, B etc. changes their inherent physico-chemical properties to a large extent. Hence tremendous possibilities remain to explore these carbonaceous nanomaterials in various catalysis fields including chemical synthesis, energy storage (batteries and super capacitors), fuel-cells, environmental remediation and organism degradation. These outstanding benefits of carbon based materials have made them extremely important in various research areas. The continuous development of these carbonaceous nanomaterials and their composites might introduce new properties as well as new active sites for challenging applications. Carbon nanodots are the recent inclusion to the nanocarbon family. The excellent photoluminescence properties of carbon nanodots have directed their application in different fields including sensing, optoelectronics, bio imaging, nanomedicine, etc. Although they are widely explored in sensing as well as bio-medical application, their inherent photocatalytic capability towards organic synthesis has not been explored much. So, the development of carbon nanodots towards organic synthesis may result in an important alternative to the traditional transition metal based catalysts. There are still huge scope towards (i) high performance carbon catalyst specific for desired products, (ii) development of chiral carbon nanomaterials for enantioselective synthesis, (iii) affordable methods for large scale synthesis, industrial scalability and economic viability, (iv) detailed elucidation of catalytic mechanism that can bring further improvements in catalytic activity and (v) stability of the catalyst to maintain excellent catalytic activity during recycling. Overall, development of carbon related catalysts with broader applications is imminent towards green and sustainable chemistry.



Dr. Biju Majumdar obtained his B.Sc in Chemistry from B. Borooah College, Guwahati in 2009 and M.Sc in Organic Chemistry from Gauhati University in 2011. Then he joined Indian Institute of Technology Indore as a Ph.D. student in 2012 under the supervision of Dr. Tridib K. Sarma. His research topic was “Development of Carbonaceous Nanomaterials based Heterogeneous Catalytic Systems for Organic Transformations”

Dr. Biju Majumdar

DOB: 31/12/1988